

Doctoral thesis

学位論文

Cosmology in vector-tensor theories  
with interaction between dark components

(暗黒成分間の相互作用を伴う  
ベクトル-テンソル理論における宇宙論)

March, 2021 (2021 年 3 月)

Shintaro Nakamura (中村 進太郎)

Department of Physics, Faculty of Science,  
Tokyo University of Science

(東京理科大学 理学研究科 物理学専攻)

# Abstract

In this thesis, we consider dark energy models based on vector-tensor theories in which a massive vector field is coupled to not only gravity but also cold dark matter (CDM). In such models, the late-time cosmic acceleration is driven by the vector field.

First, in massive vector-tensor theories (where the vector field is not coupled to CDM), we study the cross-correlation between the integrated Sachs-Wolfe (ISW) effect in cosmic microwave background (CMB) and galaxy distribution. The cross-correlation can be a probe to distinguish several dark energy models. For instance, the sign of the ISW-galaxy cross-correlation in  $\Lambda$ CDM is positive, while that in scalar Galileon is negative. It is caused by the difference of the time evolution of the effective gravitational coupling felt by light. We find that, due to the existence of intrinsic vector modes, the cross-correlation in vector-tensor theories can be positive, unlike that in scalar-tensor theories. We place observational constraints on a vector dark energy model by running the Markov chain Monte Carlo (MCMC) code. As the observational data, we use cosmic microwave background, baryon acoustic oscillations, type Ia supernovae, local measurements of the Hubble expansion rate, redshift-space distortions, and the ISW-galaxy cross-correlations. We show that even if we consider the ISW-galaxy cross-correlation data, the vector dark energy model is statistically favored over the  $\Lambda$ CDM model.

Secondly, we investigate an additional interaction with energy transfer between vector dark energy and CDM. In this case, the continuity equations for the vector field and CDM have interacting terms associated with the additional coupling. In the small-scale limit, the new interaction does not affect the conditions for the absence of ghosts and gradient instabilities for tensor and vector perturbations, while those for scalar perturbations include the dependence of the additional coupling. The interaction also affects the no-ghost condition for CDM density perturbations. We consider a concrete model with the energy exchange between dark components. In comparison to the uncoupled case, we find that the dark energy equation of state during matter-dominated epoch can be closer to  $-1$  as long as CDM partially decay to the vector field. Since the no-ghost condition for CDM density perturbations should be satisfied in whole cosmological epoch, the dark energy equation of state during the matter era has the upper limit.

Finally, we consider a new coupled vector dark energy model in which the vector field interacts with CDM through the momentum transfer. Such a situation can be realized for the interaction between a vector field and the four-velocity of CDM. In this case, the background continuity equations for the vector field and CDM do not have interacting terms, unlike the case with

energy transfer. On the other hand, the interaction affects the evolution of cosmological perturbations. For instance, the stability conditions for scalar perturbations have the dependence of the new interaction with the momentum transfer. Moreover, the effective gravitational coupling for CDM has the different time evolution from that for baryons. In particular, the former can be smaller than the Newtonian gravitational constant around today. We show that this property leads to the existence of the lower linear growth rate of matter density perturbations than that in  $\Lambda$ CDM. It means that our model has a possibility for reducing the  $\sigma_8$  tension between high-redshift and low-redshift observations.

## Acknowledgement

I would like to express my gratitude to my supervisor Professor Shinji Tsujikawa for his continual guidance and encouragement through the course of the work. I am deeply grateful to Ryotaro Kase for useful discussions and comments. I appreciate Antonio De Felice for interesting collaborations.

# Contents

<b>1</b>	<b>Introduction</b>	<b>6</b>
<b>2</b>	<b>Observational evidence of dark energy</b>	<b>11</b>
2.1	Standard cosmology . . . . .	11
2.2	Comoving distance . . . . .	16
2.3	Supernovae type Ia . . . . .	17
2.4	Cosmic microwave background . . . . .	19
<b>3</b>	<b>Overview of dark energy models</b>	<b>22</b>
3.1	Cosmological constant . . . . .	22
3.2	Dynamical dark energy . . . . .	27
3.3	Dark energy non-minimally coupled to gravity . . . . .	29
3.4	Dark energy coupled to dark matter . . . . .	32
3.5	Vector dark energy . . . . .	34
3.6	After the event GW170817 . . . . .	34
<b>4</b>	<b>Massive vector-tensor theories</b>	<b>36</b>
4.1	Generalized Proca theories . . . . .	36
4.2	Dynamics on cosmological background . . . . .	41
4.3	Conditions for avoiding ghosts and gradient instabilities . . . .	44
4.4	Concrete dark energy models . . . . .	55
<b>5</b>	<b>Integrated Sachs-Wolfe effect in massive vector-tensor theories</b>	<b>63</b>
5.1	Definition of matter density perturbation and gravitational potentials . . . . .	63
5.2	Effective gravitational couplings felt by matter and light . . .	64
5.3	ISW-galaxy cross-correlations . . . . .	67
5.4	Observational constraints . . . . .	77
5.5	Summary of Chapter 5 . . . . .	86

<b>6</b>	<b>Energy transfer between vector dark energy and cold dark matter</b>	<b>87</b>
6.1	Energy transfer and background equations . . . . .	87
6.2	Conditions for avoiding ghosts and gradient instabilities . . . .	91
6.3	Concrete model with energy transfer . . . . .	98
6.4	Summary of Chapter 6 . . . . .	108
<b>7</b>	<b>Momentum transfer between vector dark energy and cold dark matter</b>	<b>109</b>
7.1	Coupled generalized Proca theories with momentum transfer .	109
7.2	Cosmological perturbations and stability conditions . . . . .	114
7.3	Effective gravitational couplings for CDM and baryons . . . .	123
7.4	Concrete models with momentum transfer . . . . .	130
7.5	Summary of Chapter 7 . . . . .	139
<b>8</b>	<b>Summary</b>	<b>140</b>

# Chapter 1

## Introduction

In our universe, there are two types of dark components: dark energy, which is the source of accelerated expansion of the universe, and dark matter, which is the main component that forms the large-scale structure of the universe. Recent observations[1] show that the current universe is composed of dark energy (about 70%), dark matter (about 25%), baryons (about 5%), and radiation (about 0.01%). The origins of dark components are difficult to deal within the framework of general relativity and the standard model of elementary particles. It may suggest the existence of a theory that goes beyond them.

Dark energy is defined as the source of late-time cosmic acceleration. The phenomenon was first discovered in 1998 from the observations of supernovae type Ia (SN Ia) in high redshifts by two observational groups independently, which are Riess *et al.* in the High-redshift Supernova Search Team [2] and Perlmutter *et al.* in the Supernova Cosmology Project [3]. Since the standard matter like baryons, leptons, and photons only gives rise to the decelerated cosmic expansion, we need an additional energy source to explain the late-time cosmic acceleration. After the discovery, other observations such as Cosmic Microwave Background (CMB)[1] and Baryon Acoustic Oscillations (BAO)[4] have provided evidence of late-time cosmic acceleration independently. For instance, the measurement of the BAO distances and the growth rate of matter fluctuation by the extended Baryon Oscillation Spectroscopic Survey (eBOSS) shows the significance level of the existence of dark energy as  $11\sigma$  [5]. However, the origin of this phenomenon has not been specified yet.

The equation of state  $w_{\text{DE}}$  is a key quantity for discussing the property of dark energy at the background level. It is defined by the ratio of the energy density  $\rho_{\text{DE}}$  and the pressure  $P_{\text{DE}}$  of dark energy, as  $w_{\text{DE}} = P_{\text{DE}}/\rho_{\text{DE}}$ . In order to realize the late-time cosmic acceleration,  $w_{\text{DE}}$  has to satisfy the

bound  $w_{\text{DE}} < -1/3$ . From recent Planck observation [1], the combined analysis of SN Ia, CMB, and BAO shows the bound  $-1.06 < w_{\text{DE}} < -0.996$  at the 68% confidence level assuming a constant equation of state.

The simplest candidate for dark energy is a cosmological constant (denoted as  $\Lambda$ ), which was first introduced by Einstein in 1917. In Einstein's context, the negative pressure exerted by a cosmological constant suppresses the expansion of the universe. Recently, the cosmological constant is used to realize the acceleration of our universe. The energy density of  $\Lambda$  is constant in time, and this property is similar to the vacuum energy. In the case of the cosmological constant, we have  $P_{\text{DE}} = -\rho_{\text{DE}}$  and then  $w_{\text{DE}} = -1$ . However, if the cosmological constant is associated with the vacuum energy appearing in standard particle physics, its energy scale is much larger than the observed dark energy scale [6, 7, 8, 9]. If this problem is solved in such a way that the vacuum energy vanishes or becomes smaller than today's energy density of the universe, we need to find an alternative candidate of dark energy.

In modern cosmology, the fiducial model is called  $\Lambda$ CDM, in which the dark components are given by a cosmological constant and cold dark matter. Note that these dark components in the model do not interact directly. Although the model is simple, it can explain some properties of our Universe. However, if we adopt  $\Lambda$ CDM, it has been pointed out that there is the tension at about  $5\sigma$  level regarding Hubble constant  $H_0$  between CMB temperature anisotropies and low-redshift measurements [10, 11]. Moreover, the observational data associated with galaxy clusterings and weak lensing favor the amplitude of matter density contrast  $\sigma_8$  smaller than that constrained by CMB [12, 13]. It means that the cosmological scenario may be given by the other model instead of the  $\Lambda$ CDM.

As a natural extension of the  $\Lambda$ CDM model, we can think of dark energy as a new physical degree of freedom that varies over time. In particular, the framework in which gravity is coupled to a scalar degree of freedom is called scalar-tensor theory. In dynamical dark energy models,  $w_{\text{DE}}$  generally varies in time. It means that the equation of state  $w_{\text{DE}}$  can be a probe to find whether dark energy can be identified with the cosmological constant or not. As an example, quintessence is one of the dynamical dark energy models [14, 15, 16, 17, 18, 19, 20, 21, 22]. Such dynamical models can be distinguished from the  $\Lambda$ CDM model since the quintessence equation of state varies in time. However, there are no strong observational evidence that such models are favored over the  $\Lambda$ CDM. Unlike the quintessence, the Brans-Dicke theories [23] have a coupling between a scalar field and the Ricci scalar. Such coupling Galileon is one of the models with non-minimally derivative self-interaction of a scalar field  $\varphi$ . The equations of motion in Galileon respect the symmetry  $\partial_\mu \varphi \rightarrow \partial_\mu \varphi + b_\mu$  in Minkowski space-time. To avoid a Ostrogradski



instability [24, 25] associated with the Hamiltonian unbounded from below, the Lagrangian of Galileon is constructed to keep the equations of motion up to second order. These models are included in the general framework called Horndeski theory [26, 27, 28]. The Horndeski theory is the most general scalar-tensor theory with the second-order equations of motion. In Horndeski theory, there are three degrees of freedom in total such as two tensor modes related to the gravitational waves and one scalar degree of freedom.

We can consider not only scalar fields but also vector fields as the fields which describe the dark energy. As in scalar-tensor theory, a framework in which gravity is coupled to a vector degree of freedom is called vector-tensor theory. Unfortunately, C. Deffayet et al. [29] showed a no-go theorem in which the Galileon like Lagrangian can not be constructed for a vector field with  $U(1)$  symmetry. However, this no-go theorem does not apply to a massive vector field (dubbed Proca field) since the  $U(1)$  symmetry is broken. As the extension of Proca action, L. Heisenberg developed the generalized Proca (GP) theory[30] in which combine a massive vector field interacts with gravity. GP theory is one of the vector-tensor theories with the second-order equations of motion. In GP theory, there are five propagating degrees of freedom in total: two tensor modes in the gravitational field, two transverse modes, and one longitudinal scalar mode. In previous works, it is shown that the dark energy model with a massive vector field are preferred over the  $\Lambda$ CDM model due to the presence of a time component corresponding to the longitudinal wave mode. It means that the vector-tensor theories may reduce the tension of the Hubble constant.

The problem of  $\sigma_8$  tension needs further discussion. In general, extending the theory of gravity from general relativity, the gravitational constant varies in time and deviates from Newtonian gravitational constant. Assuming that the speed of propagation of gravitational waves is equal to the speed of light, the effective gravitational coupling in Horndeski theories tends to be larger than the Newtonian gravitational constant  $G$ . In cubic-order GP theories, the effective gravitational coupling can be the similar value to the Newtonian gravitational constant, but it can not be smaller than  $G$  as long as the ghost instabilities are absent. In those case, it is difficult to reduce the  $\sigma_8$  tension.

If dark matter decays into dark energy, there may be a possibility that the gravitational coupling with CDM is smaller than  $G$ . It means that the interaction between dark components may alleviate the  $\sigma_8$  tension. As such interaction, we can consider two type form: (i) energy transfer and (ii) momentum transfer. The former affects to the continuity equations of CDM and dark energy at the background level due to the energy exchange between these components. The latter do not affect to the background dynamics, while the effect of momentum transfer appears the perturbation dynamics through the

CDM four velocity.

In this thesis, we shall discuss the dark energy models based on vector-tensor theories with the second-order equations of motion. First, we derive the cosmological dynamics of vector dark energy and discuss the effect to the integrated Sachs-Wolfe-galaxy cross-correlation. After that, we place observational constraints on such dark energy model by running the likelihood analysis. Moreover, in order to reduce the tensions of two cosmological parameters, we consider the cases in which the vector dark energy interacts with cold dark matter through energy and momentum transfer. In the model with such energy transfer, the dark energy equation of state is different from that in the uncoupled case due to the energy exchange. For a concrete model, we find that the equation of state during the matter era is bounded from the CDM no-ghost condition. In the model with momentum transfer between dark components, the background dynamics is the same as that in the uncoupled case. Then, we can consider the dark energy model in which the  $H_0$  tension can be reduced by the existence of the temporal component of a vector field and the  $\sigma_8$  tension also may be reduced by the smaller effective gravitational coupling than  $G$ .

## Structure of the thesis

This thesis is organized as follows.

- In Chap.2, we review the standard cosmology and the observational evidence for the late-time cosmic acceleration.
- In Chap.3, we highlight several approaches to trying to solve the problem of dark energy.
- In Chap.4, we introduce generalized Proca theories as one of the vector-tensor theories, and we review dark energy models based on the theories.
- In Chap.5, we discuss integrated Sachs-Wolfe (ISW) effect which appears in CMB power spectrum. We also place the constraints to the vector dark energy models by using some observational data, such as CMB, BAO, SN Ia, Hubble expansion rate, Redshift space distortion (RSD), and ISW-galaxy cross-correlations.
- In Chap.6, we provide an additional interaction corresponding to energy transfer between a massive vector field (as dark energy) and cold dark

matter, We also discuss the evolution of dark energy equation of state in this case.

- In Chap.7, we consider the interaction between a massive vector field and four velocity of cold dark matter which corresponds to momentum transfer between these.
- Chap.8 is devoted to the summary of this thesis.

## Units and conventions

Throughout this thesis, we use the signature  $(-, +, +, +)$  for the four dimensional space-time metric. We adopt natural units  $c = \hbar = k_B = 1$ , where  $c$  is the speed of light,  $\hbar$  is reduced Planck's constant, and  $k_B$  is Boltzmann's constant. In these units, the Planck mass  $m_{\text{pl}}$  is related to Newtonian gravitational constant  $G$  as  $m_{\text{pl}}^2 = 1/G$ . We also denote the reduced Planck mass as  $M_{\text{pl}}$ , which is related to the Planck mass  $m_{\text{pl}}$  as  $M_{\text{pl}} = m_{\text{pl}}/\sqrt{8\pi}$ . Then,  $M_{\text{pl}}$  can be expressed as  $G$  in the form  $M_{\text{pl}}^2 = 1/(8\pi G)$  in the natural units.

# Chapter 2

## Observational evidence of dark energy

In this chapter, we will review the evidence of dark energy from some observations. To discuss the observational evidence, at first, we introduce standard cosmology and the condition for acceleration of the universe. After that, we show the observables for type Ia supernovae and the parameters associated with the shift of the acoustic peaks of cosmic microwave background. The explanation is based on Refs. [33, 34]. We also review the results from Planck collaboration.

### 2.1 Standard cosmology

At first, we consider that the universe consists of radiation, non-relativistic matter, and dark energy. Also, we assume that gravity is described by general relativity (GR). Let us begin with the following action:

$$S_{\text{SC}} = \int d^4x \sqrt{-g} \left[ \frac{M_{\text{pl}}^2}{2} R + \mathcal{L}_r + \mathcal{L}_m + \mathcal{L}_{\text{DE}} \right], \quad (2.1)$$

with the 4-dimensional metric defined by

$$ds^2 = g_{\mu\nu} dx^\mu dx^\nu, \quad (2.2)$$

where  $g$  is a determinant of the metric tensor  $g_{\mu\nu}$ ,  $R$  is the Ricci scalar,  $M_{\text{pl}}$  is the reduced Planck mass,  $\mathcal{L}_I$  are the Lagrangian densities for radiation (labeled as  $r$ ), non-relativistic matter (labeled as  $m$ ), and dark energy (labeled as DE). The non-relativistic matter consists of baryons and dark matter. In this section, we do not specify the concrete model of dark energy. Varying

the action with respect to the metric  $g_{\mu\nu}$ , we obtain the Einstein equation

$$M_{\text{pl}}^2 G_{\mu\nu} = T_{\mu\nu}^{(m)} + T_{\mu\nu}^{(r)} + T_{\mu\nu}^{(\text{DE})}, \quad (2.3)$$

where  $G_{\mu\nu}$  is the Einstein tensor, and  $T_{\mu\nu}^I$  are the energy-momentum tensors defined by

$$T_{\mu\nu}^{(I)} = -\frac{2}{\sqrt{-g}} \frac{\delta(\sqrt{-g}\mathcal{L}_I)}{\delta g^{\mu\nu}}, \quad (2.4)$$

for  $I = m, r, \text{DE}$ .

To discuss the cosmological dynamics, we consider the homogeneous and isotropic background, which is called Friedmann-Lemaître-Robertson-Walker (FLRW) space-time, is given by the following line element

$$ds^2 = -dt^2 + a^2(t)d\sigma^2, \quad (2.5)$$

where  $a(t)$  is a scale factor which depends on the cosmic time  $t$  alone, and  $d\sigma^2$  is the time-independent metric of the 3-dimensional space

$$d\sigma^2 = \frac{dr^2}{1 - Kr} + r^2(d\theta^2 + \sin^2\theta d\phi^2), \quad (2.6)$$

with a constant curvature  $K$ . Here, we have used polar coordinates given by  $(x^1, x^2, x^3) = (r, \theta, \phi)$ . When  $K = 0$ , which means the “flat” FLRW background, the 3-dimensional metric  $d\sigma^2$  can be expressed as

$$d\sigma^2 = dx^2 + dy^2 + dz^2, \quad (2.7)$$

by using Cartesian coordinates given by  $(x^1, x^2, x^3) = (x, y, z)$  with the relations  $x = r \sin\theta \sin\phi$ ,  $y = r \sin\theta \cos\phi$ , and  $z = r \cos\theta$ .

We consider that the matter species in the universe are described as the perfect fluids, so the energy-momentum tensors (2.4) have only diagonal components, as

$$T^{(I)\mu}{}_{\nu} = \text{diag}(-\rho_I, P_I, P_I, P_I), \quad (2.8)$$

where  $\rho_I$  and  $P_I$  are the energy density and the pressure for each matter species ( $I = r, m, \text{DE}$ ), respectively. Then, the (00) and (ii) components of the Einstein equation reduce to the Friedmann equations given by, respectively,

$$3M_{\text{pl}}^2 H^2 + \frac{3M_{\text{pl}}^2 K}{a^2} = \rho_r + \rho_m + \rho_{\text{DE}} \equiv \rho, \quad (2.9)$$

$$M_{\text{pl}}^2(3H^2 + 2\dot{H}) + \frac{M_{\text{pl}}^2 K}{a^2} = -P_r - P_m - P_{\text{DE}} \equiv -P, \quad (2.10)$$

where a dot represents a derivative with respect to cosmic time,  $H \equiv \dot{a}/a$  is the Hubble expansion rate,  $\rho$  and  $P$  are the total energy density and the total pressure in the universe. These equations are important to discuss cosmic expansion history. Taking the time derivative of Eq. (2.9) and using Eq. (2.10), it follows that

$$\dot{\rho} + 3H(\rho + P) = 0, \quad (2.11)$$

which corresponds to the continuity equation for the perfect fluid. The continuity equation (2.11) is related to the conservation law of energy-momentum tensor.

We introduce the equation of state of the perfect fluid defined by

$$w \equiv P/\rho. \quad (2.12)$$

Then, substituting Eq. (2.9) into (2.10), we obtain

$$\frac{\ddot{a}}{a} = -\frac{\rho}{6M_{\text{pl}}^2} (1 + 3w). \quad (2.13)$$

The universe with the positive energy density  $\rho > 0$  accelerates for  $\ddot{a} > 0$ , while it decelerates for  $\ddot{a} < 0$ . In the other word, the condition for realizing the acceleration is given by

$$w < -\frac{1}{3}, \quad (2.14)$$

from Eq. (2.13).

Since the pressure of radiation is proportional to the energy density as  $P_r = \rho_r/3$  from statistical mechanics, the equation of state for radiation  $w_r$  is given by

$$w_r = \frac{P_r}{\rho_r} = \frac{1}{3}. \quad (2.15)$$

For non-relativistic matter like dust, the pressure  $P_m$  can be negligible relative to the energy density  $\rho_m$ , so the equation of state for non-relativistic matter  $w_m$  is given by

$$w_m = \frac{P_m}{\rho_m} \simeq 0. \quad (2.16)$$

In the epoch dominated radiation or non-relativistic matter, the right hand side of Eq. (2.13) is always negative, and both Eqs. (2.15) and (2.16) do not

satisfy the condition Eq. (2.14). It means that the universe decelerates as long as the radiation or matter is the dominant factor.

To estimate the time evolution of the scale factor, we consider the case in which the fluid equation of state  $w$  is constant. Then, integrating Eq. (2.11), we obtain the relation

$$\rho \propto a^{-3(1+w)}. \quad (2.17)$$

For radiation and non-relativistic matter, these equations of state are given by Eqs. (2.15) and (2.16), so these energy densities evolve as, respectively,

$$\rho_r \propto a^{-4}, \quad \rho_m \propto a^{-3}. \quad (2.18)$$

For  $w > -1$ , substituting Eq. (2.17) into Eq. (2.9) and integrating the equation, it follows that

$$a \propto t^{2/[3(1+w)]}. \quad (2.19)$$

In the radiation dominated epoch, the scale factor evolves as  $a \propto t^{1/2}$ , while the scale factor in the matter dominated epoch evolves as  $a \propto t^{2/3}$ . When the equation of state  $w$  is in the range  $-1 < w < -1/3$ , the universe exhibits an acceleration.

For  $w = -1$ , the case corresponds to the universe dominated by the cosmological constant. In this case,  $\rho$  is constant from Eq. (2.17), so the Hubble parameter  $H$  is also constant from Eq. (2.9). Then, the scale factor grows exponentially, as

$$a \propto \exp(Ht), \quad (2.20)$$

in which the accelerating universe can be realized.

For  $w < -1$ , due to the scale factor given by Eq. (2.19) decreases with time, the universe collapses. The expanding solution with  $w < -1$  is given by

$$a \propto (t_s - t)^{2/[3(1+w)]}, \quad (2.21)$$

where  $t_s$  is a constant. This solution is valid for  $t < t_s$ . In this case, the Hubble expansion rate  $H$  and its time derivative  $\dot{H}$  reduce, respectively, to

$$H = -\frac{2}{3(1+w)(t_s - t)}, \quad \dot{H} = -\frac{2}{3(1+w)(t_s - t)^2}. \quad (2.22)$$

Then, the Ricci scalar  $R$  is expressed as

$$R = 6 \left( 2H^2 + \dot{H} + \frac{K}{a^2} \right) = \frac{4(1-3w)}{3(1+w)^2(t_s - t)^2} + \frac{6K}{a^2}. \quad (2.23)$$

When the cosmic time  $t$  approaches  $t_s$ , both the scale factor  $a$  and the Ricci scalar  $R$  diverge at that time. In this case, the universe has a big-rip singularity at which the evolution of the universe ends. Therefore, in the framework of GR, it is difficult to realized the expanding universe with  $w_{\text{DE}} < -1$  without the theoretical singularity. However, the region  $w_{\text{DE}} < -1$  is allowed from observations. As we will see later, that situation can be realized in the models which are described by the extension of gravity theory from GR.

Here, we introduce the redshift

$$z = \frac{a_0}{a} - 1, \quad (2.24)$$

where the present epoch corresponds to  $z = 0$ . In the following we take the present scale factor  $a_0$  to be unity, i.e.,  $a_0 = 1$ , then the scale factor is in the range  $0 < a \leq 1$ . The redshift  $z$  is related to the effect that the wavelength from the observed object is stretched in proportion to the scale factor in an expanding universe. As long as the recessional velocity  $v_{\text{re}}$  of the object is much smaller than the speed of light  $c$ , the redshift  $z$  is proportional to the recessional velocity, as  $z \simeq v_{\text{re}}/c$ .

In 1929, E. Hubble reported the relation between distance and recessional velocity of galaxies. The distance of galaxy was measured by the observation of apparent luminosity of Cepheid variable star, and the recessional velocity is estimated by the redshift. He showed that the recessional velocity of the object is proportional to the distance, and our universe is expanding.

From Eq. (2.18) and Eq. (2.24), the energy densities of radiation and matter can be expressed in the form

$$\rho_r = \rho_{r0} (1 + z)^4, \quad \rho_m = \rho_{m0} (1 + z)^3, \quad (2.25)$$

where  $\rho_{r0}$  and  $\rho_{m0}$  are today's values of the energy densities for radiation and matter. Taking the time derivative of Eq. (2.24) and integrating Eq. (2.11) with the redshift  $z$ , it follows that

$$\rho_{\text{DE}} = \rho_{\text{DE}0} \exp \left[ \int_0^z \frac{3 \{1 + w_{\text{DE}}(\tilde{z})\}}{1 + \tilde{z}} d\tilde{z} \right], \quad (2.26)$$

where  $\rho_{\text{DE}0}$  is today's value of the energy density for dark energy. This means that the evolution of dark energy is characterized by the equation of state  $w_{\text{DE}}$ .

To discuss time evolution of compositional ratio of each matter species in the universe along the expansion, we introduce the following quantities called density parameters,

$$\Omega_I \equiv \frac{\rho_I}{3M_{\text{pl}}^2 H^2}, \quad \Omega_K \equiv -\frac{K}{a^2 H^2}, \quad (2.27)$$



for  $I = r, m, \text{DE}$ . From Eq. (2.9), the sum of  $\Omega_I$  and  $\Omega_K$  is always unity,

$$\Omega_r + \Omega_m + \Omega_{\text{DE}} + \Omega_K = 1. \quad (2.28)$$

This relation holds in the whole cosmological epoch. Hence, Substituting Eqs. (2.25) and (2.26) into Eq. (2.28), it follows that

$$\begin{aligned} \frac{H^2(z)}{H_0^2} = & \Omega_{r0}(1+z)^4 + \Omega_{m0}(1+z)^3 + \Omega_{\text{DE}0} \exp \left[ \int_0^z \frac{3\{1 + w_{\text{DE}}(\tilde{z})\}}{1 + \tilde{z}} d\tilde{z} \right] \\ & + \Omega_{K0}(1+z)^2, \end{aligned} \quad (2.29)$$

where  $H_0$  is today's value of Hubble expansion rate (called Hubble constant), and  $\Omega_{I0}$ ,  $\Omega_{K0}$  are today's values of each density parameter given by, respectively,

$$\Omega_{I0} \equiv \frac{\rho_{I0}}{3M_{\text{pl}}^2 H_0^2}, \quad \Omega_{K0} \equiv -\frac{K}{a_0^2 H_0^2}, \quad (2.30)$$

for  $I = r, m, \text{DE}$ . When today's values of  $H_0, \Omega_{I0}, \Omega_{K0}$  and a concrete equation of state  $w_{\text{DE}}$  are given, we can estimate the evolution of the Hubble expansion rate.

The Hubble constant  $H_0$  is usually written as

$$H_0 = 100 h \text{ km s}^{-1} \text{ Mpc}^{-1} = 2.1332h \times 10^{-42} \text{ GeV}, \quad (2.31)$$

with a dimensionless constant  $h$  which describes the uncertainty on the value  $H_0$ , where

$$1 \text{ Mpc} = 10^6 \text{ pc} = 3.0857 \times 10^{24} \text{ cm}. \quad (2.32)$$

For today's energy density of the curvature  $\Omega_{K0}$ , the joint analysis of CMB and BAO in the Planck observation [1] shows the bound as

$$\Omega_{K0} = 0.0007 \pm 0.0019, \quad (68\% \text{ CL}). \quad (2.33)$$

This joint result suggests the today's universe is close to the flat geometry. In the following, we focus on the cosmological dynamics in the flat universe  $K = 0$  unless otherwise noted.

## 2.2 Comoving distance

By redefinition of the radial coordinate, the 3-dimensional line element can be written in a more convenient form as

$$d\sigma^2 = d\chi_{\text{cd}}^2 + f_K^2(\chi_{\text{cd}})(d\theta^2 + \sin^2 \theta d\phi^2), \quad (2.34)$$

with the function

$$f_K(\chi_{\text{cd}}) = \begin{cases} \sin \chi_{\text{cd}} & (K = +1), \\ \chi_{\text{cd}} & (K = 0), \\ \sinh \chi_{\text{cd}} & (K = -1), \end{cases} \quad (2.35)$$

where the quantity  $\chi_{\text{cd}}$  is called a comoving distance.

The light propagating along the  $\chi_{\text{cd}}$  direction satisfies the geodesic equation  $ds^2 = -dt^2 + a^2 d\chi_{\text{cd}}^2 = 0$ . We consider that the light is emitted at time  $t$  with  $\chi_{\text{cd}}$  (redshift  $z$ , scale factor  $a$ ) and it reaches an observer at time  $t = t_0$  with  $\chi_{\text{cd}} = 0$  (redshift  $z = 0$ , scale factor  $a = a_0 = 1$ ). Then, from the geodesic equation, the comoving distance  $\chi_{\text{cd}}$  reads

$$\chi_{\text{cd}} = - \int_{t_0}^t \frac{d\tilde{t}}{a(\tilde{t})}. \quad (2.36)$$

Moreover, since there is the relation  $dz/dt = -H/a$ , the comoving distance can be expressed as

$$\chi_{\text{cd}} = \int_0^z \frac{d\tilde{z}}{H(\tilde{z})}. \quad (2.37)$$

## 2.3 Supernovae type Ia

Since The SN Ia has a nearly constant absolute magnitude  $M \simeq -19$  at the peak of brightness, the distance to a SN Ia can be determined by measuring its observed apparent luminosity. It is the reason why the SN Ia can be used as standard candle. The observed apparent magnitude  $m$  of SNIa is different from its absolute magnitude  $M$ , whose difference is quantified as

$$\mu(z) \equiv m(z) - M = 5 \log_{10} \left[ \frac{d_L(z)}{10 \text{ pc}} \right], \quad (2.38)$$

where  $d_L(z)$  is the luminosity distance from the observer to the source at redshift  $z$  given by

$$d_L(z) = (1 + z) \int_0^z \frac{d\tilde{z}}{H(\tilde{z})}, \quad (2.39)$$

in the flat universe. This means that the absolute magnitude is defined as the apparent magnitude of the object which is located at 10 pc from the observer. From the observable (2.38) at each redshifts by the observation of SN Ia, it is possible to place constraints on the Hubble expansion rate

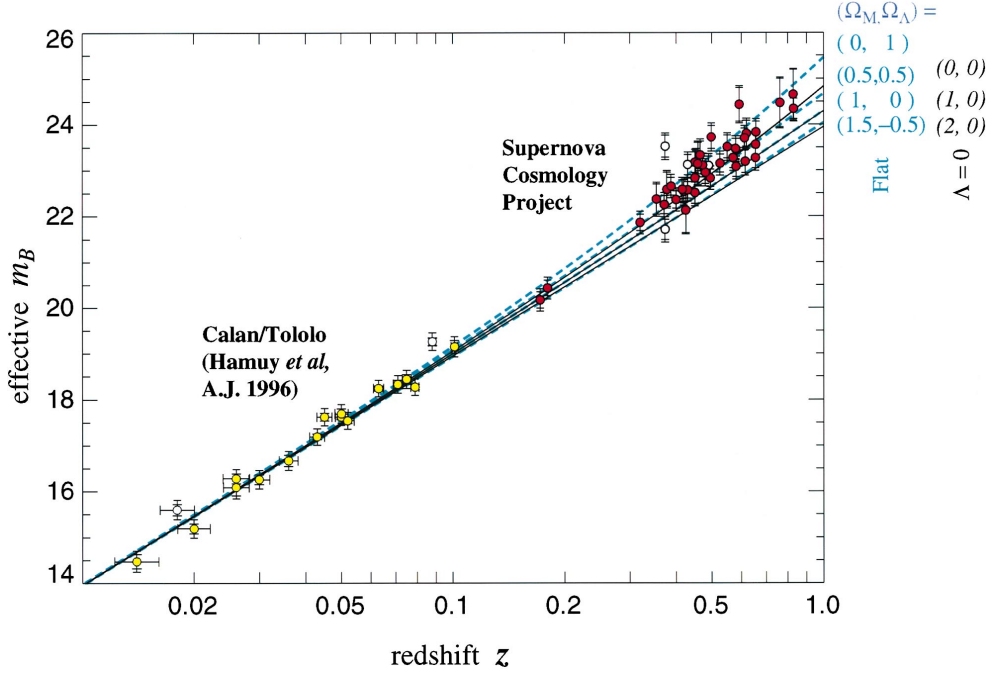


Figure 2.1: The effective apparent luminosity  $m_B$  versus the redshift  $z$  in the flat universe for 42 data from Ref.[3] and 18 data from Ref.[46]. Note that  $m_B$  involves the corrections of both data sets for the SN Ia light-curve width-luminosity relation to the apparent luminosity  $m$ . The solid curves are the theoretical prediction for  $m$  for three cosmological models without the cosmological constant. The dashed curves correspond to four cosmological models with the cosmological constant. This figure is taken from Ref.[3].

and each density parameters in the universe through the luminosity distance given by Eq. (2.39).

Fig.2.1 shows the effective apparent luminosity  $m_B$  for 42 SN Ia from Supernova Cosmology Project [3] and 18 SN Ia from the Calan/Tololo Supernova Survey [46]. We can see that the effective apparent luminosity  $m_B$  related to  $m$  increases for larger today's density parameter of dark energy (denoted as  $\Omega_\Lambda$ ). Fig.2.1 also shows the theoretical curves for some cosmological models. It means that the universe with the cosmological constant is favored over the Einstein de Sitter model ( $\Omega_{m0} = 1$  and  $\Omega_{\Lambda0} = 0$ ).

In 1998, Riess *et al.* [2] and Perlmutter *et al.* [3] released observational data of the apparent luminosity of SN Ia in the range  $0.18 < z < 0.83$ . Perlmutter *et al.* [3] carried out the likelihood analysis by using 42 data of SN Ia between  $0.18 < z < 0.83$  and 18 data perviously derived in low-redshift regimes ( $z \ll 1$ ). Assuming the flat universe with a cosmological constant, they derived the bound on the density parameter of non-relativistic matter,

as  $\Omega_{m0} = 0.28^{+0.09}_{-0.08}$  (68% CL). Since the relation (2.28) at the redshift  $z < 1$  in the flat universe reduces to  $\Omega_m + \Omega_{\text{DE}} \simeq 1$ , it means that the rest of the energy in the universe (about 70%) can be regarded as dark energy related to the late-time cosmic acceleration

After 1998, the evidence that dark energy constitutes about 70% of the today's energy density of the Universe has been confirmed by other independent observations such as CMB and BAO.

## 2.4 Cosmic microwave background

In 1964, Penzias and Wilson discovered signals which came from all parts of the sky at all times [31]. This signal was the first discovery of the CMB. The discovery of CMB provided us with independent observational evidence for the big bang cosmology. According to the big bang paradigm the Universe was initially in a hot and dense state, but the temperature decreased along with the expansion of the Universe. In the present Universe, the temperature of the CMB photon decreased to about  $3K$ . In 1992, the temperature anisotropies of the CMB were first measured at large angular separations by the COBE satellite [32]. The most recent observation of the CMB temperature anisotropies is carried out by the Planck collaboration [1] operated by the European Space Agency (ESA).

The CMB power spectrum is affected by the presence of dark energy at least in two ways. First, the change of the angular diameter distance from the last scattering surface to today leads to the shift of CMB acoustic peaks. The first effect is the shift of CMB acoustic peaks due to the change of the angular diameter distance from the last scattering surface to today. Second, there is the late-time integrated Sachs-Wolfe effect because of the time evolution of gravitational potentials induced by the presence of dark energy. In Chap.5, we will see the latter effect in detail. The first effect is usually more important to constrain the property of dark energy.

### 2.4.1 CMB shift parameters

The shift of the CMB acoustic peaks can be quantified by the two shift parameters

$$\mathcal{R} = \sqrt{\Omega_{m0}} H_0 \chi_{\text{cd}}(z_*) , \quad \ell_a = \frac{\pi \chi_{\text{cd}}(z_*)}{r_s(z_*)} , \quad (2.40)$$

where  $z_* \simeq 1090$  is the redshift of the CMB decoupling surface, and  $r_s(z_*)$  is the comoving sound horizon at the CMB decoupling defined by

$$r_s(z) = \int_z^\infty c_s H^{-1}(\tilde{z}) d\tilde{z}, \quad (2.41)$$

with  $c_s = [3\{1 + 3\rho_{b0}/(4\rho_{\gamma0})(1+z)^{-1}\}]^{-1/2}$  ( $\rho_{b0}$  and  $\rho_{\gamma0}$  are today's densities of baryons and photons, respectively). The shift parameter  $\mathcal{R}$  is associated with the overall amplitude of CMB acoustic peaks in the temperature power spectrum, whereas the multipole  $\ell_a$  determines the average acoustic structure. In the flat universe, the angular diameter distance is given by

$$d_A = \frac{1}{1+z} \int_0^z \frac{d\tilde{z}}{H(\tilde{z})}. \quad (2.42)$$

By using Eq. (2.40), It can be expressed as

$$d_A(z) = \frac{\mathcal{R}}{(1+z)H_0\sqrt{\Omega_{m0}}}, \quad (2.43)$$

which means that the shift of CMB acoustic peaks is caused by the change of the angular diameter distance from the last scattering surface to today.

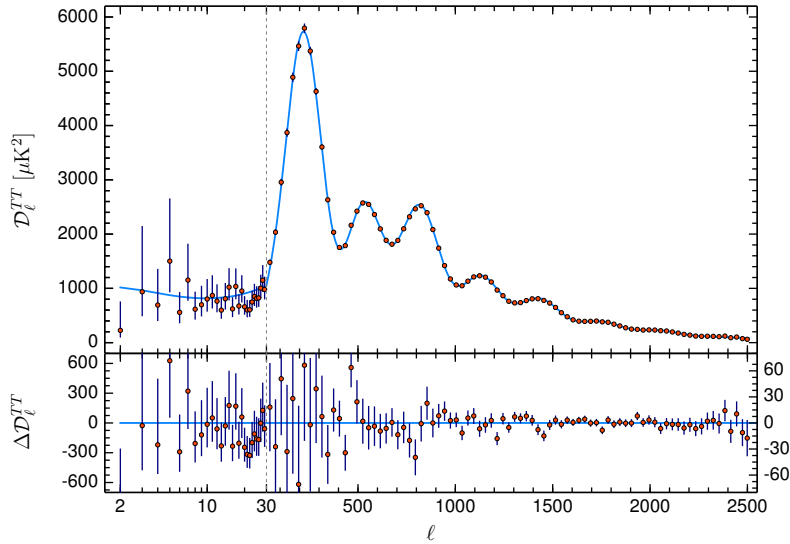


Figure 2.2: The CMB temperature power spectrum versus the multiple moment  $\ell$  from Planck 2018. The best fit theoretical spectrum in the flat  $\Lambda$ CDM is plotted as a light blue solid line in the upper panel. Note that the vertical scale is changed at  $\ell = 30$ , where the horizontal axis switches from logarithmic to linear. This figure is taken from Ref.[1].

Fig.2.2 shows the CMB temperature power spectrum obtained by the recent Planck observation [1]. We can see that the best fit case in the  $\Lambda$ CDM (a light blue solid line in the upper panel) matches the observed values with high accuracy at  $\ell \geq 30$ . The observational data in the range  $2 \leq \ell < 30$  are prone to uncertainties induced by the cosmic variance.

In Ref.[1], the dark energy equation of state is adopted the parametrization in the form

$$w_{\text{DE}}(a) = w_0 + (1 - a)w_a, \quad (2.44)$$

where  $a$  is the scale factor,  $w_0$  and  $w_a$  are assumed to be constants. In  $\Lambda$ CDM, these are chosen to be  $w_0 = -1$  and  $w_a = 0$ . In the case with  $w_a = 0$ , they showed the constraint

$$w_0 = -1.028 \pm 0.032, \quad \text{at 68\% CL.} \quad (2.45)$$

On the other hand, the equation of state with  $w_a \neq 0$  is bounded as

$$w_0 = -0.961 \pm 0.077, \quad w_a = -0.28^{+0.31}_{-0.27}, \quad \text{at 68\% CL.} \quad (2.46)$$

It means that the dark energy equations of motion  $w_{\text{DE}}$  is near  $-1$  at today, but the time evolution of  $w_{\text{DE}}$  is not excluded. Moreover, the results allow the phantom equation of state  $w_{\text{DE}} < -1$ . In Chap.3, we will see that it is possible to realize  $w_{\text{DE}} < -1$  in modified gravity theories.

# Chapter 3

## Overview of dark energy models

In this chapter, we shall review some dark energy models which were discussed in previous works. At first, we introduce a cosmological constant as the origin of dark energy, and we show the problems in  $\Lambda$ CDM model, which is a fiducial cosmological model based on a cosmological constant. Also, we review the current status of dynamical dark energy models such as quintessence. Since the quintessence can not realize the phantom equation of state  $w_{\text{DE}} < -1$  which is the region allowed from the Planck observation, we show the gravitational theories non-minimally coupled to a dynamical scalar field.

### 3.1 Cosmological constant

As the origin of dark energy, the simplest candidate is a cosmological constant  $\Lambda$ . We can take a cosmological constant into GR as the following action,

$$S_\Lambda = \int d^4x \sqrt{-g} \left[ \frac{M_{\text{pl}}^2}{2} (R - 2\Lambda) \right], \quad (3.1)$$

where  $\Lambda$  is a positive constant. Varying the action (3.1) with respect to the metric  $g_{\mu\nu}$ , we obtain the energy-momentum tensor of  $\Lambda$  as

$$T_{\mu\nu}^{(\Lambda)} = -M_{\text{pl}}^2 \Lambda g_{\mu\nu}. \quad (3.2)$$

In this case, the energy density and the pressure of the cosmological constant are given, respectively, by

$$\rho_\Lambda = M_{\text{pl}}^2 \Lambda, \quad P_{\text{DE}} = -M_{\text{pl}}^2 \Lambda, \quad (3.3)$$

on the FLRW background. It means that the cosmological constant has the negative pressure. Hence, we can see that the equation of state for  $\Lambda$  is a constant, as

$$w_{\text{DE}} = P_{\Lambda}/\rho_{\Lambda} = -1, \quad (3.4)$$

which is consistent with the bounds (2.45) and (2.46) given by Planck observation.

### 3.1.1 Cosmological constant problem

When the cosmological constant gives the dominant contribution to the Friedmann equation (2.9), it reduces to

$$3M_{\text{pl}}^2 H^2 = \rho_{\Lambda} = M_{\text{pl}}^2 \Lambda. \quad (3.5)$$

In order to realize the late-time cosmic acceleration, we require that the cosmological constant  $\Lambda$  is of the order of the square of the Hubble constant, as  $\Lambda \approx H_0^2$ . Then, the energy density of  $\Lambda$  can be estimated as [33]

$$\rho_{\Lambda} \approx M_{\text{pl}}^2 H_0^2 \approx 10^{-47} \text{GeV}^4, \quad (3.6)$$

where we have used Eq. (2.31) with  $h \approx 0.7$  and  $M_{\text{pl}} \approx 2.43 \times 10^{18} \text{GeV}$ .

We suppose that the energy density of  $\Lambda$  comes from the vacuum energy of an empty space. Hereafter, the explanation is based on Ref. [34]. We consider the vacuum energy of a free scalar field  $\varphi$  with mass  $m$  on the Minkowski space-time. Since the scalar field obeys the Klein-Gordon equation, there is the dispersion relation  $\omega = \sqrt{k^2 + m^2}$ , where  $\omega$  is the frequency, and  $k$  is the wavenumber. In this case, we can compute the vacuum expectations of the energy density and the pressure for the scalar field, respectively, as

$$\langle \rho_{\text{vac}} \rangle \equiv \langle 0 | \rho_{\varphi} | 0 \rangle = \int \frac{d^3 \mathbf{k}}{(2\pi)^3} \frac{\omega}{2} = \int \frac{d^3 \mathbf{k}}{(2\pi)^3} \frac{\sqrt{k^2 + m^2}}{2}, \quad (3.7)$$

$$\langle P_{\text{vac}} \rangle \equiv \langle 0 | P_{\varphi} | 0 \rangle = \frac{1}{3} \int \frac{d^3 \mathbf{k}}{(2\pi)^3} \frac{k^2}{2\omega} = \frac{1}{3} \int \frac{d^3 \mathbf{k}}{(2\pi)^3} \frac{k^2}{2\sqrt{k^2 + m^2}}. \quad (3.8)$$

However these diverge in the ultraviolet region. The divergences of Eqs. (3.7) and (3.8) should be regulated in such a way that the vacuum state respects the Lorentz symmetry. To do so, we employ the renormalization scheme with the Lorentz invariance formulated in a  $D$ -dimensional Minkowski space-time. To compute the vacuum expectation values of  $\rho_{\text{vac}}$  and  $P_{\text{vac}}$  by using the



renormalization scheme, we extend Eqs. (3.7) and (3.8) as

$$\langle \rho_{\text{vac}} \rangle = \mu^{4-D} \int \frac{d^{D-1} \mathbf{k}}{(2\pi)^{D-1}} \frac{\sqrt{k^2 + m^2}}{2}, \quad (3.9)$$

$$\langle P_{\text{vac}} \rangle = \frac{\mu^{4-D}}{D-1} \int \frac{d^{D-1} \mathbf{k}}{(2\pi)^{D-1}} \frac{k^2}{2\sqrt{k^2 + m^2}}, \quad (3.10)$$

where we have introduced a scale  $\mu$  in order for these to be dimensionally correct. We can compute the integral in a dimension where they converge. Then, as the analytic expression of the vacuum energy, one obtain [7, 8, 9]

$$\langle \rho_{\text{vac}} \rangle = \frac{\mu^4}{2 \cdot (4\pi)^{(D-1)/2}} \frac{\Gamma(-D/2)}{\Gamma(-1/2)} \left( \frac{m}{\mu} \right)^D, \quad (3.11)$$

where  $\Gamma(x)$  is the Gamma function which diverges at  $x = -2$ . Performing the same calculation for Eq. (3.10), it follows that

$$\langle P_{\text{vac}} \rangle = \frac{\mu^4}{4 \cdot (4\pi)^{(D-1)/2}} \frac{\Gamma(-D/2)}{\Gamma(1/2)} \left( \frac{m}{\mu} \right)^D. \quad (3.12)$$

Since the Gamma function has the property  $\Gamma(-1/2) = -2\Gamma(1/2)$ , Eq. (3.11) is expressed as

$$\langle \rho_{\text{vac}} \rangle = -\langle P_{\text{vac}} \rangle, \quad (3.13)$$

then we can obtain the equation of state of the vacuum.

To analyze the property of the divergence at  $D = 4$ , one sets  $D = 4 - \epsilon$  with the small parameter  $\epsilon$ . After that, we expand Eq. (3.11) and take the limit  $\epsilon \rightarrow 0$ . Then, Eq. (3.11) reduces to

$$\langle \rho_{\text{vac}} \rangle = -\langle P_{\text{vac}} \rangle \simeq \frac{m^4}{64\pi^2} \left[ -\frac{2}{\epsilon} + \gamma_E - \frac{3}{2} + \ln \left( \frac{m^2}{4\pi\mu^2} \right) \right], \quad (3.14)$$

where  $\gamma_E \simeq 0.5772$  is the Euler-Mascheroni constant, and we used the fact that

$$\Gamma \left( -2 + \frac{\epsilon}{2} \right) = \frac{1}{\epsilon} + \frac{3}{4} - \frac{\gamma_E}{2} + \mathcal{O}(\epsilon). \quad (3.15)$$

Using the minimal subtraction scheme, the pole  $-1/\epsilon$  is removed, and Eq. (3.14) yields [9]

$$\langle \rho_{\text{vac}} \rangle = -\langle P_{\text{vac}} \rangle \simeq \frac{m^4}{64\pi^2} \left[ \gamma_E - \frac{3}{2} + \ln \left( \frac{m^2}{4\pi\mu^2} \right) \right]. \quad (3.16)$$

Moreover, employing a non-minimal subtraction scheme, which means subtracting the terms  $\gamma_E$ ,  $-3/2$ ,  $-\ln(4\pi)$  as well as the pole  $1/\epsilon$ , the regularized energy density of the vacuum reads [7, 34]

$$\langle \rho_{\text{vac}} \rangle = -\langle P_{\text{vac}} \rangle \simeq \frac{m^4}{64\pi^2} \ln \left( \frac{m^2}{\mu^2} \right), \quad (3.17)$$

which is proportional to  $m^4$ .

For massless particles, the renormalized vacuum energy (3.17) vanishes. This means that the photon does not contribute to the vacuum energy density. However, for massive particles, it depends on the mass scale  $\mu$ . We also notice that the sign of the renormalized vacuum energy can change depending on  $m > \mu$  or  $m < \mu$ . Since the mass scale  $\mu$  is unknown, we cannot predict the concrete values of  $\langle \rho_{\text{vac}} \rangle$  and  $\langle P_{\text{vac}} \rangle$ . But, from Eq. (3.17), we can see that the vacuum energy density computed in quantum field theory receives the contribution of the fourth power of a mass  $m$ . For example, when we consider electrons with mass  $m_e \simeq 0.5\text{MeV}$ , then this contribution can be estimated as  $\langle \rho_{\text{vac}} \rangle \approx m_e^4 \approx 10^{-13}\text{GeV}^4$ . We can see that it is  $10^{34}$  times as large as  $\rho_\Lambda$  given by Eq. (3.6). It means that the electrons give rise to too much amount of vacuum energy. For the heavier particles which exist at least up to the electroweak scale, the vacuum energies associated with the heavier particles are larger than that of electrons. Hence, in order to realize a tiny value of  $\rho_{\text{vac}}$ , we need to cancel the large value associated with the finite contribution of  $m^4$ . This is known as the cosmological constant problem. In other words, the cosmological constant problem is related to the fact that the mass scale associated with dark energy is much smaller than the typical mass scales of elementary particles.

### 3.1.2 Tensions in cosmological parameters

Recently, It is pointed out that there is the tension at about  $4\text{--}6\sigma$  level between today's Hubble constant  $H_0$  constrained from CMB (high-redshift observation) and it observed by direct measurements at low redshifts. Note that, when  $H_0$  is bounded from CMB, the fiducial model is assumed to be  $\Lambda\text{CDM}$ . It means that, as long as the tension does not come from some errors of the observation, the observational data might prefer alternative theoretical candidates for dark energy to the cosmological constant.

Fig.3.1 shows the compilation of Hubble constant predictions and measurements. In fact, the result of Planck observation [1] shows that

$$H_0 = 67.4 \pm 0.50 \text{km s}^{-1} \text{Mpc}^{-1}, \quad (3.18)$$

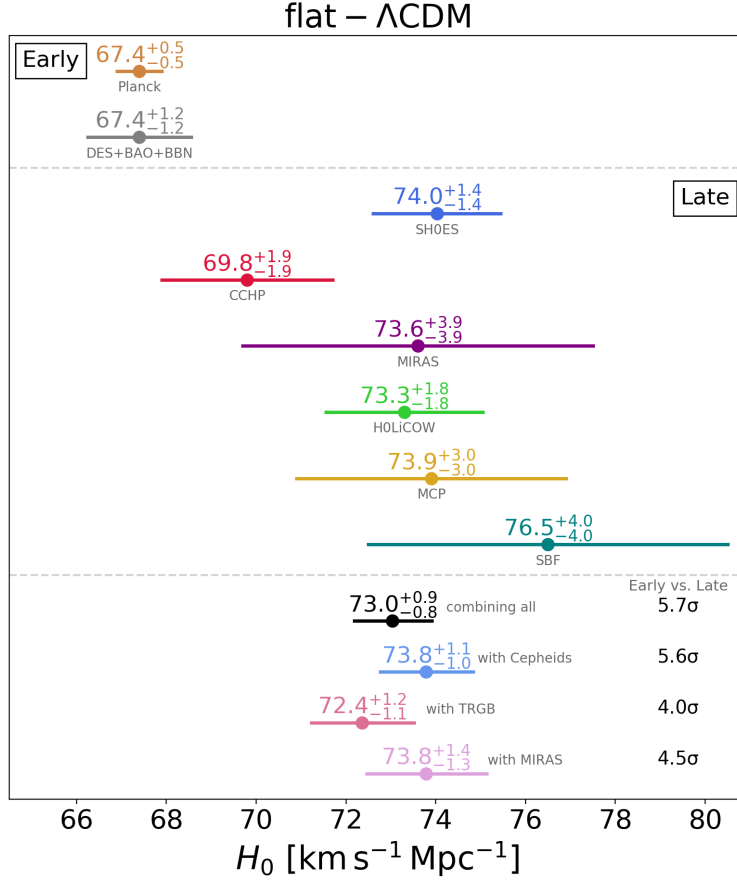


Figure 3.1: Compilation of Hubble Constant predictions and measurements. Two independent predictions based on the data in early universe [1, 10] are shown at the top left, while the middle panel shows the measurements at low redshift. The bottom panel shows combinations of the low redshift measurements and lists the tension with the early universe predictions. This figure is taken from [https://github.com/vbonvin/H0\\_tension](https://github.com/vbonvin/H0_tension)[11].

in  $\Lambda$ CDM. On the other hand, the low-redshift measurement of SN Ia and Cepheids by the SH0ES team [43] shows

$$H_0 = 74.0 \pm 1.4 \text{ km s}^{-1} \text{ Mpc}^{-1}, \quad (3.19)$$

which is quite different from the bound from Planck 2018. Note that the fourth data from the top in Fig.3.1 is presented by the CCHP collaboration [176]. They used Tip of the Red Giant Branch (TRGB) measurements to calibrate some SN Ia in stead of Cepheids to connect the distance ladder. In Fig.3.1, we can see that the combining analysis with the independent approaches to measure  $H_0$  in the late universe yields tension with the values in the early universe between  $4.0\sigma$  and  $5.8\sigma$ . This shows that the discrepancy

does not depend on the use of any method. This problem is called “the Hubble tension”.

As well as the Hubble constant, there are the tension of the today’s amplitude of matter density fluctuations  $\sigma_8$ , which is averaged over by the sphere with radius  $8h^{-1}\text{Mpc}$ . The value of  $\sigma_8$  has estimated from observations of large-scale structure such as the weak lensing of distant galaxies, and the abundance of galaxy clusters is smaller than that inferred from CMB. This tension is at about  $2\sigma$  level between the Planck data in the  $\Lambda\text{CDM}$  and local measurements. For instance, Planck derives [1]

$$S_8 \equiv \sigma_8(\Omega_m/0.3)^{0.5} = 0.832 \pm 0.013, \quad (3.20)$$

where they use the useful parameter  $S_8 \equiv$  for the observational analysis instead of  $\sigma_8$  itself. On the other hand, as two examples of the local measurements, the observation of galaxy clustering and weak lensing by the Dark Energy Survey (DES) collaboration shows [13]

$$S_8 = 0.783^{+0.021}_{-0.025}, \quad (3.21)$$

and a tomographic weak gravitational lensing analysis from the Kilo Degree Survey (KiDS) shows [12]

$$S_8 = 0.745 \pm 0.039. \quad (3.22)$$

Although the  $\sigma_8$  tension is milder than the  $H_0$  tension, these tensions might hint new physics beyond the standard cosmology based on  $\Lambda\text{CDM}$ .

## 3.2 Dynamical dark energy

When the cosmological constant problem is solved in such a way that the vacuum energy vanishes or the value is much smaller than today’s energy density of the universe, then we need to find an alternative mechanism for explaining the origin of dark energy. Note that, even if the cosmological constant problem is solved in those ways, the observational tensions of cosmological parameters remain. As one of the possibilities for explaining the origin of dark energy, there are the models with dynamical dark energy in which the equation of state  $w_{\text{DE}}$  varies in time.

## Quintessence and k-essence

For example, quintessence is a dark energy model described by a scalar field  $\varphi$  with a potential  $V(\varphi)$ . The action is given by

$$S_{\text{quint}} = \int d^4x \sqrt{-g} \left[ \frac{M_{\text{pl}}^2}{2} R - \frac{1}{2} \partial_\mu \varphi \partial^\mu \varphi - V(\varphi) \right], \quad (3.23)$$

where  $R$  is the scalar curvature, and the symbol  $\nabla_\mu$  is the covariant derivative operator. The first term in Eq. (3.23) corresponds to Einstein-Hilbert term, and the second term is the kinetic term of scalar field  $\varphi$ . In this case, the energy density and the pressure of a quintessence field are given, respectively, by

$$\rho_\varphi = \frac{\dot{\varphi}^2}{2} + V(\varphi), \quad P_\varphi = \frac{\dot{\varphi}^2}{2} - V(\varphi). \quad (3.24)$$

Then, the equation of state in quintessence is expressed as

$$w_{\text{DE,quint}} = \frac{\dot{\varphi}^2/2 - V(\varphi)}{\dot{\varphi}^2/2 + V(\varphi)} = -1 + \frac{\dot{\varphi}^2}{\dot{\varphi}^2/2 + V(\varphi)}, \quad (3.25)$$

which varies in time, and the value is always larger than  $-1$ , i.e.,  $w_{\text{DE}} > -1$ .

The quintessence potentials can be classified into three subclasses called (i) thawing models, (ii) tracking freezing models, and (iii) scaling freezing models. The observational constraints on these quintessence models have been discussed in Refs.[183, 214] for instance. In thawing models, the scalar field almost never evolves in early time, but it starts to evolve at late time. For the thawing models, if we put the prior  $w_0 \geq -1$ , where  $w_0$  is today's value of  $w_{\text{DE}}$ , the likelihood analysis in Ref.[214] showed that the upper bound  $w_0 < -0.496$  (95% CL). The thawing quintessence with  $-1 < w_0 < -0.5$  are still allowed observationally, however, there is no statistical evidence that the models with  $w_0 > -1$  are favored over the  $\Lambda$ CDM. In both tracking and scaling freezing models, the evolution of quintessence potential is fast in the early cosmological epoch, and it slows down at late time. These freezing models can be classified by the evolution of  $w_{\text{DE}}$  at early times. In the tracking freezing models, a wide range of initial conditions converges to a common cosmic evolution, that is the tracker solution. If we put the prior  $w_0 \geq -1$ , the joint analysis in Ref.[214] showed that the bound  $-1 < w_0 < -0.923$  (95% CL), which means the model coincides with the  $\Lambda$ CDM around today. In the scaling freezing models, the dark energy equation of state scales as the background fluid like matter. The result in Ref.[214] showed that the observational data favor the case in which a transition from

a scaling matter epoch to dark energy dominated epoch occurs at a very early time, and the dark energy equation of state is close to  $-1$  after the transition. Therefore, unfortunately, the current observational data are not precise enough to distinguish statistically these freezing models from the  $\Lambda$ CDM.

The quintessence can be extended to the model dubbed k-essence, in which the Lagrangian is a arbitrary function of the scalar field  $\varphi$  and its kinetic term, i.e.,

$$S_K = \int d^4x \sqrt{-g} \left[ \frac{M_{\text{pl}}^2}{2} R + K(\varphi, X_\varphi) \right], \quad (3.26)$$

where  $X_\varphi = -\nabla_\mu \varphi \nabla^\mu \varphi / 2$  is the kinetic term of  $\varphi$ , and  $K$  is a arbitrary function of  $\varphi$  and  $X_\varphi$ . In k-essence, the equation of state is also in the range  $w_{\text{DE}} > -1$  as long as the energy density of scalar field is positive and the theoretical instabilities are absent. In other words, even if we extend to the k-essence as the dynamical dark energy, the dark energy equation of state cannot be smaller than  $-1$ .

### 3.3 Dark energy non-minimally coupled to gravity

The bound from the observations allows the range  $w_{\text{DE}} < -1$ . However, the dark energy models described by simple modification of matter (like quintessence) can not realize that situation without the theoretical instabilities. If the field associated with the dark energy is non-minimally coupled to gravity, then it is possible to realize the dark energy equation of state smaller than  $-1$  without having instabilities.

#### Brans-Dicke theory

One of the examples with a non-minimally coupling between a scalar field and gravity is Brans-Dicke (BD) theory given by the following action [23]

$$S_{\text{BD}} = \int d^4x \sqrt{-g} \left[ \frac{M_{\text{pl}}^2}{2} \varphi R - \frac{M_{\text{pl}}^2 \omega_{\text{BD}}}{2\varphi} X_\varphi - V(\varphi) \right], \quad (3.27)$$

where  $\omega_{\text{BD}}$  is called the BD parameter. In the limit  $\omega_{\text{BD}} \rightarrow \infty$ , the BD theory reduces to general relativity. The present tightest solar system constraint on the post-Newtonian parameter comes from the time-delay effect of the Cassini tracking for the Sun. When the potential  $V(\varphi)$  does not exist, from local

gravitational experiments in the solar system, the BD parameter is bounded in the range

$$\omega_{\text{BD}} > 40000, \quad (3.28)$$

for a massless scalar field. It means that the difference between the BD theory and general relativity needs to be very small, then it is difficult to distinguish the model based on the BD theory from the  $\Lambda$ CDM. Note that this bound can not be applied to a massive scalar field with a potential  $V(\varphi)$ .

### Galileon theory

The Galileon is a scalar field with the symmetry (called ‘‘Galilean shift symmetry’’) under the transformation  $\varphi \rightarrow \varphi + b_\mu x^\mu + c$ , where  $b_\mu$  and  $c$  are constant vector and scalar, respectively. Also, in order to avoid ghost instabilities (dubbed Ostrogradski ghost [24, 25]), we demand that the Galileon’s equation of motion is of second order. Then, in Minkowski space-time, the general Lagrangian density of the Galileon is given by

$$\begin{aligned} \mathcal{L} = & c_1 \varphi + c_2 X_\varphi - c_3 X_\varphi \square \varphi + c_4 X_\varphi [(\square \varphi)^2 - \partial_\mu \partial_\nu \varphi \partial^\mu \partial^\nu \varphi] \\ & - \frac{c_5}{3} X_\varphi [(\square \varphi)^3 - 3 \square \varphi \partial_\mu \partial_\nu \varphi \partial^\mu \partial^\nu \varphi + 2 \partial_\mu \partial_\nu \varphi \partial^\nu \partial^\lambda \varphi \partial_\lambda \partial^\mu \varphi], \end{aligned} \quad (3.29)$$

where  $\square \varphi = \partial_\mu \partial^\mu \varphi$ , and  $c_i$  are constants. Although the Lagrangian density (3.29) contains the second derivatives of the field, the field equation of motion is still of second order.

In order to the cosmological application of the Galileon, the Galileon in Minkowski space-time should be extended to that in the curved space-time. To do so, one can promote the partial derivatives  $\partial_\mu$  to covariant derivatives  $\nabla_\mu$  in Eq. (3.29). However, such way of covariantization leads to higher derivatives in the field equation of motion. For example, after just replacing  $\partial_\mu$  with  $\nabla_\mu$  and deriving the field equation from Eq. (3.29), the fourth term in Eq. (3.29) leads to the terms with the higher derivative of  $\phi$  such as

$$\nabla^\mu [\nabla_\mu \nabla_\nu \nabla^\nu \phi - \nabla_\nu \nabla_\mu \nabla^\nu \phi] = -\nabla^\mu (R_{\mu\nu} \nabla^\nu \phi), \quad (3.30)$$

in the equation of motion for the scalar field. Such higher derivative terms can be eliminated by adding ‘‘counter terms’’ to Eq. (3.29). After that, in curved space-time, the covariant Galileon model is given by the following action

$$S_{\text{Gal}} = \int d^4x \sqrt{-g} \left[ \frac{M_{\text{pl}}^2}{2} R + \frac{1}{2} \sum_{i=1}^5 c_i \mathcal{L}_i^{(\text{Gal})} \right], \quad (3.31)$$

where

$$\mathcal{L}_1^{(\text{Gal})} = \varphi, \quad (3.32)$$

$$\mathcal{L}_2^{(\text{Gal})} = (\nabla\varphi)^2, \quad (3.33)$$

$$\mathcal{L}_3^{(\text{Gal})} = \square\varphi (\nabla\varphi)^2, \quad (3.34)$$

$$\mathcal{L}_4^{(\text{Gal})} = (\nabla\varphi)^2 \left[ 2(\square\varphi)^2 - 2\nabla_\mu\nabla_\nu\varphi\nabla^\mu\nabla^\nu\varphi - \frac{R}{2}(\nabla\varphi)^2 \right], \quad (3.35)$$

$$\begin{aligned} \mathcal{L}_5^{(\text{Gal})} = (\nabla\varphi)^2 [ & (\square\varphi)^3 - 3(\square\varphi)\nabla_\mu\nabla_\nu\varphi\nabla^\mu\nabla^\nu\varphi + 2\nabla^\nu\nabla_\mu\varphi\nabla^\rho\nabla_\nu\varphi\nabla^\mu\nabla_\rho\varphi \\ & - 6G_{\nu\rho}\nabla_\mu\varphi\nabla^\nu\nabla^\mu\varphi\nabla^\rho\varphi ], \end{aligned} \quad (3.36)$$

with the five constants  $c_i$ ,  $(\nabla\varphi)^2 = \nabla_\mu\varphi\nabla^\mu\varphi$  and  $\square\varphi = \nabla_\mu\nabla^\mu\varphi$ . The action (3.31) leads to second-order equations of motion for both the scalar field and the metric. The last terms in  $\mathcal{L}_4^{(\text{Gal})}$  and  $\mathcal{L}_5^{(\text{Gal})}$  correspond to the counter terms, and there counter terms are unique. Note that, in curved space-time, the Galilean symmetry is broken in the covariant Galileon theory due to the existence of the terms related to the first derivatives of  $\phi$  in the field equations.

Ref.[35] has shown that, for the covariant Galileon theory with a late-time de Sitter attractor, there is a tracker solution that attracts cosmological solutions with different initial conditions to a common trajectory. The dark energy equation of state along the tracker solution exhibits the phantom like evolution given by  $w_{\text{DE}} = -7/3$  (radiation era)  $\rightarrow -2$  (matter era)  $\rightarrow -1$  (de Sitter era). Note that, even though  $w_{\text{DE}}$  of the tracker solution is negative in whole cosmological epoch, the ghost instabilities do not appear.

In Ref.[37], the likelihood analysis for the dark energy model based on the covariant Galileon is carried out. It showed that the solutions approaching the tracker solution at late times can be consistent with the combined data analysis of SN Ia, CMB, and BAO, while the solution with the early tracking is disfavored from the data due to the large deviation of  $w_{\text{DE}}$  from  $-1$ . Hence, the late-time tracking solution of covariant Galileon is allowed from the observational data. Moreover, in Ref.[38], the authors carried out the likelihood analysis with the data of CMB, BAO, SNIa, local measurements of  $H_0$ , and weak gravitational lensing. The result shows that the tracker solution in covariant Galileon are statistically ruled out by cosmological data.

## Horndeski theory

Several dark energy models based on the extension of gravity theory with a scalar field belong to Horndeski theory which is the most general scalar-tensor



theory with the second-order equations of motion. The action of Horndeski theory is given by

$$S_H = \int d^4x \sqrt{-g} \sum_{i=2}^5 \mathcal{L}_i^{(H)}, \quad (3.37)$$

with

$$\mathcal{L}_2^{(H)} = G_2^{(H)}(\varphi, X_\varphi), \quad (3.38)$$

$$\mathcal{L}_3^{(H)} = G_3^{(H)}(\varphi, X_\varphi) \square \varphi, \quad (3.39)$$

$$\mathcal{L}_4^{(H)} = G_4^{(H)}(\varphi, X_\varphi) R + G_{4,X_\varphi}^{(H)} [(\square \varphi)^2 - \nabla_\mu \nabla_\nu \varphi \nabla^\nu \nabla^\mu \varphi], \quad (3.40)$$

$$\begin{aligned} \mathcal{L}_5^{(H)} = & G_5^{(H)}(\varphi, X_\varphi) G_{\mu\nu} \nabla^\mu \nabla^\nu \varphi - \frac{1}{6} G_{5,X_\varphi}^{(H)} [(\square \varphi)^3 - 3 \square \varphi \nabla_\nu \nabla_\rho \varphi \nabla^\rho \nabla^\nu \varphi \\ & + 2 \nabla_\mu \nabla_\nu \varphi \nabla^\rho \nabla^\mu \varphi \nabla^\nu \nabla_\rho \varphi], \end{aligned} \quad (3.41)$$

where the arbitrary functions  $G_i^{(H)}$  depend on both  $\varphi$  and  $X_\varphi$ , and  $G_{i,X_\varphi}^{(H)} \equiv \partial G_i / \partial X_\varphi$ . When we impose the shift symmetry  $\varphi \rightarrow \tilde{\varphi} = \varphi + \text{constant}$ , these arbitrary functions depend on  $X_\varphi$  alone.

The Horndeski action (3.37) contains many dark energy models which were discussed in the previous works. For example, the k-essence (3.26) corresponds to the case with the arbitrary functions chosen to be

$$G_2^{(H)} = K(\varphi, X_\varphi), \quad G_4^{(H)} = \frac{M_{\text{pl}}^2}{2}, \quad G_3^{(H)} = G_5^{(H)} = 0. \quad (3.42)$$

The Brans-Dicke theory given by (3.27) corresponds to the case with

$$G_2^{(H)} = -\frac{M_{\text{pl}}^2 \omega_{\text{BD}}}{2\varphi} X_\varphi - V(\varphi), \quad G_4^{(H)} = \frac{M_{\text{pl}}^2}{2} \varphi, \quad G_3^{(H)} = G_5^{(H)} = 0, \quad (3.43)$$

and the covariant Galileon theory given by (3.31) is included as

$$\begin{aligned} G_2^{(H)} &= \frac{c_1}{2} \varphi - c_2 X_\varphi, \quad G_3^{(H)} = -c_3 X_\varphi, \\ G_4^{(H)} &= -c_4 X_\varphi^2, \quad G_5^{(H)} = 3c_5 X_\varphi^2. \end{aligned} \quad (3.44)$$

### 3.4 Dark energy coupled to dark matter

From the observations, the energy density of dark energy is the same order as that of dark matter in the present universe. It means that there may be some relation between the dark components. If the baryon is also coupled

to dark energy, this gives rise to a fifth force. However, such a fifth force has not been experimentally observed inside the solar system, so it should be suppressed inside the solar system where local gravity experiments are carried out. Hence, there is a possibility that the baryon has an interaction with dark energy on cosmological scales, but in such cases we need some screening mechanism to suppress the propagation of the fifth force in local regions of the universe.

Several different forms of the interaction between dark components have been proposed in previous works. For a canonical scalar field  $\varphi$ , Wetterich [145] first proposed a coupled quintessence scenario in which  $\varphi$  interacts with CDM. In this model, the continuity equation of dark energy is sourced by the term  $Q\rho_c\dot{\varphi}$ , where  $Q$  is a coupling constant,  $\rho_c$  is the CDM energy density, and  $\dot{\varphi}$  is the time derivative of  $\varphi$ . Such interaction can be realized in the form

$$\nabla^\mu T_{\mu\nu}^{(\varphi)} = -QT_c\nabla_\nu\varphi, \quad \nabla^\mu T_{\mu\nu}^{(c)} = +QT_c\nabla_\nu\varphi, \quad (3.45)$$

Then, the continuity equations of a scalar field and CDM are given, respectively, by

$$\dot{\rho}_\varphi + 3H(\rho_\varphi + P_\varphi) = -Q\rho_c\dot{\varphi} \quad (3.46)$$

$$\dot{\rho}_c + 3H\rho_c = Q\rho_c\dot{\varphi}, \quad (3.47)$$

We can see that such an interaction gives rise to the energy exchange between CDM and the scalar field. In this case, the quintessence field  $\varphi$  drives the cosmic acceleration in the presence of a shallow potential  $V(\varphi)$ , e.g., the exponential potential  $V(\varphi) = V_0 e^{-\lambda\varphi/M_{\text{Pl}}}$  with  $|\lambda| < \mathcal{O}(1)$  (where  $M_{\text{Pl}}$  is the reduced Planck mass) [14, 15, 16, 17, 18]. Amendola [147] showed that there exists a scaling  $\varphi$ -matter-dominated epoch ( $\varphi$ MDE) during which the coupling gives rise to a constant dark energy density parameter  $\Omega_\varphi = 2Q^2/3$ .

As another possibility of the coupling between dark components, the scalar field  $\phi$  interacts with cold dark matter through a momentum transfer. This interaction is based on the field derivative coupled with the CDM four velocity  $u_c^\mu$  such as

$$Z_\varphi = u_c^\mu \nabla_\mu \varphi. \quad (3.48)$$

Such interaction does not affect to the continuity equations unlike the energy transfer, while the dynamics of cosmological perturbations is different from that in the uncoupled case. In Ref. [201], it was shown that the quadratic interacting Lagrangian of the form  $\mathcal{L}_{\text{int}} = \sqrt{-g}Z^2$  can lead to an interesting possibility for alleviating the problem of  $\sigma_8$  tension by suppressing the growth of large-scale structures. This property comes from a pure momentum transfer between dark components.

### 3.5 Vector dark energy

So far, we have reviewed scalar-tensor theories with one scalar degree of freedom. We can consider the models in which the cosmic acceleration is driven by an Abelian vector field  $A_\mu$ . Unfortunately, there are the no-go theorem in which one can not construct Galileon like interactions for single spin-1 field with Lorentz and gauge invariance in any dimensions [29]. However, this no-go theorem does not apply to massive spin 1 fields since one of the assumptions of the theorem, the gauge invariance, is dropped. It means that it is possible to successfully construct derivative self-interactions for the vector field with a broken  $U(1)$  symmetry. A systematical construction of these interactions with only 3 propagating degrees of freedom was performed in Ref. [30] with the requirement that the longitudinal mode of the vector field  $A_\mu$  possesses non-trivial interactions which belong to the class of Galileon/Horndeski theories in the limit  $A_\mu \rightarrow \nabla_\mu \varphi$ .

In Chap.4, we will show the construction of generalized Proca theories and the cosmological dynamics briefly.

### 3.6 After the event GW170817

In 2017, the gravitational waves (GW) from binary neutron star merger was observed by LIGO, Virgo[92]. From the observational data of this event, the propagating speed of the gravitational waves is bounded as

$$-3 \times 10^{-15} \leq \frac{c_T}{c} - 1 \leq 7 \times 10^{-16}, \quad (3.49)$$

for the redshift  $z \leq 0.009$ , where  $c$  is the speeds of light. It means that the propagating speed of gravitational waves is almost the same as speed of light. In general, the modification of general relativity gives rise to the difference between the speeds of gravitational waves and light. Hence, the bound (3.49) can constrain the cosmological models based on the extension of gravity theory.

In Horndeski theories, the propagating speed of gravitational waves on FLRW background is expressed as

$$c_T^2 = 1 + \frac{2\varphi^2 G_{4,X_\varphi}^{(H)} + \varphi^2(\varphi H - \dot{\varphi}) G_{5,X_\varphi}^{(H)}}{2G_4^{(H)} - 2\varphi^2 G_{4,X_\varphi}^{(H)} - H\varphi^3 G_{5,X_\varphi}^{(H)}}. \quad (3.50)$$

If the functions  $G_4$  and  $G_5$  are not related to each other, the condition for satisfying  $c_T^2 \equiv 1$  is given by

$$G_{4,X_\varphi}^{(H)} = 0, \quad G_{5,X_\varphi}^{(H)} = 0. \quad (3.51)$$

Then, the action (3.37) reduces to

$$S_H = \int d^4x \sqrt{-g} \left[ G_2^{(H)}(\varphi, X_\varphi) + G_3^{(H)}(\varphi, X_\varphi) \square \varphi + G_4^{(H)}(\varphi) R \right], \quad (3.52)$$

with  $c_T^2 = 1$ . As long as we consider this action, the bound (3.49) is automatically satisfied. For example, the action (3.52) includes the subclasses such as quintessence (3.23), k-essence (3.26), Brans-Dicke theory (3.27), and cubic-order Galileon (in which  $\mathcal{L}_4^{(\text{Gal})}$  and  $\mathcal{L}_5^{(\text{Gal})}$  in the action (3.31) are ignored). Moreover, the interaction between two dark components given by Eq. (3.45) and (3.48) do not change the propagating speeds of gravitational waves (see also Ref. [202]). Hence, these models still survive from the viewpoint of the bound (3.49).

In generalized Proca theories, we can obtain the similar conditions to Eq. (3.51). For this point, we will see in Sec.4.3.2.

# Chapter 4

## Massive vector-tensor theories

In this chapter, we shall introduce the generalization of Proca theories. We present the background equations of motion in the presence of a temporal component of the vector field and a matter fluid on the FLRW background. We also derive conditions for avoiding ghost and gradient instabilities of cosmological perturbations. For this purpose, we define cosmological perturbations which are included in metric, a Proca field, and matter sector in this chapter. After that, we discuss concrete dark energy models based on the generalized Proca theories.

### 4.1 Generalized Proca theories

In Ref.[30], the generalization of the Proca action was constructed by L. Heisenberg. We shall review the construction of generalized Proca theories in both Minkowski and curved space-time.

#### 4.1.1 Action in Minkowski space-time

Original Proca theory with a massive vector field  $A_\mu$  is given by the following action in Minkowski space-time,

$$S_{\text{Proca}} = \int d^4x \left[ -\frac{1}{4} F_{\mu\nu} F^{\mu\nu} + m^2 X \right], \quad (4.1)$$

where  $m$  is the mass of vector field, the field strength is defined by  $F_{\mu\nu} = \partial_\mu A_\nu - \partial_\nu A_\mu$ , and

$$X = -\frac{1}{2} A_\mu A^\mu. \quad (4.2)$$

Due to the existence of the mass term, the  $U(1)$  gauge symmetry is broken in this theory. Then, as the propagating degrees of freedom, the longitudinal mode arises besides two transverse polarizations.

In the following, we review the generalization of the Proca theories. In general, the vector field can be decomposed into the derivative of a scalar field  $\pi$  and a divergence-free vector  $b_\mu$ , as  $A_\mu = \partial_\mu \pi + b_\mu$  with  $\partial_\mu b^\mu = 0$ . We would like to construct the general action which gives rise to the equations of motion including up to second-order derivative terms for both  $\pi$  and  $A_\mu$ . It means that the action should be constructed of at most second-order derivative terms in  $\pi$  and first-order derivative terms in  $A_\mu$ . This situation can be realized by the Lagrangian densities in the form

$$\mathcal{L}_{n+2} = -\frac{g_{n+2}(X)}{(4-n)!} \varepsilon^{\mu_1 \dots \mu_n \lambda_1 \dots \lambda_{4-n}} \varepsilon_{\nu_1 \dots \nu_n \lambda_1 \dots \lambda_{4-n}} \partial_{\mu_1} A_{\nu_1} \partial_{\mu_2} A_{\nu_2} \dots \partial_{\mu_n} A_{\nu_n}, \quad (4.3)$$

for  $n = 0, 1, 2, 3, 4$ , where  $g_{n+2}(X)$  is the function of  $X$ , the symbol  $\partial_\mu$  is the partial derivative operator, and  $\varepsilon^{\mu\nu\alpha\beta}$  is the anti-symmetric Levi-Civita tensor which satisfies the normalization  $\varepsilon^{\mu\nu\alpha\beta} \varepsilon_{\mu\nu\alpha\beta} = -4!$ .

Let us discuss the Lagrangian densities corresponding to  $n = 0, 1, 2, 3, 4$ , in detail. For  $n = 0$ , the Lagrangian density (4.3) reduces to

$$\mathcal{L}_2 = -\frac{g_2(X)}{24} \varepsilon^{\lambda_1 \lambda_2 \lambda_3 \lambda_4} \varepsilon_{\lambda_1 \lambda_2 \lambda_3 \lambda_4} = g_2(X). \quad (4.4)$$

We note that  $\mathcal{L}_2$  does not have the derivative terms acting on the vector field. Therefore, the function  $g_2$  can also depend on all the possible terms with  $U(1)$  symmetry such as  $F_{\mu\nu} F^{\mu\nu}$  and  $F_{\mu\nu} \tilde{F}^{\mu\nu}$ , where  $\tilde{F}$  is the dual strength tensor defined by

$$\tilde{F}^{\mu\nu} = \frac{1}{2} \varepsilon^{\mu\nu\alpha\beta} F_{\alpha\beta}, \quad (4.5)$$

with the anti-symmetric Levi-Civita tensor  $\varepsilon^{\mu\nu\alpha\beta}$ . Moreover, even if we consider the terms which do not contain any time derivative of the temporal component, the propagating degrees of freedom do not increase. It means that the function  $g_2$  can also have the dependence on the terms like  $A^\mu A^\nu F_\mu{}^\alpha F_{\nu\alpha}$ . Then, the Lagrangian density  $\mathcal{L}_2$  can be extended to

$$\mathcal{L}_2 = g_2(A_\mu, F_{\mu\nu}, \tilde{F}_{\mu\nu}). \quad (4.6)$$

which contains all the contractions between  $A_\mu$ ,  $F_{\mu\nu}$ , and  $\tilde{F}_{\mu\nu}$ . For examples,  $g_2$  contains the gauge-invariant terms  $(F_{\mu\nu} F^{\mu\nu})^n$ , the parity-violating terms

$(F_{\mu\nu}\tilde{F}_{\mu\nu})^n$ , and the terms  $A^\mu A^\nu F_\mu{}^\alpha F_{\nu\alpha}$ . Actually, the independent terms can be constructed by the scalar quantities

$$F = -\frac{1}{4}F_{\mu\nu}F^{\mu\nu}, \quad (4.7)$$

$$\tilde{F} = F_{\mu\nu}\tilde{F}^{\mu\nu}, \quad (4.8)$$

$$Y = A^\mu A^\nu F_\mu{}^\alpha F_{\nu\alpha}, \quad (4.9)$$

and  $X = -A_\mu A^\mu/2$ . In the following, we do not consider the parity violation, so the dependence of  $\tilde{F}$  in  $g_2$  is ignored. Hence, the Lagrangian density  $\mathcal{L}_2$  can be expressed as

$$\mathcal{L}_2 = g_2(X, F, Y). \quad (4.10)$$

For  $n = 1$ , Eq. (4.3) reduces to

$$\begin{aligned} \mathcal{L}_3 &= -\frac{g_3(X)}{6}\epsilon^{\mu_1\lambda_1\lambda_2\lambda_3}\epsilon^{\nu_1}_{\lambda_1\lambda_2\lambda_3}\partial_{\mu_1}A_{\nu_1} \\ &= g_3(X)\partial_\mu A^\mu, \end{aligned} \quad (4.11)$$

which contains the derivative term  $\partial_\mu A^\mu$ . So, the function  $g_3$  can not have the dependence of  $F_{\mu\nu}$  unlike the function  $g_2$  in  $\mathcal{L}_2$ .

The Lagrangian densities (4.3) for  $n = 2, 3$  are given, respectively, by

$$\begin{aligned} \mathcal{L}_4 &= -\frac{g_4(X)}{2}\epsilon^{\mu_1\mu_2\lambda_1\lambda_2}\epsilon^{\nu_1\nu_2}_{\lambda_1\lambda_2}\partial_{\mu_1}A_{\nu_1}\partial_{\mu_2}A_{\nu_2} \\ &= g_4(X) [(\partial_\mu A^\mu)^2 - \partial_\mu A_\nu \partial^\nu A^\mu], \end{aligned} \quad (4.12)$$

$$\begin{aligned} \mathcal{L}_5 &= -g_5(X)\epsilon^{\mu_1\mu_2\mu_3\lambda_1}\epsilon^{\nu_1\nu_2\nu_3}_{\lambda_1}\partial_{\mu_1}A_{\nu_1}\partial_{\mu_2}A_{\nu_2}\partial_{\mu_3}A_{\nu_3} \\ &= g_5(X) [(\partial_\mu A^\mu)^3 - 3\partial_\mu A^\mu \partial_\nu A_\rho \partial^\rho A^\nu + 2\partial_\mu A_\nu \partial^\rho A^\mu \partial^\nu A_\rho]. \end{aligned} \quad (4.13)$$

Moreover, unlike the case in Horndeski theories, there are the terms derived by exchanging some of the indices in Eqs. (4.12) and (4.13) such as

$$\begin{aligned} \mathcal{L}_4^V &= -\frac{\tilde{f}_4(X)}{2}\epsilon^{\mu_1\mu_2\lambda_1\lambda_2}\epsilon^{\nu_1\nu_2}_{\lambda_1\lambda_2}\partial_{\mu_1}A_{\mu_2}\partial_{\nu_1}A_{\nu_2} \\ &= \tilde{f}_4(X) [\partial_\mu A_\nu \partial^\mu A^\nu - \partial_\mu A_\nu \partial^\nu A^\mu] \\ &= -2\tilde{f}_4(X)F, \end{aligned} \quad (4.14)$$

and

$$\begin{aligned} \mathcal{L}_5^V &= -\tilde{f}_5(X)\epsilon^{\mu_1\mu_2\mu_3\lambda_1}\epsilon^{\nu_1\nu_2\nu_3}_{\lambda_1}\partial_{\mu_1}A_{\mu_2}\partial_{\mu_3}A_{\nu_1}\partial_{\nu_2}A_{\nu_3} \\ &= \tilde{f}_5(X) [\partial_\mu A^\nu (\partial_\nu A_\rho \partial^\rho A^\mu - \partial_\rho A^\mu \partial^\rho A_\nu) + \partial_\mu A^\mu (\partial_\rho A_\nu - \partial_\nu A_\rho) \partial^\rho A^\nu] \\ &= \tilde{f}_5(X)\tilde{F}^{\alpha\mu}\tilde{F}^\beta{}_\mu\partial_\alpha A_\beta, \end{aligned} \quad (4.15)$$

where  $\tilde{f}_4(X)$  and  $\tilde{f}_5(X)$  are functions of  $X$ . Both  $\mathcal{L}_4$  and  $\mathcal{L}_5$  vanish in the scalar limit  $A_\mu \rightarrow \partial_\mu \varphi$ , so these Lagrangian densities correspond to intrinsic vector modes. Since  $\mathcal{L}_4^V = -2\tilde{f}_4(X)F$ , it can be absorbed into the Lagrangian density  $\mathcal{L}_2$  defined by Eq. (4.10). On the other hand, the interaction  $\mathcal{L}_5$  can not be absorbed into the other Lagrangian densities.

For  $n = 4$ , Eq. (4.3) gives rise to the sixth-order Lagrangian density

$$\mathcal{L}_6 = -g_6(X)\varepsilon^{\mu_1\mu_2\mu_3\mu_4}\varepsilon_{\mu_1\mu_2\mu_3\mu_4}\partial_{\mu_1}A_{\nu_1}\partial_{\mu_2}A_{\nu_2}\partial_{\mu_3}A_{\nu_3}\partial_{\mu_4}A_{\nu_4}. \quad (4.16)$$

Note that this vanishes by taking the scalar limit  $A_\mu \rightarrow \partial_\mu \varphi$ . Actually,  $\mathcal{L}_6$  corresponds to the total derivative, so it does not affect to the equations of motion. Hence, we have ignored  $\mathcal{L}_6$ .

As with  $\mathcal{L}_4^V$  and  $\mathcal{L}_5^V$ , we can also consider another Lagrangian density in the form

$$\mathcal{L}_6^V = -\tilde{f}_6(X)\varepsilon^{\mu_1\mu_2\mu_3\mu_4}\varepsilon_{\mu_1\mu_2\mu_3\mu_4}\partial_{\mu_1}A_{\mu_2}\partial_{\nu_1}A_{\nu_2}\partial_{\mu_3}A_{\nu_3}\partial_{\mu_4}A_{\nu_4}, \quad (4.17)$$

where  $\tilde{f}_6(X)$  is a function of  $X$ . This Lagrangian density also vanishes in the scalar limit  $A_\mu \rightarrow \partial_\mu \varphi$ . This contains the terms which depend on  $F_{\mu\nu}$  and  $\tilde{F}_{\mu\nu}$ , and these terms can be absorbed into  $\mathcal{L}_2$ . Ignoring such terms in  $\mathcal{L}_6$ , the non-trivial terms in  $\mathcal{L}_6$  can be expressed as

$$\tilde{\mathcal{L}}_6 = \tilde{g}_6(X)\tilde{F}^{\alpha\beta}\tilde{F}^{\mu\nu}\partial_\alpha A_\mu\partial_\beta A_\nu, \quad (4.18)$$

where  $\tilde{g}_6(X)$  is a function of  $X$ . The Lagrangian density  $\tilde{\mathcal{L}}_6$  corresponds to the intrinsic vector contribution.

Finally, in Minkowski space-time, the action of generalized Proca theories is given by

$$S_{\text{MinGP}} = \int d^4x \left[ \sum_{i=2}^5 \mathcal{L}_i + \tilde{\mathcal{L}}_6 \right], \quad (4.19)$$

where

$$\mathcal{L}_2 = g_2(X, F, Y), \quad (4.20)$$

$$\mathcal{L}_3 = g_3(X)\partial_\mu A^\mu, \quad (4.21)$$

$$\mathcal{L}_4 = g_4(X) [(\partial_\mu A^\mu)^2 - \partial_\mu A_\nu \partial^\nu A^\mu], \quad (4.22)$$

$$\begin{aligned} \mathcal{L}_5 = g_5(X) [(\partial_\mu A^\mu)^3 - 3\partial_\mu A^\mu \partial_\nu A_\rho \partial^\rho A^\nu + 2\partial_\mu A_\nu \partial^\rho A^\mu \partial^\nu A_\rho] \\ + \tilde{f}_5(X)\tilde{F}^{\alpha\mu}\tilde{F}^\beta{}_\mu\partial_\alpha A_\beta, \end{aligned} \quad (4.23)$$

$$\tilde{\mathcal{L}}_6 = \tilde{g}_6(X)\tilde{F}^{\alpha\beta}\tilde{F}^{\mu\nu}\partial_\alpha A_\mu\partial_\beta A_\nu. \quad (4.24)$$

Note that we take the Lagrangian density  $\mathcal{L}_5^V$  into  $\mathcal{L}_5$ . The equations of motion following from this action are at most of second order. Also, the number of propagating degrees of freedom is the same as that in the original Proca theory.



### 4.1.2 Action in curved space-time

To apply the generalized Proca theories to cosmology, we should extend the action (4.19) to that in curved space-time. If we just replace the partial derivatives in the action (4.19) with the covariant derivatives in curved space-time, the equations of motion following from  $\mathcal{L}_2$  and  $\mathcal{L}_3$  are still of second order, while  $\mathcal{L}_4$ ,  $\mathcal{L}_5$  and  $\tilde{\mathcal{L}}_6$  lead to the equations of motion with the higher derivatives than second order. In fact, this situation also appears in the construction of Horndeski theories in curved space-time.

Fortunately, these higher-order derivative terms in the action can be eliminated by adding non-minimal couplings  $G_4(X)R$ ,  $G_5(X)G_{\mu\nu}\nabla^\mu A^\nu$ , and  $G_6(X)L^{\mu\nu\alpha\beta}\nabla_\mu A_\nu\nabla_\alpha A_\beta$  to the Lagrangian densities  $\mathcal{L}_4$ ,  $\mathcal{L}_5$ , and  $\tilde{\mathcal{L}}_6$ , respectively, where  $G_4(X)$ ,  $G_5(X)$ , and  $G_6(X)$  are functions of  $X$ , and the quantity  $L^{\mu\nu\alpha\beta}$  is a double dual Riemann tensor defined by

$$L^{\mu\nu\alpha\beta} = \frac{1}{4}\epsilon^{\mu\nu\rho\sigma}\epsilon^{\alpha\beta\gamma\delta}R_{\rho\sigma\gamma\delta}. \quad (4.25)$$

Moreover, in order to keep the equations of motion up to second order, the functions  $g_4(X)$ ,  $g_5(X)$ , and  $\tilde{g}_6(X)$  in Eqs. (4.22)-(4.24) should be chosen as

$$g_4(X) \rightarrow G_{4,X}, \quad g_5(X) \rightarrow -G_{5,X}/6, \quad \tilde{g}_6(X) \rightarrow G_{6,X}/2, \quad (4.26)$$

where  $G_{i,X} \equiv \partial G_i/\partial X$ .

In summary, the action of generalized Proca theories in curved space-time is given by

$$S_{\text{GP}} = \int d^4x \sqrt{-g} \sum_{i=2}^6 \mathcal{L}_i, \quad (4.27)$$

with

$$\mathcal{L}_2 = G_2(X, F, Y), \quad (4.28)$$

$$\mathcal{L}_3 = G_3(X)\nabla_\mu A^\mu, \quad (4.29)$$

$$\mathcal{L}_4 = G_4(X)R + G_{4,X}(X) [(\nabla_\mu A^\mu)^2 - \nabla_\mu A_\nu \nabla^\nu A^\mu], \quad (4.30)$$

$$\begin{aligned} \mathcal{L}_5 = & G_5(X)G_{\mu\nu}\nabla^\mu A^\nu - \frac{1}{6}G_{5,X}(X) [(\nabla_\mu A^\mu)^3 - 3\nabla_\mu A^\mu \nabla_\nu A_\rho \nabla^\rho A^\nu \\ & + 2\nabla_\mu A_\nu \nabla^\rho A^\mu \nabla^\nu A_\rho] - \tilde{g}_5(X)\tilde{F}^{\alpha\mu}\tilde{F}^\beta_\mu \nabla_\alpha A_\beta, \end{aligned} \quad (4.31)$$

$$\mathcal{L}_6 = G_6(X)L^{\mu\nu\alpha\beta}\nabla_\mu A_\nu \nabla_\alpha A_\beta + \frac{1}{2}G_{6,X}(X)\tilde{F}^{\alpha\beta}\tilde{F}_{\mu\nu}\nabla_\alpha A_\mu \nabla_\beta A_\nu, \quad (4.32)$$

where  $G_{i,X} \equiv \partial G_i/\partial X$ , and the quantities  $\tilde{F}^{\mu\nu}$ ,  $F$ , and  $Y$  are defined by Eqs. (4.5), (4.7), and (4.9) with  $F_{\mu\nu} = \nabla_\mu A_\nu - \nabla_\nu A_\mu$ . Actually, it is also possible

to include the dependence of  $F^{\mu\nu}\tilde{F}_{\mu\nu}$  in  $\mathcal{L}_2$ . However, when we impose the parity invariance, then such term does not affect the cosmological dynamics. Generalized Proca theories have five propagating degrees of freedom in total, which are one longitudinal scalar mode, two vector polarizations, and two tensor polarization. As we will see later, we shall confirm the number of degrees of freedom on FLRW background<sup>1</sup>.

In the limit  $A_\mu \rightarrow \nabla_\mu\varphi$ ,  $\mathcal{L}_6$  and the last term in  $\mathcal{L}_5$  vanish, then the action (4.27) reduces to the action of shift-symmetric Horndeski theories, in which the arbitrary functions in the action (3.37) depend on  $X_\varphi$  alone, i.e.,  $G_i^{(H)} = G_i^{(H)}(X_\varphi)$ .

## 4.2 Dynamics on cosmological background

### 4.2.1 Profile of metric, vector field, and matter

Let us study the cosmological dynamics on the flat FLRW background given by the line element

$$ds^2 = -dt^2 + a^2(t)\delta_{ij}dx^i dx^j, \quad (4.33)$$

where  $t$  is cosmic time, and  $a(t)$  is a scale factor which depends on  $t$ .

To keep the spatial isotropy of the background, the vector field  $A^\mu$  on the background is characterized by a temporal component only, as follows

$$A^\mu = (\phi(t), 0, 0, 0). \quad (4.34)$$

In this case, the mass term  $X$  defined by Eq.(4.2) can be expressed as  $X = \phi^2/2$  on the background. Note that we treat the spatial components of vector field as the perturbations.

To discuss the cosmological dynamics, we consider the matter sector is given by perfect fluid described by the following action [112, 171],

$$S_M = - \sum_{I=m,r} \int d^4x \left[ \sqrt{-g} \rho_I(n_I) + J_I^\mu \{ \partial_\mu \ell_I + \mathcal{A}_{I1} \partial_\mu \mathcal{B}_{I1} + \mathcal{A}_{I2} \partial_\mu \mathcal{B}_{I2} \} \right], \quad (4.35)$$

where the subscripts  $I = m, r$  represent non-relativistic matter and radiations, respectively. The energy density  $\rho_I$  depends on the fluid number

---

<sup>1</sup>In Ref.[30], it confirms that the number of degrees of freedom in generalized Proca theories is maintained five in total on any space-time.

density  $n_I$ . The vector field  $J_I^\mu$  is related to  $n_I$  according to

$$n_I = \sqrt{\frac{J_I^\mu J_I^\nu g_{\mu\nu}}{g}}. \quad (4.36)$$

The quantity  $\ell_I$  contains background quantity and scalar perturbations, whereas  $\mathcal{A}_{I1}$ ,  $\mathcal{A}_{I2}$ ,  $\mathcal{B}_{I1}$ ,  $\mathcal{B}_{I2}$  are associated with vector perturbations. Due to the transverse condition for the vector modes, a third component like  $\mathcal{A}_{I3}\partial_\mu\mathcal{B}_{I3}$  is redundant in the action (4.35). Therefore, the fundamental fields over which this action will be varied are  $g_{\mu\nu}$ ,  $J_\mu$ ,  $\ell$ ,  $\mathcal{A}_{1,2}$  and  $\mathcal{B}_{1,2}$ . The Schutz-Sorkin action is particularly convenient for dealing with the dynamics of vector perturbations.

The fluid four-velocity  $u_{I\mu}$  is defined by

$$u_{I\mu} = \frac{J_{I\mu}}{n_I\sqrt{-g}}, \quad (4.37)$$

which obeys the relation  $u_I^\mu u_{I\mu} = -1$  from Eq. (4.36). Then, varying the action (4.35) with respect to  $g_{\mu\nu}$ , we obtain the energy-momentum tensor of each perfect fluid given by

$$T_{I\mu\nu} = (\rho_I + P_I) u_{I\mu} u_{I\nu} + P_I g_{\mu\nu}, \quad (4.38)$$

where  $\rho_I$  and  $P_I$  correspond to the energy density and pressure, respectively. The fluid pressure  $P_I$  is defined by

$$P_I = n_I \rho_{I,n_I} - \rho_I, \quad (4.39)$$

with the notation  $\rho_{I,n_I} \equiv \partial\rho_I/\partial n_I$ .

Variation the action (4.35) with respect to  $\ell_I$  leads to

$$\partial_\mu J_I^\mu = 0, \quad (4.40)$$

which holds for each  $I = m, r$ . Varying the action (4.35) with respect to  $J_I^\mu$  and using the property  $\partial n_I / \partial J_I^\mu = J_{I\mu} / (n_I g)$ , it follows that

$$\partial_\mu \ell_I = u_{I\mu} \rho_{I,n_I} - \mathcal{A}_{I1} \partial_\mu \mathcal{B}_{I1} - \mathcal{A}_{I2} \partial_\mu \mathcal{B}_{I2}, \quad (4.41)$$

where  $I = m, r$ .

### 4.2.2 Background equations of motion

We consider the total action given by

$$S = S_{\text{GP}} + S_M, \quad (4.42)$$

where  $S_{\text{GP}}$  and  $S_M$  are defined by Eqs. (4.27) and (4.35), respectively. Since the fluid four-velocity in its rest frame is given by

$$u_I^\mu = (1, 0, 0, 0), \quad (4.43)$$

Eq. (4.37) leads to

$$J_I^0 = n_I a^3, \quad (4.44)$$

which corresponds to the particle number of each matter species. Moreover, From Eq. (4.40), we can see that

$$\mathcal{N}_I \equiv J_I^0 = n_I a^3 = \text{constant}, \quad (4.45)$$

which means that the particle number  $\mathcal{N}_I$  is conserved. In other words, the number density of each matter species obeys

$$\dot{n}_I + 3Hn_I = 0, \quad \text{for } I = m, r, \quad (4.46)$$

where a dot denotes a derivative with respect to  $t$ , and  $H$  is the Hubble expansion rate defined by  $H = \dot{a}/a$ .

From the time derivative of  $\rho_I$  given by  $\dot{\rho}_I(n) = \rho_{I,n}\dot{n}$  on the background and using Eq. (2.18) and (2.22), the energy density  $\rho_I(n_I)$  of each matter component obeys

$$\dot{\rho}_I + 3H(\rho_I + P_I) = 0. \quad (4.47)$$

We consider the case in which the pressures of non-relativistic matters and radiations satisfy

$$P_m = 0, \quad P_r = \rho_r/3, \quad (4.48)$$

respectively. Then, the energy densities of each matter components obey

$$\dot{\rho}_m + 3H\rho_m = 0, \quad (4.49)$$

$$\dot{\rho}_r + 4H\rho_r = 0, \quad (4.50)$$

Varying the action (4.27) with respect to the (00) and (ii) components of metric  $g_{\mu\nu}$ , it follows that

$$G_2 - G_{2,X}\phi^2 - 3G_{3,X}H\phi^3 + 6G_4H^2 - 6(2G_{4,X} + G_{4,XX}\phi^2)H^2\phi^2 + G_{5,XX}H^3\phi^5 + 5G_{5,X}H^3\phi^3 = \rho_m + \rho_r, \quad (4.51)$$

$$G_2 - \dot{\phi}\phi^2G_{3,X} + 2G_4(3H^2 + 2\dot{H}) - 2G_{4,X}\phi(3H^2\phi + 2H\dot{\phi} + 2\dot{H}\phi) - 4G_{4,XX}H\dot{\phi}\phi^3 + G_{5,X}H\phi^2(2\dot{H}\phi + 2H^2\phi + 3H\dot{\phi}) + G_{5,XX}H^2\dot{\phi}\phi^4 = -P_m - P_r. \quad (4.52)$$

where  $G_{i,X} \equiv \partial G_i / \partial X$ , and we use the property Eq. (4.39).

Also varying the action (4.27) with respect to  $A^\mu$ , we obtain the following equation,

$$\phi(G_{2,X} + 3G_{3,X}\phi H + 6G_{4,X}H^2 + 6G_{4,XX}\phi^2H^2 - 3G_{5,X}\phi H^3 - G_{5,XX}\phi^3H^3) = 0. \quad (4.53)$$

Note that, among five Eqs. (4.49)-(4.53), four of them are independent.

From Eq. (4.53), we can see that there are two branches of solutions. One of them is a trivial solution  $\phi = 0$  in which case the temporal component of the vector field does not contribute to the background dynamics. Another solutions are given by the equation

$$G_{2,X} + 3G_{3,X}\phi H + 6G_{4,X}H^2 + 6G_{4,XX}\phi^2H^2 - 3G_{5,X}\phi H^3 - G_{5,XX}\phi^3H^3 = 0, \quad (4.54)$$

then the field  $\phi$  is directly related to the Hubble expansion rate  $H$  since the functions  $G_i$  depend on  $X = \phi^2/2$  on the background. It means that there are the de-Sitter solutions characterized by constant  $H$  and  $\phi$ . Therefore, we shall focus on the solution satisfying Eq. (4.54) in the following discussion.

## 4.3 Conditions for avoiding ghosts and gradient instabilities

### 4.3.1 Definition of cosmological perturbations

We show the conditions for the absence of ghosts and gradient instabilities for tensor, vector, and scalar perturbations on the flat FLRW background. Let us consider the linearly perturbed line element in the flat gauge given by

$$ds^2 = -(1 + 2\alpha)dt^2 + 2(\partial_i B + V_i)dt dx^i + a^2(t)(\delta_{ij} + h_{ij})dx^i dx^j, \quad (4.55)$$

where  $\alpha, B$  are scalar perturbations,  $V_i$  is vector perturbation, and  $h_{ij}$  is tensor perturbation. The vector and tensor perturbations satisfy the transverse and traceless conditions, such that

$$\partial^i V_i = 0, \quad (4.56)$$

$$\partial^i h_{ij} = 0, \quad h^i_i = 0. \quad (4.57)$$

The massive vector field  $A^\mu$  contains both scalar and vector modes, as follows

$$A^0 = \phi + \delta\phi, \quad A^i = \frac{1}{a^2(t)} \delta^{ij} (\partial_j \chi_V + E_j), \quad (4.58)$$

where  $\delta\phi$  and  $\chi_V$  are the scalar perturbations, and  $E_j$  is the vector perturbation satisfying the transverse condition

$$\partial^i E_i = 0. \quad (4.59)$$

Then, the components of  $A_\mu$  yields

$$A_0 = g_{00} A^0 + g_{0i} A^i \simeq -\phi - (\delta\phi + 2\phi\alpha), \quad (4.60)$$

$$A_i = g_{i0} A^0 + g_{ij} A^j \simeq \partial_i \psi + Y_i, \quad (4.61)$$

up to linear order in scalar and vector perturbations, where

$$\psi \equiv \chi_V + \phi(t)B, \quad (4.62)$$

$$Y_i \equiv E_i + \phi(t)V_i. \quad (4.63)$$

As we will see later, the perturbations  $\psi$  and  $Y_i$  correspond to the dynamical scalar and vector degrees of freedom, respectively.

For matter sector, the vector field  $J_I^\mu$  also has both scalar and vector perturbations, as

$$J_I^0 = \mathcal{N}_I + \delta J_I, \quad J_I^i = \frac{1}{a^2} \delta^{ij} (\partial_j \delta j_I + W_{Ij}), \quad (4.64)$$

where  $\mathcal{N}_I$  is the background particle number of each matter species given by Eq. (4.45),  $\delta J_I$  and  $\delta j_I$  are scalar perturbations, and  $W_{Ij}$  is the vector perturbation satisfying the transverse condition

$$\partial^j W_{Ij} = 0. \quad (4.65)$$

The spatial component of four-velocity  $u_{I\mu}$  also can be expressed in the form

$$u_{Ii} = -\partial_i v_I + v_{Ii}, \quad \text{for } I = m, r, \quad (4.66)$$

where  $v_I$  is the scalar velocity potential, and  $v_{Ii}$  is the intrinsic vector mode satisfying the transverse condition

$$\partial^i v_{Ii} = 0. \quad (4.67)$$

Since the fluid four-velocity in its rest frame is given by Eq. (4.43), the temporal and spatial components of Eq. (4.41) reduce to, respectively,

$$\dot{\ell}_I = -\rho_{I,n_I}, \quad (4.68)$$

$$\partial_i \ell_I + \mathcal{A}_{I1} \partial_i \mathcal{B}_{I1} + \mathcal{A}_{I2} \partial_i \mathcal{B}_{I2} = u_{Ii} \rho_{I,n_I}. \quad (4.69)$$

Substituting Eq. (4.66) into Eq. (4.69), it follows that

$$\partial_i \ell_I + \mathcal{A}_{I1} \partial_i \mathcal{B}_{I1} + \mathcal{A}_{I2} \partial_i \mathcal{B}_{I2} = -\rho_{I,n_I} \partial_i v_I + \rho_{I,n_I} v_{Ii}, \quad (4.70)$$

up to linear order in perturbations. The coefficients in front of the perturbed quantities in Eq. (4.70) are time-dependent background quantities. The rotational-free scalar part  $\partial_i \ell_I$  needs to be identical to the spatial derivative of scalar perturbations on the right-hand-side of Eq. (4.70), while the divergence-free vector part  $\mathcal{A}_{I1} \partial_i \mathcal{B}_{I1} + \mathcal{A}_{I2} \partial_i \mathcal{B}_{I2}$  is equivalent to the corresponding intrinsic vector perturbations on the same right-hand-side. Then, Eq.(4.70) gives the following relations,

$$\partial_i \ell_I = -\rho_{I,n_I} \partial_i v_I, \quad (4.71)$$

$$\mathcal{A}_{I1} \partial_i \mathcal{B}_{I1} + \mathcal{A}_{I2} \partial_i \mathcal{B}_{I2} = \rho_{I,n_I} v_{Ii}. \quad (4.72)$$

Since  $\rho_{I,n_I}$  in Eq. (4.71) is the background quantity which depends on time alone, the integrated solution to Eq. (4.71) is given by

$$\ell_I = \bar{C}_I(t) - \rho_{I,n_I} v_I. \quad (4.73)$$

Here, the time-dependent function  $\bar{C}_I(t)$  is determined by the  $\mu = 0$  component of Eq. (4.41), as

$$\bar{C}_I(t) = - \int^t \rho_{I,n_I}(\tilde{t}) d\tilde{t}. \quad (4.74)$$

Then, the scalar quantity  $\ell_I$  is given by

$$\ell_I = - \int^t \rho_{I,n_I}(\tilde{t}) d\tilde{t} - \rho_{I,n_I} v_I, \quad (4.75)$$

which contains the velocity potential  $v_I$ .

Since the linear perturbations with different wave numbers do not mix on the FLRW background, we can consider a configuration with which all the perturbations propagate in one direction,  $z$ . Then, the vector perturbations  $X_i = V_i, W_{Ii}, E_i, v_{Ii}$  depend on  $t$  and  $z$ . The components of  $X_i$  consistent with the divergence-free conditions  $\partial^i X_i = 0$  are chosen to be

$$X_i = (X_1(t, z), X_2(t, z), 0) . \quad (4.76)$$

For the Lagrange multipliers  $\mathcal{A}_{I1}, \mathcal{A}_{I2}, \mathcal{B}_{I1}, \mathcal{B}_{I2}$ , we can choose them in the following forms [209]

$$\mathcal{A}_{I1} = \delta\mathcal{A}_{I1}(t, z), \quad \mathcal{A}_{I2} = \delta\mathcal{A}_{I2}(t, z), \quad (4.77)$$

$$\mathcal{B}_{I1} = x + \delta\mathcal{B}_{I1}(t, z), \quad \mathcal{B}_{I2} = y + \delta\mathcal{B}_{I2}(t, z), \quad (4.78)$$

where  $\delta\mathcal{A}_{I1}, \delta\mathcal{A}_{I2}, \delta\mathcal{B}_{I1}, \delta\mathcal{B}_{I2}$  are perturbed quantities. The vector perturbations  $\delta\mathcal{A}_{Ii} = (\delta\mathcal{A}_{I1}(t, z), \delta\mathcal{A}_{I2}(t, z), 0)$  and  $\delta\mathcal{B}_{Ii} = (\delta\mathcal{B}_{I1}(t, z), \delta\mathcal{B}_{I2}(t, z), 0)$  satisfy the transverse conditions  $\partial^i \delta\mathcal{A}_{Ii} = 0$  and  $\partial^i \delta\mathcal{B}_{Ii} = 0$ . The vector field  $\mathcal{B}_{Ii}$ , which is orthogonal to the  $z$  direction, can be chosen to have the background components  $\bar{\mathcal{B}}_{Ii} = (b_1 x, b_2 y, 0)$  with arbitrary constants  $b_1$  and  $b_2$ . In Eq. (4.78) both  $b_1$  and  $b_2$  are normalized to be 1, in which case the left-hand side of Eq. (4.72) reduces to the linear perturbation  $\delta\mathcal{A}_{Ii}$  (with  $i = 1, 2$ ). This is consistent with the fact that the right-hand-side of Eq. (4.72) consists of the perturbations at linear order. To doing so, from Eq. (4.72), the field  $\delta\mathcal{A}_{Ii}$  can be written in the form

$$\delta\mathcal{A}_{Ii} = \rho_{I, n_I} v_{Ii} . \quad (4.79)$$

### 4.3.2 Tensor perturbations

For the tensor perturbation, due to the conditions (4.57), there are two polarization modes  $h_+$  and  $h_\times$ , as

$$h_{ij} = h_+ e_{ij}^+ + h_\times e_{ij}^\times . \quad (4.80)$$

In Fourier space with the comoving wave number  $\mathbf{k}$ , the unit bases obey the relations

$$e_{ij}^+(\mathbf{k}) e_{ij}^+(-\mathbf{k})^* = 1, \quad e_{ij}^\times(\mathbf{k}) e_{ij}^\times(-\mathbf{k})^* = 1, \quad e_{ij}^+(\mathbf{k}) e_{ij}^\times(-\mathbf{k})^* = 0, \quad (4.81)$$

Expanding the action (4.27) up to second order in the tensor perturbations and using the background Eq. (4.52), it follows that the terms containing  $h_+^2$  and  $h_\times^2$  identically vanish. Then, the resulting second-order action of



tensor perturbations is given by

$$S_T^{(2)} = \sum_{\lambda=+, \times} \int dt d^3x a^3 \frac{q_T}{8} \left[ \dot{h}_\lambda^2 + c_T^2 \frac{k^2}{a^2} h_\lambda^2 \right], \quad (4.82)$$

in Fourier space with  $k = |\mathbf{k}|$ , where

$$q_T = 2G_4 - 2\phi^2 G_{4,X} + H\phi^3 G_{5,X}, \quad (4.83)$$

$$c_T^2 = 1 + \frac{2\phi^2 G_{4,X} + \phi^2 \dot{\phi} G_{5,X} - H\phi^3 G_{5,X}}{q_T}. \quad (4.84)$$

The tensor ghost is absent under the condition  $q_T > 0$ , while the gradient instability on small scales can be avoided under the condition  $c_T^2 > 0$ . Note that the quantity  $c_T^2$  corresponds to the propagating speed squared of the gravitational wave.

When we assume that  $c_T \equiv c = 1$  in order to satisfy the bound (3.49), as long as the functions  $G_4$  and  $G_5$  are not related to each other, the arbitrary functions in quartic and quintic interaction are constrained as

$$G_{4,X} = 0, \quad G_{5,X} = 0, \quad (4.85)$$

which mean the functions  $G_4$  and  $G_5$  reduce to be constants. For the quadratic action (4.30), it includes the action of general relativity which is given by  $G_4 = M_{\text{pl}}^2/2$  with the reduced Planck mass  $M_{\text{pl}}$ . For the function  $G_5$ , it affects the cosmological dynamics only through the derivatives with respect to  $X$  (e.g.,  $G_{5,X}$  and  $G_{5,XX}$ ). Therefore, we can set the functions  $G_4$  and  $G_5$  as

$$G_4 = \text{constant} \equiv \frac{M_{\text{pl}}^2}{2}, \quad G_5 = \text{constant} \equiv 0, \quad (4.86)$$

in order to satisfy the bound (3.49).

### 4.3.3 Vector perturbations

There are four quantities  $V_i$ ,  $E_i$ ,  $W_i$ , and  $v_i$  as vector perturbations, and these obey the transverse conditions given by Eqs. (4.56), (4.59), (4.65), (4.67), respectively. Then, as we have mentioned already, we can consider that the components of these vector fields are chosen to be Eq. (4.76).

At first, expanding Eq. (4.35) up to quadratic order in vector perturbations, then the resulting second-order action of vector perturbations is given

by

$$(S_M^{(2)})_V = \int dt d^3x a^3 \sum_{I=m,r} \sum_{i=1}^2 \left[ \frac{1}{2a^2} \left\{ \frac{\rho_{I,n_I}}{\mathcal{N}_I} (W_{Ii}^2 + \mathcal{N}_I^2 V_i^2) + 2\rho_{I,n_I} V_i W_{Ii} - a^3 \rho_I V_i^2 \right\} \right. \\ \left. - \mathcal{N}_I \delta \mathcal{A}_{Ii} \delta \dot{\mathcal{B}}_{Ii} - \frac{1}{a^2} W_{Ii} \delta \mathcal{A}_{Ii} \right], \quad (4.87)$$

where  $\mathcal{N}_I$  are constants given by Eq.(4.45), and  $\delta \mathcal{A}_{Ii}$  and  $\delta \mathcal{B}_{Ii}$  are chosen to be Eqs. (4.77)-(4.78). Since the fields  $W_{Ii}$ ,  $\delta \mathcal{A}_{Ii}$ ,  $\delta \mathcal{B}_{Ii}$  are only in the matter action, we can vary the action (4.87) with respect to these perturbations independently of the full second-order action. Then, varying the second-order matter action (4.87) with respect to  $W_{Ii}$ ,  $\delta \mathcal{A}_{Ii}$  and  $\delta \mathcal{B}_{Ii}$ , we obtain the following relations, respectively,

$$W_{Ii} = \frac{\mathcal{N}_I}{\rho_{I,n_I}} (\delta \mathcal{A}_{Ii} - \rho_{I,n_I} V_i), \quad (4.88)$$

$$W_{Ii} + a^2 \mathcal{N}_I \delta \dot{\mathcal{B}}_{Ii} = 0, \quad (4.89)$$

$$\delta \mathcal{A}_{Ii} = C_{Ii}, \quad (4.90)$$

where  $C_{Ii}$  are constants in time for  $I = m, r$ . From Eqs. (4.79) and (4.90), we obtain the relation

$$\rho_{I,n_I} v_{Ii} = \frac{\rho_I + P_I}{n_I} v_{Ii} = C_{Ii} \quad (4.91)$$

where we use Eq.(4.39). The relation (4.91) is associated with the conservation of the energy-momentum tensor of the perfect fluid. This is the same relation as that in GR, and it means that the vector perturbation  $v_i$  is non-dynamical. Substituting Eqs. (4.88) and (4.79) into Eq. (4.89), it follows that

$$v_{Ii} = V_i - a^2 \delta \dot{\mathcal{B}}_{Ii}. \quad (4.92)$$

After substituting Eqs. and integrating out the perturbations, the resulting second-order matter action reduces to

$$(S_M^{(2)})_V = \int dt d^3x \sum_{i=1}^2 \frac{a}{2} [n_I \rho_{I,n_I} v_{Ii}^2 - \rho_I V_i^2]. \quad (4.93)$$

Let us expand the full action (4.27) with Eq. (4.93) up to second order in vector perturbations. After integrating out the perturbations  $W_{Ii}$  and

$\delta\mathcal{A}_{I_i}$  and using the background equations (4.51)-(4.53), then the second-order action for vector perturbations yields

$$S_V^{(2)} = \int dt d^3x \sum_{i=1}^2 \frac{a}{2} \left[ q_V \dot{Y}_i^2 - \frac{\mathcal{C}_1}{a^2} (\partial Y_i)^2 - \mathcal{C}_2 Y_i^2 + \frac{q_T}{2a^2} (\partial V_i)^2 \right. \\ \left. + \frac{\phi}{a^2} (2G_{4,X} - G_{5,X} H \phi) \partial V_i \partial Z_i + \sum_{I=m,r} (\rho_I + P_I) \left( V_i - a^2 \delta \dot{\mathcal{B}}_{Ii} \right)^2 \right], \quad (4.94)$$

where the vector field  $Y_i$  is defined by Eq. (4.63), and

$$q_V \equiv G_{2,F} + 2G_{2,Y} \phi^2 - 4g_5 H \phi + 2G_6 H^2 + 2G_{6,X} H^2 \phi^2, \quad (4.95)$$

$$\mathcal{C}_1 \equiv q_V + 2 \left[ G_6 \dot{H} - G_{2,Y} \phi^2 - (\phi - \dot{H} \phi)(g_5 - G_{6,X} H \phi) \right], \quad (4.96)$$

$$\mathcal{C}_2 \equiv 2(2G_{4,X} - G_{5,X} H \phi) \dot{H} + (G_{3,X} + 4G_{4,XX} H \phi - G_{5,X} H^2 - G_{5,XX} \phi^2 H^2) \dot{\phi} \\ + 2q_V H^2 + \frac{d}{dt} (q_V H). \quad (4.97)$$

In Fourier space with the comoving wavenumber  $k = |\mathbf{k}|$ , variation of the action (4.94) with respect to  $V_I$ , leads to

$$\frac{q_T}{2} \frac{k^2}{a^2} V_i = - \sum_{I=m,r} \frac{\mathcal{N}_I \mathcal{C}_{Ii}}{a^3} - \frac{\phi}{2} (2G_{4,X} - G_{5,X} H \phi) \frac{k^2}{a^2} Y_i, \quad (4.98)$$

where we use Eqs. (4.91) and (4.92). It means that the dynamics of  $V_i$  is determined by  $Y_i$  and the constants  $\mathcal{C}_{Ii}$ . Integrating out the non-dynamical fields  $v_i$ ,  $V_i$  and taking the small-scale limit ( $k \rightarrow \infty$ ), finally, the resulting second-order action for the perturbations  $Y_i$  in Fourier space reduces to

$$S_V^{(2)} \simeq \sum_{i=1}^2 \int dt d^3x \frac{a}{2} q_V \left[ \dot{Y}_i^2 + c_V^2 \frac{k^2}{a^2} Y_i^2 \right], \quad (4.99)$$

where

$$c_V^2 \equiv 1 + \frac{\phi^2 (2G_{4,X} - G_{5,X} H \phi)^2}{2q_T q_V} \\ - \frac{2[G_{2,Y} \phi^2 - G_6 \dot{H} - (g_5 - G_{6,X} H \phi)(H \phi - \dot{\phi})]}{q_V}. \quad (4.100)$$

We can see that there are two dynamical degrees of freedom  $Y_1$  and  $Y_2$  for the intrinsic vector modes.

When the arbitrary functions  $G_2$ ,  $g_5$ ,  $G_6$  are chosen to be

$$G_2(X, Y, F) = \tilde{G}_2(X) + F, \quad g_5 = 0 = G_6, \quad (4.101)$$

and  $G_{4,5}$  satisfy the condition (4.85), where the function  $\tilde{G}_2$  depends on  $X$  alone, then both  $q_V$  and  $c_V^2$  reduce to be unity in whole cosmological epoch.

#### 4.3.4 Scalar perturbations

In the following, we shall focus on the dark energy models satisfying the bound (3.49). To do so, we consider the following action

$$S_{\text{CGP}} = \int d^4x \sqrt{-g} \left[ \frac{M_{\text{pl}}^2}{2} R + G_2(X, F) + G_3(X) \nabla_\mu A^\mu \right], \quad (4.102)$$

which is the action of cubic-order generalized Proca theories satisfying the condition (4.85). Here, the first term in square brackets of Eq. (4.102) is the same as Einstein-Hilbert term with reduced Planck mass  $M_{\text{pl}}$ . Note that, we have imposed that  $G_2$  does not depend on  $Y = A^\mu A^\nu F_\mu^\alpha F_{\nu\alpha}$ . In fact, the contribution  $Y$  to  $\mathcal{L}_2$  affects to the second-order action for scalar perturbations only through the quantity  $q_V$ . Since  $G_2$  depends on  $F$ , we can discuss the dynamics of the scalar perturbations without loss of generality, even if  $G_2$  does not have the dependence of  $Y$ . In this case, the background equations of motion (4.51)-(4.53) reduce to, respectively,

$$3M_{\text{pl}}^2 H^2 + G_2 - G_{2,X} \phi^2 - 3G_{3,X} H \phi^3 = \rho_m + \rho_r, \quad (4.103)$$

$$M_{\text{pl}}^2 (3H^2 + 2\dot{H}) + G_2 - \dot{\phi} \phi^2 G_{3,X} = -P_m - P_r, \quad (4.104)$$

$$\phi (G_{2,X} + 3G_{3,X} \phi H) = 0. \quad (4.105)$$

Also, the quantities, which are related to the stability conditions for tensor and vector perturbations, reduce to

$$q_T = M_{\text{pl}}^2, \quad c_T^2 = 1, \quad (4.106)$$

$$q_V = 1, \quad c_V^2 = 1. \quad (4.107)$$

Then, the ghosts and gradient instabilities for tensor and vector perturbations are automatically avoided. Moreover, since  $c_T^2$  is unity, the bound (3.49) is also satisfied.

To study the propagation of scalar perturbations, we first define the density perturbation  $\delta\rho_I$  of each matter fluid ( $I = m, r$ ), as

$$\delta\rho_I \equiv \frac{\rho_{I,n_I}}{a^3} \delta J_I, \quad (4.108)$$

where  $\rho_{I,n_I}$  solely depends on the number density  $n_I$ . By defining  $\delta\rho_I$  in this way, the perturbation of number density  $n_I$ , expanded up to second order, can be expressed as

$$\delta n_I = \frac{\delta\rho_I}{\rho_{I,n_I}} - \frac{(\mathcal{N}_I \partial B + \partial\delta j_I)^2}{2\mathcal{N}_I a^5}, \quad (4.109)$$

whose first term on the right hand side is consistent with the left hand side.

Expanding the matter action (4.35) up to second order in scalar perturbations and varying the resulting quadratic-order action with respect to  $\delta j_I$ , it follows that

$$\partial\delta j_I = -\mathcal{N}_I (\partial B + \partial v_I), \quad \text{for } I = m, r, \quad (4.110)$$

which can be used to eliminate the non-dynamical fields  $\delta j_I$  from the matter action. We note that the relations (4.110) also follow from Eq. (4.66) and the property  $n_I \sqrt{-g} u_{Ii} = J_{Ii} = \mathcal{N}_I \partial_i B + \partial_i \delta j_I$  for scalar perturbations up to linear order. The propagation speed squares of matter perfect fluids are defined as

$$c_I^2 = \frac{n_I \rho_{I,n_I}}{\rho_{I,n_I}}, \quad (4.111)$$

with  $I = m, r$ . We focus on the case in which  $c_I^2$  for non-relativistic matters and radiations are given, respectively, by

$$c_m^2 = +0, \quad c_r^2 = \frac{1}{3}. \quad (4.112)$$

Expanding the action  $S_{\text{CGP}}$  up to quadratic order in scalar perturbations and using the background Eqs. (4.51)-(4.53), the second-order action arising from (4.42) reads

$$\begin{aligned} S_S^{(2)} = & \int dt d^3x a^3 \left\{ \sum_{I=m,r} \left\{ \left[ n_I \rho_{I,n_I} \frac{\partial^2 B}{a^2} - \dot{\delta\rho}_I - 3H (1 + c_I^2) \delta\rho_I \right] v_I \right. \right. \\ & - \frac{n_I \rho_{I,n_I}}{2} \frac{(\partial v_I)^2}{a^2} - \frac{c_I^2}{2n_I \rho_{I,n_I}} (\delta\rho_I)^2 - \alpha \delta\rho_I \Big\} - w_3 \frac{(\partial\alpha)^2}{a^2} + w_4 \alpha^2 \\ & - \left[ (3Hw_1 - 2w_4) \frac{\delta\phi}{\phi} - w_3 \frac{\partial^2(\delta\phi)}{a^2\phi} - w_3 \frac{\partial^2\dot{\psi}}{a^2\phi} + w_6 \frac{\partial^2\psi}{a^2} \right] \alpha \\ & - \frac{w_3}{4} \frac{(\partial\delta\phi)^2}{a^2\phi^2} + w_5 \frac{(\delta\phi)^2}{\phi^2} - \left[ \frac{(w_6\phi + w_2)\psi}{2} - \frac{w_3}{2} \dot{\psi} \right] \frac{\partial^2(\delta\phi)}{a^2\phi^2} \\ & \left. - \frac{w_3}{4\phi^2} \frac{(\partial\dot{\psi})^2}{a^2} + \frac{w_7}{2} \frac{(\partial\psi)^2}{a^2} + \left( w_1\alpha + \frac{w_2\delta\phi}{\phi} \right) \frac{\partial^2 B}{a^2} \right\}, \quad (4.113) \end{aligned}$$

with <sup>2</sup>

$$w_1 = -\phi^3 G_{3,X} - 2M_{\text{pl}}^2 H, \quad (4.114)$$

$$w_2 = w_1 + 2M_{\text{pl}}^2 H = -\phi^3 G_{3,X}, \quad (4.115)$$

$$w_3 = -2\phi^2 q_V, \quad (4.116)$$

$$w_4 = \frac{1}{2}\phi^4 G_{2,XX} - \frac{3}{2}H\phi^3(G_{3,X} - \phi^2 G_{3,XX}) - 3M_{\text{pl}}^2 H^2, \quad (4.117)$$

$$w_5 = w_4 - \frac{3}{2}H(w_1 + w_2), \quad (4.118)$$

$$w_6 = \frac{1}{\phi}w_2 = -\phi^2 G_{3,X}, \quad (4.119)$$

$$w_7 = \frac{\dot{\phi}}{\phi^3}w_2 = -\dot{\phi}G_{3,X}. \quad (4.120)$$

Here, the field  $\psi$  is defined by Eq. (4.62), which corresponds to the scalar perturbation of  $A_i$ .

Varying (4.113) with respect to nondynamical fields  $\alpha$ ,  $B$ ,  $\delta\phi$ ,  $v_m$ , and  $v_r$  in Fourier space, respectively, we obtain the following equations,

$$\sum_{I=m,r} \delta\rho_I - 2w_4\alpha + (3Hw_1 - 2w_4) \frac{\delta\phi}{\phi} + \frac{k^2}{a^2} (\mathcal{Y} + w_1B - w_6\psi) = 0, \quad (4.121)$$

$$\sum_{I=m,r} n_I \rho_{I,n_I} v_I + w_1\alpha + w_2 \frac{\delta\phi}{\phi} = 0, \quad (4.122)$$

$$(3Hw_1 - 2w_4)\alpha - 2w_5 \frac{\delta\phi}{\phi} + \frac{k^2}{a^2} \left[ \frac{\mathcal{Y}}{2} + w_2B - \left( \frac{w_2}{\phi} + w_6 \right) \frac{\psi}{2} \right] = 0, \quad (4.123)$$

$$\delta\dot{\rho}_I + 3H(1 + c_I^2)\delta\rho_I + \frac{k^2}{a^2} n_I \rho_{I,n_I} (B + v_I) = 0, \quad \text{for } I = m, r, \quad (4.124)$$

where

$$\mathcal{Y} \equiv \frac{w_3}{\phi} \left( \dot{\psi} + \delta\phi + 2\phi\alpha \right). \quad (4.125)$$

Variations of the action (4.113) with respect to the dynamical perturbations  $\psi$ ,  $\delta\rho_m$ , and  $\delta\rho_r$  lead to, respectively,

$$\dot{\mathcal{Y}} + \left( H - \frac{\dot{\phi}}{\phi} \right) \mathcal{Y} + 2\phi(w_6\alpha + w_7\psi) + (w_2 + w_6\phi) \frac{\delta\phi}{\phi} = 0, \quad (4.126)$$

$$\dot{v}_I - 3Hc_I^2 v_I - c_I^2 \frac{\delta\rho_I}{\rho_I + P_I} - \alpha = 0, \quad \text{for } I = m, r. \quad (4.127)$$

---

<sup>2</sup>In full generalized Proca theories with the arbitrary functions  $G_4$  and  $G_5$ , the functions  $w_{1,2,4,5,6,7}$  include the terms associated with these arbitrary functions. Then,  $w_{6,7}$  are not related to  $w_2$ .

We can eliminate the non-dynamical perturbations from the action (4.113) by solving Eqs. (4.121)-(4.124) for  $\alpha$ ,  $B$ ,  $\delta\phi$ ,  $v_m$ ,  $v_r$ . After the integration by parts, the resulting second-order action in Fourier space can be expressed in the form,

$$S_S^{(2)} = \int dt d^3x a^3 \left( \dot{\vec{\chi}}^t \mathbf{K} \dot{\vec{\chi}} - \frac{k^2}{a^2} \vec{\chi}^t \mathbf{G} \vec{\chi} - \vec{\chi}^t \mathbf{M} \vec{\chi} - \frac{k}{a} \vec{\chi}^t \mathbf{B} \dot{\vec{\chi}} \right), \quad (4.128)$$

where  $\mathbf{K}$ ,  $\mathbf{G}$ ,  $\mathbf{M}$  and  $\mathbf{B}$  are  $3 \times 3$  matrices. The vector field  $\vec{\chi}^t$  is composed of the dynamical perturbations, as

$$\vec{\chi}^t = (\psi, \delta\rho_m/k, \delta\rho_r/k). \quad (4.129)$$

The matrices  $\mathbf{K}$  and  $\mathbf{G}$  is associated with the kinetic terms and the gradient terms of three scalar modes, respectively. The matrix  $\mathbf{M}$  is related to the masses of three scalar modes, and the leading-order contributions are at most of the order  $k^0$ . In the small scale limit ( $k \rightarrow \infty$ ), the second term on the right hand side of Eq. (4.128) dominates over the third and fourth terms.

In the small-scale limit, the non-vanishing components of  $\mathbf{K}$  and  $\mathbf{G}$  are given, respectively, by

$$K_{11} = \frac{H^2 M_{\text{pl}}^2 (3w_1^2 + 4M_{\text{pl}}^2 w_4)}{\phi^2 (w_1 - 2w_2)^2}, \quad (4.130)$$

$$K_{22} = \frac{a^2}{2n_m \rho_{m,n_m}}, \quad K_{33} = \frac{a^2}{2n_r \rho_{r,n_r}}, \quad (4.131)$$

and

$$G_{11} = \mathcal{G} + \dot{\mu} + H\mu - \frac{w_2^2}{2(w_1 - 2w_2)^2 \phi^2} [n_m \rho_{m,n_m} + n_r \rho_{r,n_r}], \quad (4.132)$$

$$G_{22} = \frac{a^2 c_m^2}{2n_m \rho_{m,n_m}}, \quad G_{33} = \frac{a^2 c_r^2}{2n_r \rho_{r,n_r}}, \quad (4.133)$$

where

$$\mathcal{G} \equiv -\frac{4H^2 M_{\text{pl}}^4 w_2^2}{\phi^2 w_3 (w_1 - 2w_2)^2} - \frac{\dot{\phi}}{2\phi^3} w_2, \quad \mu \equiv \frac{H M_{\text{pl}}^2 w_2}{\phi^2 (w_1 - 2w_2)}. \quad (4.134)$$

The scalar ghosts are absent for  $K_{11} > 0$ ,  $K_{22} > 0$ , and  $K_{33} > 0$ . Since  $n_m \rho_{m,n_m} = \rho_m > 0$  and  $n_r \rho_{r,n_r} = 4\rho_r/3 > 0$ , the last two conditions trivially hold. The first condition is satisfied for

$$q_S \equiv 3w_1^2 + 4M_{\text{pl}}^2 w_4 > 0. \quad (4.135)$$

In the small scale limit, the second-order action (4.113) gives rise to the dispersion relation

$$\det \left( \omega^2 \mathbf{K} - \frac{k^2}{a^2} \mathbf{G} \right) = 0, \quad (4.136)$$

with the frequency  $\omega$ . The scalar propagation speed  $c_s$  is defined as  $c_s^2 = \omega^2 a^2 / k^2$ . The propagation speed squared associated with the perturbation  $\psi$  is given by  $c_S^2 = G_{11}/K_{11}$ . To avoid the Laplacian instability, we require that

$$c_S^2 = \frac{1}{K_{11}} \left[ \mathcal{G} + \dot{\mu} + H\mu - \frac{w_2^2}{2(w_1 - 2w_2)^2 \phi^2} \left( \rho_m + \frac{4}{3} \rho_r \right) \right] \geq 0. \quad (4.137)$$

The matter propagation speed squares, which correspond to the ratios  $G_{22}/K_{22}$  and  $G_{33}/K_{33}$  for non-relativistic matter and radiation respectively, reduce to  $c_m^2 = 0$ , and  $c_r^2 = 1/3$ . These mean there are no Laplacian instabilities for the two matter perfect fluids.

In cubic-order generalized Proca theories, the quantity  $c_S^2$  given by Eq. (4.137) reduces to

$$c_S^2 = \frac{2M_{\text{pl}}^2}{q_S} \left[ (2G_{3,X} + G_{3,XX}\phi^2) \dot{\phi} + G_{3,X} H \phi \right] + \frac{(G_{3,X}\phi^3)^2}{q_S} \left[ \frac{2M_{\text{pl}}^2}{q_V \phi^2} - 1 \right], \quad (4.138)$$

where

$$q_S = 3G_{3,X}\phi^2 \left( G_{3,X}\phi^2 - \frac{2M_{\text{pl}}^2 \dot{H}}{\dot{\phi}} \right), \quad (4.139)$$

by using the background equations (4.103)-(4.105), and Eqs. (4.114)-(4.117), (4.131), (4.134).

## 4.4 Concrete dark energy models

To study the cosmological dynamics relevant to the late-time cosmic acceleration, we consider a concrete model of dark energy given by the action (4.42) with

$$\begin{aligned} G_2(X, F) &= q_V F + b_2 X^{p_2}, & G_3(X) &= b_3 X^{p_3}, & G_4(X) &= \frac{M_{\text{pl}}^2}{2}, \\ G_5(X) &= 0, & G_6(X) &= 0 \end{aligned} \quad (4.140)$$



where  $q_V, b_2, b_3, p_2, p_3$  are constants. In this model, the background Eq. (4.53) yields

$$2^{1-p_2} b_2 p_2 \dot{\phi}^{2p_2-1} + 3 \cdot 2^{1-p_3} b_3 p_3 H \dot{\phi}^{2p_3} = 0. \quad (4.141)$$

Eq. (4.141) shows that  $H$  is related to  $\phi$  according to

$$\phi^p H = \lambda = \text{constant}, \quad (4.142)$$

where the power  $p$  is a constant with

$$p = 2p_3 - 2p_2 + 1. \quad (4.143)$$

Then, the two terms in Eq. (4.141) have the same power-law dependence of  $\phi$ . Provided that

$$p > 0, \quad (4.144)$$

the temporal vector component  $\phi$  grows with the decrease of  $H$ . As the vector-field density dominates over the background fluid density, the solutions enter the epoch of cosmic acceleration and finally approach the de Sitter fixed point characterized by constant  $\phi$  [44]. Then, from Eq. (4.141), the coefficients  $b_2, b_3$  are related with each other, as

$$b_3 = -\frac{2^{(p+1)/2} p_2 b_2}{3\lambda(p + 2p_2 - 1)}. \quad (4.145)$$

In the following, we shall study the dynamics of background and perturbations for the functions (4.140) with the powers (4.143).

#### 4.4.1 Background dynamics and equation of state

In the model given by Eqs. (4.140), the background equations (4.51) and (4.52) yield

$$3M_{\text{pl}}^2 H^2 = \rho_r + \rho_m - b_2 \left( \frac{\phi^2}{2} \right)^{p_2}, \quad (4.146)$$

$$M_{\text{pl}}^2 (3H^2 + 2\dot{H}) = -b_2 \left( \frac{\phi^2}{2} \right)^{p_2} + b_3 p_3 \dot{\phi} \phi^2 \left( \frac{\phi^2}{2} \right)^{p_3-1} - P_m - P_r, \quad (4.147)$$

Then, Eq. (4.146) can be expressed as

$$\Omega_{\text{DE}} + \Omega_m + \Omega_r = 1, \quad (4.148)$$

where  $\Omega_I$  (for  $I = \text{DE}, m, r$ ) are the density parameters of dark energy, matter, and radiation, which are given by

$$\Omega_{\text{DE}} = -\frac{2^{-p_2} b_2 \phi^{2p_2}}{3M_{\text{pl}}^2 H^2}, \quad (4.149)$$

$$\Omega_m = \frac{\rho_m}{3M_{\text{pl}}^2 H^2}, \quad (4.150)$$

$$\Omega_r = \frac{\rho_r}{3M_{\text{pl}}^2 H^2}. \quad (4.151)$$

Note that Eq. (4.148) is a relation between each of the density parameters, so one of them is estimated by the others, such as  $\Omega_m = 1 - \Omega_{\text{DE}} - \Omega_r$ . By imposing the condition  $\Omega_{\text{DE}} > 0$ , the constants  $b_2$  is constrained to be negative,

$$b_2 < 0. \quad (4.152)$$

Then, we can consider that the coefficient  $b_2$  is related to the mass  $m$  of the vector field, as

$$b_2 = -m^2 M_{\text{pl}}^{2(1-p_2)}. \quad (4.153)$$

Differentiating Eq. (4.141) with respect to  $t$  and using Eq. (4.147), we can solve for  $\dot{\phi}$  and  $\dot{H}$  as follows<sup>3</sup>

$$\epsilon_\phi \equiv \frac{\dot{\phi}}{\phi H} = \frac{3 - 3\Omega_{\text{DE}} + \Omega_r}{2p(1 + s\Omega_{\text{DE}})}, \quad (4.154)$$

$$\epsilon_H \equiv \frac{\dot{H}}{H^2} = -\frac{3 - 3\Omega_{\text{DE}} + \Omega_r}{2(1 + s\Omega_{\text{DE}})}, \quad (4.155)$$

where

$$s = \frac{p_2}{p}. \quad (4.156)$$

Then, the density parameters  $\Omega_{\text{DE}}$  and  $\Omega_r$  obey the differential equations,

$$\Omega'_{\text{DE}} = \frac{(1 + s)\Omega_{\text{DE}}(3 - 3\Omega_{\text{DE}} + \Omega_r)}{1 + s\Omega_{\text{DE}}}, \quad (4.157)$$

$$\Omega'_r = -\frac{\Omega_r[1 - \Omega_r + (3 + 4s)\Omega_{\text{DE}}]}{1 + s\Omega_{\text{DE}}}, \quad (4.158)$$

---

<sup>3</sup>From Eq. (7.142), the relation between  $\dot{\phi}$  and  $\dot{H}$  reads  $p\dot{\phi}/\phi + \dot{H}/H = 0$  with  $\phi \neq 0$ . It is consistent with the relation between Eqs. (4.154) and (4.155).

where a prime represents a derivative with respect to  $\mathcal{N} = \ln a$  which is called e-folding number. For a given value of  $s$  and initial conditions of  $\Omega_{\text{DE}}$  and  $\Omega_r$ , each density parameter is known by integrating Eqs. (4.157) and (4.158). We shall impose the condition

$$1 + s > 0, \quad (4.159)$$

to avoid diverging  $\Omega_{\text{DE}}$  in the interval  $0 \leq \Omega_{\text{DE}} \leq 1$ .

The dark energy equation of state in Eq. (7.30) and effective equation of state in Eq. (7.32) are given by

$$w_{\text{DE}} = -\frac{3(1+s) + s\Omega_r}{3(1+s\Omega_{\text{DE}})}, \quad (4.160)$$

$$w_{\text{eff}} \equiv -1 - \frac{2\dot{H}}{3H^2} = \frac{\Omega_r - 3(1+s)\Omega_{\text{DE}}}{3(1+s\Omega_{\text{DE}})}, \quad (4.161)$$

respectively.

For the dynamical system given by Eqs. (4.157) and (4.158), there are three fixed points as follows:

$$(a) \quad (\Omega_{\text{DE}}, \Omega_r) = (0, 1) \quad (\text{radiation-dominated point}), \quad (4.162)$$

$$(b) \quad (\Omega_{\text{DE}}, \Omega_r) = (0, 0) \quad (\text{matter-dominated point}), \quad (4.163)$$

$$(c) \quad (\Omega_{\text{DE}}, \Omega_r) = (1, 0) \quad (\text{de Sitter point}). \quad (4.164)$$

At each fixed point, the equations of state (4.160) and (4.161) reduce to

$$(a) \quad w_{\text{DE}} = -1 - \frac{4}{3}s, \quad w_{\text{eff}} = \frac{1}{3}, \quad (4.165)$$

$$(b) \quad w_{\text{DE}} = -1 - s, \quad w_{\text{eff}} = 0, \quad (4.166)$$

$$(c) \quad w_{\text{DE}} = -1, \quad w_{\text{eff}} = -1. \quad (4.167)$$

To discuss the stability of the fixed points, we consider small perturbations  $\delta\Omega_{\text{DE}}$  and  $\delta\Omega_r$  around them, and these obey the following relation

$$\begin{pmatrix} \delta\Omega'_{\text{DE}} \\ \delta\Omega'_r \end{pmatrix} = \mathcal{M} \begin{pmatrix} \delta\Omega_{\text{DE}} \\ \delta\Omega_r \end{pmatrix}, \quad \mathcal{M} = \begin{pmatrix} \frac{\partial f_1}{\partial \Omega_{\text{DE}}} & \frac{\partial f_1}{\partial \Omega_r} \\ \frac{\partial f_2}{\partial \Omega_{\text{DE}}} & \frac{\partial f_2}{\partial \Omega_r} \end{pmatrix}, \quad (4.168)$$

where the function  $f_1$  and  $f_2$  correspond to the r.h.s. of Eqs. (4.157) and (4.158), respectively. Note that the components of a matrix  $\mathcal{M}$  should be

evaluated at the fixed points. Then, eigenvalues of the matrix  $\mathcal{M}$  for each fixed point are given, respectively, by

$$(a) \quad \mu_1 = 4(1 + s), \quad \mu_2 = 1, \quad (4.169)$$

$$(b) \quad \mu_1 = 3(1 + s), \quad \mu_2 = -1, \quad (4.170)$$

$$(c) \quad \mu_1 = -3, \quad \mu_2 = -4. \quad (4.171)$$

When  $1 + s > 0$ , the fixed point (a) corresponding the radiation dominated epoch is unstable because of the positivity of the two eigenvalues. In this case, the point (b), which can be regarded as the matter dominated epoch, corresponds to a saddle. The de Sitter point (c) is always stable since the two eigenvalues are negative. Hence, the cosmological trajectory is characterized by the sequence of these fixed points such as (a)→(b)→(c). Then, the dark energy equation of state  $w_{\text{DE}}$  evolves from  $w_{\text{DE}} = -1 - 4s/3$  to  $w_{\text{DE}} = -1 - s$  during early cosmological epoch, and it finally approaches  $w_{\text{DE}} = -1$  at the de Sitter attractor. The similar evolution is realized for the tracker solution in extended scalar Galileon theories [39]. In that case, since there is the second time derivative of scalar field  $\ddot{\phi}$  in the background equations of motion, we can choose initial conditions where the cosmological evolution are not on the tracker solution. In vector dark energy models given by (4.140), since the background equations do not have the terms related to  $\ddot{\phi}$ , the deviation from the tracker solution does not allow.

In Fig. 4.1, we show the evolution of  $w_{\text{DE}}$  for three different values of the parameter  $s$ . The dark energy equation of state for  $s = 1$  (which is corresponded to the case (i) in Fig. 4.1) evolves as  $w_{\text{DE}} = -7/3 \rightarrow -2 \rightarrow -1$ . The evolution is consistent with the analytic estimation that we mentioned above. This behavior of  $w_{\text{DE}}$  is the same as that of the tracker solution which found for scalar Galileon [35, 36]. Unfortunately, this case for  $s = 1$  is in tension with the combined observational constraints of SNIa, CMB, and BAO due to the large deviation of  $w_{\text{DE}}$  from -1 during early time cosmological epoch. The dark energy equation of state for smaller  $|s|$  tends to be closer to  $-1$  in the radiation and matter epochs. For examples, the values of  $w_{\text{DE}}$  for  $s = 1/2$  and  $s = 1/5$  during the matter-dominated epoch are given, respectively, by  $w_{\text{DE}} = -1.5$  and  $w_{\text{DE}} = -1.2$  (which are corresponded to the cases (ii) and (iii) shown in Fig. 4.1). For tracker solutions in extended scalar Galileon theories, the likelihood analysis based on the data of SNIa, CMB, and BAO has given the bound  $0 \leq s \leq 0.36$  (95%CL)[40]. For the models given by Eq. (4.140), the combined analysis based on the data of SNIa, CMB, BAO, and local measurements of the Hubble expansion rate has given the bound  $0.157 \leq s \leq 0.372$  [45]. Since the models reduce to the  $\Lambda$ CDM in the limit  $s \rightarrow 0$ , it means that the model with  $s > 0$  is favored

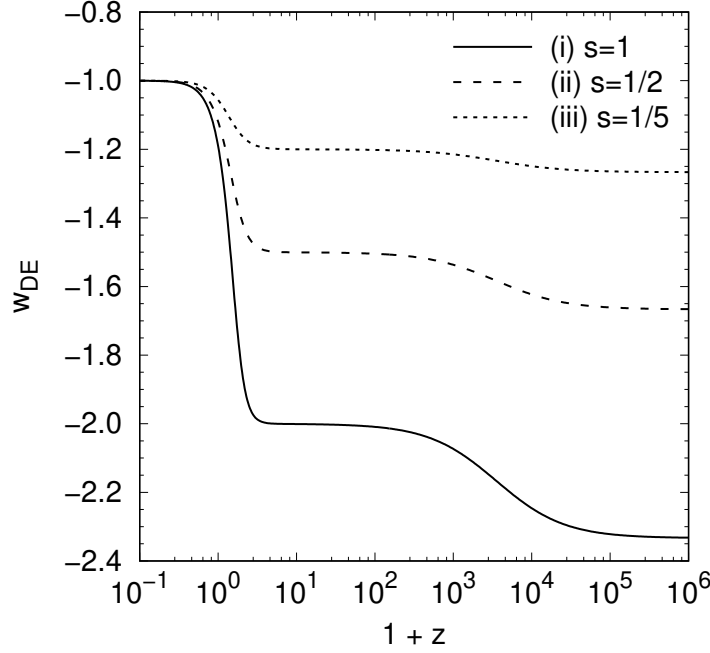


Figure 4.1: Evolution of  $w_{\text{DE}}$  versus  $1+z$ , where  $z$  is the redshift, for the three cases (i)  $s = 1$ , (ii)  $s = 1/2$ , (iii)  $s = 1/5$ . In each case the initial conditions of  $\Omega_{\text{DE}}$  and  $\Omega_r$  are chosen to be (i)  $\Omega_{\text{DE}} = 1.0 \times 10^{-42}$ ,  $\Omega_r = 0.998$  at  $z = 1.7 \times 10^6$ , (ii)  $\Omega_{\text{DE}} = 1.5 \times 10^{-36}$ ,  $\Omega_r = 0.9996$  at  $z = 9.0 \times 10^6$ , and (iii)  $\Omega_{\text{DE}} = 1.0 \times 10^{-42}$ ,  $\Omega_r = 0.998$  at  $z = 1.7 \times 10^6$ . Then, their today's values are  $\Omega_{\text{DE}}(z=0) \simeq 0.68$  and  $\Omega_r(z=0) \simeq 10^{-4}$ , respectively. This figure corresponds to the left panel of the figure 2 in Ref. [44], and the author remake the figure.

over  $\Lambda\text{CDM}$ .

#### 4.4.2 Stability conditions

In the model given by Eq. (4.140), the quantities  $q_T$  and  $q_V$  defined by Eqs. (4.83) and (4.95), which are related to the no-ghost conditions for tensor and vector perturbations, reduce to

$$q_T = M_{\text{pl}}^2, \quad q_V = 1. \quad (4.172)$$

Then, the tensor and vector ghosts are always absent in this model. Also, the propagating speeds of tensor and vector perturbations  $c_T^2$  and  $c_V^2$ , which are given by Eqs. (4.84) and (4.100), reduce to, respectively,

$$c_T^2 = 1, \quad c_V^2 = 1, \quad (4.173)$$

Hence, the Laplacian instabilities of tensor and vector perturbations are always absent in this model. Moreover, the propagating speed of gravitational

waves is equivalent to that of light. It means that this model is consistent with the bound (3.49) constrained by the GW170817 event [92].

For scalar perturbations, the quantities (4.131) and (4.135) reduce to, respectively,

$$K_{11} = \frac{3M_{\text{pl}}^2 H^2 p^2 s \Omega_{\text{DE}} (1 + s \Omega_{\text{DE}})}{\phi^2 (1 - ps \Omega_{\text{DE}})^2}, \quad (4.174)$$

$$q_S = 12M_{\text{pl}}^4 H^2 p^2 s \Omega_{\text{DE}} (1 + s \Omega_{\text{DE}}). \quad (4.175)$$

The no-ghost condition for scalar perturbations corresponds to  $q_S > 0$ . It means that the scalar ghosts are absent for

$$s > 0. \quad (4.176)$$

under which the dark energy equation of state (4.160) during the radiation and matter eras is in the range  $w_{\text{DE}} < -1$ . At early times ( $\Omega_{\text{DE}} \ll 1$ ),  $K_{11}$  has the dependence,

$$K_{11} \propto \Omega_{\text{DE}}^{(ps-1)/[p(1+s)]}. \quad (4.177)$$

In order to avoid the approach of  $K_{11}$  to 0 in the asymptotic past ( $\Omega_{\text{DE}} \rightarrow 0$ ), we require that  $(ps - 1)/[p(1 + s)] \leq 0$ . Under the conditions (4.144) and (4.176), this translates to

$$0 < ps \leq 1, \quad \text{or} \quad 0 < p_2 \leq 1. \quad (4.178)$$

From Eq. (4.138), the Laplacian instability of scalar perturbations is absent for

$$c_S^2 = \frac{6ps + 5p - 3 + (2ps + p - 1)\Omega_r + [3 - 3p - 2ps(2 + p)]\Omega_{\text{DE}} - 2p^2 s^2 \Omega_{\text{DE}}^2}{6p^2 (1 + s\Omega_{\text{DE}})^2} + \frac{2s\Omega_{\text{DE}}}{3q_V u^2 (1 + s\Omega_{\text{DE}})} > 0 \quad (4.179)$$

where  $q_V = 1$  for the model (4.140), and the quantity  $u$  is the normalized temporal vector component defined by

$$u \equiv \frac{\phi}{M_{\text{pl}}}. \quad (4.180)$$

By using Eqs. (4.142), (4.149), and (4.153), the normalized temporal vector component can be expressed as

$$u = \left( \frac{3 \cdot 2^{p_2} \lambda^2}{M_{\text{pl}}^{2p} m^4} \Omega_{\text{DE}} \right)^{1/[2p(1+s)]}. \quad (4.181)$$

To avoid the divergence of  $c_S^2$  in the asymptotic past, we further impose the condition

$$p(1+s) \geq 1, \quad (4.182)$$

since the last term of Eq. (4.179) is proportional to  $(\Omega_{\text{DE}})^{[p(1+s)-1]/[p(1+s)]}$ .

During the radiation, matter, and de Sitter epochs, the propagating speed squared (4.179) reduces, respectively, to

$$(c_S^2)_{\text{rad}} = \frac{p(3+4s)-2}{3p^2}, \quad (4.183)$$

$$(c_S^2)_{\text{mat}} = \frac{p(5+6s)-3}{6p^2}, \quad (4.184)$$

$$(c_S^2)_{\text{dS}} = \frac{1}{3p(1+s)} \left[ 1 - ps + \left( \frac{2}{3^{1/p}} \right)^{1/(1+s)} \frac{ps}{\lambda_V} \right], \quad (4.185)$$

where

$$\lambda_V \equiv q_V \left[ \left( \frac{\phi}{M_{\text{pl}}} \right)^p \frac{H}{m} \right]^{2/[p(1+s)]} = q_V \left( \frac{\lambda}{M_{\text{pl}}^p m} \right)^{2/[p(1+s)]}. \quad (4.186)$$

On using the conditions (4.172), (4.176), (4.178), and (4.182), it follows that  $(c_S^2)_{\text{rad}}$ ,  $(c_S^2)_{\text{mat}}$ , and  $(c_S^2)_{\text{dS}}$  are all positive.

# Chapter 5

## Integrated Sachs-Wolfe effect in massive vector-tensor theories

To confront the dark energy model in GP theories with the observations of RSDs and ISW-galaxy cross-correlations, we need to study the evolution of matter density perturbations and gravitational potentials. In small-scale, we derive the gravitational couplings felt by matter and light under the quasi-static approximation. We show that the sign of ISW-galaxy cross-correlation in vector-tensor theories can be positive, unlike that in scalar-tensor theories. It is caused by the existence of the intrinsic vector modes. Moreover, we place the observational constraints on the vector dark energy model. We find that our dark energy model based on cubic-order generalized Proca theories is favored over  $\Lambda$ CDM even if we consider the ISW-galaxy cross-correlations as the additional data.

### 5.1 Definition of matter density perturbation and gravitational potentials

For our purpose, we consider a perfect fluid of non-relativistic matter with the sound speed squared  $c_m^2$  close to  $+0$ . The gauge-invariant matter density contrast is defined by

$$\delta \equiv \frac{\delta\rho_m}{\rho_m} + 3Hv_m. \quad (5.1)$$

We also introduce the two Bardeen gravitational potentials [113]:

$$\Psi \equiv \alpha + \dot{B}, \quad \Phi \equiv HB. \quad (5.2)$$



The gravitational potential associated with the bending of light rays is defined by

$$\psi_{\text{ISW}} \equiv \Psi - \Phi, \quad (5.3)$$

which plays a key role for the ISW effect in CMB measurements.

In Fourier space with the coming wavenumber  $k = |\mathbf{k}|$ , we relate  $\Psi$  and  $\Phi$  with the matter density contrast  $\delta$ , as

$$\frac{k^2}{a^2} \Psi = -4\pi G \mu \rho_m \delta, \quad (5.4)$$

$$\frac{k^2}{a^2} \psi_{\text{ISW}} = -8\pi G \Sigma \rho_m \delta, \quad (5.5)$$

where  $G$  is the Newton gravitational constant. The quantities  $\mu$  and  $\Sigma$  are dimensionless (positive) gravitational couplings felt by matter and light, respectively [114, 115, 116, 117, 118, 119]. We can express  $\Sigma$  in the form

$$\Sigma = \frac{\mu}{2} (1 + \eta), \quad (5.6)$$

where  $\eta$  is the gravitational slip parameter defined by

$$\eta \equiv -\Phi/\Psi. \quad (5.7)$$

## 5.2 Effective gravitational couplings felt by matter and light

We first briefly review the gravitational couplings and the evolution of non-relativistic matter perturbations in GP theories. In this case, Eqs. (4.124) and (4.127) reduce, respectively, to

$$\dot{\delta} - 3\dot{\mathcal{V}} + \frac{k^2}{a^2} (B + v_m) = 0, \quad (5.8)$$

$$\dot{v}_m = \alpha, \quad (5.9)$$

where  $\mathcal{V} \equiv H v_m$ . Taking the time derivative of Eq. (5.8) and using Eq. (5.9), it follows that

$$\ddot{\delta} + 2H\dot{\delta} + \frac{k^2}{a^2} \Psi = 3\ddot{\mathcal{V}} + 6H\dot{\mathcal{V}}. \quad (5.10)$$

For the theories in which the matter growth rate is not significantly different from that in GR,  $\dot{\delta}$  is at most of order  $H\delta$ . Then, from Eq. (5.8), the velocity potential can be estimated as  $|\mathcal{V}| \lesssim (aH/k)^2 |\delta|$ . For the perturbations deep inside the Hubble radius ( $k^2 \gg a^2 H^2$ ), the two terms on the right hand side

of Eq. (5.10) can be neglected relative to those on the left hand side. In this case, Eq. (5.10) reduces to

$$\ddot{\delta} + 2H\dot{\delta} - 4\pi G\mu\rho_m\delta \simeq 0, \quad (5.11)$$

where we used Eq. (5.4).

The dimensionless gravitational coupling  $\mu$  is known by solving the other perturbation equations of motion derived in Ref. [44]. For the modes deep inside the sound horizon ( $c_s^2 k^2/a^2 \gg H^2$ ), we can resort to the so-called quasi-static approximation under which the dominant terms in the perturbation equations are those containing  $\delta\rho_m$  and  $k^2/a^2$  [120, 79].

Employing the quasi-static approximation for Eqs. (4.121) and (4.123), we obtain

$$\delta\rho_m \simeq -\frac{k^2}{a^2}(\mathcal{Y} + w_1 B - w_6 \psi), \quad (5.12)$$

$$\mathcal{Y} \simeq \left(\frac{w_2}{\phi} + w_6\right)\psi - 2w_2 B = \frac{2w_2}{\phi}\psi - 2w_2 B, \quad (5.13)$$

Substituting Eq. (5.13) into Eq. (5.12), it follows that

$$\delta\rho_m \simeq -\frac{k^2}{a^2} \left[ (w_1 - 2w_2)B + \frac{w_2}{\phi}\psi \right]. \quad (5.14)$$

This can be expressed in terms of  $\Psi$ , as

$$\delta\rho_m \simeq -\frac{k^2}{a^2} \left[ \frac{(w_1 - 2w_2)}{H}\Phi + \frac{w_2}{\phi}\psi \right], \quad (5.15)$$

where we used Eq. (5.2). We eliminate the quantity  $v_m$  from Eqs. (4.122) and (4.124), and then we obtain

$$\dot{\delta\rho_m} + 3H\delta\rho_m + \frac{k^2}{a^2} \left( \rho_m B - w_1 \alpha - \frac{w_2}{\phi} \delta\phi \right) = 0. \quad (5.16)$$

We take the time derivative of Eq. (5.14) and eliminate the terms  $\dot{\delta\rho_m}$  and  $\delta\rho_m$  in Eq. (5.16).

$$\mathcal{Y} = \frac{w_3}{\phi} \left( \dot{\psi} + \delta\phi + 2\phi\alpha \right) \simeq \left( \frac{w_2}{\phi} + w_6 \right) \psi - 2w_2 B \quad (5.17)$$

We note that the combination of perturbations  $\alpha + \dot{B}$  can be expressed in terms of the Bardeen gravitational potential  $\Psi$ . After these process, we obtain

$$\phi^2(w_1 - 2w_2)w_3\Psi + \mu_1\Phi + \mu_2\psi \simeq 0, \quad (5.18)$$

where

$$\mu_1 \equiv \frac{\phi^2}{H} [(\dot{w}_1 - 2\dot{w}_2 + Hw_1 - \rho_m)w_3 - 2w_2(w_2 + Hw_3)] , \quad (5.19)$$

$$\mu_2 \equiv \phi(w_2^2 + Hw_2w_3 + \dot{w}_2w_3) + w_2(w_6\dot{\phi}^2 - w_3\dot{\phi}) . \quad (5.20)$$

On the other hand, we can take the time derivative of Eq. (5.13) and eliminate the terms  $\dot{\mathcal{Y}}$  and  $\mathcal{Y}$  in Eq. (4.126). This process leads to

$$2\phi^2w_2\Psi + \mu_3\Phi + \mu_4\psi \simeq 0 , \quad (5.21)$$

where

$$\mu_3 \equiv \frac{2\phi}{Hw_3}\mu_2 , \quad (5.22)$$

$$\begin{aligned} \mu_4 \equiv & -\frac{1}{w_3} \left[ \phi^3(w_6^2 + 2w_3w_7) + \phi^2(2w_2w_6 + Hw_3w_6 + w_3\dot{w}_6) \right. \\ & \left. + \phi \left\{ w_2^2 + Hw_2w_3 + w_3(\dot{w}_2 - \dot{\phi}w_6) \right\} - 2\dot{\phi}w_2w_3 \right] . \end{aligned} \quad (5.23)$$

Then, one can solve Eqs. (5.15), (5.18), (5.21) for  $\Psi$ ,  $\Phi$ , and  $\psi$ , as

$$\Psi \simeq -\frac{H(\mu_2\mu_3 - \mu_1\mu_4)}{\phi\mu_5} \frac{a^2}{k^2} \rho_m \delta , \quad (5.24)$$

$$\Phi \simeq \frac{\phi H [2w_2\mu_2 - w_3\mu_4(w_1 - 2w_2)]}{\mu_5} \frac{a^2}{k^2} \rho_m \delta , \quad (5.25)$$

$$\psi \simeq \frac{\phi H [w_1w_3\mu_3 - 2w_2(\mu_1 + w_3\mu_3)]}{\mu_5} \frac{a^2}{k^2} \rho_m \delta , \quad (5.26)$$

where

$$\begin{aligned} \mu_5 \equiv & (w_1 - 2w_2) [\phi(w_1 - 2w_2)w_3\mu_4 - 2\phi w_2\mu_2] \\ & + Hw_2 [2w_2(\mu_1 + w_3\mu_3) - w_1w_3\mu_3] . \end{aligned} \quad (5.27)$$

We note that we used the approximation  $\delta \simeq \delta\rho_m/\rho_m$ , which is valid deep inside the sound horizon.

From Eqs. (5.4) and (5.7), the effective gravitational coupling felt by matter and the gravitational slip parameter are given, respectively, by [89]

$$\mu = \frac{2M_{\text{pl}}^2 H(\mu_2\mu_3 - \mu_1\mu_4)}{\phi\mu_5} , \quad (5.28)$$

$$\eta = \frac{\phi^2 [2w_2\mu_2 - w_3\mu_4(w_1 - 2w_2)]}{\mu_2\mu_3 - \mu_1\mu_4} . \quad (5.29)$$

The effective gravitational coupling felt by light  $\Sigma$  is given by Eq. (5.6) with Eqs. (5.28) and (5.29).

On using the definitions of  $w_1, \dots, w_7$  in Eqs. (4.114)-(4.120) and the background Eqs. (4.103)-(4.104), the following equalities hold

$$2\phi^2 (w_1 - w_2) w_3 = 2\mu_1 + \mu_3 w_3 = -4H\phi^2 M_{\text{pl}}^2 w_3, \quad (5.30)$$

$$2\mu_2 + \mu_4 w_3 = 0. \quad (5.31)$$

Then, in cubic-order generalized Proca theories given by Eq. (4.102), Eq. (5.29) reduces to

$$\eta = 1, \quad (5.32)$$

and hence there is no gravitational slip in the cubic-order GP theories. It means that

$$\Psi = -\Phi, \quad (5.33)$$

which shows the absence of an anisotropic stress. Moreover, on using Eq. (4.138) and the definitions of  $w_1, \dots, w_7$  in Eqs. (4.114)-(4.120), the following equalities hold

$$\mu_2 \mu_3 - \mu_1 \mu_4 = -4\phi^5 H q_V [q_S c_S^2 + (\phi^3 G_{3,X})^2], \quad (5.34)$$

$$\mu_5 = -8M_{\text{pl}}^2 H^2 \phi^4 q_V q_S c_S^2. \quad (5.35)$$

Finally, in cubic-order GP theories, the effective gravitational couplings felt by matter and light reduce to

$$\mu = \Sigma = 1 + \frac{(\phi^3 G_{3,X})^2}{q_S c_S^2}. \quad (5.36)$$

In this case, the gravitational interactions felt by matter and light are equivalent to each other. Under the absence of ghosts and Laplacian instabilities of scalar perturbations, the gravitational interactions are enhanced ( $\mu = \Sigma > 1$ ) compared to those in GR ( $\mu = \Sigma = 1$ ). Since  $\mu$  and  $\Sigma$  do not depend on  $k$  under the quasi-static approximation, the matter density contrast  $\delta$  evolves in a scale-independent way according to Eq. (5.11) for the perturbations inside the sound horizon.

### 5.3 ISW-galaxy cross-correlations

In this section, we derive the power spectrum of ISW-galaxy cross-correlations in a general way without specifying gravitational theories. During the matter

era the gravitational potential  $\psi_{\text{ISW}}$  does not typically change in time, but the dominance of dark energy leads to the variation of  $\psi_{\text{ISW}}$  at low redshifts. This leaves an imprint on temperature anisotropies of CMB photons freely streaming from the last scattering surface to today. The ISW contribution  $\Delta T_{\text{ISW}}$  to the CMB temperature perturbation divided by the average temperature  $T$  can be quantified by the integral with respect to the redshift  $z = 1/a - 1$ , such that

$$\frac{\Delta T_{\text{ISW}}(\hat{n})}{T} = - \int_0^{z_r} dz \frac{\partial \psi_{\text{ISW}}}{\partial z}, \quad (5.37)$$

where  $\hat{n}$  is a unit vector along the line of sight and  $z_r$  is the redshift at recombination.

The clustering of galaxies occurs by the growth of matter density contrast  $\delta$ . For the theories in which the dimensionless gravitational coupling  $\mu$  does not depend on the wavenumber  $\mathbf{k}$ , we can express the Fourier-space perturbation  $\delta$  at the redshift  $z$  in the form

$$\delta(z, \mathbf{k}) = \frac{D(z)}{D_0} \delta(0, \mathbf{k}), \quad (5.38)$$

where we introduced the growth factor  $D(z)$  with today's value  $D_0 \equiv D(z = 0)$ . The fluctuations in the angular distribution of galaxies can be quantified as

$$\frac{\Delta N_{\text{Galaxy}}(\hat{n})}{N} = \int_0^{z_r} dz b_s^A \phi^A(z) \delta(z, \hat{n} \chi_{\text{cd}}(z)), \quad (5.39)$$

where  $b_s^A$  is a bias factor,  $\phi^A(z)$  is a window function, and  $\chi_{\text{cd}} = \int_0^z H^{-1}(\tilde{z}) d\tilde{z}$  is a comoving distance. The label  $A$  stands for different galaxy catalogues. For the window function, we choose the following form [106]

$$\phi^A(z) = \frac{\beta_0}{\Gamma[(\alpha_0 + 1)/\beta_0]} \left( \frac{z}{z_0} \right)^{\alpha_0} \exp \left[ - \left( \frac{z}{z_0} \right)^{\beta_0} \right], \quad (5.40)$$

where  $\Gamma[x]$  is the gamma function and  $\alpha_0, \beta_0, z_0$  are positive constants. The values of these constants are different depending on the galaxy surveys. The function (5.40), which is positive, satisfies the normalization  $\int_0^\infty dz \phi^A(z) = 1$  and it has a peak around  $z = z_0$ . To confront our model with the observational data, we select the two galaxies surveys: 2 Micron All-Sky Survey (2MASS) and SDSS, in which case the window functions for galaxy bins are considerably peaked at particular redshifts [106]. The 2MASS galaxy catalogue can be fitted by the window function (5.40) with  $(z_0, \alpha_0, \beta_0) = (0.072, 1.901, 1.752)$ . For the SDSS catalogue, we choose the parameters  $(z_0, \alpha_0, \beta_0) = (0.113, 3.457, 1.197)$ .

In the following, we also assume that the bias  $b_s^A$  is scale-independent as well as time-independent in the range of redshift intervals allowed by  $\phi^A(z)$ . This is a reasonable assumption for galaxy catalogues with the peaked window function mentioned above.

Let us consider a perturbation  $X(z, \chi_{\text{cd}} \hat{n})$  that depends on  $z$  and the product of comoving distance  $\chi$  and unit vector  $\hat{n}$ . Then, the perturbation  $X(\hat{n})$ , which corresponds to the integration of  $X(z, \chi_{\text{cd}} \hat{n})$  with respect to  $z$  from  $z = 0$  to  $z = \infty$ , can be expanded in terms of spherical harmonics  $Y_{lm}(\hat{n})$ , as

$$X(\hat{n}) = \int_0^\infty dz X(z, \chi_{\text{cd}} \hat{n}) = \sum_{l,m} a_{lm}^X Y_{lm}(\hat{n}), \quad (5.41)$$

where  $a_{lm}^X = \int d\Omega X(\hat{n}) Y_{lm}^*(\hat{n})$  with the solid angle  $\Omega$ . The Fourier-series expansion of  $X(z, \chi \hat{n})$  is given by

$$X(z, \chi_{\text{cd}} \hat{n}) = \int \frac{d^3 k}{(2\pi)^3} X(z, \mathbf{k}) e^{i\mathbf{k} \cdot \chi \hat{n}}. \quad (5.42)$$

On using the relation  $\int d\Omega e^{i\mathbf{k} \cdot \mathbf{r}} Y_{lm}^*(\hat{r}) = 4\pi i^l j_l(kr) Y_{lm}^*(\hat{k})$ , where  $\hat{r} = \mathbf{r}/r$ ,  $\hat{k} = \mathbf{k}/k$ , with the spherical Bessel function  $j_l(x)$ , the coefficient  $a_{lm}^X$  is expressed as

$$a_{lm}^X = \frac{i^l}{2\pi^2} \int dz \int d^3 k X(z, \mathbf{k}) j_l(k\chi) Y_{lm}^*(\hat{k}). \quad (5.43)$$

The coefficients  $a_{lm}^{\text{ISW}}$  and  $a_{lm}^{\text{Galaxy}}$ , which are associated with the ISW signal and galaxy clusterings respectively, can be derived by substituting  $X \rightarrow -\partial\psi_{\text{ISW}}/\partial z$  and  $X \rightarrow b_s^A \phi^A(z)(D(z)/D_0)\delta(0, \mathbf{k})$  into Eq. (5.43). In doing so, we exploit the properties  $1+z = e^{-\mathcal{N}}$  and  $dz/d\mathcal{N} = -e^{-\mathcal{N}}$  between the redshift  $z$  and the  $e$ -folding number  $\mathcal{N} = \ln a$ . Then, it follows that [121]

$$a_{lm}^{\text{ISW}} = \frac{-i^l}{2\pi^2 D_0} \int d\mathcal{N}_1 \int d^3 k_1 Z_{\text{ISW}}(\mathcal{N}_1) \delta(0, \mathbf{k}_1) j_l(k_1 \chi_1) Y_{lm}^*(\hat{k}_1), \quad (5.44)$$

$$a_{lm}^{\text{Galaxy}} = \frac{-i^l}{2\pi^2 D_0} \int d\mathcal{N}_2 e^{-\mathcal{N}_2} \int d^3 k_2 b_s^A \phi^A(\mathcal{N}_2) D(\mathcal{N}_2) \delta(0, \mathbf{k}_2) j_l(k_2 \chi_2) Y_{lm}^*(\hat{k}_2), \quad (5.45)$$

where  $\chi_I \equiv \chi(\mathcal{N}_I)$  with  $I = 1, 2$ , and  $Z_{\text{ISW}}$  is defined by

$$\frac{\partial\psi_{\text{ISW}}}{\partial\mathcal{N}} = Z_{\text{ISW}}(\mathcal{N}, k) \frac{\delta(0, \mathbf{k})}{D_0}. \quad (5.46)$$

The cross-correlation between the ISW signal in CMB and the galaxy fluctuations is quantified as

$$\left\langle \frac{\Delta T_{\text{ISW}}(\hat{n}_1)}{T} \frac{\Delta N_{\text{Galaxy}}(\hat{n}_2)}{N} \right\rangle = \sum_{l=0}^{\infty} \frac{2l+1}{4\pi} C_l^{\text{IG}} \mathcal{P}_l(\cos \theta), \quad (5.47)$$

where  $\mathcal{P}_l$  is the Legendre polynomial with the angle  $\theta$  between the unit vectors  $\hat{n}_1$  and  $\hat{n}_2$ , and  $C_l^{\text{IG}}$  is the ISW-galaxy cross-correlation amplitude given by

$$C_l^{\text{IG}} = \left\langle a_{lm}^{\text{ISW}} (a_{lm}^{\text{Galaxy}})^* \right\rangle. \quad (5.48)$$

Substituting Eqs. (5.44) and (5.45) into Eq. (5.48), we obtain

$$\begin{aligned} C_l^{\text{IG}} &= \frac{2b_s^A}{\pi D_0^2} \int_{k_m}^{k_M} dk k^2 P_\delta(k) \\ &\times \int_{\mathcal{N}_i}^0 d\mathcal{N}_1 Z_{\text{ISW}}(\mathcal{N}_1, k) j_l[k\chi_1] \int_{\mathcal{N}_i}^0 d\mathcal{N}_2 e^{-\mathcal{N}_2} \phi^A(\mathcal{N}_2) D(\mathcal{N}_2) j_l[k\chi_2], \end{aligned} \quad (5.49)$$

$$(5.50)$$

where  $k_m$  and  $k_M$  are minimum and maximum wavenumbers, respectively,  $\mathcal{N}_i$  is the initial value of  $\mathcal{N}$  in the deep matter era, and  $P_\delta$  is the matter power spectrum defined by

$$\langle \delta(0, \mathbf{k}_1) \delta^*(0, \mathbf{k}_2) \rangle = (2\pi)^3 \delta_D^{(3)}(\mathbf{k}_1 - \mathbf{k}_2) P_\delta(k_1). \quad (5.51)$$

Similarly, the galaxy-galaxy correlation amplitude can be computed as

$$\begin{aligned} C_l^{\text{GG}} &= \left\langle a_{lm}^{\text{Galaxy}} (a_{lm}^{\text{Galaxy}})^* \right\rangle \\ &= \frac{2(b_s^A)^2}{\pi D_0^2} \int_{k_m}^{k_M} dk k^2 P_\delta(k) \left( \int_{\mathcal{N}_i}^0 d\mathcal{N} e^{-\mathcal{N}} \phi^A(\mathcal{N}) D(\mathcal{N}) j_l[k\chi_{\text{cd}}(\mathcal{N})] \right)^2. \end{aligned} \quad (5.52)$$

On using the transfer function  $T_m(k)$  from the deep radiation era to the matter-dominated epoch, the matter power spectrum can be expressed as

$$P_\delta(k) = 2\pi^2 \delta_H^2 T_m^2(k) \left( \frac{k}{H_0} \right)^{n_s} H_0^{-3}, \quad (5.53)$$

where  $\delta_H$  and  $n_s$  are the amplitude and the spectral index of primordial scalar perturbations, respectively. We employ the transfer function  $T_m(k)$  advocated by Eisenstein and Hu [122, 123]. Substituting Eq. (5.53) into

Eqs. (5.50) and (5.52), it follows that

$$C_l^{\text{IG}} = 4\pi b_s^A \bar{\delta}_H^2 \int_{k_m}^{k_M} \frac{dk}{k} \left( \frac{k}{H_0} \right)^{n_s+3} T_m^2(k) \\ \times \int_{\mathcal{N}_i}^0 d\mathcal{N}_1 Z_{\text{ISW}}(\mathcal{N}_1, k) j_l[k\chi_1] \int_{\mathcal{N}_i}^0 d\mathcal{N}_2 e^{-\mathcal{N}_2} \phi^A(\mathcal{N}_2) D(\mathcal{N}_2) j_l[k\chi_2], \quad (5.54)$$

$$C_l^{\text{GG}} = 4\pi (b_s^A)^2 \bar{\delta}_H^2 \int_{k_m}^{k_M} \frac{dk}{k} \left( \frac{k}{H_0} \right)^{n_s+3} T_m^2(k) \\ \times \int_{\mathcal{N}_i}^0 d\mathcal{N}_1 e^{-\mathcal{N}_1} \phi^A(\mathcal{N}_1) D(\mathcal{N}_1) j_l[k\chi_1] \int_{\mathcal{N}_i}^0 d\mathcal{N}_2 e^{-\mathcal{N}_2} \phi^A(\mathcal{N}_2) D(\mathcal{N}_2) j_l[k\chi_2], \quad (5.55)$$

where

$$\bar{\delta}_H \equiv \frac{\delta_H}{D_0}. \quad (5.56)$$

The quantity  $Z_{\text{ISW}}$  plays a key role for determining the sign of  $C_l^{\text{IG}}$ . We recall that the gravitational potential  $\psi_{\text{ISW}}$  is related to  $\delta$  according to Eq. (5.5). The density  $\rho_m$  is given by  $\rho_m = 3M_{\text{pl}}^2 H_0^2 \Omega_{m0} (1+z)^3$ , where  $\Omega_{m0}$  is today's density parameter of non-relativistic matter. Using the relation (5.38), we can express  $\psi_{\text{ISW}}$  in the form

$$\psi_{\text{ISW}} = -\frac{3H_0^2 \Omega_{m0}}{k^2} e^{-\mathcal{N}} D\Sigma \frac{\delta(0, \mathbf{k})}{D_0}. \quad (5.57)$$

Taking the  $\mathcal{N}$ -derivative of Eq. (5.57) and comparing it with Eq. (7.1), it follows that

$$Z_{\text{ISW}}(\mathcal{N}, k) = \frac{3H_0^2 \Omega_{m0}}{k^2} e^{-\mathcal{N}} D\Sigma \mathcal{F}, \quad (5.58)$$

where we introduced the following quantity

$$\mathcal{F} \equiv 1 - \frac{D'}{D} - \frac{\Sigma'}{\Sigma} = 1 - (\ln D\Sigma)'. \quad (5.59)$$

Substituting Eq. (5.58) into Eq. (5.54), we obtain

$$C_l^{\text{IG}} = \frac{12\pi b_s^A \bar{\delta}_H^2 \Omega_{m0}}{H_0^{n_s+1}} \int dk k^{n_s} T_m^2(k) \\ \times \int_{\mathcal{N}_i}^0 d\mathcal{N}_1 e^{-\mathcal{N}_1} D(\mathcal{N}_1) \Sigma(\mathcal{N}_1) \mathcal{F}(\mathcal{N}_1) j_l(k\chi_1) \int_{\mathcal{N}_i}^0 d\mathcal{N}_2 e^{-\mathcal{N}_2} D(\mathcal{N}_2) \phi^A(\mathcal{N}_2) j_l(k\chi_2), \quad (5.60)$$



For the large wavenumber  $k$ , it is useful to employ the following Limber approximation for an arbitrary  $k$ -dependent function  $f(k)$ :

$$\int dk k^2 f(k) j_l(k\chi_1) j_l(k\chi_2) \simeq \frac{\pi}{2} \frac{\delta(\chi_1 - \chi_2)}{\chi_1^2} f\left(\frac{l_{12}}{\chi_1}\right), \quad (5.61)$$

where  $l_{12} \equiv l + 1/2$ . Applying the approximation (5.61) to Eq. (5.60) and using Eq. (5.53) and the relation  $d\mathcal{N}/d\chi_{\text{cd}} = -aH$ , we obtain

$$C_l^{\text{IG}} \simeq \frac{6\pi^2 b_s^A \bar{\delta}_H^2 \Omega_{m0}}{l_{12}^2} \int_{\mathcal{N}_i}^0 d\mathcal{N} e^{-\mathcal{N}} \frac{H}{H_0} \left(\frac{l_{12}}{\bar{\chi}_{\text{cd}}}\right)^{n_s} T_m^2 \left(\frac{l_{12} H_0}{\bar{\chi}_{\text{cd}}}\right) \phi^A D^2 \Sigma \mathcal{F}, \quad (5.62)$$

where  $\bar{\chi}_{\text{cd}} \equiv H_0 \chi_{\text{cd}}$ .

The negative ISW-galaxy cross-correlation ( $C_l^{\text{IG}} < 0$ ) can occur for the models in which  $\mathcal{F} < 0$  at low redshifts, which translates to

$$(\ln D\Sigma)' > 1. \quad (5.63)$$

Since  $C_l^{\text{IG}}$  is the integral with respect to  $\mathcal{N}$  from the deep matter era to today, the condition (5.63) is necessary but not sufficient for realizing  $C_l^{\text{IG}} < 0$ . As we will see in Sec. 5.3.1, even if  $\mathcal{F}$  becomes negative at low redshifts, there are cases in which  $C_l^{\text{IG}}$  is positive.

Writing the factor  $D'/D$  in Eq. (5.59) in terms of the matter density parameter  $\Omega_m$  and the growth index  $\gamma$ , as  $D'/D = (\Omega_m)^\gamma$ , it follows that  $\mathcal{F} = 1 - (\Omega_m)^\gamma - \Sigma'/\Sigma$ . In the  $\Lambda$ CDM model, the growth index is well approximated by  $\gamma \simeq 0.55$  at low redshifts [124]. Since  $\Sigma = 1$  in this case, we have  $\mathcal{F} = 1 - (\Omega_m)^\gamma > 0$  and hence the ISW-galaxy cross-correlation is positive in the  $\Lambda$ CDM model.

In modified gravity theories the growth index is generally different from 0.55. In  $f(R)$  gravity, for example, it is in the range  $0.40 \lesssim \gamma \lesssim 0.55$  [125]. The observational data of RSDs and the clustering of luminous red galaxies placed the bound  $\gamma = 0.56 \pm 0.05$  for constant  $\gamma$  [126], so the quantity  $1 - (\Omega_m)^\gamma$  is positive for the redshift  $z$  relevant to the galaxy surveys ( $z \lesssim 2$ ). To realize the negative ISW-galaxy cross-correlation, it is at least necessary to satisfy the condition

$$\Sigma' > 0 \quad (5.64)$$

at low redshifts.

Before closing this subsection, we explain how to compute the quantities  $\bar{\delta}_H$  and  $b_s^A$  in the expression of Eq. (5.62). We first consider the part of  $k$ -integrals in Eqs. (5.54) and (5.55) depending on the window function and introduce the following quantity

$$I \equiv \int_{k_m}^{k_M} \frac{dk}{k} \left(\frac{k}{H_0}\right)^{n_s+3} [T_m(k) w_{\text{TH}}(8h^{-1}, k)]^2, \quad (5.65)$$

where  $w_{\text{TH}}$  is the top-hat function defined by

$$w_{\text{TH}}(r, k) = \frac{3[\sin(kr) - kr \cos(kr)]}{(kr)^3}. \quad (5.66)$$

The quantity (5.65) is evaluated at the scale  $r = 8h^{-1}$  Mpc, where  $h$  is the normalized Hubble constant given by  $H_0 = 100 h \text{ km s}^{-1} \text{ Mpc}^{-1}$ . For the scalar spectral index  $n_s$ , we choose the best-fit value  $n_s = 0.9649$  constrained from the Planck 2018 data [1].

We define today's amplitude of over density at the scale  $8h^{-1}$  Mpc, as

$$\sigma_8(0) \equiv \delta_H \sqrt{I}. \quad (5.67)$$

From Eq. (5.38) the value of  $\sigma_8$  at the initial redshift  $z_i$  in the deep matter era is related to  $\sigma_8(0)$ , as  $\sigma_8(z_i) = \sigma_8(0) D(z_i)/D_0$ . Then, the perturbation  $\bar{\delta}_H = \delta_H/D_0$  is expressed as

$$\bar{\delta}_H = \frac{\sigma_8(z_i)}{D(z_i)} \frac{1}{\sqrt{I}}. \quad (5.68)$$

Provided that the evolution of perturbations in the deep matter era is close to that in the  $\Lambda$ CDM model, the initial growth factor can be chosen as  $D(z_i) = a_i = e^{\mathcal{N}_i}$ . Today's growth factor  $D_0$  is known by solving Eq. (5.11) for  $\delta$ . Since the scalar-field contribution to the dynamics of perturbations tends to be negligible at higher redshifts in our model, we choose the same early-time initial conditions as those in the  $\Lambda$ CDM model. In particular, we consider initial conditions for  $\sigma_8(z_i)$ , such that  $\sigma_8(z_i) = \sigma_8(z_i)^{\Lambda\text{CDM}}$ , and find  $\sigma_8(z_i)^{\Lambda\text{CDM}}$  by using  $\sigma_8(z_i)^{\Lambda\text{CDM}} = \sigma_8(0)^{\Lambda\text{CDM}} e^{\mathcal{N}_i}/D_0^{\Lambda\text{CDM}}$ . For  $\sigma_8(0)^{\Lambda\text{CDM}}$ , we choose the Planck best-fit value  $\sigma_8(0)^{\Lambda\text{CDM}} = 0.811$  [1]. Since the initial condition for  $\sigma_8(z_i)$  is now fixed, the value of  $\bar{\delta}_H$  is known from Eq. (5.68).

For the bias factor  $b_s^A$ , we normalize it by using the observed best-fit galaxy-galaxy correlation spectrum  $C_l^{\text{GG}}$ . The analysis of Ref. [127] using the galaxy spectrum data of 2MASS surveys combined with the WMAP data showed that the best-fit value of bias is  $b_s^{2\text{MASS}} = 1.4$ . For the SDSS survey, the galaxy spectrum is consistent with the WMAP best-fit  $\Lambda$ CDM cosmology with the bias factor  $b_s^{\text{SDSS}} = 1$  [106]. Then, for each galaxy survey, we can compute the galaxy power spectrum  $C_{l,\text{best}}^{\text{GG}}$  by using the best-fit bias and best-fit cosmological parameters constrained from WMAP. We write the power spectrum (5.55) in the form  $C_l^{\text{GG}} = 4\pi(b_s^A)^2 \bar{\delta}_H^2 Y_l^{\text{GG},A}$  and define the  $\chi^2$  estimator:

$$\chi_{\text{bias},A}^2 \equiv \sum_{l=2}^{150} \left[ C_{l,\text{best}}^{\text{GG}} - 4\pi(b_s^A)^2 \bar{\delta}_H^2 Y_l^{\text{GG},A} \right]^2. \quad (5.69)$$

The bias can be fixed by minimizing  $\chi_{\text{bias},A}^2$ . Solving  $\partial\chi_{\text{bias},A}^2/\partial b_s^A = 0$  for  $b_s^A$ , it follows that

$$b_s^A = \sqrt{\frac{\sum_l C_{l,\text{best}}^{\text{GG}} Y_l^{\text{GG},A}}{4\pi\bar{\delta}_H^2 \sum_l (Y_l^{\text{GG},A})^2}}. \quad (5.70)$$

Computing  $b_s^A$  from Eq. (5.70) for dark energy models in GP theories, we have confirmed that the bias depends only mildly on the model parameters (typically within a few percent difference). This means that, as in the minimal theory of massive gravity [121], using the power spectrum  $C_{l,\text{best}}^{\text{GG}}$  derived for the best-fit  $\Lambda$ CDM cosmology is a reasonable prescription for the bias estimation.

### 5.3.1 ISW-galaxy cross-correlations in GP theories

Let us consider the dark energy model in GP theories characterized by the functions (4.140). From Eq. (5.36), the quantities  $\mu$  and  $\Sigma$  are expressed as

$$\mu = \Sigma = 1 + \frac{s\Omega_{\text{DE}}}{3(1+s\Omega_{\text{DE}})c_S^2}. \quad (5.71)$$

During the radiation and matter eras, the scalar propagation speed squares are given, respectively, by Eqs. (4.183) and (4.184). Since  $\Omega_{\text{DE}} \ll 1$  in these epochs,  $\mu$  and  $\Sigma$  are close to 1.

On using Eq. (4.185) at the de Sitter solution ( $\Omega_{\text{DE}} = 1$ ), it follows that

$$\mu_{\text{dS}} = \Sigma_{\text{dS}} = 1 + \left[ \frac{1-ps}{ps} + \left( \frac{2}{3^{1/p}} \right)^{1/(1+s)} \frac{1}{\lambda_V} \right]^{-1}, \quad (5.72)$$

In the last equality, we used the fact that the model (4.140) satisfies  $q_V = 1$  (under which there is no issue of the strong coupling problem). The intrinsic vector mode affects  $\mu_{\text{dS}}$  and  $\Sigma_{\text{dS}}$  through the quantity  $\lambda_V$ . Since  $\lambda > 0$  and  $p(1+s) \geq 1$ , both  $\mu_{\text{dS}}$  and  $\Sigma_{\text{dS}}$  are larger than 1. In the limit  $\lambda_V \rightarrow \infty$ , Eq. (5.72) reduces to  $\mu_{\text{dS}} = \Sigma_{\text{dS}} \rightarrow 1/(1-ps)$ , which corresponds to the values in cubic-order Horndeski (scalar-tensor) theories. In another limit  $\lambda_V \rightarrow 0$ , we have  $\mu_{\text{dS}} = \Sigma_{\text{dS}} \rightarrow 1$  and hence the evolution of perturbations is similar to that in GR.

In the left panel of Fig. 5.1, we show the evolution of  $\Sigma$  ( $= \mu$ ) for four different values of  $\lambda_V$  with  $q_V = 1$ . The other model parameters are chosen to be  $s = 0.2$  and  $p = 3$  with today's matter density parameter  $\Omega_m(z=0) = 0.32$ . In the  $\Lambda$ CDM model, the quantity  $\Sigma$  is equivalent to 1 throughout the cosmological evolution. This case can be regarded as the limit  $\lambda_V \rightarrow 0$  in

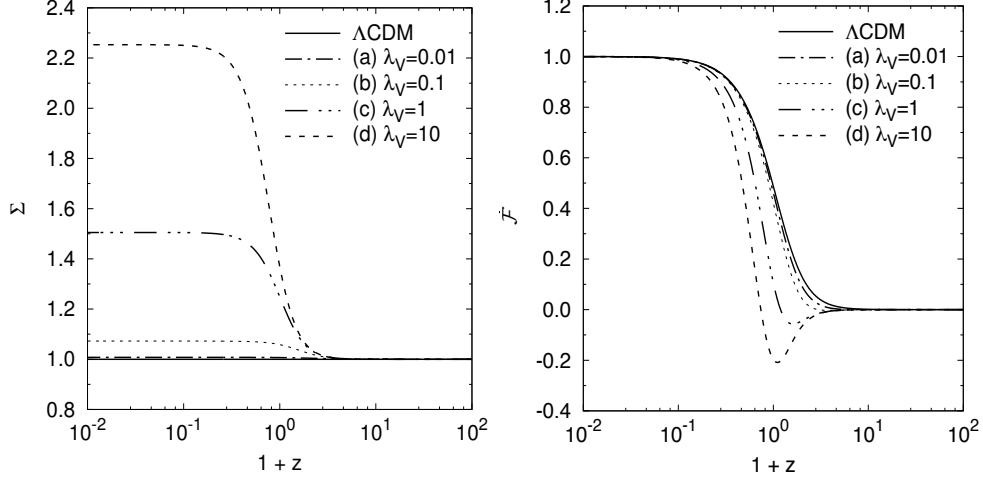


Figure 5.1: Evolution of  $\Sigma$  (left) and  $\mathcal{F}$  (right) versus  $1+z$  for  $s = 0.2$ ,  $p = 3$ , and  $\Omega_{m0} = 0.32$  with four different values of  $\lambda_V$ : (a)  $\lambda_V = 0.01$ , (b)  $\lambda_V = 0.1$ , (c)  $\lambda_V = 1$ , and (d)  $\lambda_V = 10$ . The solid line corresponds to the evolution of  $\Sigma$  and  $\mathcal{F}$  in the  $\Lambda$ CDM model. For  $\lambda_V \gtrsim 1$ , the perturbation enters the region  $\mathcal{F} < 0$  at low redshifts.

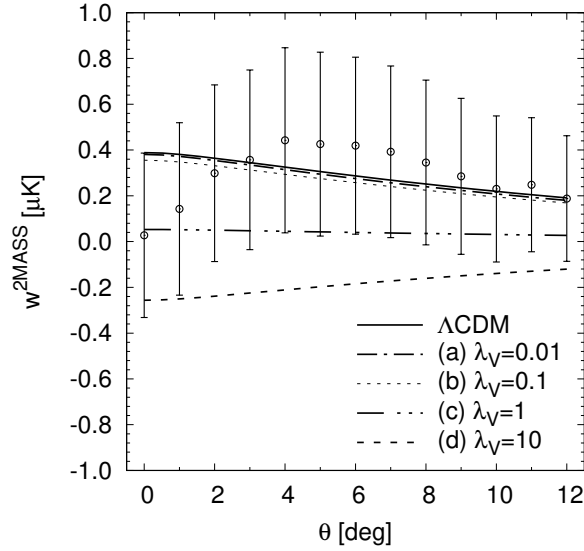


Figure 5.2: The ISW-galaxy cross-correlation observable  $w^{2MASS}$  versus the angle  $\theta$  (representing the deviation from the center of galaxy datasets) for the model parameters same as those used in Fig. 5.1 with  $n_s = 0.9649$ ,  $\sigma_8(0) = 0.811$ , and  $h = 0.696$ . We also show the data points of 2MASS measurements with error bars [106] (derived by the jackknife error estimation method).

Eq. (5.72). As estimated from Eqs. (5.71),  $\Sigma$  is close to 1 in the deep matter era for any value of  $\lambda_V$  under consideration. The deviation of  $\Sigma$  from 1 starts to occur at low redshifts. For larger  $\lambda_V$ , the deviation of  $\Sigma$  from 1 tends to be more significant. This reflects the fact that, for increasing  $\lambda_V$ , the de Sitter value  $\Sigma_{\text{dS}}$  in Eq. (5.72) gets larger, e.g.,  $\Sigma_{\text{dS}} = 1.07$  for  $\lambda_V = 0.1$  and  $\Sigma_{\text{dS}} = 2.25$  for  $\lambda_V = 10$  in the numerical simulation of Fig. 5.1.

In the right panel of Fig. 5.1, we also plot the evolution of the quantity  $\mathcal{F}$  defined by Eq. (5.59) for the same model parameters as those used in the left panel. In all the cases the quantity  $\mathcal{F}$  starts to evolve from the value close to +0 and finally approaches the asymptotic value 1, but the intermediate evolution of  $\mathcal{F}$  is different depending on the parameter  $\lambda_V$ . In the  $\Lambda$ CDM model we have  $\mathcal{F} > 0$  throughout the cosmological evolution, so the ISW-galaxy cross-correlation is positive. In GP theories, the growth of  $\Sigma$  occurs at low redshifts, in which case  $\mathcal{F}$  can be negative. With the model parameters used in Fig. 5.1, the perturbation temporally enters the region  $\mathcal{F} < 0$  for  $\lambda_V \gtrsim 1$ . When  $\lambda_V \gg 1$  the minimum value of  $\mathcal{F}$  is largely negative, so it is expected that the strong negative ISW-galaxy cross-correlation occurs.

The observable associated with the ISW-galaxy cross-correlation is given by

$$w^A(\theta) \equiv T_{\text{CMB}} \sum_{l=0}^{\infty} \frac{2l+1}{4\pi} C_l^{\text{IG},A} \mathcal{P}_l(\cos \theta), \quad (5.73)$$

where  $T_{\text{CMB}} = 2.7255 \text{ K}$  and  $\theta$  is the angle characterizing the deviation from the center of galaxy datasets. For the calculation of  $C_l^{\text{IG}}$ , we employ the formula (5.62) derived under the Limber approximation. In Fig. 5.2, we plot  $w^{2\text{MASS}}$  versus  $\theta$  corresponding to 2MASS galaxy surveys for the same model parameters as those adopted in Fig. 5.1 with  $n_s = 0.9649$ ,  $\sigma_8(0) = 0.811$ , and  $h = 0.696$ . In Fig. 5.2, the data points from the 2MASS survey are also shown with error bars. We note that the bias factor has been computed according to the formula (5.70) for the window function (5.40) fitted to the 2MASS survey. The numerical values of  $b_s^{2\text{MASS}}$  for  $\lambda_V = 0.01, 0.1, 1, 10$  are 1.497, 1.487, 1.475, 1.471, respectively, so the bias depends weakly on the model parameters.

For the models with  $\lambda_V < \mathcal{O}(0.1)$  and the  $\Lambda$ CDM model, we have  $w^{2\text{MASS}}(\theta) > 0$  for any angle  $\theta$ , so they can be compatible with the 2MASS data. As we see in Fig. 5.2, the model with  $\lambda_V = 1$  has a marginal positive ISW-galaxy cross-correlation. In this case the perturbation temporally enters the region  $\mathcal{F} < 0$ , but the positive contribution to  $C_l^{\text{IG},2\text{MASS}}$  at high redshifts leads to  $w^{2\text{MASS}}(\theta) > 0$ . For  $\lambda_V = 10$ , the minimum value of  $\mathcal{F}$  is largely negative and hence  $w^{2\text{MASS}}(\theta) < 0$  for any angle  $\theta$ . In Fig. 5.2, we observe that the models with  $\lambda_V \gtrsim 1$  are in tension with the 2MASS data. Thus, we have

shown that the models with the large increase of  $\Sigma$  at low redshifts (such as the cases (c) and (d) in Fig. 5.1) can be strongly constrained from the ISW-galaxy cross-correlation data.

## 5.4 Observational constraints

In this section, we place observational constraints on the model given by the functions (4.140) by employing the ISW-galaxy cross-correlation data from the 2MASS and SDSS surveys [106] as well as other observational data from CMB, BAO, SN Ia,  $H(z)$ , and RSDs. The latter datasets were also used in the likelihood analysis of Ref. [45] to constrain the dark energy model in full GP theories, so we first briefly overview such a statistical method and then explore whether our dark energy model with  $c_T^2 = 1$  can be compatible with all the data including the ISW-galaxy cross-correlation.

### 5.4.1 Priors on the model parameters

The present dark energy model has the following five free parameters:

$$\Omega_{m0}, \quad h, \quad s, \quad p, \quad \lambda_V. \quad (5.74)$$

At the background level, there are three free parameters  $\Omega_{m0}, h, s$ , so we have only one additional quantity  $s$  to those in the  $\Lambda$ CDM model. At the level of perturbations, there are seven free parameters in full GP theories studied in Ref. [45]. Now, we are considering the cubic-order GP theories with  $c_T^2 = 1$ , so this reduces the number of free parameters to six. Moreover we are considering the model with  $q_V = 1$ , so we are left with the five parameters given by Eq. (5.74). We have chosen the parameter  $\lambda_V$  instead of  $\lambda$ , as the former is directly related to the effect of intrinsic vector modes on  $\mu$  and  $\Sigma$ .

In the MCMC simulation, we set the following priors on the parameter space of five model parameters.

- Today's density parameter of non-relativistic matter:  $0.1 \leq \Omega_{m0} \leq 0.5$ .
- The normalized Hubble constant:  $0.6 \leq h \leq 0.8$ .
- The deviation parameter from the  $\Lambda$ CDM model:  $0 < s \leq 1$ .
- The power  $p$ :  $0 < p \leq 25$ .
- The parameter  $\lambda_V$ :  $10^{-13} \leq \lambda_V \leq 15$ .

In addition, we need to take into account the conditions for the absence of ghosts and Laplacian instabilities of scalar perturbations. They are given by

- $Q_S > 0$  and  $c_S^2 > 0$  in the whole cosmological epoch.
- $0 < ps \leq 1$  to avoid the strong coupling at early times, see Eq. (4.178).
- $p(1 + s) \geq 1$  for avoiding the divergence of  $c_S^2$  at early times, see Eq. (4.182).

The other model parameters are known from the five parameters in Eq. (5.74), say,  $p_2 = sp$  and  $p_3 = [p(1 + 2s) - 1]/2$ .

### 5.4.2 Observational data

We briefly explain the likelihood method and observational data used in our MCMC analysis. For more details, we refer the readers to Ref. [45].

#### (A) CMB

To constrain the model from the CMB data, we resort to the following two CMB shift parameters:

$$l_a = \frac{\pi\chi(z_*)}{r_s(z_*)}, \quad \mathcal{R} = \sqrt{\Omega_{m0}}H_0\chi(z_*), \quad (5.75)$$

where  $\chi(z) = \int_0^z H^{-1}(\tilde{z})d\tilde{z}$  is the coming distance, and  $r_s(z) = \int_z^\infty c_s H^{-1}(\tilde{z})d\tilde{z}$  is the coming sound horizon with  $c_s = [3\{1 + 3\rho_{b0}/(4\rho_{\gamma0})(1 + z)^{-1}\}]^{-1/2}$  ( $\rho_{b0}$  and  $\rho_{\gamma0}$  are today's densities of baryons and photons, respectively). In the following, we fix today's baryon density parameter  $\Omega_{b0} = \rho_{b0}/(3M_{\text{pl}}^2 H_0^2)$  to the Planck best-fit value  $\Omega_{b0} = 0.02226$  [51]. For the decoupling redshift  $z_*$ , we employ the fitting formula of Hu and Sugiyama [128].

The mean values of CMB shift parameters constrained from the Planck 2015 data are  $\langle l_a \rangle = 301.77$  and  $\langle \mathcal{R} \rangle = 1.4782$  with the deviations  $\sigma(l_a) = 0.090$  and  $\sigma(\mathcal{R}) = 0.0048$ , respectively [129, 51]. The  $\chi^2$  statistics for these parameters is defined by

$$\chi_{\text{CMB}}^2 = \mathbf{V}^T \mathbf{C}^{-1} \mathbf{V}, \quad (5.76)$$

where  $\mathbf{V}^T \equiv ((l_a - \langle l_a \rangle)/\sigma(l_a), (\mathcal{R} - \langle \mathcal{R} \rangle)/\sigma(\mathcal{R}))$ , and  $\mathbf{C}^{-1}$  is the inverse of the normalized covariance matrix  $\mathbf{C}$ . The components of  $\mathbf{C}$  are given by  $C_{11} = C_{22} = 1$  and  $C_{12} = C_{21} = 0.3996$ .

**(B) BAO**

The observable associated with the BAO measurements is the ratio  $r_{\text{BAO}}(z_j) \equiv r_s(z_d)/D_V(z_j)$  between the sound horizon  $r_s(z_d)$  at the redshift  $z_d$  where baryons are released from the Compton drag of photons and the dilation scale  $D_V(z_j)$  at the observed redshifts  $z_j$ . For the drag redshift  $z_d$ , we use the fitting formula of Eisenstein and Hu [122]. The dilation scale is defined by

$$D_V(z) = [z(1+z)^2 D_A^2(z) H^{-1}(z)]^{1/3}, \quad (5.77)$$

where  $D_A(z) = (1+z)^{-1} \int_0^z H^{-1}(\tilde{z}) d\tilde{z}$  is the angular diameter distance. For given  $N$  data of  $r_{\text{BAO}}(z_j)$  with the error  $\sigma(z_j)$ , the  $\chi^2$  estimator in BAO measurements is given by

$$\chi_{\text{BAO}}^2 = \sum_{j=1}^N \frac{[r_{\text{BAO}}(z_j) - \langle r_{\text{BAO}}(z_j) \rangle]^2}{\sigma^2(z_j)}, \quad (5.78)$$

where  $\langle r_{\text{BAO}}(z_j) \rangle$  is the mean observed value of each data. We exploit the BAO data extracted from the surveys of 6dFGS [52], SDSS-MGS [53], BOSS [54], BOSS CMASS [55], and Wiggle Z [56].

**(C) SN Ia**

The SN Ia has a nearly constant absolute magnitude  $M \simeq -19$  at the peak of brightness. The observed apparent magnitude  $m$  of SNIa is different from its absolute magnitude  $M$ , whose difference is quantified as

$$\mu(z) \equiv m(z) - M = 5 \log_{10} \left[ \frac{d_L(z)}{10 \text{ pc}} \right], \quad (5.79)$$

where  $d_L(z) = (1+z) \int_0^z H^{-1}(\tilde{z}) d\tilde{z}$  is the luminosity distance from the observer to the source at redshift  $z$ . The  $\chi^2$  estimator in SN Ia measurements is defined by

$$\chi_{\text{SNIa}}^2 = \sum_{j=1}^N \frac{[\mu(z_j) - \langle \mu_{\text{obs}}(z_j) \rangle]^2}{\sigma^2(z_j)}, \quad (5.80)$$

where  $N$  is the number of datasets, and  $\langle \mu_{\text{obs}}(z_j) \rangle$  is the mean observed value of  $\mu(z_j)$  with the error  $\sigma(z_j)$ . We use the Union 2.1 datasets [47] for the computation of  $\chi_{\text{SNIa}}^2$ .



### (D) Local measurements of the Hubble expansion rate

The direct measurement of the Hubble constant from the observations of Cepheids placed the bound  $h = 0.7324 \pm 0.0174$  [42]. In addition, the Hubble expansion rate  $H(z)$  at redshift  $z$  can be constrained from the measurement of the ratio  $r_H(z) \equiv r_s(z_d)/H^{-1}(z)$  in BAO measurements. We define the  $\chi^2$  statistics associated with the local measurements of  $H$ , as

$$\chi_H^2 = \frac{(h - 0.7324)^2}{0.0174^2} + \sum_{j=1}^3 \frac{[r_H(z_j) - \langle r_H(z_j) \rangle]^2}{\sigma^2(z_j)}, \quad (5.81)$$

where  $\langle r_H(z_j) \rangle$  is the mean observed value of  $r_H(z_j)$  at redshift  $z_j$  with the error  $\sigma(z_j)$ . We exploit the three data provided by the BOSS measurement [54].

### (E) RSDs

The RSD measurement can constrain the following quantity

$$y(z) \equiv f(z)\sigma_8(z), \quad (5.82)$$

where  $f(z) \equiv \delta'/\delta$  is the linear growth rate of the matter density contrast. To compute  $y(z)$  in our model, we resort to Eq. (5.11) derived under the quasi-static approximation for perturbations deep inside the sound horizon. This equation can be expressed as

$$\delta'' + \frac{1 + (3 + 4s)\Omega_{\text{DE}}}{2(1 + s\Omega_{\text{DE}})}\delta' - \frac{3}{2}\mu(1 - \Omega_{\text{DE}})\delta = 0, \quad (5.83)$$

where  $\mu$  is given by Eq. (5.71) with the scalar propagation speed squared (4.179). In the deep matter era ( $\Omega_{\text{DE}} \ll 1$ ) we have  $\mu \simeq 1$ , so the evolution of  $\delta$  is similar to that in the  $\Lambda$ CDM model. We express  $\delta$  in Fourier space as Eq. (5.38) and choose the initial conditions  $D' = D = e^{\mathcal{N}_i}$  at  $\mathcal{N}_i = -6$ . Since the growth rate  $D(z)$  is known after solving Eq. (5.83), we obtain  $\sigma_8(z) = \sigma_8(0)D(z)/D_0$  and  $y(z)$  by adopting the Planck best-fit value  $\sigma_8(0) = 0.811$  [1].

If there are  $N$  datasets with the mean observed value  $\langle y_{\text{obs}}(z_j) \rangle$  and the error  $\sigma(z_j)$ , the  $\chi^2$  estimator for RSD measurements is defined as

$$\chi_{\text{RSD}}^2 = \sum_{j=1}^N \frac{[y(z_j) - \langle y_{\text{obs}}(z_j) \rangle]^2}{\sigma^2(z_j)}. \quad (5.84)$$

We use the observational data given in Refs. [130, 131, 132, 133, 134, 135, 136, 137, 138] for the computation of  $\chi_{\text{RSD}}^2$ .

### (F) ISW-galaxy cross-correlations

The observable quantity associated with the ISW-galaxy cross-correlation is given by Eq. (5.73). Then, we define the corresponding  $\chi^2$  estimator, as

$$\chi_{\text{IG}}^2 = \sum_A \sum_{j=1}^N \frac{[w^A(\theta_j) - \langle w_{\text{obs}}^A(\theta_j) \rangle]^2}{(\sigma_j^A)^2}, \quad (5.85)$$

where  $N$  is the number of datasets,  $\langle w_{\text{obs}}^A(\theta_j) \rangle$  is the mean observed value of  $w^A(\theta_j)$  with the error  $\sigma_j^A$  on the data, and the subscript “ $A$ ” stands for different galaxy surveys. To calculate  $w^A(\theta_j)$  theoretically, we utilize the cross-correlation power spectrum (5.62) with the Planck 2018 best-fit values  $n_s = 0.9649$  and  $\sigma_8(0) = 0.811$ . For each model parameter, the quantities  $\bar{\delta}_H$  and  $b_s^A$  in Eq. (5.62) are computed according to the formulas (5.68) and (5.70), respectively. For the observational data of  $\langle w_{\text{obs}}^A(\theta_j) \rangle$  and  $\sigma_j^A$ , we choose those of 2MASS and SDSS surveys given in Ref. [106].

### 5.4.3 Likelihood results

We perform the MCMC sampling over the allowed five-dimensional parameter space and compute the following  $\chi^2$  statistics

$$\chi^2 = \chi_{\text{CMB}}^2 + \chi_{\text{BAO}}^2 + \chi_{\text{SNIa}}^2 + \chi_H^2 + \chi_{\text{RSD}}^2 + \chi_{\text{IG}}^2. \quad (5.86)$$

The best-fit model corresponds to the case in which  $\chi^2$  is minimized.

In Fig. 5.3, we show one-dimensional probability distributions for each parameter and two-dimensional observational contours for the combination of the five parameters (5.74). The middle dashed lines in one-dimensional probability distributions represent the best-fit parameters. Considering the background expansion history alone with the data of CMB, BAO, SN Ia, and  $H(z)$ , there exists a global minimum of  $\chi^2$  corresponding to the best-fit values of  $\Omega_{m0}$ ,  $h$ ,  $s$ . In the full MCMC analysis including the RSD and ISW-galaxy cross-correlation data, the global minimum of  $\chi^2$  is not uniquely fixed. In other words, there are several different sets of parameters giving the similar lowest values of  $\chi^2$ . One of examples for such a set of model parameters is given by

$$\Omega_{m0} = 0.301, \quad h = 0.697, \quad s = 0.185, \quad p = 3.078, \quad \lambda_V = 4.370 \times 10^{-8}, \quad (5.87)$$

with the minimal value

$$\chi_{\text{min}}^2 = 618.9. \quad (5.88)$$

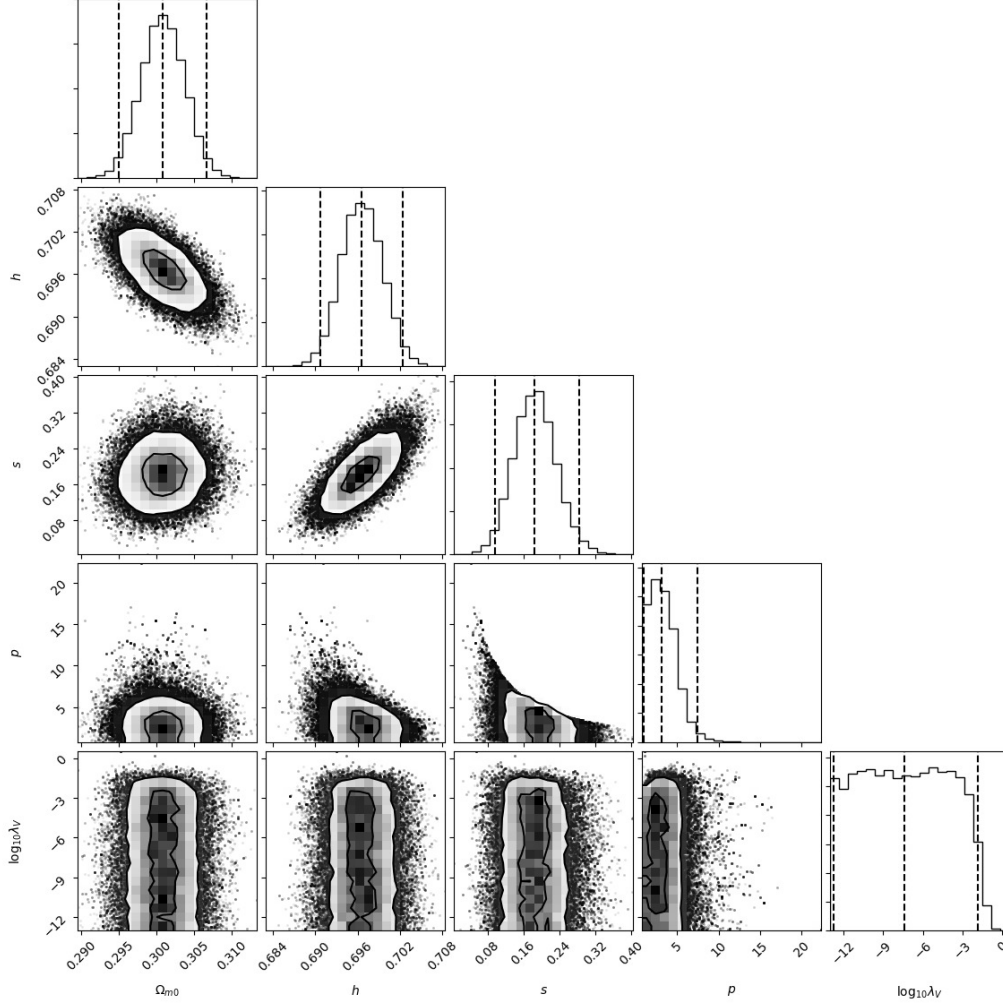


Figure 5.3: Observational bounds on the five model parameters  $\Omega_{m0}$ ,  $h$ ,  $s$ ,  $p$ ,  $\lambda_V$  derived by the joint data analysis of CMB, BAO, SN Ia,  $H_0$ , RSDs, and the ISW-galaxy cross-correlation with the catalogues of 2MASS and SDSS. The vertical dashed lines represent the best fit (central) and the  $2\sigma$  confidence limits (outside). The quantities  $\Omega_{m0}$ ,  $h$ , and  $s$  are tightly constrained from the background expansion history. The parameter  $p$  is bounded from above from the theoretical prior  $ps \leq 1$ . The quantity  $\lambda_V$  is constrained to be  $\lambda_V < 0.015$  from the RSD and ISW-galaxy cross-correlation data.

The  $2\sigma$  bounds corresponding to these parameters are

$$\Omega_{m0} = 0.301^{+0.006}_{-0.006}, \quad h = 0.697^{+0.006}_{-0.006}, \quad s = 0.185^{+0.100}_{-0.089}, \quad (5.89)$$

$$p = 3.078^{+4.317}_{-2.119}, \quad \bar{\lambda}_V \leq \lambda_V < 0.015, \quad (5.90)$$

where  $\bar{\lambda}_V$  is the lower limit of the assumed prior.

The observational bounds on  $\Omega_{m0}$ ,  $h$ , and  $s$  are similar to those derived in Ref. [45] in full GP theories without the ISW-galaxy cross-correlation data. This means that the background expansion history mostly determines the observational constraints on these three parameters. The model with  $s = 0$ , i.e., the  $\Lambda$ CDM model, is outside the  $2\sigma$  likelihood contour, so it is disfavored over the best-fit model with (5.88) in cubic-order GP theories.

We carry out the independent MCMC sampling for the  $\Lambda$ CDM model by varying the two parameters  $\Omega_{m0}$  and  $h$ . We find that the best-fit  $\Lambda$ CDM model corresponds to  $\Omega_{m0} = 0.299$  and  $h = 0.687$  with  $\chi^2_{\Lambda\text{CDM}} = 642.7$ , whose  $\chi^2$  is larger than (5.88). In GP theories, the existence of the additional parameter  $s$  to those in the  $\Lambda$ CDM model can reduce the tensions of the parameters  $h$  and  $\Omega_{m0}$  between CMB and low-redshift measurements. In particular, the normalized Hubble constant  $h$  shifts to the region between the best-fit values of CMB ( $h \simeq 0.67$ ) [1] and local measurements of  $H_0$  ( $h \simeq 0.73$ ) [42].

The observational contour in the two-dimensional  $(p, s)$  plane of Fig. 5.3 is bounded by the prior  $ps \leq 1$  arising from the absence of the strong coupling problem of scalar perturbations in the asymptotic past. Compared to the  $2\sigma$  upper limit  $p < 22.6$  derived in Ref. [45] without imposing the prior  $ps \leq 1$ , the upper bound on  $p$  is now reduced to  $p < 7.4$ .

As we see in the one-dimensional probability distribution of  $\lambda_V$  in Fig. 5.3, the central value of  $\lambda_V$  is not well constrained from the data, but there exists the  $2\sigma$  upper limit  $\lambda_V < 0.015$ . In the limit that  $\lambda_V \rightarrow 0$ , we recover the values  $\mu_{\text{ds}} = \Sigma_{\text{ds}} = 1$  in GR. On using the best-fit parameters  $s = 0.185$  and  $p = 3.078$  with the bound  $\lambda_V < 0.015$ , we obtain the limit  $\mu_{\text{ds}} = \Sigma_{\text{ds}} < 1.011$  from Eq. (5.72). Thus, we have shown that the existence of the intrinsic vector mode can give rise to the values of  $\mu$  and  $\Sigma$  close to those in GR. This behavior does not occur in scalar-tensor theories, as they correspond to the other limit  $\lambda_V \rightarrow \infty$ .

We discuss the dynamics of background and perturbations for the best-fit model given by the parameters (5.87). As we see in the left panel of Fig. 5.4, the best-fit model has the dark energy equation of state  $w_{\text{DE}} = -1.185$  during the matter era, which is followed by the approach to the de Sitter attractor ( $w_{\text{DE}} = -1$ ). This is in stark contrast to the  $\Lambda$ CDM model in which  $w_{\text{DE}}$  is always equivalent to  $-1$ . On the other hand, in the right panel of Fig. 5.4, we

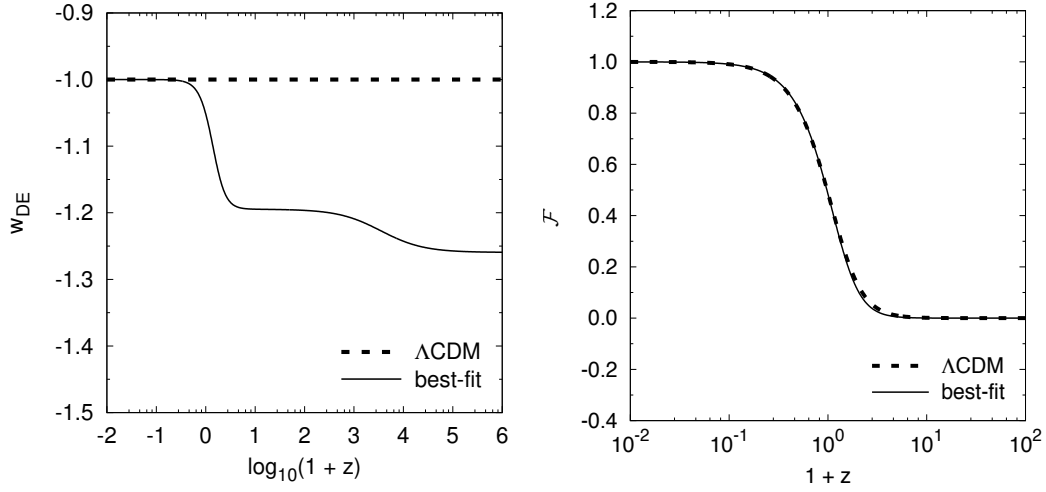


Figure 5.4: (Left) Evolution of  $w_{DE}$  versus  $1+z$  for the best-fit model parameters given by Eq. (5.87) (solid line) and for the  $\Lambda$ CDM model (dashed line). (Right) Evolution of the quantity  $\mathcal{F}$  defined by Eq. (5.59) for the two models corresponding to the left panel. The background dynamics of the best-fit model in GP theories is different from that in  $\Lambda$ CDM model, while the dynamics of perturbations is similar to each other.

find that the evolution of the quantity  $\mathcal{F}$ , which appears in the ISW-galaxy cross-correlation spectrum  $C_l^{IG}$ , is almost identical to that in the  $\Lambda$ CDM model. Indeed, substituting the best-fit values (5.87) into Eq. (5.72), we obtain  $\mu_{ds} - 1 = \Sigma_{ds} - 1 = 3.3 \times 10^{-8}$  and hence both  $\mu$  and  $\Sigma$  are very close to 1 throughout the cosmic expansion history.

In Fig. 5.5, we plot the ISW-galaxy cross-correlation observable  $w^A(\theta)$  associated with two galaxy surveys for the best-fit model parameters (5.87). Again, the theoretical curve in this model, which has the positive cross-correlation, is similar to that in the best-fit  $\Lambda$ CDM model. As we see in the left panel of Fig. 5.5, the best-fit model can fit the 2MASS data quite well. In the SDSS case, the model does not exhibit good fits to the data for  $\theta < 7$  degrees. To increase the values of  $w^{SDSS}(\theta)$  for the compatibility with the data, we require that the quantity  $\Sigma$  is smaller than 1. However, this is not possible for cubic-order GP theories in which  $\Sigma > 1$  under the absence of ghost and Laplacian instabilities. Then, the MCMC likelihood analysis finds the minimum value of  $\chi^2$  with  $\Sigma$  very close to 1. In Fig. 5.2, we observe that the model with  $\lambda_V = 0.1$  looks consistent with the 2MASS ISW-galaxy cross-correlation data. However, the fact that this model is outside the  $2\sigma$  limit  $\lambda_V < 0.015$  means that it is still in tension with the SDSS ISW-galaxy cross-correlation data.

The RSD measurements provide constraints on the dimensionless gravitational coupling  $\mu$ , which is same as  $\Sigma$  in cubic-order GP theories. The RSD

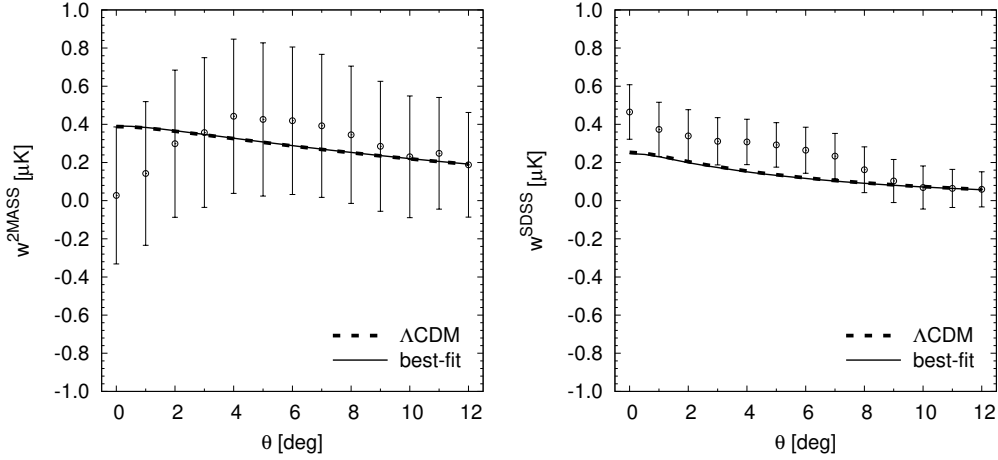


Figure 5.5: The ISW-galaxy cross-correlation observable  $w^A$  versus  $\theta$  for the 2MASS (left) and SDSS (right) surveys for the best-fit model with the parameters (5.87) (solid line) and for the best-fit  $\Lambda$ CDM model (dashed line). We also show the observational data with error bars in each galaxy survey. The cross-correlations predicted by the two models are almost the same as each other.

data [130, 131, 132, 133, 134, 135, 136, 137, 138] tend to favor the cosmic growth rate similar to that in GR or even smaller. Hence the models with  $\mu$  close to 1 are also favored from the RSD measurements. We performed the MCMC simulation without using the ISW-galaxy cross-correlation data and obtained the  $2\sigma$  limit  $\lambda_V < 0.029$ . Since this is weaker than the bound  $\lambda_V < 0.015$  derived by the full likelihood analysis, the ISW-galaxy data provide a more stringent bound on  $\lambda_V$  than that constrained from the RSD data.

For the best-fit model parameters, the powers in the functions  $G_2$  and  $G_3$  are given by  $p_2 = 0.4$  and  $p_3 = 1.0$ . In this case, the coupling  $G_3 = b_3 X^{p_3}$  corresponds to that in the cubic vector Galileon. In scalar-tensor theories, if the cubic Galileon gives the dominant contribution to the dark energy density, this leads to the negative ISW-galaxy cross-correlation incompatible with the observational data [109, 110, 111]. In GP theories, the existence of intrinsic vector modes can make the cubic vector Galileon compatible with the ISW-galaxy cross-correlation data by reducing  $\Sigma$  to the value close to 1. Thus, the dark energy model in GP theories can be observationally distinguished from the corresponding counterpart in scalar-tensor theories.

While  $\chi^2_{\min} = 618.9$  is smaller than  $\chi^2_{\Lambda\text{CDM}} = 642.7$ , our model has more free parameters than those in the  $\Lambda$ CDM model. To make comparison with these two models by taking into account the number of degrees of freedom, we resort to the Akaike information criterion (AIC) [139] and Bayesian in-

formation criterion (BIC) [140]. They are defined, respectively, by

$$\text{AIC} = \chi^2 + 2\mathcal{P}, \quad \text{BIC} = \chi^2 + \mathcal{P} \ln(N_{\text{data}}), \quad (5.91)$$

where  $\mathcal{P}$  is the number of model parameters, and  $N_{\text{data}}$  is the number of data points. For the best-fit model parameters (5.87), we obtain  $\text{AIC} = 628.9$  and  $\text{BIC} = 651.2$ . They are smaller than their best-fit values in the  $\Lambda\text{CDM}$  model:  $\text{AIC} = 646.7$  and  $\text{BIC} = 655.6$ . Thus, even with the AIC and BIC, our model is statistically favored over the  $\Lambda\text{CDM}$  model.

## 5.5 Summary of Chapter 5

In this chapter, we studied the evolution of matter density perturbations. We derived the effective gravitational couplings felt by matter and light under the quasi-static approximation. We found that there is no gravitational slip in the cubic-order GP theories. It means that the effective gravitational coupling felt by matter is the same as that felt by light. Due to the existence of the intrinsic vector modes, the effective gravitational coupling can be similar to that in  $\Lambda\text{CDM}$ . This property leads to the positive sign of the ISW-galaxy cross-correlation, unlike that in scalar Galileon. We also placed the constraint on the vector dark energy model by using the recent observational data. As the results, the model with  $s > 0$  is still favored, then our model can reduce the Hubble tension between high- and low- redshift. Moreover, the observational data statistically prefer the vector dark energy model to  $\Lambda\text{CDM}$ .

# Chapter 6

## Energy transfer between vector dark energy and cold dark matter

In this chapter, we shall study the cosmology of cubic-order GP theories in which a massive vector field is directly coupled to cold dark matter with the energy transfer. At first, we derive the background equations on the flat FLRW space-time and the dark energy equation of state. Due to the existence of the energy exchange between dark components, the continuity equations for dark energy and dark matter have the interacting terms. Then, the evolution of the dark energy equation of state is different from that in the uncoupled case. We also derive conditions for the absence of ghosts and gradient instabilities in the small-scale limit. The stability conditions for tensor and vector perturbations in the small-scale limit are the same as those in the case without the energy transfer, while the conditions for scalar perturbations include the terms associated with the additional interaction. Moreover, we consider a concrete vector dark energy model with the energy transfer. In the model, the additional interaction affects dark energy equation of state during matter era. Then, even if we consider the power-law model with integer powers, we can realize the case in which the dark energy equation of state is closer to  $-1$  as long as cold dark matter partially decays to vector dark energy.

### 6.1 Energy transfer and background equations

We consider the case in which both baryons and radiation are uncoupled to the vector field. On the other hand, we assume that  $A_\mu$  is coupled to cold



dark matter (CDM) with the interacting action

$$S_{\text{ET}} = \int d^4x \sqrt{-g} Q f_1(X) T_c, \quad (6.1)$$

where  $Q$  is a dimensionless coupling constant,  $f_1$  is a function of  $X = -A_\mu A^\mu/2$ , and  $T_c$  is the trace of CDM energy-momentum tensor  $(T_c)^\mu{}_\mu$ . Note that the energy-momentum tensor of each matter component is given by the form as Eq. (4.38). We focus on the case in which the CDM pressure vanishes, i.e.,

$$P_c = 0, \quad (6.2)$$

then the interacting action (6.1) reduces to

$$S_{\text{ET}} = - \int d^4x \sqrt{-g} Q f_1(X) \rho_c(n_c). \quad (6.3)$$

For our purpose, we consider the total action given by

$$S = S_{\text{CGP}} + S_M + S_{\text{ET}}, \quad (6.4)$$

where  $S_{\text{CGP}}$  is the action of cubic-order generalized Proca theories given by Eq. (4.102). For the matter action  $S_M$ , we consider the perfect fluids of CDM, baryons, and radiation, which are labelled by  $I = c, b, r$ , respectively. The perfect fluids can be described by the Schutz-Sorkin action,

$$S_M = - \sum_{I=c,b,r} \int d^4x \left[ \sqrt{-g} \rho_I(n_I) + J_I^\mu (\partial_\mu \ell_I + \mathcal{A}_{I1} \partial_\mu \mathcal{B}_{I1} + \mathcal{A}_{I2} \partial_\mu \mathcal{B}_{I2}) \right]. \quad (6.5)$$

Note that the action (6.5) is the same form as Eq. (4.35), and non-relativistic matter in Eq. (4.35) is decomposed as CDM and baryons in Eq. (6.5).

### 6.1.1 Equations of motion

Variation the action (6.4) with respect to  $\ell_I$  leads to

$$\partial_\mu J_I^\mu = 0, \quad (6.6)$$

which holds for each  $I = c, b, r$ . Since the fluid four-velocity in its rest frame is given by Eq. (4.43) and then Eq. (4.37) leads to Eq. (4.44), we obtain

$$\mathcal{N}_I \equiv J_I^0 = n_I a^3 = \text{constant}, \quad (6.7)$$

which means that the particle number  $\mathcal{N}_I$  is still conserved. In other words, the number density of each matter species (including CDM) obeys

$$\dot{n}_I + 3Hn_I = 0, \quad \text{for } I = c, b, r, \quad (6.8)$$

even if the additional interaction (6.3) exists.

We vary the action (6.4) with respect to  $J_I^\mu$  by keeping in mind that the interaction action (6.3) has the dependence of  $J_c^\mu$ . After that, employing the relation  $\partial n_I / \partial J_I^\mu = J_{I\mu} / (n_I g)$ , we obtain

$$\partial_\mu \ell_I + \mathcal{A}_{I1} \partial_\mu \mathcal{B}_{I1} + \mathcal{A}_{I2} \partial_\mu \mathcal{B}_{I2} = u_{I\mu} \rho_{I,n_I}, \quad \text{for } I = b, r, \quad (6.9)$$

$$\partial_\mu \ell_c + \mathcal{A}_{c1} \partial_\mu \mathcal{B}_{c1} + \mathcal{A}_{c2} \partial_\mu \mathcal{B}_{c2} = u_{c\mu} \rho_{c,n_c} [1 + Qf_1]. \quad (6.10)$$

Eqs. (6.9) for baryons and radiation are the same form as Eq. (4.41), while Eq. (6.10) for CDM has an additional term which is related to the coupling constant  $Q$ .

On using Eqs. (4.39), (6.8) and the property  $\dot{\rho}_I(n) = \rho_{I,n} \dot{n}$ , the energy density  $\rho_I(n_I)$  of each matter component obeys

$$\dot{\rho}_I + 3H(\rho_I + P_I) = 0. \quad (6.11)$$

We consider the case in which the pressures of baryons and radiation satisfy

$$P_b = 0, \quad P_r = \rho_r/3, \quad (6.12)$$

respectively, with the vanishing CDM pressure (6.2). Then, the energy densities of three matter components obey

$$\dot{\rho}_c + 3H\rho_c = 0. \quad (6.13)$$

$$\dot{\rho}_b + 3H\rho_b = 0, \quad (6.14)$$

$$\dot{\rho}_r + 4H\rho_r = 0, \quad (6.15)$$

Varying the action (6.4) with respect to the (00) and (ii) components of metric  $g_{\mu\nu}$ , it follows that

$$3M_{\text{pl}}^2 H^2 = -G_2 + (1 + Qf_1) \rho_c + \rho_b + \rho_r, \quad (6.16)$$

$$M_{\text{pl}}^2 (2\dot{H} + 3H^2) = -G_2 + G_{3,X} \phi^2 \dot{\phi} - \frac{1}{3} \rho_r, \quad (6.17)$$

Also, taking the variation of the action (5.4) with respect to  $\phi$ , we obtain the following equation of motion

$$\phi (G_{2,X} + 3G_{3,X} H \phi - Qf_{1,X} \rho_c) = 0, \quad (6.18)$$

Since we focus on the case  $\phi \neq 0$ , then Eq. (6.18) reduces to

$$G_{2,X} + 3G_{3,X}H\phi - Qf_{1,X}\rho_c = 0. \quad (6.19)$$

Taking the limit  $Q \rightarrow 0$ , Eqs. (6.16) and (6.18) reduce to Eqs. (4.103) and (4.105), respectively. On the other hand, since we focus on the case that CDM has no pressure, Eq. (6.17) is the same form as Eq. (4.104) with Eqs. (6.2) and (6.12).

We define the energy density of CDM containing the effect of interactions with the vector field, such that

$$\tilde{\rho}_c \equiv (1 + Qf_1)\rho_c. \quad (6.20)$$

On using Eq. (6.13), we find that  $\tilde{\rho}_c$  obeys the differential equation:

$$\dot{\tilde{\rho}}_c + 3H\tilde{\rho}_c = \frac{Qf_{1,X}\phi\dot{\phi}}{1 + Qf_1}\tilde{\rho}_c. \quad (6.21)$$

While the CDM particle number is conserved for the energy density  $\rho_c$ , this is not the case for  $\tilde{\rho}_c$  due to the interaction with the vector field appearing on the right hand side of Eq. (6.21).

We also define the energy density  $\rho_{\text{DE}}$  and pressure  $P_{\text{DE}}$  of dark energy (arising from the vector field), as

$$\rho_{\text{DE}} = -G_2, \quad (6.22)$$

$$P_{\text{DE}} = G_2 - G_{3,X}\phi^2\dot{\phi}, \quad (6.23)$$

with the equation of state

$$w_{\text{DE}} \equiv \frac{P_{\text{DE}}}{\rho_{\text{DE}}} = -1 + \frac{G_{3,X}\phi^2\dot{\phi}}{G_2}. \quad (6.24)$$

Taking the time derivative of Eq. (6.22) and using Eqs. (6.19) and (6.23), it follows that

$$\dot{\rho}_{\text{DE}} + 3H(\rho_{\text{DE}} + P_{\text{DE}}) = -\frac{Qf_{1,X}\phi\dot{\phi}}{1 + Qf_1}\tilde{\rho}_c. \quad (6.25)$$

Comparing Eq. (6.21) with Eq. (6.25), it is clear that the vector field and CDM interact with each other through the couplings with opposite signs. Also, this means that  $\tilde{\rho}_c$  is regarded as the physical energy density of CDM rather than  $\rho_c$ .

## 6.2 Conditions for avoiding ghosts and gradient instabilities

In this section, we derive conditions for the absence of ghosts and Laplacian instabilities in the small-scale limit. For this purpose, we consider the perturbed line element given by (4.33) and the perturbations of a Proca field given by (4.58).

For matter sector, we take the same way as that in Sec. 4.3.1, and we decompose non-relativistic matter as CDM and baryons. Then, the vector field  $J_I^\mu$  and the spatial component of four-velocity  $u_{I\mu}$  can be expressed in the form,

$$J_I^0 = \mathcal{N}_I + \delta J_I, \quad J_I^i = \frac{1}{a^2} \delta^{ij} (\partial_j \delta J_I + W_{Ij}), \quad (6.26)$$

$$u_{Ii} = -\partial_i v_I + v_{Ii}, \quad (6.27)$$

for  $I = c, b, r$ , where  $\mathcal{N}_I$  is the background particle number of each matter species given by Eq. (6.7),  $\delta J_I$  and  $\delta J_I$  are scalar perturbations,  $v_I$  is the scalar velocity potential,  $W_{Ij}$  and  $v_{Ii}$  are the vector perturbations satisfying the transverse conditions

$$\partial^j W_{Ij} = 0. \quad (6.28)$$

$$\partial^i v_{Ii} = 0, \quad (6.29)$$

which hold for  $I = c, b, r$ . Also, for the Lagrange multiplier  $\mathcal{A}_{I1}$ ,  $\mathcal{A}_{I2}$ ,  $\mathcal{B}_{I1}$ ,  $\mathcal{B}_{I2}$  in the matter action (6.5), these depend on the cosmic time  $t$  and one direction  $z$  as the forms given by Eqs. (4.77) and (4.78).

In this case, the temporal components of Eqs. (6.9) and (6.10) are given, respectively, by

$$\dot{\ell}_I = -\rho_{I,n_I}, \quad \text{for } I = b, r, \quad (6.30)$$

$$\dot{\ell}_c = -[1 + Qf_1] \rho_{c,n_c}. \quad (6.31)$$

On the other hands, the spatial components of Eqs. (6.9) and (6.10) reduce to, respectively,

$$\partial_i \ell_I + \mathcal{A}_{I1} \partial_i \mathcal{B}_{I1} + \mathcal{A}_{I2} \partial_i \mathcal{B}_{I2} = u_{Ii} \rho_{I,n_c}, \quad \text{for } I = b, r, \quad (6.32)$$

$$\partial_i \ell_c + \mathcal{A}_{c1} \partial_i \mathcal{B}_{c1} + \mathcal{A}_{c2} \partial_i \mathcal{B}_{c2} = u_{ci} \rho_{c,n_c} [1 + Qf_1]. \quad (6.33)$$

Substituting (6.27) into Eqs. (6.32) and (6.33), it follows that

$$\partial_i \ell_c + \mathcal{A}_{c1} \partial_i \mathcal{B}_{c1} + \mathcal{A}_{c2} \partial_i \mathcal{B}_{c2} = -[1 + Qf_1(t)] \rho_{c,n_c} \partial_i v_c + [1 + Qf_1(t)] \rho_{c,n_c} v_{ci}, \quad (6.34)$$

up to linear order in perturbations. We note that the coefficients in front of the perturbed quantities in Eq. (6.34) are time-dependent background quantities. Decomposing Eq. (6.34) as the rotational-free scalar part and the divergence-free vector part, then we obtain the following relations,

$$\partial_i \ell_c = -[1 + Qf_1(t)] \rho_{c,n_c} \partial_i v_c \quad (6.35)$$

$$\mathcal{A}_{c1} \partial_i \mathcal{B}_{c1} + \mathcal{A}_{c2} \partial_i \mathcal{B}_{c2} = [1 + Qf_1(t)] \rho_{c,n_c} v_{ci}, \quad (6.36)$$

for CDM. The integrated solution to Eq. (6.35) is  $\ell_c = \bar{C}_c(t) - [1 + Qf_1(t)] \rho_{c,n_c} v_c$ . Here, the time-dependent function  $\bar{C}_c(t)$  is determined by the  $\mu = 0$  component of Eq. (6.10), as  $\bar{C}_c(t) = -\int^t [1 + Qf_1(\tilde{t})] \rho_{c,n_c}(\tilde{t}) d\tilde{t}$ . In doing so, the scalar quantity  $\ell_I$  is given by

$$\ell_c = -\int^t [1 + Qf_1(\tilde{t})] \rho_{c,n_c}(\tilde{t}) d\tilde{t} - [1 + Qf_1(t)] \rho_{c,n_c} v_c, \quad (6.37)$$

which contains the velocity potential  $v_c$  and the terms related to the additional interaction (6.3) like  $Qf_1$ . Also, substituting Eqs. (4.77)-(4.78) into Eq. (6.36) and expanding the resulting equation up to linear order, we obtain the relation

$$\delta \mathcal{A}_{ci} = [1 + Qf_1(t)] \rho_{c,n_c} v_{ci}. \quad (6.38)$$

For baryons and radiation, by following the same procedure, we obtain the relations analogous to Eqs. (6.37) and (6.38), respectively, as

$$\ell_I = -\int^t \rho_{I,n_I}(\tilde{t}) d\tilde{t} - \rho_{I,n_I} v_I, \quad (6.39)$$

$$\delta \mathcal{A}_{Ii} = \rho_{I,n_I} v_{Ii}, \quad (6.40)$$

with  $I = b, r$ . These are the same as those in uncoupled case given by Eqs. (4.75) and (4.79).

### 6.2.1 Tensor and vector perturbations

The tensor perturbation is expressed in terms of the sum of two polarization modes, as  $h_{ij} = h_+ e_{ij}^+ + h_\times e_{ij}^\times$ . In Fourier space with the comoving wavenumber  $\mathbf{k}$ , the unit bases  $e_{ij}^+$  and  $e_{ij}^\times$  satisfy the normalizations (4.81).

Along the same procedure as Sec. 4.3.2, expanding the action (6.4) up to second order in  $h_{ij}$  and using the background Eq. (6.17), then we obtain the second-order action of tensor perturbations given by

$$S_T^{(2)} = \sum_{\lambda=+,\times} \int dt d^3x a^3 \frac{q_T}{8} \left[ \dot{h}_\lambda^2 - \frac{c_T^2}{a^2} (\partial h_\lambda)^2 \right], \quad (6.41)$$

where

$$q_T = M_{\text{pl}}^2, \quad c_T^2 = 1. \quad (6.42)$$

The action (6.41) is the same as that in general relativity. Hence the propagation of tensor perturbations is not modified by the non-vanishing coupling  $Q$ . Since the speed  $c_T$  of gravitational waves is equivalent to 1, the coupled dark energy theories given by (6.4) are consistent with the bound (3.49) arising from the GW170817 event [92].

As for vector perturbations, we first expand the actions (6.5) and (6.3) up to second order. The resulting quadratic-order actions are given, respectively, by

$$(S_M^{(2)})_V = \int dt d^3x \sum_{I=c,b,r} \sum_{i=1}^2 \left[ \frac{1}{2a^2} \left\{ \frac{\rho_{I,n_I}}{\mathcal{N}_I} (W_{Ii} + \mathcal{N}_I V_i)^2 - a^3 \rho_I V_i^2 \right\} \right. \\ \left. - \mathcal{N}_I \delta \mathcal{A}_{Ii} \delta \dot{\mathcal{B}}_{Ii} - \frac{1}{a^2} W_{Ii} \delta \mathcal{A}_{Ii} \right], \quad (6.43)$$

$$(S_{\text{ET}}^{(2)})_V = \int dt d^3x \sum_{i=1}^2 Q \left[ \frac{f_1}{2a^2} \left\{ \frac{\rho_{c,n_c}}{\mathcal{N}_c} (W_{ci} + \mathcal{N}_c V_i)^2 - a^3 \rho_c V_i^2 \right\} \right. \\ \left. + \frac{a f_{1,X} \rho_c}{2} (E_i + 2\phi V_i) E_i \right]. \quad (6.44)$$

where Eq. (6.43) is the same form as Eq. (4.87). Varying the action  $(S_M^{(2)})_V + (S_{\text{ET}}^{(2)})_V$  with respect to  $W_{Ii}$  and using Eqs. (6.38) and (6.40), it follows that

$$W_{Ii} = \mathcal{N}_i (v_{Ii} - V_i), \quad (6.45)$$

which hold for  $I = c, b, r$ . We note that the relations (6.45) also follow from Eq. (6.27) and the property  $n_I \sqrt{-g} u_{Ii} = J_{Ii} = \mathcal{N}_I V_i + W_{Ii}$  for vector perturbations up to linear order. Substituting the relation (6.45) into Eqs. (6.43)-(6.44) and varying  $(S_M^{(2)})_V + (S_{\text{ET}}^{(2)})_V$  with respect to  $v_{Ii}$  and  $\delta \mathcal{B}_{Ii}$ , we obtain

$$v_{Ii} = V_i - a^2 \delta \dot{\mathcal{B}}_{Ii}, \quad (6.46)$$

$$\delta \mathcal{A}_{Ii} = C_{Ii}, \quad (6.47)$$

where  $C_{Ii}$  are constants in time.

After integrating out the perturbations  $W_{Ii}$  and  $\delta \mathcal{A}_{Ii}$ , the resulting second-

order action in the matter sector yields

$$(S_M^{(2)})_V + (S_{\text{ET}}^{(2)})_V = \int dt d^3x \frac{a}{2} \sum_{i=1}^2 \left[ \sum_{I=b,r,c} (n_I \rho_{I,n_I} v_{Ii}^2 - \rho_I V_i^2) + Q \{ (n_c \rho_{c,n_c} v_{ci}^2 - \rho_c V_i^2) f_1 + \rho_c f_{1,X} E_i (2\phi V_i + E_i) \} \right]. \quad (6.48)$$

Eq. (6.48) has the terms related to the coupling constant  $Q$ . Taking the limit  $Q \rightarrow 0$ , Eq. (6.48) reduces to Eq. (4.87) which is the second-order matter action in uncoupled case.

We now expand the action (6.4) up to second order in vector perturbations. Then, the total quadratic-order action for vector perturbations yields

$$S_V^{(2)} = \int dt d^3x \sum_{i=1}^2 \frac{a}{2} \left[ q_V \dot{Y}_i^2 - \frac{q_V}{a^2} (\partial Y_i)^2 - G_{3,X} \dot{\phi} Y_i^2 + \frac{q_T}{2a^2} (\partial V_i)^2 + \rho_b v_{bi}^2 + \frac{4}{3} \rho_r v_{ri}^2 + (1 + Q f_1) \rho_c v_{ci}^2 \right], \quad (6.49)$$

where

$$q_V \equiv G_{2,F}. \quad (6.50)$$

Varying the action (6.49) with respect to  $V_i$  in Fourier space with the comoving wavenumber  $k = |\mathbf{k}|$ , we obtain

$$\frac{q_T}{2} a k^2 V_i = -(\mathcal{N}_b C_{bi} + \mathcal{N}_r C_{ri} + \mathcal{N}_c C_{ci}), \quad (6.51)$$

which can be used to eliminate the fourth term in Eq. (6.49). Taking the small-scale limit ( $k \rightarrow \infty$ ), the action (6.49) reduces to

$$S_V^{(2)} \simeq \sum_{i=1}^2 \int dt d^3x \frac{a}{2} q_V \left[ \dot{Y}_i^2 + c_V^2 \frac{k^2}{a^2} Y_i^2 \right], \quad (6.52)$$

where

$$c_V^2 = 1. \quad (6.53)$$

The two dynamical fields  $Y_1$  and  $Y_2$  propagate with the speed  $c_V$  equivalent to 1, so there are no Laplacian instabilities of vector perturbations. The no-ghost condition corresponds to  $q_V > 0$ , i.e.,

$$G_{2,F} > 0. \quad (6.54)$$

From the above discussion, it is clear that the coupling  $Q$  does not affect the stability conditions of vector perturbations in the small-scale limit.

### 6.2.2 Scalar perturbations

To study the propagation of scalar perturbations, as the same way in Sec. 4.3.4, we define the density perturbation  $\delta\rho_I$  of each matter fluid ( $I = c, b, r$ ), as

$$\delta\rho_I \equiv \frac{\rho_{I,n_I}}{a^3} \delta J_I. \quad (6.55)$$

Then, we can express the perturbation of number density  $n_I$  up to quadratic-order as

$$\delta n_I = \frac{\delta\rho_I}{\rho_{I,n_I}} - \frac{(\mathcal{N}_I \partial B + \partial \delta j_I)^2}{2\mathcal{N}_I a^5}, \quad (6.56)$$

which hold for  $I = c, b, r$ .

Expanding  $S_M + S_{\text{ET}}$  up to second order in scalar perturbations and varying the resulting quadratic-order action with respect to  $\delta j_I$ , we obtain the relations

$$\partial \delta j_I = -\mathcal{N}_I (\partial B + \partial v_I), \quad \text{for } I = c, b, r, \quad (6.57)$$

which can be used to eliminate the non-dynamical fields  $\delta j_I$  from the matter action. The propagation speed squares of matter perfect fluids are defined as

$$c_I^2 = \frac{n_I \rho_{I,n_I n_I}}{\rho_{I,n_I}}, \quad (6.58)$$

with  $I = c, b, r$ . We consider the case in which  $c_I^2$  for CDM, baryons, and radiations are given, respectively, by

$$c_c^2 = +0, \quad c_b^2 = +0, \quad c_r^2 = \frac{1}{3}. \quad (6.59)$$

Expanding the total action (6.4) up to second order in scalar perturbations and using the background Eqs. (6.16)-(6.18), the second-order action arising from (6.4) reads <sup>1</sup>

$$S_S^{(2)} = S_{Q=0}^{(2)} + S_Q^{(2)}, \quad (6.60)$$

---

<sup>1</sup>Here, since we would like to separate the terms related to the coupling constant  $Q$  from the others, the second-order action is written by using  $\rho_c$  which is corresponded to CDM with the number density conservation. One can rewrite this action in terms of  $\tilde{\rho}_c$  as needed.



where

$$\begin{aligned}
S_{Q=0}^{(2)} = & \int dt d^3x a^3 \left\{ \sum_{I=m,r} \left\{ \left[ n_I \rho_{I,n_I} \frac{\partial^2 B}{a^2} - \dot{\delta\rho}_I - 3H (1 + c_I^2) \delta\rho_I \right] v_I \right. \right. \\
& - \frac{n_I \rho_{I,n_I}}{2} \frac{(\partial v_I)^2}{a^2} - \frac{c_I^2}{2n_I \rho_{I,n_I}} (\delta\rho_I)^2 - \alpha \delta\rho_I \left. \right\} - w_3 \frac{(\partial\alpha)^2}{a^2} + w_4 \alpha^2 \\
& - \left[ (3Hw_1 - 2w_4) \frac{\delta\phi}{\phi} - w_3 \frac{\partial^2(\delta\phi)}{a^2\phi} - w_3 \frac{\partial^2\dot{\psi}}{a^2\phi} + w_6 \frac{\partial^2\psi}{a^2} \right] \alpha \\
& - \frac{w_3}{4} \frac{(\partial\delta\phi)^2}{a^2\phi^2} + w_5 \frac{(\delta\phi)^2}{\phi^2} - \left[ \frac{(w_6\phi + w_2)\psi}{2} - \frac{w_3}{2} \dot{\psi} \right] \frac{\partial^2(\delta\phi)}{a^2\phi^2} \\
& - \frac{w_3}{4\phi^2} \frac{(\partial\dot{\psi})^2}{a^2} + \frac{w_7}{2} \frac{(\partial\psi)^2}{a^2} + \left( w_1\alpha + \frac{w_2\delta\phi}{\phi} \right) \frac{\partial^2 B}{a^2} \left. \right\}, \quad (6.61)
\end{aligned}$$

and

$$\begin{aligned}
S_Q^{(2)} = & \int dt d^3x a^3 Q \left[ \left( n_c \rho_{c,n_c} \frac{\partial^2 B}{a^2} - \dot{\delta\rho}_c - 3H \delta\rho_c \right) f_1 v_c - \frac{n_c \rho_{c,n_c} f_1}{2} \frac{(\partial v_c)^2}{a^2} \right. \\
& \left. - (f_1 + f_{1,X} \phi^2) \alpha \delta\rho_c - f_{1,X} \phi \delta\phi \delta\rho_c - \frac{1}{2} f_{1,XX} \phi^2 \rho_c (\phi\alpha + \delta\phi)^2 \right], \quad (6.62)
\end{aligned}$$

where the functions  $w_i$  ( $i = 1, 2, \dots, 7$ ) in Eq. (6.61) are the same as that given by Eqs. (4.114)-(4.120). Hence, the action  $S_{Q=0}^{(2)}$  coincides with Eq. (4.113) in uncoupled case. The coupling  $Q$  gives rise to the additional action  $S_Q^{(2)}$  to  $S_{Q=0}^{(2)}$ .

Varying (6.60) with respect to the non-dynamical fields  $\alpha$ ,  $B$ ,  $\delta\phi$ ,  $v_c$ ,  $v_b$ , and  $v_r$  in Fourier space, respectively, it follows that

$$\begin{aligned}
& \sum_{I=c,b,r} \delta\rho_I - 2w_4\alpha + (3Hw_1 - 2w_4) \frac{\delta\phi}{\phi} + \frac{k^2}{a^2} (\mathcal{Y} + w_1 B - w_6 \psi) \\
& = -Q(f_1 + f_{1,X} \phi^2) \delta\rho_c - Q f_{1,XX} \phi^3 \rho_c (\phi\alpha + \delta\phi), \quad (6.63)
\end{aligned}$$

$$\sum_{I=c,b,r} (\rho_I + P_I) v_I + w_1\alpha + w_2 \frac{\delta\phi}{\phi} = -n_c \rho_{c,n_c} Q f_1 v_c, \quad (6.64)$$

$$\begin{aligned}
& (3Hw_1 - 2w_4) \alpha - 2w_5 \frac{\delta\phi}{\phi} + \frac{k^2}{a^2} \left[ \frac{1}{2} \mathcal{Y} + w_2 B - \frac{1}{2} \left( \frac{w_2}{\phi} + w_6 \right) \psi \right] \\
& = -Q f_{1,X} \phi^2 \delta\rho_c - Q f_{1,XX} \phi^3 \rho_c (\phi\alpha + \delta\phi), \quad (6.65)
\end{aligned}$$

$$\delta\dot{\rho}_I + 3H(1 + c_I^2)\delta\rho_I + \frac{k^2}{a^2}(\rho_I + P_I)(B + v_I) = 0, \quad \text{for } I = c, b, r, \quad (6.66)$$

where the quantity  $\mathcal{Y}$  is defined by Eq. (4.125). Taking the limit  $Q \rightarrow 0$ , the right hand sides of Eqs. (6.63)-(6.65) are vanished, then these equations reduce to Eq. (4.121)-(4.123), respectively.

The dynamical perturbations correspond to the four fields  $\psi$  and  $\delta\rho_I$  ( $I = c, b, r$ ). Solving Eqs. (6.63)-(6.66) for  $\alpha$ ,  $B$ ,  $\delta\phi$ ,  $v_c$ ,  $v_b$ ,  $v_r$  and substituting them into Eq. (6.60), the second-order action in Fourier space is expressed in the form

$$S_S^{(2)} = \int dt d^3x a^3 \left( \dot{\vec{\mathcal{X}}}^t \mathbf{K} \dot{\vec{\mathcal{X}}} - \frac{k^2}{a^2} \vec{\mathcal{X}}^t \mathbf{G} \vec{\mathcal{X}} - \vec{\mathcal{X}}^t \mathbf{M} \vec{\mathcal{X}} - \vec{\mathcal{X}}^t \mathbf{B} \dot{\vec{\mathcal{X}}} \right), \quad (6.67)$$

where  $\mathbf{K}$ ,  $\mathbf{G}$ ,  $\mathbf{M}$  and  $\mathbf{B}$  are  $4 \times 4$  matrices, and the vector field  $\vec{\mathcal{X}}^t$  is given by

$$\vec{\mathcal{X}}^t \equiv (\psi, \delta\rho_c/k, \delta\rho_b/k, \delta\rho_r/k). \quad (6.68)$$

Neither  $\mathbf{M}$  nor  $\mathbf{B}$  contains the  $k^2/a^2$  term. If there are the terms including the  $k^2/a^2$  dependence in  $\mathbf{B}$ , it can be absorbed into  $\mathbf{G}$  after the integration by parts. Taking the small-scale limit, the non-vanishing matrix components are

$$K_{11} = \frac{H^2 M_{\text{pl}}^2 (3w_1^2 + 4M_{\text{pl}}^2 w_4 - 2Q\rho_c M_{\text{pl}}^2 f_{1,XX} \phi^4)}{\phi^2 (w_1 - 2w_2)^2}, \quad (6.69)$$

$$K_{22} = \frac{a^2(1 + Qf_1)}{2n_c \rho_{c,n_c}}, \quad K_{33} = \frac{a^2}{2n_b \rho_{b,n_b}}, \quad K_{44} = \frac{a^2}{2n_r \rho_{r,n_r}}, \quad (6.70)$$

and

$$G_{11} = \mathcal{G} + \dot{\mu} + H\mu - \frac{w_2^2}{2(w_1 - 2w_2)^2 \phi^2} [n_c \rho_{c,n_c} (1 + Qf_1) + n_b \rho_{b,n_b} + n_r \rho_{r,n_r}], \quad (6.71)$$

$$G_{22} = 0, \quad G_{33} = 0, \quad G_{44} = \frac{a^2 c_r^2}{2n_r \rho_{r,n_r}}, \quad (6.72)$$

where

$$\mathcal{G} \equiv -\frac{4H^2 M_{\text{pl}}^4 w_2^2}{\phi^2 w_3 (w_1 - 2w_2)^2} - \frac{\dot{\phi}}{2\phi^3} w_2, \quad \mu \equiv \frac{H M_{\text{pl}}^2 w_2}{\phi^2 (w_1 - 2w_2)}. \quad (6.73)$$

The scalar ghosts are absent for  $K_{11} > 0$ ,  $K_{22} > 0$ ,  $K_{33} > 0$ , and  $K_{44} > 0$ . Since  $n_b \rho_{b,n_b} = \rho_b > 0$  and  $n_r \rho_{r,n_r} = 4\rho_r/3 > 0$ , the last two conditions trivially hold. The first condition is satisfied for

$$q_S \equiv 3w_1^2 + 4M_{\text{pl}}^2 w_4 - 2Q\rho_c M_{\text{pl}}^2 f_{1,XX} \phi^4 > 0. \quad (6.74)$$

Since  $n_c \rho_{c,n_c} = \rho_c > 0$ , the second condition translates to

$$q_c \equiv 1 + Qf_1 > 0. \quad (6.75)$$

For negative value of  $Qf_1$ , this gives the upper bound on  $|Qf_1|$ .

In the large  $k$  limit, the second-order action (6.60) gives rise to the dispersion relation

$$\det \left( \omega^2 \mathbf{K} - \frac{k^2}{a^2} \mathbf{G} \right) = 0, \quad (6.76)$$

with the frequency  $\omega$ . The scalar propagation speed  $c_s$  is defined as  $c_s^2 = \omega^2 a^2 / k^2$ . The propagation speed squared associated with the perturbation  $\psi$  is given by  $c_s^2 = G_{11}/K_{11}$ . To avoid the Laplacian instability, we require that

$$c_s^2 = \frac{1}{K_{11}} \left[ \mathcal{G} + \dot{\mu} + H\mu - \frac{w_2^2}{2(w_1 - 2w_2)^2 \phi^2} \left\{ \rho_c (1 + Qf_1) + \rho_b + \frac{4}{3} \rho_r \right\} \right] \geq 0. \quad (6.77)$$

The matter propagation speed squares, which correspond to the ratios  $G_{22}/K_{22}$ ,  $G_{33}/K_{33}$ ,  $G_{44}/K_{44}$  for CDM, baryons, and radiations respectively, reduce to  $c_c^2 = 0$ ,  $c_b^2 = 0$ , and  $c_r^2 = 1/3$ . Hence there are no Laplacian instabilities for the three matter perfect fluids.

The CDM perturbation  $\delta\rho_c$  is associated with the perturbation of number-density dependent quantity  $\rho_c(n_c)$ , which is not identical to the perturbation  $\delta\tilde{\rho}_c$  absorbing the contribution of coupling  $Qf_1$  (related to the background CDM density  $\tilde{\rho}_c = [1 + Qf_1]\rho_c$ ). In Eqs. (6.63) and (6.65), however, we observe that  $\delta\rho_c$  is coupled to the scalar perturbation  $\psi$  arising from the vector field. Indeed, the effect of coupling appears in the expressions of  $q_s$  and  $c_s^2$  derived above. Unlike the background CDM density  $\rho_c$  obeying Eq. (6.13), the interaction between  $\delta\rho_c$  and  $\psi$  manifests itself at the level of linear perturbations.

## 6.3 Concrete model with energy transfer

In this section, we propose a concrete coupled vector dark energy model and study the background cosmological dynamics by paying particular attention to the evolution of  $w_{\text{DE}}$ . Let us consider the model given by the functions

$$G_2(X, F) = b_2 X + F, \quad G_3(X) = b_3 X^{p_3}, \quad f_1(X) = \left( \frac{X}{M_{\text{pl}}^2} \right)^q, \quad (6.78)$$

where  $b_2$ ,  $b_3$ ,  $p_3$ , and  $q$  are constants. Since  $G_{2,F} = 1$  in this model, the no-ghost condition (6.54) of vector perturbations is automatically satisfied.

For the functions (6.78), Eq. (6.19) reduces to

$$b_2 + 3 \cdot 2^{1-p_3} b_3 p_3 H \phi^{2p_3-1} - Qq \cdot 2^{1-q} M_{\text{pl}}^{-2q} \rho_c \phi^{2(q-1)} = 0. \quad (6.79)$$

For  $Q = 0$ , there is the solution where  $\phi$  solely depends on  $H$ , such that  $\phi \propto H^{-1/(2p_3-1)}$ . As long as the energy density of  $A_\mu$  is subdominant to that of background fluids during the radiation and matter eras, the Hubble parameter evolves as  $H \propto 1/t$  and hence the temporal vector component grows as  $\phi \propto t^{1/(2p_3-1)}$  for  $p_3 > 1/2$ . Finally, the solutions approach stable de Sitter attractors characterized by constant  $\phi$  [44].

For  $Q \neq 0$ , we would like to focus on the case where the third term in Eq. (6.79) is subdominant to the constant  $b_2$  in the radiation era and temporally approaches a constant after the onset of matter dominance. In doing so, we deal with the second term in Eq. (6.79) as a constant during the matter era (as in the case  $Q = 0$ ), in which case  $\phi \propto t^{1/(2p_3-1)}$ . On using the property  $\rho_c \propto a^{-3} \propto t^{-2}$  in this epoch, the third term in Eq. (6.79) is proportional to  $t^{(2q-4p_3)/(2p_3-1)}$ . For  $q$  satisfying the relation

$$q = 2p_3, \quad (6.80)$$

all the terms in Eq. (6.79) are constants during the matter era.

For the choice (6.80), the third term in Eq. (6.79) is subdominant to other two terms during the radiation dominance. Indeed, exploiting the solutions  $\phi \propto t^{1/(2p_3-1)}$  and  $\rho_c \propto a^{-3} \propto t^{-3/2}$  in this epoch, the third term in Eq. (6.79) grows in proportion to  $t^{1/2}$  toward a constant value in the matter era. After the onset of late-time cosmic acceleration, the coupling term in Eq. (6.79) starts to decrease toward 0 by reflecting the fact that  $\rho_c$  decreases faster than  $t^{-2}$ . Finally, the solutions approach the de Sitter fixed point satisfying

$$b_2 + 3 \cdot 2^{1-p_3} b_3 p_3 H_{\text{dS}} \phi_{\text{dS}}^{2p_3-1} = 0, \quad (6.81)$$

where the subscript “dS” represents the values on the de Sitter point.

### 6.3.1 Autonomous system

In the following, we focus on the background cosmological dynamics for the power  $q$  satisfying the relation (6.80). In doing so, it is convenient to define

$$\Omega_{\text{DE}} \equiv \frac{\rho_{\text{DE}}}{3M_{\text{pl}}^2 H^2} = -\frac{b_2 \phi^2}{6M_{\text{pl}}^2 H^2}, \quad (6.82)$$

$$\Omega_I \equiv \frac{\rho_I}{3M_{\text{pl}}^2 H^2}, \quad (6.83)$$

$$\tilde{\Omega}_c \equiv \frac{\tilde{\rho}_c}{3M_{\text{pl}}^2 H^2} = (1 + Qf_1) \Omega_c, \quad (6.84)$$

where  $I = c, b, r$ . From Eq. (6.16), the CDM density parameter  $\tilde{\Omega}_c$ , which accommodates the interaction with the vector field, can be expressed as

$$\tilde{\Omega}_c = 1 - \Omega_{\text{DE}} - \Omega_b - \Omega_r. \quad (6.85)$$

Taking the derivatives of  $\Omega_{\text{DE}}$ ,  $\Omega_b$ ,  $\Omega_r$ , and  $\Omega_c$  with respect to  $\mathcal{N} \equiv \ln a$  and using the continuity Eqs. (6.14)-(6.13), it follows that

$$\Omega'_{\text{DE}} = 2\Omega_{\text{DE}} (\epsilon_\phi - \epsilon_h), \quad (6.86)$$

$$\Omega'_b = -\Omega_b (3 + 2\epsilon_h), \quad (6.87)$$

$$\Omega'_r = -2\Omega_r (2 + \epsilon_h), \quad (6.88)$$

$$\Omega'_c = -\Omega_c (3 + 2\epsilon_h), \quad (6.89)$$

where

$$\epsilon_\phi \equiv \frac{\dot{\phi}}{H\phi}, \quad \epsilon_h \equiv \frac{\dot{H}}{H^2}. \quad (6.90)$$

After differentiating Eq. (6.19) with respect to  $t$  and using Eq. (6.17), we can solve them for  $\dot{\phi}$  and  $\dot{H}$ . In doing so, we exploit Eqs. (6.85) and (6.19) to eliminate  $\rho_c$  and  $b_3$ . Defining the dimensionless variable

$$r_Q \equiv \frac{Q f_{1,X} \rho_c}{b_2} = -2p_3 Q \left( \frac{u^2}{2} \right)^{2p_3} \frac{\Omega_c}{\Omega_{\text{DE}}}, \quad \text{with} \quad u \equiv \frac{\phi}{M_{\text{pl}}}, \quad (6.91)$$

we obtain

$$\epsilon_\phi = \frac{u'}{u} = \frac{3(1 + r_Q) + (1 - r_Q)(\Omega_r - 3\Omega_{\text{DE}})}{2(1 + r_Q) + 2(1 - r_Q)^2 s \Omega_{\text{DE}}} s, \quad (6.92)$$

$$\epsilon_h = \frac{H'}{H} = -\frac{(1 + r_Q)(3 + \Omega_r - 3\Omega_{\text{DE}}) - 6r_Q(1 - r_Q)s \Omega_{\text{DE}}}{2(1 + r_Q) + 2(1 - r_Q)^2 s \Omega_{\text{DE}}}, \quad (6.93)$$

where

$$s \equiv \frac{1}{2p_3 - 1}. \quad (6.94)$$

In what follows, we focus on the theories with  $p_3 > 1/2$ , i.e.,  $s > 0$ . We also consider the case in which  $\Omega_{\text{DE}}$  is positive, i.e.,  $b_2 < 0$ .

When  $Q = 0$ , the parameter  $s$  characterizes the deviation of  $w_{\text{DE}}$  from  $-1$  [44, 169]. At the background level, our coupled dark energy model has two additional parameters  $Q$  and  $s$  relative to those in the  $\Lambda$ CDM model. The variable  $r_Q$ , which corresponds to the ratio between the third and first terms on the left hand side of Eq. (6.19), obeys the differential equation

$$r'_Q = r_Q \left( \frac{2}{s} \epsilon_\phi - 3 \right). \quad (6.95)$$

For given constants  $Q$  and  $s$ , the background cosmological dynamics is known by integrating Eqs. (6.86)-(6.88) and Eq. (6.95) with Eqs. (6.92) and (6.93). In doing so, we need to specify the initial conditions of  $\Omega_{\text{DE}}$ ,  $\Omega_b$ ,  $\Omega_r$ , and  $u$  at some redshift  $z = 1/a - 1$ . The initial value of  $\Omega_c$  is determined by using Eq. (6.85) and the correspondence

$$\Omega_c = \left[ 1 + Q \left( \frac{u^2}{2} \right)^{2p_3} \right]^{-1} \tilde{\Omega}_c. \quad (6.96)$$

From Eq. (6.91), the initial condition of  $r_Q$  is known accordingly. Instead of solving Eq. (6.95), we can also integrate Eq. (6.92) for the dimensionless temporal vector component  $u = \phi/M_{\text{pl}}$ . Nevertheless, using the variable  $r_Q$  is convenient to study the effect of coupling  $Q$  on the background cosmological dynamics. Indeed, the dark energy equation of state (6.24) is simply expressed as

$$w_{\text{DE}} = -1 - \frac{2}{3}(1 - r_Q)\epsilon_\phi, \quad (6.97)$$

which shows that  $w_{\text{DE}}$  is determined by the two quantities  $r_Q$  and  $\epsilon_\phi$ .

### 6.3.2 Analytic estimation for each cosmological epoch

Before solving the above autonomous system numerically, we analytically estimate the evolution of background quantities during the radiation, matter, and accelerated epochs.

Let us begin with the early Universe in which  $\Omega_{\text{DE}}$  is much smaller than 1. Expanding  $\epsilon_\phi$  and  $\epsilon_h$  around  $\Omega_{\text{DE}} = 0$ , it follows that

$$\epsilon_\phi = \frac{3}{2}s + \frac{1 - r_Q}{2(1 + r_Q)}s\Omega_r + \mathcal{O}(\Omega_{\text{DE}}), \quad \epsilon_h = -\frac{3}{2} - \frac{1}{2}\Omega_r + \mathcal{O}(\Omega_{\text{DE}}). \quad (6.98)$$

In this regime, the dark energy equation of state can be estimated as

$$w_{\text{DE}} \simeq -1 - (1 - r_Q)s \left[ 1 + \frac{1 - r_Q}{3(1 + r_Q)}\Omega_r \right], \quad \text{for } \Omega_{\text{DE}} \ll 1. \quad (6.99)$$

In addition, the quantity  $r_Q$  approximately obeys

$$r'_Q \simeq \frac{r_Q(1 - r_Q)}{1 + r_Q}\Omega_r. \quad (6.100)$$

We would like to consider the case in which the effect of coupling  $Q$  on Eq. (6.19) is unimportant in the early radiation era, so that  $r_Q \ll 1$ . From the

above estimation, the fixed point corresponding to the radiation dominance is given by

$$P_r : (\Omega_{\text{DE}}, \Omega_b, \Omega_r, r_Q) = (0, 0, 1, 0), \quad (6.101)$$

with  $\tilde{\Omega}_c = 0$  and  $u = 0$ . In this epoch, the dark energy equation of state (6.99) reduces to

$$w_{\text{DE}} \simeq -1 - \frac{4}{3}s. \quad (6.102)$$

This value of  $w_{\text{DE}}$  is identical to that derived for  $Q = 0$  in Ref. [44, 169], so the effect of coupling  $Q$  on  $w_{\text{DE}}$  does not appear in the deep radiation epoch. However, we have  $r'_Q \simeq r_Q$  around the point  $P_r$  and hence the non-vanishing coupling  $Q$  leads to the increase of  $r_Q$  proportional to  $a$ . In the late radiation era, this growth of  $r_Q$ , together with the decrease of  $\Omega_r$ , gives rise to the departure of  $w_{\text{DE}}$  from the constant value (6.102). From Eq. (6.92) the temporal vector component obeys  $u' \simeq 2su$  around the point  $P_r$ , so it grows as  $u \propto a^{2s}$ .

After  $\Omega_r$  becomes much smaller than 1 during the matter era, we have  $\epsilon_\phi \simeq 3s/2$  and  $\epsilon_h \simeq -3/2$  from Eq. (6.98). On using Eqs. (6.87), (6.89), and (6.95), it follows that  $\Omega_b = \Omega_b^{(m)} = \text{constant}$ ,  $\Omega_c = \Omega_c^{(m)} = \text{constant}$ , and  $r_Q = r_Q^{(m)} = \text{constant}$  in this epoch. Then, the fixed point corresponding to the matter dominance is

$$P_m : (\Omega_{\text{DE}}, \Omega_b, \Omega_r, r_Q) = (0, \Omega_b^{(m)}, 0, r_Q^{(m)}) , \quad (6.103)$$

with  $\tilde{\Omega}_c = 1 - \Omega_b^{(m)}$  and  $u = 0$ . From Eq. (6.92), the quantity  $u$  approximately obeys  $u' \simeq 3su/2$  around the point  $P_m$ , so that the temporal vector component grows as  $u \propto a^{3s/2}$ . Provided that  $|Q(u^2/2)^{2p_3}| \ll 1$ ,  $\Omega_c$  is approximately equivalent to  $\tilde{\Omega}_c$ . Around the fixed point  $P_m$ , the dark energy equation of state is simply given by

$$w_{\text{DE}} \simeq w_{\text{DE}}^{(m)} \equiv -1 - \left(1 - r_Q^{(m)}\right)s, \quad (6.104)$$

where  $w_{\text{DE}}^{(m)}$  is a constant. In the limit that  $Q \rightarrow 0$ , this result coincides with the value  $w_{\text{DE}}^{(m)} = -1 - s$  derived in Refs. [44, 169]. For  $Q > 0$ ,  $r_Q^{(m)}$  is a negative constant and hence  $w_{\text{DE}}^{(m)} < -1 - s$ . On the other hand, the negative coupling  $Q$  gives rise to the value  $0 < r_Q^{(m)} < 1$ , so  $w_{\text{DE}}^{(m)}$  gets closer to  $-1$  in comparison to the  $Q = 0$  case.

The magnitude of constant  $r_Q^{(m)}$  depends on the initial condition of  $r_Q$  in the radiation era. In terms of the quantity  $Qf_1$  equivalent to the second term in the square bracket of Eq. (6.96), we can express  $r_Q$  as  $r_Q =$

$-2p_3(\Omega_c/\Omega_{\text{DE}})Qf_1$ . Even if  $|Qf_1|$  is very much smaller than 1, the quantity  $r_Q$  can be as large as the order of 0.1 due to the large term  $\Omega_c/\Omega_{\text{DE}} \gg 1$  in the matter era. In Sec. 6.3.3, we will show that the no ghost condition (6.75) puts upper limits on the value  $r_Q^{(m)}$ .

The matter fixed point  $P_m$  is different from the  $\varphi$ MDE [147] characterized by the non-vanishing constant  $\Omega_{\text{DE}}$  proportional to the coupling-constant squared  $\beta^2$ , in that  $\Omega_{\text{DE}} = 0$  on the point  $P_m$ . From Eq. (6.86), the dark energy density parameter around  $P_m$  approximately obeys  $\Omega'_{\text{DE}} = 3(1+s)\Omega_{\text{DE}}$ , so  $\Omega_{\text{DE}}$  grows as

$$\Omega_{\text{DE}} \propto a^{3(1+s)}. \quad (6.105)$$

Eventually, the contribution of  $\Omega_{\text{DE}}$  to Eq. (6.95) becomes non-negligible at the late cosmological epoch. Assuming that  $r_Q \ll 1$  in this epoch and expanding Eq. (6.95) around  $r_Q = 0$ , it follows that

$$r'_Q = -\frac{3(1+s)\Omega_{\text{DE}}}{1+s\Omega_{\text{DE}}}r_Q + \mathcal{O}(r_Q^2). \quad (6.106)$$

This means that, after the dominance of dark energy,  $r_Q$  starts to decrease from the value  $r_Q^{(m)}$ . Finally, the solutions approach the dS fixed point characterized by

$$P_{\text{dS}} : (\Omega_{\text{DE}}, \Omega_b, \Omega_r, r_Q) = (1, 0, 0, 0), \quad (6.107)$$

with  $\tilde{\Omega}_c = 0$  and  $u = u_{\text{dS}} = \text{constant}$ . Since  $\epsilon_\phi = 0 = \epsilon_h$  on this point, both  $u$  and  $H$  are constants, with the dark energy equation of state

$$w_{\text{DE}} = -1. \quad (6.108)$$

During the cosmological sequence of radiation, matter, and dS epochs,  $w_{\text{DE}}$  changes as (6.102)  $\rightarrow$  (6.104)  $\rightarrow$  (6.108).

### 6.3.3 Numerical analysis

To study the background cosmological dynamics in more detail, we numerically integrate Eqs. (6.86)-(6.88) and Eq. (6.95) for several different values of  $s$  and  $Q$ . We also discuss whether the conditions for the absence of ghosts and Laplacian instabilities in the small-scale limit are consistently satisfied. The background initial conditions in the deep radiation era (around the redshift  $z = 10^7$ ) are chosen to realize today's values  $\Omega_{\text{DE}}^{(0)} = 0.68$ ,  $\Omega_b^{(0)} \simeq 0.05$ , and  $\Omega_r^{(0)} \simeq 10^{-4}$ . We consider the case in which today's temporal vector component  $u^{(0)}$  is of order 1.

In Fig. 6.1, we plot the evolution of  $w_{\text{DE}}$  and  $r_Q$  versus  $z+1$  for  $s = 1$  and four different values of  $Q$ . When  $Q = 0$ , the dark energy equation of



state evolves as  $w_{\text{DE}} = -7/3 \rightarrow -2 \rightarrow -1$  during the radiation, matter, and dS epochs, respectively. The joint observational constraint based on SN Ia, CMB, BAOs, RSDs,  $H_0$ , and ISW-galaxy cross-correlation data give the bound  $s = 0.185^{+0.100}_{-0.089}$  (95 % CL) [170], so the model with  $s = 1$  and  $Q = 0$  is excluded due to the large deviation of  $w_{\text{DE}}$  from  $-1$  before the onset of cosmic acceleration.

If  $Q > 0$ , we observe in Fig. 6.1 that  $w_{\text{DE}}$  is smaller than  $-2$  during the matter era. This is consistent with the analytic estimation (6.104), which gives  $w_{\text{DE}}^{(m)} = -2 + r_Q^{(m)} < -2$  for  $s = 1$  and  $Q > 0$ . In case (A4) of Fig. 6.1, the numerical value of  $r_Q^{(m)}$  is about  $-0.2$  and hence  $w_{\text{DE}}^{(m)} \simeq -2.2$ . This behavior of  $w_{\text{DE}}$ , which occurs through the decay of dark energy to CDM, is in more tension with the observational data in comparison to the  $Q = 0$  case.

When  $Q < 0$ , the quantity  $r_Q^{(m)}$  is positive. In cases (A1) and (A2) of Fig. 6.1, we can confirm that  $r_Q$  temporally approaches the positive constant  $r_Q^{(m)}$  after its increase during the radiation dominance ( $r_Q \propto a$ ). This leads to  $w_{\text{DE}}$  larger than  $-2$  in the matter era, whose behavior is attributed to the decay of CDM to dark energy. After the matter-dominated epoch ends,  $w_{\text{DE}}$  starts to approach the asymptotic value  $-1$  with the decrease of  $r_Q$ . The case (A1) in Fig. 6.1 corresponds to the marginal one in which the quantity  $q_c = 1 + Qf$  is close to  $+0$  at the dS point. For  $Q < 0$ , the no-ghost condition  $q_c > 0$  constrains the field value  $u_{\text{dS}} = \phi_{\text{dS}}/M_{\text{pl}}$  in the range

$$|Q| \left( \frac{u_{\text{dS}}^2}{2} \right)^{2p_3} < 1. \quad (6.109)$$

This also puts the upper limit on the magnitude of  $r_Q^{(m)}$ . When  $s = 1$ , we numerically find the bound  $r_Q^{(m)} < 0.48$ , which translates to  $w_{\text{DE}}^{(m)} < -1.52$ . Thus, the negative coupling  $Q$  allows the possibility for realizing  $w_{\text{DE}}^{(m)}$  closer to  $-1$  relative to the  $Q = 0$  case.

Although the model with  $s = 1$  should be still difficult to be compatible with the observational data due to the upper bound  $w_{\text{DE}}^{(m)} < -1.52$ , the situation is different for the models with  $s < 1$  (i.e.,  $p_3 > 1$ ). In Fig. 6.2, we depict the evolution of  $w_{\text{DE}}$  and  $r_Q$  for  $s = 1/3$  (i.e.,  $p_3 = 2$ ) and four different values of  $Q$ . When  $Q = 0$ , we have  $w_{\text{DE}}^{(m)} = -1.33$ , in which case the model is outside the 95 % CL observational boundary [170]. As we observe in Fig. 6.2, the negative coupling  $Q$  leads to larger values of  $w_{\text{DE}}^{(m)}$  compatible with the data. In case (B2), the numerical values of  $w_{\text{DE}}$  and  $r_Q$  in the matter era are  $-1.22$  and  $0.35$ , respectively, which are consistent with the analytic estimation (6.104). The case (B1) is the marginal situation

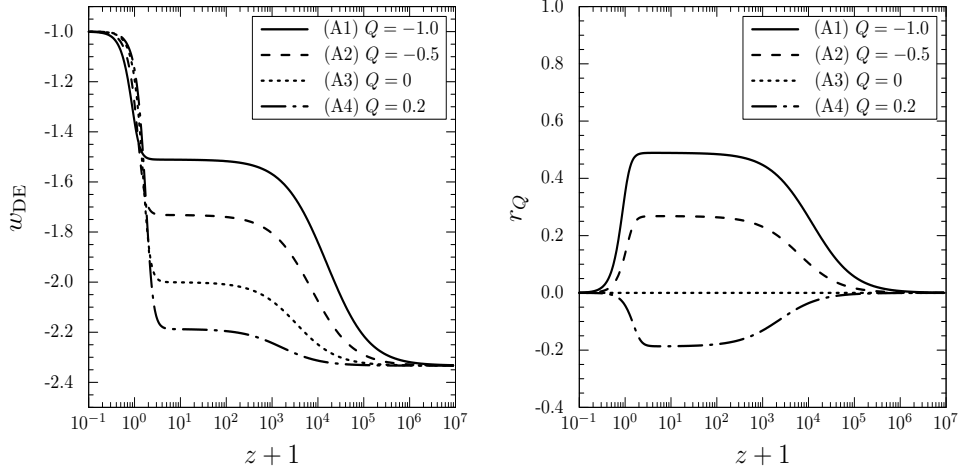


Figure 6.1: Evolution of  $w_{\text{DE}}$  (left) and  $r_Q$  (right) versus  $z+1$  for  $s = 1$  (i.e.,  $q = 2p_3 = 2$ ). Each line corresponds to the couplings (A1)  $Q = -1.0$ , (A2)  $Q = -0.5$ , (A3)  $Q = 0$ , and (A4)  $Q = 0.2$ . The initial conditions are chosen to give rise to today's values  $\Omega_{\text{DE}}^{(0)} = 0.68$ ,  $\Omega_b^{(0)} \simeq 0.05$ ,  $\Omega_r^{(0)} \simeq 10^{-4}$ , and  $u^{(0)} = 1.04$  (at the redshift  $z = 0$ ). In case (A1), the no-ghost condition  $q_c > 0$  is marginally satisfied on the dS fixed point.

in which the quantity  $q_c$  at the dS point is close to  $+0$ . This corresponds to the maximum dark energy equation of state  $w_{\text{DE}}^{(m)} = -1.14$  with  $r_Q^{(m)} = 0.59$ . Thus, for  $s = 1/3$ , the negative coupling  $Q$  gives rise to  $w_{\text{DE}}^{(m)}$  in the range  $-1.33 < w_{\text{DE}}^{(m)} < -1.14$ . This alleviates the problem of observational incompatibility of the model with  $s = 1/3$  and  $Q = 0$ . The positive coupling does not improve the situation, see case (B4) of Fig. 6.2.

In the above discussion, the no-ghost condition  $q_c > 0$  on the dS solution is crucial to put an upper bound on the value of  $w_{\text{DE}}^{(m)}$ . As we showed in Sec. 6.3.2, the temporal vector component  $u = \phi/M_{\text{pl}}$  increases during the radiation and matter epochs. Around the dS fixed point there is the approximate relation  $u'/u \simeq 3(1 - \Omega_{\text{DE}})s/[2(1 + s\Omega_{\text{DE}})]$ , so  $u$  also grows toward the constant value  $u_{\text{dS}}$ . This means that, under the condition (6.109), the no-ghost condition  $q_c > 0$  of CDM is satisfied during the whole cosmic expansion history. The other no-ghost condition (6.74) of the vector field translates to

$$q_S = 12M_{\text{pl}}^4 H^2 \Omega_{\text{DE}} \left[ \frac{1 + r_Q}{s} + (1 - r_Q)^2 \Omega_{\text{DE}} \right] > 0. \quad (6.110)$$

Provided that  $r_Q > -1$ , the condition (6.110) is always satisfied. This is the case for  $Q < 0$ , under which  $r_Q > 0$ .

On using the background equations of motion, the vector propagation

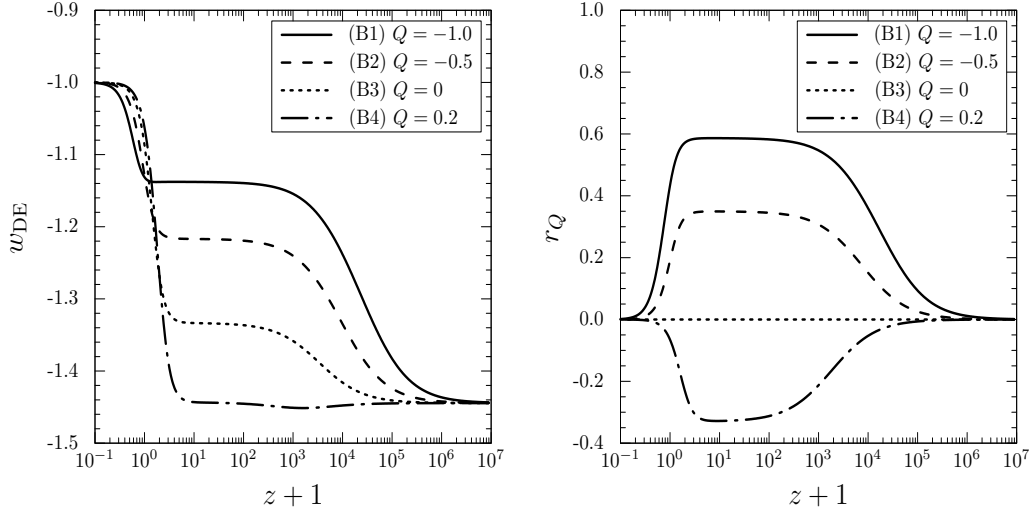


Figure 6.2: Evolution of  $w_{\text{DE}}$  (left) and  $r_Q$  (right) versus  $z+1$  for  $s = 1/3$  (i.e.,  $q = 2p_3 = 4$ ) with the different couplings: (B1)  $Q = -1.0$ , (B2)  $Q = -0.5$ , (B3)  $Q = 0$ , and (B4)  $Q = 0.2$ . Today's values of  $\Omega_{\text{DE}}^{(0)}$ ,  $\Omega_b^{(0)}$ , and  $\Omega_r^{(0)}$  are the same as those in Fig. 6.1, while  $u^{(0)} = 1.166$ .

speed squared (6.77) can be expressed as

$$c_S^2 = \frac{s\tilde{s}(2s - \tilde{s})(5 + 3s) - 2\tilde{s}^4\Omega_{\text{DE}}^2 - \tilde{s}^2[(7 + 3s)s - 2(1 + s)\tilde{s}]\Omega_{\text{DE}} + s\tilde{s}^2(1 + s)\Omega_r}{6(\tilde{s}^2\Omega_{\text{DE}} + 2s - \tilde{s})^2} + \frac{2\tilde{s}^2\Omega_{\text{DE}}}{3q_V u^2(\tilde{s}^2\Omega_{\text{DE}} + 2s - \tilde{s})}, \quad (6.111)$$

where  $\tilde{s} = (1 - r_Q)s$ , and  $q_V = 1$  for the model under consideration. On the fixed points  $P_r$ ,  $P_m$ , and  $P_{\text{ds}}$ , Eq. (6.111) reduces, respectively, to

$$(c_S^2)_r = \frac{s(2s + 3)}{3}, \quad (c_S^2)_m = \frac{s(5 + 3s)(1 - r_Q^{(m)})}{6(1 + r_Q^{(m)})}, \quad (c_S^2)_{\text{ds}} = \frac{2s}{3(1 + s)q_V u_{\text{ds}}^2}. \quad (6.112)$$

Since we are considering the case  $s > 0$ , both  $(c_S^2)_r$  and  $(c_S^2)_{\text{ds}}$  are positive under the absence of vector ghosts ( $q_V > 0$ ). During the matter era, the condition  $(c_S^2)_m \geq 0$  gives

$$-1 < r_Q^{(m)} \leq 1, \quad (6.113)$$

which is satisfied for all the cases shown in Figs. 6.1 and 6.2. The quantity  $|r_Q|$  reaches the maximum value  $|r_Q^{(m)}|$  during the matter era, so the no-ghost condition (6.110) automatically holds under the bound (6.113).

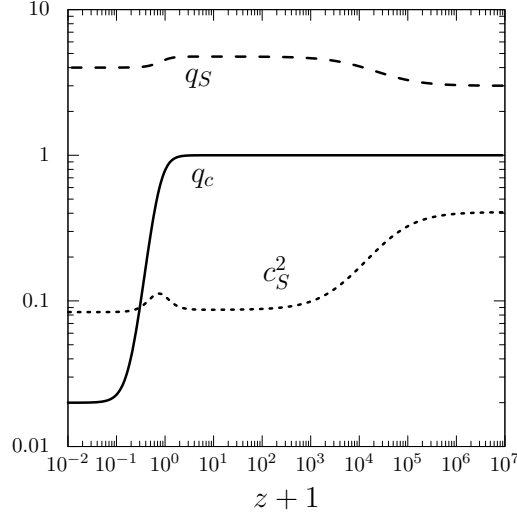


Figure 6.3: Evolution of  $q_c$ ,  $q_s$  and  $c_s^2$  versus  $z + 1$  for the case (B1) in Fig. 6.2, i.e.,  $s = 1/3$  and  $Q = -1.0$ . Today's values of  $\Omega_{\text{DE}}$ ,  $\Omega_b$ ,  $\Omega_r$ , and  $u$  are chosen in the same way as those in Fig. 6.2. The quantity  $q_s$  is divided by the positive quantity  $12M_{\text{pl}}^4 H^2 \Omega_{\text{DE}}$ .

In order to confirm the above analytic estimations, we compute the quantities  $q_c$ ,  $q_s$  and  $c_s^2$  by numerically integrating the autonomous equations. Figure 6.3 is such an example, which corresponds to the case (B1) in Fig. 6.2. We recall that this is close to the marginal case in which the condition  $q_c > 0$  is satisfied on the dS solution. In Fig. 6.3, we observe that  $q_c$  starts to deviate from 1 at low redshifts and it finally approaches the asymptotic value 0.02. As estimated from Eq. (6.110),  $q_s$  is always positive during the whole cosmological evolution. Since  $s = 1/3$ ,  $q_V = 1$ ,  $r_Q^{(m)} = 0.59$ , and  $u_{\text{dS}} = 1.41$  for the case (B1) in Fig. 6.2, the analytic estimations (6.112) give the values  $(c_s^2)_r = 0.407$ ,  $(c_s^2)_m = 0.086$ , and  $(c_s^2)_{\text{dS}} = 0.084$ , respectively. They are in good agreement with their numerical values computed in Fig. 6.3. We note that  $c_s^2$  also remains positive during the transition from the matter era to the dS epoch.

As long as the no-ghost condition  $q_c > 0$  of CDM is satisfied on the dS solution, the numerical simulations of Figs. 6.1 and 6.2 show that  $|r_Q|$  does not exceed 1. In this case, there are neither ghosts ( $q_s > 0$ ) nor Laplacian instabilities ( $c_s^2 > 0$ ) for the longitudinal scalar mode of  $A_\mu$ . In other words, under the condition (6.109), all the stability conditions associated with scalar perturbations are consistently satisfied. We found that the maximum allowed values of  $w_{\text{DE}}$  consistent with the stability conditions are  $w_{\text{DE}}^{(m)} = -1.52$  for  $s = 1$  and  $w_{\text{DE}}^{(m)} = -1.14$  for  $s = 1/3$ . For smaller  $s$ ,  $w_{\text{DE}}^{(m)}$  increases further,

e.g.,  $w_{\text{DE}}^{(m)} = -1.07$  for  $s = 1/5$  (i.e.,  $p_3 = 3$ ). This upper limit of  $w_{\text{DE}}^{(m)}$  is mostly determined by the product  $Qf_1 = Q(u^2/2)^{2p_3}$ , which means that both coupling constant  $Q$  and temporal vector component  $u$  affect the evolution of  $w_{\text{DE}}$  after the onset of matter dominance.

## 6.4 Summary of Chapter 6

In this chapter, we studied the vector dark energy model with the energy transfer between dark components. We derived the background equations of motion and the dark energy equation of state with the additional interaction  $Qf_1(X)$ . Moreover, we obtained the stability conditions for cosmological perturbations. We found that  $q_T$ ,  $c_T^2$ ,  $q_V$ ,  $c_V^2$  in the small-scale limit are not affected by the new interaction, while the stability conditions for scalar perturbations  $q_S$  and  $c_S^2$  have the interacting term associated with the energy transfer. The no-ghost condition for CDM also include the interacting term  $Qf_1(X)$ . Finally, we consider a concrete dark energy model described by the power-law function of  $X$ . We showed that the dark energy equation of state during matter-dominated epoch is closer to  $-1$  than that in the case with  $Q = 0$  as long as CDM decays the vector dark energy. If the vector dark energy decays CDM,  $w_{\text{DE}}^{(m)}$  becomes larger than that in the uncoupled case. Since  $q_c$  should be positive in whole cosmological epoch, there is the upper limit of  $w_{\text{DE}}^{(m)}$ .

## Chapter 7

# Momentum transfer between vector dark energy and cold dark matter

In this chapter, we shall discuss cosmology with momentum transfer between dark components. At first, we introduce the new interaction based on vector-tensor theories and derive the background equations of motion. Then, we can see that the momentum transfer does not affect the background dynamics. After that, we derive the stability conditions for cosmological perturbations and the effective gravitational couplings for CDM and baryons. We confirm that the new interaction does not affect the propagating speed of gravitational waves, while the propagating speed squared of scalar mode is different from that in uncoupled case. Moreover, due to the existence of momentum transfer, the effective gravitational coupling for CDM can be smaller than the Newtonian gravitational constant at late time. Then, the linear growth rate of the matter contrast becomes smaller than that in  $\Lambda$ CDM. It means that the  $\sigma_8$  tension may be able to be reduced by the existence of the momentum transfer between dark components.

### 7.1 Coupled generalized Proca theories with momentum transfer

Since the properties of dark sectors are unknown, we would like to consider possible interactions between them which are present at the level of Lagrangian. In coupled GP theories, there exists a simple interaction between

CDM and vector dark energy quantified by a scalar combination,

$$Z = -u_c^\mu A_\mu. \quad (7.1)$$

where we assume that CDM is described by a perfect fluid with the four-velocity  $u_c^\mu$ .

The action of our coupled GP theories with the quantity  $Z$  is given by

$$S = \int d^4x \sqrt{-g} \left[ \frac{M_{\text{pl}}^2}{2} R - \frac{1}{4} F_{\mu\nu} F^{\mu\nu} + f_2(X, Z) + G_3(X) \nabla_\mu A^\mu \right] + S_M, \quad (7.2)$$

where the function  $f_2$ , which is the generalization of  $G_2(X)$  in original GP theories, depends on both  $X$  and  $Z$ . For the matter action  $S_M$ , we consider the perfect fluids of CDM, baryons, and radiation, which are labelled by  $I = c, b, r$ , respectively. The perfect fluids can be described by the action (6.5).

From Eq. (4.37), the scalar combination  $Z$  defined by Eq. (7.1) can be expressed as

$$Z = -\frac{g^{\mu\nu} J_{c\mu} A_\nu}{n_c \sqrt{-g}}. \quad (7.3)$$

Neither radiation nor baryons are assumed to be coupled to the vector field.

### 7.1.1 Covariant equations of motion

We shall derive the covariant equations of motion by varying (7.2) with respect to several variables in the action. Variation with respect to  $\ell_I$  leads to

$$\partial_\mu J_I^\mu = 0, \quad (7.4)$$

which holds for each  $I = c, b, r$ . On using the property  $J_I^\mu = n_I \sqrt{-g} u_I^\mu$  and the relation  $\partial_\mu (\sqrt{-g} u_I^\mu) = \sqrt{-g} \nabla_\mu u_I^\mu$ , Eq. (7.4) translates to

$$n_I \nabla_\mu u_I^\mu + u_I^\mu \partial_\mu n_I = 0. \quad (7.5)$$

Since  $\rho_I$  depends only on  $n_I$ , there is the relation,

$$(\rho_I + P_I) \partial_\mu n_I = n_I \partial_\mu \rho_I, \quad (7.6)$$

where the fluid pressure  $P_I$  is defined by Eq. (4.39). On using Eqs. (7.5) and (7.6), we obtain

$$u_I^\mu \partial_\mu \rho_I + (\rho_I + P_I) \nabla_\mu u_I^\mu = 0. \quad (7.7)$$

We vary the action (7.2) with respect to  $J_c^\mu$  by keeping in mind that the scalar combination  $Z$  of Eq. (7.3) depends on  $J_c^\mu$ . On using the property  $\partial n_I / \partial J_I^\mu = J_{I\mu} / (n_I g)$ , it follows that

$$\partial_\mu \ell_c = u_{c\mu} \rho_{c,n_c} - \frac{f_{2,Z}}{n_c} (A_\mu - Z u_{c\mu}) - \mathcal{A}_{c1} \partial_\mu \mathcal{B}_{c1} - \mathcal{A}_{c2} \partial_\mu \mathcal{B}_{c2}. \quad (7.8)$$

For baryons and radiation, there is no dependence of  $J_b^\mu$  and  $J_r^\mu$  in the function  $f_2$ , so that

$$\partial_\mu \ell_I = u_{I\mu} \rho_{I,n_I} - \mathcal{A}_{I1} \partial_\mu \mathcal{B}_{I1} - \mathcal{A}_{I2} \partial_\mu \mathcal{B}_{I2}, \quad (7.9)$$

where  $I = b, r$ .

The covariant Einstein equations of motion follow by varying the action (7.2) with respect to  $g^{\mu\nu}$ . In doing so, we use the following properties,

$$\delta n_I = \frac{n_I}{2} (g_{\mu\nu} - u_{I\mu} u_{I\nu}) \delta g^{\mu\nu}, \quad (7.10)$$

$$\delta X = -\frac{1}{2} A_\mu A_\nu \delta g^{\mu\nu}, \quad (7.11)$$

$$\delta Z = \left( \frac{1}{2} Z u_{c\mu} u_{c\nu} - u_{c\mu} A_\nu \right) \delta g^{\mu\nu}, \quad (7.12)$$

together with  $\delta \sqrt{-g} = -(1/2) \sqrt{-g} g_{\mu\nu} \delta g^{\mu\nu}$ . Then, the resulting covariant equations are given by

$$M_{\text{pl}}^2 G_{\mu\nu} = \sum_{I=c,b,r} T_{\mu\nu}^{(I)} + T_{\mu\nu}^{(A)}, \quad (7.13)$$

where  $G_{\mu\nu}$  is the Einstein tensor, and

$$T_{\mu\nu}^{(I)} = (\rho_I + P_I) u_{I\mu} u_{I\nu} + P_I g_{\mu\nu}, \quad (7.14)$$

$$\begin{aligned} T_{\mu\nu}^{(A)} = & F_{\mu\rho} F_\nu{}^\rho - \frac{1}{4} g_{\mu\nu} F_{\rho\sigma} F^{\rho\sigma} + f_2 g_{\mu\nu} + f_{2,X} A_\mu A_\nu + f_{2,Z} Z u_{c\mu} u_{c\nu} \\ & + G_{3,X} (A_\mu A_\nu \nabla_\rho A^\rho + g_{\mu\nu} A^\lambda A_\rho \nabla_\lambda A^\rho - A_\rho A_\mu \nabla_\nu A^\rho - A_\rho A_\nu \nabla_\mu A^\rho). \end{aligned} \quad (7.15)$$

Varying the action (7.2) with respect to  $A_\nu$ , the equation for the vector field yields

$$\nabla_\mu F^{\mu\nu} - f_{2,X} A^\nu - f_{2,Z} u_c^\nu + G_{3,X} (A^\mu \nabla^\nu A_\mu - A^\nu \nabla^\mu A_\mu) = 0. \quad (7.16)$$

Taking the covariant derivative of Eq. (7.13) leads to

$$\sum_{I=c,b,r} \nabla^\mu T_{\mu\nu}^{(I)} + \nabla^\mu T_{\mu\nu}^{(A)} = 0. \quad (7.17)$$



On using the property (7.7), it follows that

$$u_I^\nu \nabla^\mu T_{\mu\nu}^{(I)} = 0, \quad (7.18)$$

which holds for  $I = c, b, r$ . This corresponds to the continuity equation for each perfect fluid. If CDM is the only fluid component, we have  $u_c^\nu \nabla^\mu T_{\mu\nu}^{(A)} = -u_c^\nu \nabla^\mu T_{\mu\nu}^{(c)} = 0$  from Eqs. (7.17) and (7.18). Since we are considering coupled GP theories with the momentum transfer alone, there are no explicit interacting terms associated with the energy exchange. This property is different from interacting GP theories with the energy transfer studied in Chap. 6. We note that the momentum exchange between the vector field and CDM occurs through Eq. (7.17).

### 7.1.2 Background equations of motion

We derive the background equations on the flat FLRW spacetime given by the line element (4.33). The vector-field profile and the fluid four-velocities consistent with this background are given by Eqs. (4.34) and (4.43), respectively. Also, the four-velocities of each perfect fluid are given by Eq. (4.43) in its rest frame.

From Eq. (7.18), the fluid continuity equations are given by

$$\dot{\rho}_I + 3H(\rho_I + P_I) = 0, \quad (7.19)$$

with  $I = c, b, r$ .

From the (00) and (ii) components of Einstein equations (7.13), we obtain

$$3M_{\text{pl}}^2 H^2 = \sum_{I=c,b,r} \rho_I - f_2 + (f_{2,X}\phi + f_{2,Z} + 3G_{3,X}H\phi^2)\phi, \quad (7.20)$$

$$M_{\text{pl}}^2 (2\dot{H} + 3H^2) = - \sum_{I=c,b,r} P_I - f_2 + G_{3,X}\phi^2\dot{\phi}. \quad (7.21)$$

The  $\nu = 0$  component of Eq. (7.16) translates to

$$f_{2,X}\phi + f_{2,Z} + 3G_{3,X}H\phi^2 = 0. \quad (7.22)$$

We define the dark energy density  $\rho_{\text{DE}}$  and pressure  $P_{\text{DE}}$ , as

$$\rho_{\text{DE}} = -f_2 + (f_{2,X}\phi + f_{2,Z} + 3G_{3,X}H\phi^2)\phi = -f_2, \quad (7.23)$$

$$P_{\text{DE}} = f_2 - G_{3,X}\phi^2\dot{\phi}, \quad (7.24)$$

where we used Eq. (7.22) in the second equality of Eq. (7.23). Taking the time derivative of Eq. (7.23) and exploiting Eq. (7.22), we obtain

$$\dot{\rho}_{\text{DE}} + 3H(\rho_{\text{DE}} + P_{\text{DE}}) = 0, \quad (7.25)$$

which corresponds to the continuity equation in the dark energy sector. We can see that, even if the dark components interact each other through the momentum transfer, these continuity equations do not have any additional terms unlike Eqs. (6.21) and (6.25) in the case with energy transfer.

Taking the time derivative of Eq. (7.22) and combining it with Eq. (7.21), it follows that

$$\dot{\phi} = \frac{\phi^4 G_{3,X}}{q_S} (3\rho_c + 3\rho_b + 4\rho_r), \quad (7.26)$$

$$\dot{H} = -\frac{q_S - 3\phi^6 G_{3,X}^2}{6M_{\text{pl}}^2 q_S} (3\rho_c + 3\rho_b + 4\rho_r), \quad (7.27)$$

where

$$\begin{aligned} q_S = & 3\phi^3 (2H\phi^2 M_{\text{pl}}^2 G_{3,XX} + \phi^3 G_{3,X}^2 + 4HM_{\text{pl}}^2 G_{3,X}) \\ & + 2\phi^2 M_{\text{pl}}^2 (\phi^2 f_{2,XX} + 2\phi f_{2,XZ} + f_{2,ZZ} + f_{2,X}). \end{aligned} \quad (7.28)$$

As we will show later in Sec. 7.2, the quantity  $q_S$  must be positive to avoid the ghost in the scalar sector. In this case, the right hand sides of Eqs. (7.26) and (7.27) do not cross the singular point  $q_S = 0$ .

We also introduce the density parameters,

$$\Omega_I = \frac{\rho_I}{3M_{\text{pl}}^2 H^2}, \quad \Omega_{\text{DE}} = \frac{\rho_{\text{DE}}}{3M_{\text{pl}}^2 H^2}. \quad (7.29)$$

as well as the equations of state

$$w_I = \frac{P_I}{\rho_I}, \quad w_{\text{DE}} = \frac{P_{\text{DE}}}{\rho_{\text{DE}}} = -1 + \frac{G_{3,X}\phi^2\dot{\phi}}{f_2}. \quad (7.30)$$

Then, Eq. (7.20) is expressed as

$$\sum_{I=c,b,r} \Omega_I + \Omega_{\text{DE}} = 1. \quad (7.31)$$

The effective equation of state is given by

$$w_{\text{eff}} = \sum_{I=c,b,r} w_I \Omega_I + w_{\text{DE}} \Omega_{\text{DE}} = -1 - \frac{2\dot{H}}{3H^2}, \quad (7.32)$$

where we used Eq. (7.21) in the second equality. The  $Z$  dependence in  $f_2$  affects the evolution of  $\phi$  through the term  $f_{2,Z}$  in Eq. (7.22). The dark energy equation of state  $w_{\text{DE}}$  is also modified by the vector-CDM interaction.

## 7.2 Cosmological perturbations and stability conditions

In this section, we derive the conditions for the absence of ghosts and gradient instabilities for the cosmological perturbations in the theories given by the action (7.2). Again, we consider the perturbed line element given by (4.33) and the perturbations of a Proca field given by (4.58). The spatial component of four velocity  $u_{I\mu}$  can be expressed in the form as Eq. (6.27) with the transverse condition (6.29).

For CDM, substituting Eqs. (4.61) and (6.27) into the spatial component of Eq. (7.8), it follows that

$$\begin{aligned} \partial_i \ell_c + \mathcal{A}_{c1} \partial_i \mathcal{B}_{c1} + \mathcal{A}_{c2} \partial_i \mathcal{B}_{c2} = & -\rho_{c,n_c} \partial_i v_c - \frac{f_{2,Z}}{n_c} (\partial_i \psi + \phi \partial_i v_c) \\ & + \rho_{c,n_c} v_{ci} - \frac{f_{2,Z}}{n_c} (Y_i - \phi v_{ci}) , \end{aligned} \quad (7.33)$$

up to linear order in perturbations. From the rotational-free scalar part  $\partial_i \ell_c$  of Eq. (7.33),

$$\partial_i \ell_c = -\rho_{c,n_c} \partial_i v_c - \frac{f_{2,Z}}{n_c} (\partial_i \psi + \phi \partial_i v_c) , \quad (7.34)$$

The integrated solution to Eq. (7.34) is  $\ell_c = \bar{C}_c(t) - \rho_{c,n_c} v_c - (f_{2,Z}/n_c) (\psi + \phi v_c)$ . The function  $\bar{C}_c(t)$  is determined by the temporal component of Eq. (7.8), as  $\bar{C}_c(t) = -\int^t \rho_{c,n_c}(\tilde{t}) d\tilde{t}$ . Then, the scalar quantity  $\ell_c$  is given by

$$\ell_c = -\int^t \rho_{c,n_c}(\tilde{t}) d\tilde{t} - \rho_{c,n_c} v_c - \frac{f_{2,Z}}{n_c} (\psi + \phi v_c) , \quad (7.35)$$

which contains the velocity potential  $v_c$  and the dynamical perturbation  $\psi$ . We recall that the energy-momentum tensors (7.14) and (7.15) were obtained after eliminating  $\ell_c$  on account of Eq. (7.8). The terms  $-\rho_{c,n_c} v_c$  and  $-(f_{2,Z}/n_c) (\psi + \phi v_c)$  in Eq. (7.35) contribute to Eqs. (7.14) and (7.15), respectively, as the perturbed energy-momentum tensors.

On the other hands, the divergence-free vector part of Eq. (7.33) gives the following relation,

$$\mathcal{A}_{c1} \partial_i \mathcal{B}_{c1} + \mathcal{A}_{c2} \partial_i \mathcal{B}_{c2} = \rho_{c,n_c} v_{ci} - \frac{f_{2,Z}}{n_c} (Y_i - \phi v_{ci}) . \quad (7.36)$$

Substituting Eqs. (4.77)-(4.78) into Eq. (7.36) and expanding it up to linear order, then it follows that

$$\delta \mathcal{A}_{ci} = \rho_{c,n_c} v_{ci} - \frac{f_{2,Z}}{n_c} (Y_i - \phi v_{ci}) . \quad (7.37)$$

which contains the intrinsic vector modes  $v_{ci}$  and  $Y_i$ .

On using Eq. (7.9), the relations for baryons and radiation analogous to Eqs. (7.35) and (7.37) are given, respectively, by

$$\ell_I = - \int^t \rho_{I,n_I}(\tilde{t}) d\tilde{t} - \rho_{I,n_I} v_I, \quad (7.38)$$

$$\delta\mathcal{A}_{Ii} = \rho_{I,n_I} v_{Ii}, \quad (7.39)$$

for  $I = b, r$ , which are the same form as Eqs. (4.75) and (4.79) since both baryons and radiation are not interacted to the vector field.

### 7.2.1 Tensor and vector perturbations

Along the same procedure as Sec. 4.3.2, expanding the action (7.2) up to quadratic order in the components of tensor perturbations  $h_+$  and  $h_\times$ , we end up with the second-order action of tensor perturbations,

$$S_T^{(2)} = \sum_{\lambda=+,\times} \int dt d^3x \frac{M_{\text{pl}}^2}{8} a^3 \left[ \dot{h}_\lambda^2 - \frac{1}{a^2} (\partial h_\lambda)^2 \right]. \quad (7.40)$$

This is equivalent to the corresponding action of tensor perturbations in general relativity, so the speed of gravitational waves  $c_T$  is equivalent to that of light. Hence, as well as the case of energy transfer, the coupled GP theories with momentum transfer are consistent with the bound (3.49) constrained by the GW170817 event [92].

For vector perturbations, the intrinsic vector modes appear in each term of (7.2), so we sum up all those contributions to the action. For this purpose, we use the fact that  $\ell_I$  ( $I = c, b, r$ ) are scalar quantities satisfying Eqs. (7.35) and (7.38), so the term  $J_I^\mu \partial_\mu \ell_I$  in the matter action (6.5) does not contribute to the quadratic-order action of vector perturbations. Vary the resulting second-order action with respect to  $W_{Ii}$  and  $\delta\mathcal{A}_{Ii}$ , it follows that

$$W_{Ii} = \left( \frac{\delta\mathcal{A}_{Ii}}{\rho_{I,n_I}} - V_i \right) \mathcal{N}_i, \quad (7.41)$$

$$\delta\mathcal{A}_{Ii} = \rho_{I,n_I} \left( V_i - a^2 \delta\mathcal{B}_{Ii} \right). \quad (7.42)$$

The perturbations  $\delta\mathcal{A}_{ci}$  and  $\delta\mathcal{A}_{Ii}$  ( $I = b, r$ ) are related to the spatial components of four-velocities according to Eqs. (7.37) and (7.39), respectively. Then, we have

$$V_i - a^2 \delta\mathcal{B}_{ci} = v_{ci} - \frac{f_{2,Z}}{\rho_c + P_c} (Y_i - \phi v_{ci}), \quad (7.43)$$

$$V_i - a^2 \delta\mathcal{B}_{Ii} = v_{Ii}, \quad (\text{for } I = b, r), \quad (7.44)$$

where we used Eq. (4.39). In the following, we exploit Eqs. (7.41) and (7.42) to eliminate the variables  $W_{Ii}$  and  $\delta\mathcal{A}_{Ii}$  from the second-order action. On using the background Eqs. (7.20) and (7.22), the second-order action of vector perturbations yields

$$S_V^{(2)} = \int dt d^3x \sum_{i=1}^2 \frac{a}{2} \left[ \dot{Y}_i^2 - \frac{1}{a^2} (\partial Y_i)^2 - \frac{1}{\phi} \left( G_{3,X} \phi \dot{\phi} - f_{2,Z} \right) Y_i^2 + \frac{M_{\text{pl}}^2}{2a^2} (\partial V_i)^2 \right. \\ \left. - 2f_{2,Z} V_i Y_i + \sum_{I=b,r} (V_i - a^2 \delta \dot{\mathcal{B}}_{Ii})^2 (\rho_I + P_I) \right. \\ \left. + (V_i - a^2 \delta \dot{\mathcal{B}}_{ci})^2 (\rho_c + P_c + \phi f_{2,Z}) + 2a^2 f_{2,Z} Y_i \delta \dot{\mathcal{B}}_{ci} \right]. \quad (7.45)$$

In Fourier space with the comoving wavenumber  $k = |\mathbf{k}|$ , we vary the action (7.45) with respect to  $V_i$ ,  $\delta \mathcal{B}_{ci}$ , and  $\delta \mathcal{B}_{Ii}$  ( $I = b, r$ ). This leads to

$$\frac{M_{\text{pl}}^2 k^2}{2a^2} V_i + (\rho_c + P_c + \phi f_{2,Z}) \left( V_i - a^2 \delta \dot{\mathcal{B}}_{ci} \right) - f_{2,Z} Y_i \\ + \sum_{I=b,r} (\rho_I + P_I) \left( V_i - a^2 \delta \dot{\mathcal{B}}_{Ii} \right) = 0, \quad (7.46)$$

$$\left[ (\rho_c + P_c + \phi f_{2,Z}) \left( V_i - a^2 \delta \dot{\mathcal{B}}_{ci} \right) - f_{2,Z} Y_i \right] a^3 = \mathcal{C}_{ci}, \quad (7.47)$$

$$(\rho_I + P_I) \left( V_i - a^2 \delta \dot{\mathcal{B}}_{Ii} \right) a^3 = \mathcal{C}_{Ii}, \quad (\text{for } I = b, r), \quad (7.48)$$

where  $\mathcal{C}_{Ii}$  (with  $I = c, b, r$ ) are constants in time. Notice that all the combinations in the form  $V_i - a^2 \delta \dot{\mathcal{B}}_{Ii}$  (with  $I = c, b, r$ ) can be rewritten in terms of the perfect fluid and Proca physical quantities by means of Eqs. (7.43) and (7.44). Substituting Eqs. (7.47) and (7.48) into Eq. (7.46), we obtain

$$V_i = -\frac{2}{M_{\text{pl}}^2 k^2 a} \sum_{I=c,b,r} \mathcal{C}_{Ii}, \quad (7.49)$$

which decays as  $|V_i| \propto a^{-1}$ . Plugging Eqs. (7.43) and (7.44) into Eqs. (7.47) and (7.48), it follows that

$$v_{ci} = \frac{(\rho_c + P_c) \mathcal{C}_{ci} + [2(\rho_c + P_c) + \phi f_{2,Z}] f_{2,Z} a^3 Y_i}{(\rho_c + P_c + \phi f_{2,Z})^2 a^3}, \quad (7.50)$$

$$v_{Ii} = \frac{\mathcal{C}_{Ii}}{(\rho_I + P_I) a^3}, \quad (\text{for } I = b, r). \quad (7.51)$$

While the velocity of baryons  $v_{bi}$  stays constant since  $\rho_b \propto n_b$  and  $P_b = 0$ , the CDM velocity  $v_{ci}$  is instead affected by the dynamical field  $Y_i$ .

Integrating out the Lagrange multiplier  $V_i$  by means of Eq. (7.46), the action gets its reduced form, with the field  $Y_i$  and the contributions from  $\delta\dot{\mathcal{B}}_{ci}$ , and  $\delta\dot{\mathcal{B}}_{Ii}$  ( $I = b, r$ ). On taking the small-scale limit  $k \rightarrow \infty$ , the dominant contributions to the second-order action of vector perturbations are given by

$$S_V^{(2)} \simeq \sum_{i=1}^2 \int dt d^3x \frac{a}{2} \left\{ q_V \left[ \dot{Y}_i^2 - c_V^2 \frac{k^2}{a^2} Y_i^2 \right] + (\rho_c + P_c + \phi f_{2,Z}) a^4 \delta\dot{\mathcal{B}}_{ci}^2 + \sum_{I=b,r} (\rho_I + P_I) a^4 \delta\dot{\mathcal{B}}_{Ii}^2 \right\}, \quad (7.52)$$

where

$$q_V = 1, \quad c_V^2 = 1. \quad (7.53)$$

Hence there are neither ghosts nor Laplacian instabilities for the dynamical perturbations  $Y_i$ , with the propagating speed equivalent to that of light. As we are going to see in Sec. 7.2.2, the same no-ghost condition for the field  $\delta\mathcal{B}_{ci}$ , will reappear in the scalar perturbation sector, so that we will postpone its study for later. Since the instability of  $Y_i$  is absent, the violent growth of  $v_{ci}$  does not occur through Eq. (7.50). This is the same conclusion as that found for uncoupled GP theories in Sec 4.3.3. Hence the existence of dynamical vector perturbations does not affect the anisotropy in structure formation. The constant  $q_V$  different from 1 arises for more general Lagrangians containing intrinsic vector modes, say,  $\mathcal{L}_F = -q_V F_{\mu\nu} F^{\mu\nu}/4$ .

The above discussion shows that the new interaction associated with the momentum transfer affects the small-scale stability conditions of neither tensor nor for the Proca vector perturbations.

### 7.2.2 Scalar perturbations

Let us derive conditions for the absence of ghosts and Laplacian instabilities for scalar perturbations. From Eq. (4.36), the perturbation of each fluid number density  $n_I$ , which is expanded up to second order, is given by

$$\delta n_I = \frac{\delta\rho_I}{\rho_{I,n_I}} - \frac{(\mathcal{N}_I \partial\chi + \partial\delta j_I)^2}{2\mathcal{N}_I a^5}, \quad (7.54)$$

where  $\delta\rho_I$  is the density perturbation related to  $\delta J_I$ , as

$$\delta\rho_I = \frac{\rho_{I,n_I}}{a^3} \delta J_I. \quad (7.55)$$

The fluid sound speed squares are defined by

$$c_I^2 = \frac{n_I \rho_{I,n_I n_I}}{\rho_{I,n_I}}, \quad (7.56)$$

which are  $c_c^2 = +0$ ,  $c_b^2 = +0$ , and  $c_r^2 = 1/3$  for CDM, baryons, and radiation, respectively.

On using the property  $n_I \sqrt{-g} u_{Ii} = J_{Ii} = J_I^0 g_{0i} + J_I^j g_{ij} = \mathcal{N}_I \partial_i B + \partial_i \delta j_I$  for linear perturbations, it follows that

$$\partial \delta j_I = -\mathcal{N}_I (\partial B + \partial v_I). \quad (7.57)$$

This relation is used to eliminate the non-dynamical variable  $\delta j_I$ .

In total, there are ten perturbed quantities associated with the scalar mode:  $\alpha, B$  for the metric components,  $\delta\phi, \psi$  for the vector field, and  $v_I, \delta\rho_I$  (with  $I = c, b, r$ ) for each matter component. Expanding the action (7.2) up to second order in scalar perturbations and integrating it by parts, the quadratic-order action yields

$$S_S^{(2)} = \int dt d^3x (L_{\text{GP}} + L_Z + L_M), \quad (7.58)$$

where

$$\begin{aligned} L_{\text{GP}} = a^3 & \left[ \left( w_1 \alpha + \frac{w_2 \delta\phi}{\phi} \right) \frac{\partial^2 B}{a^2} - w_3 \frac{(\partial\alpha)^2}{a^2} + \tilde{w}_4 \alpha^2 - \frac{w_3}{4} \frac{(\partial\delta\phi)^2}{a^2 \phi^2} + \tilde{w}_5 \frac{(\delta\phi)^2}{\phi^2} \right. \\ & - \left\{ (3Hw_1 - 2\tilde{w}_4) \frac{\delta\phi}{\phi} - \frac{w_3}{a^2 \phi} \left( \partial^2 \delta\phi + \partial^2 \dot{\psi} \right) + w_6 \frac{\partial^2 \psi}{a^2} \right\} \alpha - \frac{w_3}{4\phi^2} \frac{(\partial\dot{\psi})^2}{a^2} \\ & \left. - \left\{ \frac{(w_6 \phi + w_2) \psi}{2} - \frac{w_3}{2} \dot{\psi} \right\} \frac{\partial^2 (\delta\phi)}{a^2 \phi^2} + \frac{w_7}{2} \frac{(\partial\psi)^2}{a^2} \right], \quad (7.59) \end{aligned}$$

$$\begin{aligned} L_Z = a^3 & \left[ \frac{\phi f_{2,Z}}{\rho_c + P_c} \left\{ (\rho_c + P_c) \frac{\partial^2 B}{a^2} - \dot{\delta\rho}_c - 3H (1 + c_c^2) \delta\rho_c \right\} v_c - \phi f_{2,Z} \frac{(\partial v_c)^2}{2a^2} \right. \\ & + f_{2,Z} \psi \frac{\partial^2 B}{a^2} + \frac{f_{2,Z}}{\rho_c + P_c} \dot{\psi} \delta\rho_c + \frac{f_{2,XZ} \phi \dot{\phi} + f_{2,ZZ} \dot{\phi} + 3f_{2,Z} H}{\rho_c + P_c} \psi \delta\rho_c \\ & \left. + \frac{1}{2} (2\phi^3 f_{2,XZ} + \phi^2 f_{2,ZZ} - \phi f_{2,Z}) \left( \alpha + \frac{\delta\phi}{\phi} \right)^2 + \frac{f_{2,Z}}{2\phi a^2} (\partial\psi)^2 \right], \quad (7.60) \end{aligned}$$

$$\begin{aligned} L_M = a^3 & \sum_{I=c,b,r} \left[ \left\{ (\rho_c + P_c) \frac{\partial^2 B}{a^2} - \dot{\delta\rho}_I - 3H (1 + c_I^2) \delta\rho_I \right\} v_I \right. \\ & \left. - \frac{\rho_c + P_c}{2} \frac{(\partial v_I)^2}{a^2} - \frac{c_I^2}{2(\rho_c + P_c)} (\delta\rho_I)^2 - \alpha \delta\rho_I \right], \quad (7.61) \end{aligned}$$

with  $w_{1,2,3,6,7}$  given by Eqs. (4.114)-(4.116) and Eqs.(4.119)-(4.120) , and

$$\tilde{w}_4 = \frac{1}{2}\phi^4 f_{2,XX} - \frac{3}{2}H\phi^3(G_{3,X} - \phi^2 G_{3,XX}) - 3M_{\text{pl}}^2 H^2 , \quad (7.62)$$

$$\tilde{w}_5 = \tilde{w}_4 - \frac{3}{2}H(w_1 + w_2) . \quad (7.63)$$

Note that the function  $f_{2,XX}$  in  $\tilde{w}_4$  is the generalization of  $G_{2,XX}$  in  $w_4$  given by Eq. (4.117). The contribution of intrinsic vector modes to the scalar perturbation equations appears only through the quantity  $w_3 = -2\phi^2 q_V$ . In the theory given by the action (7.2),  $q_V$  is equivalent to 1.

There are six non-dynamical variables  $\alpha, B, \delta\phi, v_c, v_b, v_r$ , while the dynamical perturbations correspond to the four fields  $\psi, \delta\rho_c, \delta\rho_b, \delta\rho_r$ . Varying the action (7.58) with respect to the six non-dynamical fields in Fourier space, it follows that

$$\begin{aligned} \sum_{I=c,b,r} \delta\rho_I - 2\tilde{w}_4\alpha + (3Hw_1 - 2\tilde{w}_4) \frac{\delta\phi}{\phi} + \frac{k^2}{a^2} (\mathcal{Y} + w_1B - w_6\psi) \\ = (2\phi^3 f_{2,XZ} + \phi^2 f_{2,ZZ} - \phi f_{2,Z}) \left( \alpha + \frac{\delta\phi}{\phi} \right) , \end{aligned} \quad (7.64)$$

$$\sum_{I=c,b,r} (\rho_I + P_I) v_I + w_1\alpha + w_2 \frac{\delta\phi}{\phi} = -f_{2,Z} (\phi v_c + \psi) , \quad (7.65)$$

$$\begin{aligned} (3Hw_1 - 2\tilde{w}_4) \alpha - 2\tilde{w}_5 \frac{\delta\phi}{\phi} + \frac{k^2}{a^2} \left[ \frac{1}{2}\mathcal{Y} + w_2B - \frac{1}{2} \left( \frac{w_2}{\phi} + w_6 \right) \psi \right] \\ = (2\phi^3 f_{2,XZ} + \phi^2 f_{2,ZZ} - \phi f_{2,Z}) \left( \alpha + \frac{\delta\phi}{\phi} \right) , \end{aligned} \quad (7.66)$$

$$\dot{\delta\rho}_I + 3H(1 + c_I^2) \delta\rho_I + \frac{k^2}{a^2} (\rho_I + P_I) (B + v_I) = 0 , \quad \text{for } I = c, b, r , \quad (7.67)$$

where the quantity  $\mathcal{Y}$  is the same as that given by Eq. (4.125). When the function  $f_2$  does not depend on the quantity  $Z$ , then Eqs. (7.64)-(7.66) reduce to Eqs. (4.121)-(4.123), respectively.

Variations of the action (7.58) with respect to the four dynamical perturbations lead to

$$\dot{\mathcal{Y}} + \left( H - \frac{\dot{\phi}}{\phi} \right) \mathcal{Y} + 2\phi(w_6\alpha + w_7\psi) + (w_2 + w_6\phi) \frac{\delta\phi}{\phi} = -2f_{2,Z} (\phi v_c + \psi) , \quad (7.68)$$



$$\dot{v}_c - 3Hc_c^2 v_c - c_c^2 \frac{\delta \rho_c}{\rho_c + P_c} - \alpha = -\frac{1}{a^3(\rho_c + P_c)} \frac{\partial}{\partial t} [a^3 f_{2,Z} (\phi v_c + \psi)] , \quad (7.69)$$

$$\dot{v}_I - 3Hc_I^2 v_I - c_I^2 \frac{\delta \rho_I}{\rho_I + P_I} - \alpha = 0 , \quad \text{for } I = b, r . \quad (7.70)$$

In the case with  $f_{2,Z} = 0$ , then Eqs. (7.68) and (7.69) reduce to Eqs. (4.126) and (4.127), respectively.

Solving Eqs. (7.64)-(7.67) for the non-dynamical fields  $\alpha$ ,  $B$ ,  $\delta\phi$ ,  $v_c$ ,  $v_b$ ,  $v_r$  and substituting the results into the action (7.58), then these perturbations are eliminated from the action (7.58). After the integration by parts, the resulting second-order action in Fourier space can be expressed in the form,

$$S_S^{(2)} = \int dt d^3x a^3 \left( \dot{\vec{\mathcal{X}}}^t \mathbf{K} \dot{\vec{\mathcal{X}}} - \frac{k^2}{a^2} \vec{\mathcal{X}}^t \mathbf{G} \vec{\mathcal{X}} - \vec{\mathcal{X}}^t \mathbf{M} \vec{\mathcal{X}} - \frac{k}{a} \vec{\mathcal{X}}^t \mathbf{B} \dot{\vec{\mathcal{X}}} \right) , \quad (7.71)$$

where  $\mathbf{K}$ ,  $\mathbf{G}$ ,  $\mathbf{M}$  and  $\mathbf{B}$  are  $4 \times 4$  matrices. The leading-order contributions to the matrix component  $\mathbf{M}$  are at most of the order  $k^0$ . The vector field  $\vec{\mathcal{X}}^t$  is composed of the dynamical perturbations, as

$$\vec{\mathcal{X}}^t = (\psi, \delta\rho_c/k, \delta\rho_b/k, \delta\rho_r/k) . \quad (7.72)$$

In the small-scale limit ( $k \rightarrow \infty$ ), the non-vanishing components of  $\mathbf{K}$  and  $\mathbf{G}$  are given, respectively, by

$$K_{11} = \frac{H^2 M_{\text{pl}}^2}{\phi^2 (w_1 - 2w_2)^2} [3w_1^2 + 4M_{\text{pl}}^2 \tilde{w}_4 + 2M_{\text{pl}}^2 (2\phi^3 f_{2,XZ} + \phi^2 f_{2,ZZ} - \phi f_{2,Z})] , \quad (7.73)$$

$$K_{22} = \frac{a^2(\rho_c + P_c + \phi f_{2,Z})}{2(\rho_c + P_c)^2} , \quad K_{33} = \frac{a^2}{2(\rho_b + P_b)} , \quad K_{44} = \frac{a^2}{2(\rho_r + P_r)} , \quad (7.74)$$

and

$$G_{11} = \mathcal{G} + \dot{\mu} + H\mu - \frac{w_2^2}{2(w_1 - 2w_2)^2 \phi^2} \sum_{I=c,b,r} (\rho_I + P_I) - \frac{4f_{2,Z} H^2 M_{\text{pl}}^4}{2(w_1 - 2w_2)^2 \phi} , \quad (7.75)$$

$$G_{22} = \frac{a^2 c_c^2}{2(\rho_c + P_c)} , \quad G_{33} = \frac{a^2 c_b^2}{2(\rho_b + P_b)} , \quad G_{44} = \frac{a^2 c_r^2}{2(\rho_r + P_r)} , \quad (7.76)$$

where

$$\mathcal{G} = -\frac{4H^2 M_{\text{pl}}^4 w_2^2}{\phi^2 w_3 (w_1 - 2w_2)^2} - \frac{\dot{\phi}}{2\phi^3} w_2 , \quad \mu = \frac{H M_{\text{pl}}^2 w_2}{\phi^2 (w_1 - 2w_2)} . \quad (7.77)$$

The anti-symmetric matrix  $\mathbf{B}$  has the leading-order off-diagonal components, which are given by

$$B_{12} = -B_{21} = -\frac{aHM_{\text{pl}}^2 f_{2,Z}}{(w_1 - 2w_2)(\rho_c + P_c)}. \quad (7.78)$$

The diagonal components of  $\mathbf{B}$  are lower than the order  $k^0$ .

In the following, we will consider perfect fluids obeying the weak energy conditions  $\rho_I + P_I > 0$  (with  $I = c, b, r$ ). In this case, the no-ghost conditions for baryons and radiation ( $K_{33} > 0$  and  $K_{44} > 0$ ) are automatically satisfied. The absence of ghosts for the dynamical perturbations  $\psi$  and  $\delta\rho_c$  requires that

$$q_S = 3w_1^2 + 4M_{\text{pl}}^2 \tilde{w}_4 + 2M_{\text{pl}}^2 (2\phi^3 f_{2,XZ} + \phi^2 f_{2,ZZ} - \phi f_{2,Z}) > 0, \quad (7.79)$$

$$q_c = 1 + \frac{\phi f_{2,Z}}{\rho_c + P_c} > 0, \quad (7.80)$$

respectively. By using Eq. (7.22), one can easily confirm that  $q_S$  given by Eq. (7.79) is identical to the quantity (7.28) appearing in the denominators of background Eqs. (7.26) and (7.27). The  $Z$  dependence in the coupling  $f_2$  affects the no-ghost conditions of both the Proca field and CDM.

To avoid a strong-coupling problem for the Proca field, we need to impose at any time, for high  $k$ 's, that the diagonal term  $K_{11}$  never vanishes or approaches zero. Similarly, the element  $K_{22}\rho_c^2$  should satisfy the same no strong-coupling condition<sup>1</sup>. Other matter fields trivially satisfy the no strong-coupling condition.

The propagation of baryons and radiation is not modified by the matrix  $\mathbf{B}$ , so their sound speeds are  $c_b^2 = G_{33}/K_{33}$  and  $c_r^2 = G_{44}/K_{44}$ , respectively. On the other hand, the off-diagonal components (7.78) affect the propagation of dynamical perturbations  $\mathcal{X}_1 \equiv \psi$  and  $\mathcal{X}_2 \equiv \delta\rho_c/k$ . We substitute the solutions  $\mathcal{X}_j = \tilde{\mathcal{X}}_j e^{i(\omega t - kx)}$  (with  $j = 1, 2$  and  $\omega$  is a frequency) to their equations of motion following from the action (7.71). To derive the dispersion relations in the small-scale limit, we pick up terms of the orders  $\omega^2$ ,  $\omega k$ , and  $k^2$ . Then, we obtain

$$\omega^2 \tilde{\mathcal{X}}_1 - \hat{c}_S^2 \frac{k^2}{a^2} \tilde{\mathcal{X}}_1 - i\omega \frac{k}{a} \frac{B_{12}}{K_{11}} \tilde{\mathcal{X}}_2 \simeq 0, \quad (7.81)$$

$$\omega^2 \tilde{\mathcal{X}}_2 - \hat{c}_c^2 \frac{k^2}{a^2} \tilde{\mathcal{X}}_2 - i\omega \frac{k}{a} \frac{B_{21}}{K_{22}} \tilde{\mathcal{X}}_1 \simeq 0, \quad (7.82)$$

<sup>1</sup>We have multiplied  $K_{22}$  by  $\rho_c^2$ , as this corresponds to the kinetic term for the density contrast  $\delta_c = \delta\rho_c/\rho_c$ .

where

$$\begin{aligned}\hat{c}_S^2 &= \frac{G_{11}}{K_{11}} \\ &= \frac{\phi^2(w_1 - 2w_2)^2}{H^2 M_{\text{pl}}^2 q_S} \left[ \mathcal{G} + \dot{\mu} + H\mu - \sum_{I=c,b,r} \frac{w_2^2(\rho_I + P_I) + 4f_{2,Z}\phi H^2 M_{\text{pl}}^4}{2(w_1 - 2w_2)^2 \phi^2} \right],\end{aligned}\quad (7.83)$$

$$\hat{c}_c^2 = \frac{G_{22}}{K_{22}} = \frac{c_c^2}{q_c}. \quad (7.84)$$

Since we are considering the case  $c_c^2 = +0$ , it follows that  $\hat{c}_c^2 = +0$ . Then, the two solutions to Eq. (7.82) are given by

$$\omega = 0, \quad (7.85)$$

$$\omega \tilde{\mathcal{X}}_2 = i \frac{k}{a} \frac{B_{21}}{K_{22}} \tilde{\mathcal{X}}_1. \quad (7.86)$$

The CDM has the dispersion relation (7.85), so its sound speed squared  $c_{\text{CDM}}^2 = \omega^2 a^2 / k^2$  is

$$c_{\text{CDM}}^2 = +0. \quad (7.87)$$

The perturbation  $\psi$  associated with the longitudinal scalar mode of  $A_\mu$  corresponds to the other branch (7.86), so substitution of Eq. (7.86) into Eq. (7.81) results in the dispersion relation  $\omega^2 = c_S^2 k^2 / a^2$ , with

$$c_S^2 = \hat{c}_S^2 + \Delta c_S^2, \quad (7.88)$$

where

$$\Delta c_S^2 = \frac{B_{12}^2}{K_{11} K_{22}} = \frac{2M_{\text{pl}}^2 (\phi f_{2,Z})^2}{q_S q_c (\rho_c + P_c)}. \quad (7.89)$$

Thus the interaction between the Proca field and CDM gives rise to an additional contribution  $\Delta c_S^2$  to the total sound speed squared  $c_S^2$ . The small-scale Laplacian instability is absent for

$$c_S^2 \geq 0. \quad (7.90)$$

Under the no-ghost conditions (7.79) and (7.80),  $\Delta c_S^2$  is positive. This means that, as long as  $\hat{c}_S^2$  defined by Eq. (7.83) is positive, the Laplacian instability is always absent for the perturbation  $\psi$ .

In summary, there are neither ghosts nor Laplacian instabilities for scalar perturbations under the conditions (7.79), (7.80), and (7.90). As long as  $c_c^2 = +0$ , the coupling between the Proca field and CDM does not modify the effective CDM sound speed squared  $c_{\text{CDM}}^2$ .

### 7.3 Effective gravitational couplings for CDM and baryons

To confront coupled dark energy models in GP theories with the observations of galaxy clusterings and weak lensing, we need to understand the evolution of matter density perturbations at low redshifts. For this purpose, we derive the effective gravitational couplings felt by CDM and baryon density perturbations by employing the so-called quasi-static approximation. The contribution of radiation to the background and perturbation equations of motion is ignored in the following discussion.

We consider the case in which the equations of state and the sound speed squares of CDM and baryons are given by

$$w_c = 0, \quad w_b = 0, \quad c_c^2 = 0, \quad c_b^2 = 0. \quad (7.91)$$

We also introduce the CDM and baryon density contrasts,

$$\delta_c = \frac{\delta\rho_c}{\rho_c}, \quad \delta_b = \frac{\delta\rho_b}{\rho_b}. \quad (7.92)$$

From Eq. (7.67), we obtain

$$\dot{\delta}_I = -\frac{k^2}{a^2}(\chi + v_I), \quad \text{for } I = c, b. \quad (7.93)$$

We can express Eqs. (7.69) and (7.70) in the forms,

$$\dot{v}_c = \frac{1}{q_c} \left[ \alpha - \frac{H}{\phi} \{q_c \epsilon_c + (1 - q_c) \epsilon_\phi\} \psi + \frac{1}{\phi} (1 - q_c) \dot{\psi} - H q_c \epsilon_c v_c \right], \quad (7.94)$$

$$\dot{v}_b = \alpha, \quad (7.95)$$

where

$$q_c = 1 + \frac{\phi f_{2,Z}}{\rho_c}, \quad (7.96)$$

$$\epsilon_c = \frac{\dot{q}_c}{H q_c} = \frac{(f_{2,Z} + f_{2,XZ} \phi^2 + f_{2,ZZ} \phi) \dot{\phi} + 3H \phi f_{2,Z}}{H(\phi f_{2,Z} + \rho_c)}, \quad (7.97)$$

$$\epsilon_\phi = \frac{\dot{\phi}}{H \phi}. \quad (7.98)$$

If there is no  $Z$  dependence in  $f$ , we have  $q_c = 1$  and  $\epsilon_c = 0$ , in which case  $\dot{v}_c = \alpha$ .

The gauge-invariant Bardeen potentials are defined by Eq. (5.2). Taking the time derivatives of Eq. (7.93) and using Eqs. (7.94)-(7.95), it follows that

$$\begin{aligned} \ddot{\delta}_c + (2 + \epsilon_c)H\dot{\delta}_c + \frac{k^2}{a^2}\frac{\Psi}{q_c} + \frac{k^2}{a^2}\left[\left(1 - \frac{1}{q_c}\right)\left(\frac{\dot{\Phi}}{H} - \epsilon_H\Phi\right) + \epsilon_c\Phi\right] \\ - \frac{k^2}{a^2}\frac{H}{\phi}\left[\left(1 - \frac{1}{q_c}\right)\left(\frac{\dot{\psi}}{H} - \epsilon_\phi\psi\right) + \epsilon_c\psi\right] = 0, \end{aligned} \quad (7.99)$$

$$\ddot{\delta}_b + 2H\dot{\delta}_b + \frac{k^2}{a^2}\Psi = 0, \quad (7.100)$$

where

$$\epsilon_H = \frac{\dot{H}}{H^2}. \quad (7.101)$$

In contrast to Eq. (7.100) of baryon perturbations, the evolution of CDM density contrast is nontrivially affected by the  $Z$  dependence in  $f_2$  through the quantities containing  $\Phi$ ,  $\dot{\Phi}$ ,  $\psi$ ,  $\dot{\psi}$  in Eq. (7.99). By using the quasi-static approximation in the following, we derive the closed-form expressions of  $\Psi$ ,  $\Phi$ , and  $\psi$  to estimate the gravitational couplings of CDM and baryon density perturbations.

### 7.3.1 Quasi-static approximation

We employ the quasi-static approximation for the modes deep inside the horizon, under which the dominant contributions to the perturbation equations are the terms containing  $k^2/a^2$  as well as  $\delta\rho_c$ ,  $\delta\rho_b$  and their time derivatives [210, 211, 212]. Then, from Eqs. (7.64) and (7.66), it follows that

$$\delta\rho_c + \delta\rho_b \simeq -\frac{k^2}{a^2}(\mathcal{Y} + w_1\chi - w_6\psi), \quad (7.102)$$

$$\mathcal{Y} \simeq \left(\frac{w_2}{\phi} - w_6\right)\psi - 2w_2\chi. \quad (7.103)$$

Substituting Eq. (7.103) into Eq. (7.102) and using  $\delta_I$  ( $I = c, b$ ) and  $\Phi$  defined in Eqs. (7.92) and (5.2), respectively, we obtain

$$\rho_c\delta_c + \rho_b\delta_b \simeq -\frac{k^2}{a^2}\left(\frac{w_1 - 2w_2}{H}\Phi + \frac{w_2}{\phi}\psi\right). \quad (7.104)$$

From Eqs. (4.125) and (7.103), it follows that

$$\dot{\psi} \simeq \frac{w_2 + w_6\phi}{w_3}\psi - 2\phi\left(\alpha + \frac{w_2}{w_3}\frac{\Phi}{H}\right) - \delta\phi. \quad (7.105)$$

We differentiate Eq. (7.104) with respect to  $t$  and resort to Eqs. (7.93) and (7.105) to remove  $\dot{\delta}_c$ ,  $\dot{\delta}_b$ , and  $\dot{\psi}$ . The perturbation  $\delta\phi$  can be eliminated by exploiting Eq. (7.65). After this procedure the CDM velocity potential  $v_c$  still remains, so we employ Eq. (7.93) to express it in terms of  $\dot{\delta}_c$  and  $\Phi$ , as

$$v_c = -\frac{a^2}{k^2}\dot{\delta}_c - \frac{\Phi}{H}. \quad (7.106)$$

Then, we obtain

$$\phi^2(w_1 - 2w_2)w_3\Psi + \mu_1\Phi + \mu_2\psi \simeq \frac{a^2}{k^2}w_3\phi^2(q_c - 1)\rho_c\dot{\delta}_c, \quad (7.107)$$

where

$$\mu_1 = \frac{\phi^2}{H} [(\dot{w}_1 - 2\dot{w}_2 + Hw_1 - \rho_b - q_c\rho_c)w_3 - 2w_2(w_2 + Hw_3)], \quad (7.108)$$

$$\mu_2 = \phi(w_2^2 + Hw_2w_3 + \dot{w}_2w_3) + w_2(w_6\phi^2 - w_3\dot{\phi}) + \phi w_3\rho_c(q_c - 1). \quad (7.109)$$

We also substitute Eq. (7.103) and its time derivative into Eq. (7.68) by exploiting the relations (7.105) and (7.106). This procedure leads to

$$2\phi^2w_2\Psi + \mu_3\Phi + \mu_4\psi \simeq -\frac{2a^2}{k^2}\phi^2(q_c - 1)\rho_c\dot{\delta}_c, \quad (7.110)$$

where

$$\mu_3 = \frac{2\phi}{Hw_3}\mu_2, \quad (7.111)$$

$$\begin{aligned} \mu_4 = & -\frac{1}{w_3} [\phi^3(w_6^2 + 2w_3w_7) + \phi^2(2w_2w_6 + Hw_3w_6 + w_3\dot{w}_6) \\ & + \phi\{w_2^2 + Hw_2w_3 + w_3(\dot{w}_2 - \dot{\phi}w_6)\} - 2\dot{\phi}w_2w_3] - 2\phi\rho_c(q_c - 1). \end{aligned} \quad (7.112)$$

We note that Eqs. (7.108), (7.109), (7.111) and (7.112) include the  $Z$  dependence through the quantity  $q_c$  unlike Eqs. (5.19), (5.20), (5.22) and (5.23) in the case without the  $Z$  dependence. Moreover, since  $q_c - 1 = \phi f_{2,Z}/\rho_c$ , the  $Z$  dependence gives rise to the new terms containing  $\dot{\delta}_c$  on the right-hand-sides of Eqs. (7.107) and (7.110). Combining Eq. (7.107) with (7.110) to eliminate the time derivative  $\dot{\delta}_c$ , we obtain

$$2\phi^2(w_1 - w_2)w_3\Psi + (2\mu_1 + \mu_3w_3)\Phi + (2\mu_2 + \mu_4w_3)\psi = 0. \quad (7.113)$$

On using the definitions of  $w_1, \dots, w_7$  in Eqs. (4.114)-(4.120), (7.62)-(7.63) and the background Eqs. (7.20)-(7.21), the following equalities hold

$$2\phi^2 (w_1 - w_2) w_3 = 2\mu_1 + \mu_3 w_3 = -4H\phi^2 M_{\text{pl}}^2 w_3, \quad (7.114)$$

$$2\mu_2 + \mu_4 w_3 = 0. \quad (7.115)$$

Then, Eq. (7.113) reduces to

$$\Psi = -\Phi, \quad (7.116)$$

which shows the absence of an anisotropic stress.

It is convenient to introduce the two dimensionless variables,

$$\alpha_{\text{B}} = \frac{\phi^3 G_{3,X}}{2M_{\text{pl}}^2 H}, \quad (7.117)$$

$$\hat{\nu}_S = \frac{q_S \hat{c}_S^2}{4M_{\text{pl}}^4 H^2}, \quad (7.118)$$

where

$$\begin{aligned} q_S \hat{c}_S^2 = & 2M_{\text{pl}}^2 [H\phi^5 \epsilon_\phi G_{3,XX} + H\phi^3 (1 + 2\epsilon_\phi) G_{3,X} - \rho_c (q_c - 1)] \\ & - \phi^6 G_{3,X}^2 \left( 1 + \frac{4M_{\text{pl}}^2}{w_3} \right). \end{aligned} \quad (7.119)$$

Then, the quantities  $w_1, w_2, \mu_1$ , and  $\mu_2$  appearing in Eqs. (7.104) and (7.107) are expressed, respectively, as

$$w_1 = -2HM_{\text{pl}}^2 (\alpha_{\text{B}} + 1), \quad (7.120)$$

$$w_2 = -2HM_{\text{pl}}^2 \alpha_{\text{B}}, \quad (7.121)$$

$$\mu_1 = 2H\phi^2 M_{\text{pl}}^2 w_3 (\alpha_{\text{B}}^2 + \hat{\nu}_S - 1), \quad (7.122)$$

$$\mu_2 = -2H^2 \phi M_{\text{pl}}^2 w_3 (\alpha_{\text{B}}^2 + \hat{\nu}_S). \quad (7.123)$$

On using Eq. (7.116), we can solve Eqs. (7.104) and (7.107) for  $\Psi, \Phi, \psi$ , as

$$\Psi = -\Phi \simeq -\frac{a^2}{2M_{\text{pl}}^2 k^2} \left[ \left( 1 + \frac{\alpha_{\text{B}}^2}{\hat{\nu}_S} \right) (\rho_c \delta_c + \rho_b \delta_b) + \frac{\alpha_{\text{B}}}{\hat{\nu}_S} (q_c - 1) \rho_c \frac{\dot{\delta}_c}{H} \right], \quad (7.124)$$

$$\psi \simeq \frac{a^2}{2M_{\text{pl}}^2 k^2} \frac{\phi}{H} \left[ \left\{ 1 + \frac{\alpha_{\text{B}}(\alpha_{\text{B}} - 1)}{\hat{\nu}_S} \right\} (\rho_c \delta_c + \rho_b \delta_b) + \frac{\alpha_{\text{B}} - 1}{\hat{\nu}_S} (q_c - 1) \rho_c \frac{\dot{\delta}_c}{H} \right]. \quad (7.125)$$

The time derivatives of Eqs. (7.124) and (7.125) give rise to the terms containing  $\ddot{\delta}_c$ , which contribute to Eq. (7.99) of the CDM density contrast. After eliminating  $\Psi$ ,  $\dot{\Phi}$ ,  $\Phi$ ,  $\dot{\psi}$ , and  $\psi$  from Eq. (7.99), we obtain the second-order differential equation for  $\delta_c$ , as

$$\ddot{\delta}_c + H \frac{\hat{c}_S^2}{c_S^2} \left[ 2 + \epsilon_c - \frac{3(q_c - 1)\Omega_c}{2\hat{\nu}_S q_c} \{ (q_c - 1)(1 + 2\epsilon_H + \epsilon_S) - 2q_c \epsilon_c \} \right] \dot{\delta}_c + \frac{3H\alpha_B(q_c - 1)}{2\hat{\nu}_S q_c} \frac{\hat{c}_S^2}{c_S^2} \Omega_b \dot{\delta}_b - \frac{3H^2}{2G} (G_{cc}\Omega_c \delta_c + G_{cb}\Omega_b \delta_b) \simeq 0, \quad (7.126)$$

where

$$G_{cc} = G_{cb} = \left[ 1 + \frac{\alpha_B^2}{\hat{\nu}_S} + \frac{\alpha_B}{\hat{\nu}_S} \{ (q_c - 1)(1 + \epsilon_H + \epsilon_S - \epsilon_B) - q_c \epsilon_c \} \right] \frac{1}{q_c} \frac{\hat{c}_S^2}{c_S^2} G, \quad (7.127)$$

with

$$\epsilon_B \equiv \frac{\dot{\alpha}_B}{H\alpha_B}, \quad \epsilon_S \equiv \frac{\dot{\nu}_S}{H\hat{\nu}_S}. \quad (7.128)$$

From Eqs. (7.88) and (7.89), the ratio between  $c_S^2$  and  $\hat{c}_S^2$  is

$$\frac{c_S^2}{\hat{c}_S^2} = 1 + \frac{\Delta c_S^2}{\hat{c}_S^2} = 1 + \frac{3(q_c - 1)^2 \Omega_c}{2\hat{\nu}_S q_c}. \quad (7.129)$$

The difference  $\Delta c_S^2$  between  $c_S^2$  and  $\hat{c}_S^2$ , which arises from the off-diagonal components of matrix  $\mathbf{B}$  in Eq. (7.71), vanishes for  $f_Z = 0$ .

Substituting Eq. (7.124) into Eq. (7.100), we obtain

$$\ddot{\delta}_b + 2H\dot{\delta}_b - \frac{3H\alpha_B(q_c - 1)}{2\hat{\nu}_S} \Omega_c \dot{\delta}_c - \frac{3H^2}{2G} (G_{bc}\Omega_c \delta_c + G_{bb}\Omega_b \delta_b) \simeq 0, \quad (7.130)$$

where

$$G_{bb} = G_{bc} = \left( 1 + \frac{\alpha_B^2}{\hat{\nu}_S} \right) G. \quad (7.131)$$

As long as  $\hat{c}_S^2$  is positive with the absence of ghosts ( $q_S > 0$ ), the quantity  $\hat{\nu}_S$  is positive. In coupled GP theories the Laplacian instability is absent for  $c_S^2 = \hat{c}_S^2 + \Delta c_S^2 > 0$ , so the condition  $\hat{c}_S^2 > 0$  is not mandatory. To ensure the stability during the whole cosmic expansion history, however, we do not consider the special case where the two inequalities  $\hat{c}_S^2 < 0$  and  $c_S^2 > 0$  hold. As long as  $q_S \hat{c}_S^2 > 0$ , the gravitational couplings  $G_{bb}$  and  $G_{bc}$  of baryons are larger than the Newton constant  $G$ . This enhancement of  $G_{bb}$  is attributed to the cubic-derivative coupling  $G_3(X)$  [169]. If there is no dependence of  $Z$  in  $f_2$ , we have  $q_c = 1$ ,  $\epsilon_c = 0$ , and  $c_S^2 = \hat{c}_S^2$ , so the CDM gravitational couplings (7.127) reduces to the value (7.131) of baryons.



In the presence of the coupling  $f_2(Z)$ , we observe in Eq. (7.127) that  $G_{cc}$  and  $G_{cb}$  are multiplied by the factor  $\hat{c}_S^2/(q_c c_S^2)$ . The quantity  $q_c = 1 + \phi f_{2,Z}/\rho_c$  should be close to 1 during the matter-dominated epoch ( $\phi f_{2,Z} \ll \rho_c$ ), but the magnitude of  $q_c$  becomes greater than 1 after the dominance of the vector-field density as dark energy ( $\phi f_{2,Z} \gtrsim \rho_c$ ). Moreover, as long as  $q_S \hat{c}_S^2 > 0$ , the ratio  $\hat{c}_S^2/c_S^2$  is smaller than 1. Then, it is anticipated that the interaction  $f_2(Z)$  may suppress the values of  $G_{cc}$  and  $G_{cb}$  at low redshifts. The term  $\alpha_B^2/\hat{\nu}_S$  in the square bracket of Eq. (7.127) works to enhance the CDM gravitational coupling, but there are also additional terms proportional to  $\alpha_B$  in Eq. (7.127). We will show that the terms proportional to  $\alpha_B$ , which arise from the mixture of couplings  $G_3(X)$  and  $f_2(Z)$ , can play an important role to modify the values of  $G_{cc}$  and  $G_{cb}$  during the epoch of cosmic acceleration. In Sec. 7.4, we will consider a concrete model of coupled dark energy and investigate whether the realization of  $G_{cc}$  and  $G_{cb}$  smaller than  $G$  is possible. Before doing so, we compute the values of  $G_{cc}$  and  $G_{bb}$  on the de Sitter background.

### 7.3.2 Gravitational couplings on de Sitter background

The background Eqs. (7.20)-(7.22) allow the existence of de Sitter solutions, along which  $\phi$  and  $H$  are constant with  $\rho_I = 0 = P_I$ . On this de Sitter background, we have

$$\epsilon_\phi = 0, \quad \epsilon_H = 0, \quad \epsilon_B = 0, \quad \epsilon_S = 0, \quad \epsilon_c = 3. \quad (7.132)$$

As the solutions approach the de Sitter fixed point, the quantity (7.96) behaves as  $q_c \simeq \phi f_{2,Z}/\rho_c \rightarrow \infty$ , where the positivity of  $q_c$  requires that  $\phi f_{2,Z} > 0$ . Of course, this behavior of  $q_c$  does not mean the divergence of physical quantities. Indeed, on the de Sitter background satisfying Eq. (7.132), Eq. (7.127) reduces to

$$(G_{cc})_{\text{dS}} = (G_{cb})_{\text{dS}} = -2 \frac{\alpha_B}{\hat{\nu}_S} \frac{\hat{c}_S^2}{c_S^2} G. \quad (7.133)$$

In the regime where  $q_c \gg 1$ , the terms proportional to  $\alpha_B$  in the square bracket of Eq. (7.127) completely dominates over  $\alpha_B^2/\hat{\nu}_S$ . This means that the gravitational coupling of CDM is very different from that of baryons around the de Sitter solution. The quantities (7.118) and (7.129) are given,

respectively, by

$$\hat{\nu}_S = \frac{1}{4M_{\text{pl}}^4 H^2} \left[ 2H\phi^3 M_{\text{pl}}^2 G_{3,X} - \phi^6 G_{3,X}^2 \left( 1 + \frac{4M_{\text{pl}}^2}{w_3} \right) - 2\phi M_{\text{pl}}^2 f_{2,Z} \right], \quad (7.134)$$

$$\frac{c_S^2}{\hat{c}_S^2} = 1 + \frac{\phi f_{2,Z}}{2M_{\text{pl}}^2 H^2 \hat{\nu}_S}. \quad (7.135)$$

As long as the condition  $\hat{c}_S^2 > 0$  is satisfied in addition to the absence of ghosts ( $q_S > 0$  and  $\phi f_{2,Z} > 0$ ), we have  $\hat{\nu}_S = q_S \hat{c}_S^2 / (4M_{\text{pl}}^4 H^2) > 0$  and  $c_S^2 / \hat{c}_S^2 > 1$ . Then, from Eq. (7.133),  $(G_{cc})_{\text{dS}} < 0$  for  $\alpha_B > 0$  and  $(G_{cc})_{\text{dS}} > 0$  for  $\alpha_B < 0$ . Substituting Eqs. (7.117), (7.134) and (7.135) into Eq. (7.133), it follows that

$$(G_{cc})_{\text{dS}} = (G_{cb})_{\text{dS}} = \frac{4HM_{\text{pl}}^2 w_3}{\phi^3 G_{3,X} (4M_{\text{pl}}^2 + w_3) - 2HM_{\text{pl}}^2 w_3} G, \quad (7.136)$$

while the baryon gravitational coupling (7.131) yields

$$(G_{bb})_{\text{dS}} = (G_{bc})_{\text{dS}} = \left( 1 + \frac{\phi^6 G_{3,X}^2}{4M_{\text{pl}}^4 H^2 \hat{\nu}_S} \right) G, \quad (7.137)$$

where  $\hat{\nu}_S$  is given by Eq. (7.134). One can express Eq. (7.136) in terms of  $q_V$  [see Eq. (4.116)] and  $\alpha_B$ , as

$$(G_{cc})_{\text{dS}} = (G_{cb})_{\text{dS}} = \frac{2q_V u^2}{(\alpha_B - 1)q_V u^2 - 2\alpha_B} G, \quad (7.138)$$

where

$$u = \frac{\phi}{M_{\text{pl}}}. \quad (7.139)$$

In the expression (7.138),  $u$  should be evaluated on the de Sitter fixed point. Our theory corresponds to  $q_V = 1$ , but we explicitly write  $q_V$  in Eq. (7.138) to accommodate more general intrinsic vector-mode Lagrangians like  $\mathcal{L}_F = -q_V F_{\mu\nu} F^{\mu\nu}/4$ . As we already mentioned, the sign of  $(G_{cc})_{\text{dS}}$  depends on  $\alpha_B$ . When  $\alpha_B = 1$ , for example, we have  $(G_{cc})_{\text{dS}} = -q_V u^2 G$ , while, for  $\alpha_B \gg 1$  and  $q_V u^2 \gg 1$ ,  $(G_{cc})_{\text{dS}} \simeq (2/\alpha_B)G$ . The self-accelerating solution in cubic-order extended Galileon scalar-tensor theory [39, 40] can be regarded as the weak-coupling limit  $q_V \rightarrow \infty$  in Eq. (7.138), so that  $(G_{cc})_{\text{dS}} = 2G/(\alpha_B - 1)$ . Since our coupled GP theory gives the value  $(G_{cc})_{\text{dS}} = 2u^2 G/[(\alpha_B - 1)u^2 - 2\alpha_B]$ , its observational signatures associated with the cosmic growth measurements are different from those in its scalar-tensor counterpart.

## 7.4 Concrete models with momentum transfer

To study the cosmological dynamics relevant to the late-time cosmic acceleration, we consider a concrete model of coupled dark energy given by the action (7.2) with

$$f_2(X, Z) = b_2 X^{p_2} + \beta (2X)^n Z^m, \quad G_3(X) = b_3 X^{p_3}, \quad (7.140)$$

where  $b_2, b_3, p_2, p_3$  and  $\beta, n, m$  are constants. In this model, the background Eq. (7.22) yields

$$2^{1-p_2} b_2 p_2 \phi^{2p_2-1} + 3 \cdot 2^{1-p_3} b_3 p_3 H \phi^{2p_3} + \beta (2n + m) \phi^{2n+m-1} = 0. \quad (7.141)$$

In uncoupled GP theories ( $\beta = 0$ ), Eq. (7.141) shows that  $H$  is related to  $\phi$  according to

$$\phi^p H = \lambda = \text{constant}, \quad (7.142)$$

where  $p = 2p_3 - 2p_2 + 1$ . Provided that  $p > 0$ , the temporal vector component  $\phi$  grows with the decrease of  $H$ . As the vector-field density dominates over the background fluid density, the solutions enter the epoch of cosmic acceleration and finally approach the de Sitter fixed point characterized by constant  $\phi$  [44].

In coupled GP theories which contain the  $Z$  dependence in  $f_2$ , we would like to consider the cosmological background possessing the same property as Eq. (7.142). This can be realized for the powers,

$$p_3 = \frac{1}{2} (p + 2p_2 - 1), \quad n = p_2 - \frac{m}{2}. \quad (7.143)$$

In this case, the three terms in Eq. (7.141) have the same power-law dependence of  $\phi$ . Then, from Eq. (7.141), the constants  $b_2$ ,  $b_3$ , and  $\beta$  are related with each other, as

$$b_3 = -\frac{2^{(p+1)/2} p_2 (b_2 + 2^{p_2} \beta)}{3\lambda(p + 2p_2 - 1)}. \quad (7.144)$$

In the following, we study the dynamics of background and perturbations for the functions (7.140) with the powers (7.143).

### 7.4.1 Background dynamics and theoretically consistent conditions

To study the background dynamics, we take CDM, baryons, and radiation into account as perfect fluids. The dark energy density parameter defined in

Eq. (7.29) yields

$$\Omega_{\text{DE}} = -\frac{(2^{-p_2}b_2 + \beta)\phi^{2p_2}}{3M_{\text{pl}}^2 H^2}. \quad (7.145)$$

By imposing the condition  $\Omega_{\text{DE}} > 0$ , the constants  $b_2$  and  $\beta$  are constrained to be

$$2^{-p_2}b_2 + \beta < 0. \quad (7.146)$$

From Eq. (7.31), we have

$$\Omega_b = 1 - \Omega_{\text{DE}} - \Omega_c - \Omega_r. \quad (7.147)$$

On using Eqs. (7.26) and (7.27), it follows that

$$\epsilon_\phi = \frac{3 - 3\Omega_{\text{DE}} + \Omega_r}{2p(1 + s\Omega_{\text{DE}})}, \quad (7.148)$$

$$\epsilon_H = -\frac{3 - 3\Omega_{\text{DE}} + \Omega_r}{2(1 + s\Omega_{\text{DE}})}, \quad (7.149)$$

where

$$s = \frac{p_2}{p}. \quad (7.150)$$

Then, the density parameters  $\Omega_{\text{DE}}$ ,  $\Omega_c$ , and  $\Omega_r$  obey the differential equations,

$$\Omega'_{\text{DE}} = \frac{(1 + s)\Omega_{\text{DE}}(3 - 3\Omega_{\text{DE}} + \Omega_r)}{1 + s\Omega_{\text{DE}}}, \quad (7.151)$$

$$\Omega'_c = \frac{\Omega_c[\Omega_r - 3(1 + s)\Omega_{\text{DE}}]}{1 + s\Omega_{\text{DE}}}, \quad (7.152)$$

$$\Omega'_r = -\frac{\Omega_r[1 - \Omega_r + (3 + 4s)\Omega_{\text{DE}}]}{1 + s\Omega_{\text{DE}}}, \quad (7.153)$$

where a prime represents a derivative with respect to  $\mathcal{N} = \ln a$ . For a given value of  $s$  and initial conditions of  $\Omega_{\text{DE}}$ ,  $\Omega_c$ , and  $\Omega_r$ , each density parameter is known by integrating Eqs. (7.151)-(7.153) with Eq. (7.147).

The dark energy equation of state in Eq. (7.30) and effective equation of state in Eq. (7.32) are given by

$$w_{\text{DE}} = -\frac{3(1 + s) + s\Omega_r}{3(1 + s\Omega_{\text{DE}})}, \quad (7.154)$$

$$w_{\text{eff}} = \frac{\Omega_r - 3(1 + s)\Omega_{\text{DE}}}{3(1 + s\Omega_{\text{DE}})}, \quad (7.155)$$

respectively. Apart from the fact that non-relativistic matter is separated into CDM and baryons, the background dynamics is the same as that studied

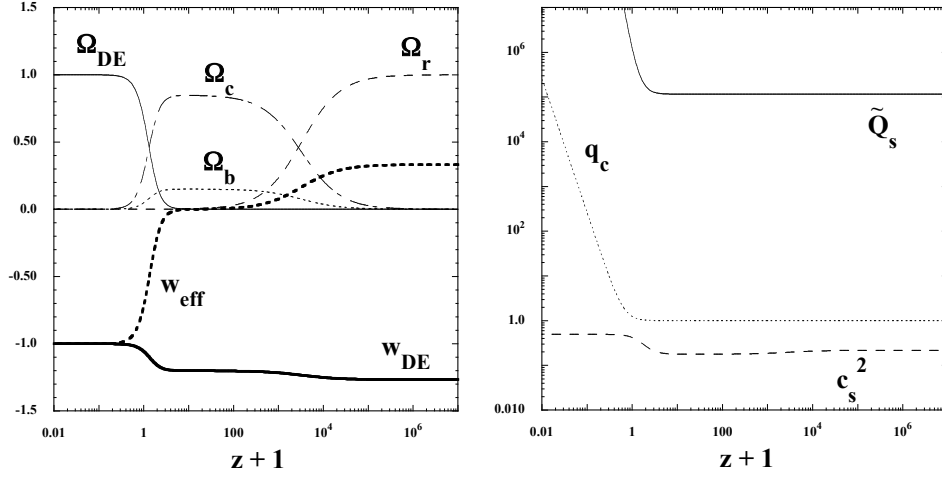


Figure 7.1: (Left) Evolution of  $w_{\text{DE}}$ ,  $w_{\text{eff}}$  and  $\Omega_{\text{DE}}$ ,  $\Omega_c$ ,  $\Omega_b$ ,  $\Omega_r$  versus  $z+1$  for  $s = 1/5$ , where  $z = 1/a - 1$  is the redshift with today's scale factor  $a = 1$ . The initial conditions of  $\Omega_{\text{DE}}$ ,  $\Omega_c$ , and  $\Omega_r$  are chosen to realize their today's values  $\Omega_{\text{DE}}(z=0) = 0.68$ ,  $\Omega_c(z=0) = 0.27$ ,  $\Omega_b(z=0) = 0.05$ , and  $\Omega_r(z=0) = 10^{-4}$ , respectively. (Right) Evolution of  $q_c$ ,  $\tilde{Q}_s = K_{11} M_{\text{pl}}^{2p}/\lambda^2$ , and  $c_s^2$  for  $p_2 = 1$ ,  $p = 5$ ,  $m = 2$ , and  $r_\beta = 0.05$  with the same initial conditions of density parameters as those used in the left panel, with today's dimensionless temporal vector component  $u(z=0) = 0.459$ .

in Ref. [44]. As we observe in Eq. (7.145), the effect of new coupling  $\beta$  can be simply absorbed into the definition of  $\Omega_{\text{DE}}$  at the background level.

During the cosmological sequence of radiation ( $\Omega_r = 1$ ,  $w_{\text{eff}} = 1/3$ ), matter ( $\Omega_c + \Omega_b = 1$ ,  $w_{\text{eff}} = 0$ ), and de Sitter ( $\Omega_{\text{DE}} = 1$ ,  $w_{\text{eff}} = -1$ ) epochs, the dark energy equation of state (7.154) changes as  $w_{\text{DE}} = -1 - 4s/3 \rightarrow -1 - s \rightarrow -1$ , respectively, see the left panel of Fig. 7.1 for the case  $s = 1/5$ . Thus the background dynamics is solely determined by the single parameter  $s$ , which characterizes the deviation from the  $\Lambda$ CDM model.

We define the density parameter associated with the coupling  $\beta$ , as

$$\Omega_\beta = \frac{\beta \phi^{2p_2}}{3M_{\text{pl}}^2 H^2}. \quad (7.156)$$

Then, the no-ghost conditions (7.79) and (7.80) translate, respectively, to

$$q_S = 12M_{\text{pl}}^4 H^2 p^2 s \Omega_{\text{DE}} (1 + s \Omega_{\text{DE}}) > 0, \quad (7.157)$$

$$q_c = 1 + \frac{m \Omega_\beta}{\Omega_c} > 0. \quad (7.158)$$

To satisfy the condition (7.157) in the asymptotic past ( $\Omega_{\text{DE}} \rightarrow +0$ ), the parameter  $s$  is in the range,

$$s > 0. \quad (7.159)$$

This means that  $w_{\text{DE}}$  is always in the phantom region ( $w_{\text{DE}} < -1$ ). Around the future de Sitter fixed point, the parameter (7.158) behaves as  $q_c \simeq m\Omega_\beta/\Omega_c$ , so its positivity requires that

$$m\Omega_\beta > 0. \quad (7.160)$$

For positive  $m$ , the inequality (7.160) implies that  $\beta > 0$ . The condition (7.160) is not obligatory for the cosmic expansion history by today, but we impose it to ensure the stability around the future de Sitter solution.

As for the no strong-coupling condition, the quantity given by Eq. (7.73) reduces to

$$K_{11} = \frac{3p^2 s M_{\text{pl}}^2 H^2 \Omega_{\text{DE}} (1 + s\Omega_{\text{DE}})}{(1 - ps\Omega_{\text{DE}})^2 \phi^2}. \quad (7.161)$$

At early times ( $\Omega_{\text{DE}} \ll 1$ ),  $K_{11}$  has the dependence,

$$K_{11} \propto \Omega_{\text{DE}}^{(ps-1)/[p(s+1)]}, \quad (7.162)$$

so that the strong coupling can be avoided for

$$0 < ps \leq 1, \quad \text{or} \quad 0 < p_2 \leq 1. \quad (7.163)$$

We remind the reader that we are considering the case  $p > 0$ , in order for the Proca field to be responsible for the late-time cosmic acceleration.

During the radiation, matter, and de Sitter epochs, the sound speed squared (7.88) reduces, respectively, to

$$(c_S^2)_{\text{ra}} = \frac{p(3+4s)-2}{3p^2} - \frac{mr_\beta}{2p^2 s}, \quad (7.164)$$

$$(c_S^2)_{\text{ma}} = \frac{p(5+6s)-3}{6p^2} - \frac{mr_\beta}{2p^2 s}, \quad (7.165)$$

$$(c_S^2)_{\text{ds}} = \frac{1}{3p(1+s)} \left( 1 - ps - \frac{4psM_{\text{pl}}^2}{w_3} \right), \quad (7.166)$$

where

$$r_\beta = \frac{\Omega_\beta}{\Omega_{\text{DE}}} = -\frac{\beta}{2^{-p_2} b_2 + \beta}. \quad (7.167)$$

As long as  $\Omega_{\text{DE}} > 0$ , the condition (7.160) translates to  $mr_\beta > 0$ . The constant  $r_\beta$  characterizes the contribution of the coupling  $\beta$  to the total dark energy density. We note that the difference (7.89) between  $c_S^2$  and  $\hat{c}_S^2$  is given by

$$\Delta c_S^2 = \frac{m^2 r_\beta^2 \Omega_{\text{DE}}}{2p^2 s (\Omega_c + mr_\beta \Omega_{\text{DE}}) (1 + s\Omega_{\text{DE}})}. \quad (7.168)$$

This quantity vanishes on the radiation and matter fixed points ( $\Omega_{\text{DE}} = 0$ ), so  $(\hat{c}_S^2)_{\text{ra}}$  and  $(\hat{c}_S^2)_{\text{ma}}$  are identical to  $(c_S^2)_{\text{ra}}$  and  $(c_S^2)_{\text{ma}}$ , respectively. On the de Sitter solution, there is the difference  $(\Delta c_S^2)_{\text{ds}} = mr_\beta/[2p^2s(1+s)]$ , so that

$$(\hat{c}_S^2)_{\text{ds}} = \frac{1}{3p(1+s)} \left( 1 - ps - \frac{4psM_{\text{pl}}^2}{w_3} \right) - \frac{mr_\beta}{2p^2s(1+s)}. \quad (7.169)$$

In Eq. (7.166), the coupling  $\beta$  disappears from  $(c_S^2)_{\text{ds}}$  due to the contribution  $(\Delta c_S^2)_{\text{ds}}$  to  $(\hat{c}_S^2)_{\text{ds}}$ . To avoid the Laplacian instability during the whole cosmological evolution, we require that  $(c_S^2)_{\text{ra}}$ ,  $(c_S^2)_{\text{ma}}$ , and  $(c_S^2)_{\text{ds}}$  are all positive.

In the right panel of Fig. 7.1, we plot the evolution of  $q_c$ ,  $\tilde{Q}_S = K_{11}M_{\text{pl}}^{2p}/\lambda^2$ , and  $c_S^2$  for the model parameters  $p_2 = 1$ ,  $p = 5$ ,  $m = 2$ , and  $r_\beta = 0.05$ . Today's values of density parameters (at the redshift  $z = 0$ ) are the same as those in the left panel, with  $u(z = 0) = \phi(z = 0)/M_{\text{pl}} = 0.459$ . Since  $s (= 1/5)$ ,  $m$ ,  $\Omega_{\text{DE}}$ , and  $r_\beta = \Omega_\beta/\Omega_{\text{DE}}$  are all positive, the no-ghost conditions (7.157) and (7.158) are automatically satisfied. Indeed, the positivities of  $\tilde{Q}_S$  and  $q_c$  can be confirmed in Fig. 7.1. Since the numerical simulation of Fig. 7.1 corresponds to  $ps = 1$ ,  $K_{11}$  stays constant in the asymptotic past ( $\Omega_{\text{DE}} \ll 1$ ), see Eq. (7.162). As we observe in Fig. 7.1, the quantity  $\tilde{Q}_S = K_{11}M_{\text{pl}}^{2p}/\lambda^2$  continues to grow toward the future de Sitter attractor, so there is no strong-coupling problem for the Proca field. This is also the case for CDM, where the quantity  $K_{22}\rho_c^2 = a^2(\rho_c + \phi f_{2,z})/2$  approaches 0 neither in the asymptotic past nor in the future.

For the model parameters used in the numerical simulation of Fig. 7.1, the analytic estimations (7.164) and (7.165) give  $(c_S^2)_{\text{ra}} = 0.217$  and  $(c_S^2)_{\text{ma}} = 0.177$ , which agree well with their numerical values in Fig. 7.1. On using the asymptotic value  $u_{\text{ds}} = \phi_{\text{ds}}/M_{\text{pl}} = 0.474$  on the de Sitter solution, we obtain  $(c_S^2)_{\text{ds}} = 0.494$  and  $(\hat{c}_S^2)_{\text{ds}} = 0.485$  from Eqs. (7.166) and (7.169). Again, they are in good agreement with their numerical values. As we observe in Fig. 7.1, the scalar sound speed squared  $c_S^2$  is always positive from the radiation era to the de Sitter epoch. Hence, for the model parameters and initial conditions used in Fig. 7.1, we realize a viable cosmology without ghosts or Laplacian instabilities.

## 7.4.2 Dynamics of matter perturbations

We proceed to the study of matter density perturbations relevant to the observations of galaxy clusterings, weak lensing, and CMB. Since we are interested in the late-time evolution of perturbations, we ignore the contributions of radiation to the background and perturbation equations.

During the matter-dominated epoch in which  $\Omega_{\text{DE}}$  is less than the order 1, we compute the CDM and baryon gravitational couplings by expanding Eqs. (7.127) and (7.131) in terms of  $\Omega_{\text{DE}}$ . Then, it follows that

$$(G_{cc})_{\text{ma}} = (G_{cb})_{\text{ma}} = [1 + \mathcal{F}\Omega_{\text{DE}} + \mathcal{O}(\Omega_{\text{DE}}^2)] G, \quad (7.170)$$

$$(G_{bb})_{\text{ma}} = (G_{bc})_{\text{ma}} = \left[1 + \frac{s}{3(c_S^2)_{\text{ma}}}\Omega_{\text{DE}} + \mathcal{O}(\Omega_{\text{DE}}^2)\right] G, \quad (7.171)$$

where

$$\mathcal{F} = \frac{s}{3(c_S^2)_{\text{ma}}} - \frac{mr_\beta\{4p(1+s)-1\}}{2p^2(c_S^2)_{\text{ma}}\Omega_c}, \quad (7.172)$$

and  $(c_S^2)_{\text{ma}}$  is given by Eq. (7.165). In the early matter era ( $\Omega_{\text{DE}} \ll 1$ ), both  $(G_{cc})_{\text{ma}}$  and  $(G_{bb})_{\text{ma}}$  are close to  $G$ . With the increase of  $\Omega_{\text{DE}}$ , the gravitational couplings (7.170) and (7.171) start to deviate from  $G$ . Since the factor  $s/[(3c_S^2)_{\text{ma}}]$  in Eq. (7.171) is positive under the absence of ghosts and Laplacian instabilities,  $(G_{bb})_{\text{ma}}$  is larger than  $G$ .

For  $(G_{cc})_{\text{ma}}$  given in Eq. (7.170), there is an extra term arising from the coupling  $\beta$  besides the positive factor  $s/[(3c_S^2)_{\text{ma}}]$ . As long as  $mr_\beta\{4p(1+s)-1\} > 0$ , the coupling  $\beta$  works to reduce  $(G_{cc})_{\text{ma}}$ . If  $\mathcal{F} < 0$  in the early matter era ( $\Omega_c \simeq 1$ ), the factor  $\mathcal{F}$  remains negative due to the decrease of  $\Omega_c$ . If  $\mathcal{F} > 0$  initially, then there is the moment at which  $\mathcal{F}$  crosses 0. This moment of transition can be quantified by the CDM density parameter, as

$$\Omega_c^{\text{T}} = \frac{3mr_\beta[4p(1+s)-1]}{2p^2s}. \quad (7.173)$$

After  $\Omega_c$  drops below  $\Omega_c^{\text{T}}$ ,  $G_{cc}$  becomes smaller than  $G$ . This transition from  $G_{cc} > G$  to  $G_{cc} < G$  occurs for the model parameters satisfying  $\Omega_c^{\text{T}} < 1$ , i.e.,  $2p^2s > 3mr_\beta[4p(1+s)-1]$ . We note that, if  $\Omega_c^{\text{T}}$  is much smaller than 1, the expansion of  $G_{cc}$  of Eq. (7.170) up to first order in  $\Omega_{\text{DE}}$  loses its validity. We are interested in the case where the weak gravitational interaction for CDM ( $G_{cc} < G$ ) is realized by today. In this case,  $\Omega_c^{\text{T}}$  is larger than today's CDM density parameter  $\Omega_c(z=0) \simeq 0.27$ , so that

$$\Omega_c^{\text{T}} > 0.27, \quad (7.174)$$

which can be regarded as a criterion for the realization of weak gravity.

The parameter  $\alpha_{\text{B}}$  defined in Eq. (7.117) is related to  $\Omega_{\text{DE}}$ , as

$$\alpha_{\text{B}} = p_2\Omega_{\text{DE}}. \quad (7.175)$$

Since we are considering the theory with  $q_V = 1$ , the CDM gravitational coupling (7.138) on the de Sitter background reduces to

$$(G_{cc})_{\text{dS}} = (G_{cb})_{\text{dS}} = \frac{2u_{\text{dS}}^2}{(p_2 - 1)u_{\text{dS}}^2 - 2p_2} G, \quad (7.176)$$



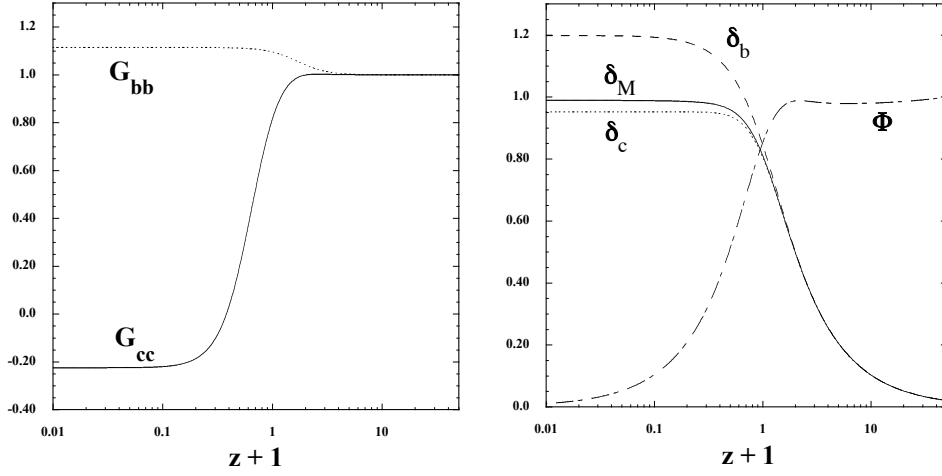


Figure 7.2: Evolution of  $G_{cc}$ ,  $G_{bb}$  (left) and  $\delta_c$ ,  $\delta_b$ ,  $\delta_M$ ,  $\Phi$  (right) versus  $z+1$  for  $p_2 = 1$ ,  $s = 1/5$ ,  $m = 2$ , and  $r_\beta = 0.05$ , with the same initial conditions of density parameters as those used in Fig. 7.1. We choose today's value of the total matter density contrast  $\delta_M$ , as  $\sigma_8(z=0) = 0.811$ . The gravitational potential  $\Phi$  is normalized by its initial value at  $z = 50$ .

where  $u_{\text{dS}} = \phi_{\text{dS}}/M_{\text{pl}}$ . Meanwhile, the baryon gravitational coupling (7.131) on the de Sitter solution yields

$$(G_{bb})_{\text{dS}} = (G_{bc})_{\text{dS}} = \left[ 1 + \frac{s}{3(1+s)(\hat{c}_S)_{\text{dS}}^2} \right] G, \quad (7.177)$$

where  $(\hat{c}_S)_{\text{dS}}^2$  is given by Eq. (7.169). As expected,  $(G_{bb})_{\text{dS}}$  is always larger than  $G$ , but this is not the case for  $(G_{cc})_{\text{dS}}$ .

In the left panel of Fig. 7.2, we show the evolution of  $G_{cc}$  and  $G_{bb}$  for  $z < 50$  by using the same model parameters and initial conditions as those given in the caption of Fig. 7.1. At high redshifts, we have  $\Omega_{\text{DE}} \ll 1$  and hence both  $G_{cc}$  and  $G_{bb}$  are close to  $G$  from Eqs. (7.170) and (7.171). In this case the quantity (7.172) is given by  $\mathcal{F} = 0.377 - 0.260/\Omega_c$ , so  $\mathcal{F}$  is initially positive. The CDM density parameter (7.173) at which  $\mathcal{F}$  crosses 0 is  $\Omega_c^{\text{T}} = 0.69$ . Numerically, we find that  $G_{cc}$  becomes smaller than  $G$  at the redshift  $z < 1.06$ . The numerical value of CDM density parameter at  $z = 1.06$  is  $\Omega_c = 0.71$ , which is close to  $\Omega_c^{\text{T}} = 0.69$  derived by the analytic estimation (7.173). As we observe in Fig. 7.2,  $G_{cc}$  starts to be smaller than  $G$  at  $z = 1.06$  and decreases toward an asymptotic negative constant after crossing  $G_{cc} = 0$ . Since this case corresponds to  $p_2 = 1$  in Eq. (7.176), we have  $(G_{cc})_{\text{dS}} = -u_{\text{dS}}^2 G = -0.225G$ , where we used the numerical value  $u_{\text{dS}} = 0.4743$  on the de Sitter attractor. This analytic estimation of  $(G_{cc})_{\text{dS}}$  is

in good agreement with the asymptotic numerical value seen in Fig. 7.2. As we estimated in Eqs. (7.171) and (7.177), the baryon gravitational coupling  $G_{bb}$  is always larger than  $G$ . For the model parameters used in Fig. 7.2, we have  $(G_{bb})_{\text{dS}} = 1.114G$  from Eq. (7.177), which agrees well with the numerical result.

For larger  $mr_\beta$ , the density parameter (7.173) at transition tends to be larger, so that the CDM perturbation enters the regime  $G_{cc} < G$  earlier. This means that, for increasing values of  $m$  and  $\beta$ , the realization of weak gravity by the momentum transfer starts to occur from higher redshifts. The gravitational coupling (7.176) on the de Sitter background depends on  $p_2$  and  $u_{\text{dS}}$ . Meanwhile, the condition for the no strong-coupling problem at early times imposes that  $0 < p_2 \leq 1$ , under which the denominator of Eq. (7.176) is always negative. Then,  $(G_{cc})_{\text{dS}}$  is negative, as seen in the numerical simulation of Fig. 7.2. In this case the gravitational interaction is no longer attractive, by reflecting the fact that CDM interacts with the self-accelerating vector field through the momentum transfer. As we mentioned in Sec. 7.3, this behavior of  $(G_{cc})_{\text{dS}}$  is mostly attributed to the mixture of couplings  $G_3(X)$  and  $f_2(Z)$ , i.e., the terms proportional to  $\alpha_B$  in Eq. (7.127). Today's CDM gravitational coupling depends on when the transition to the regime  $G_{cc} < G$  occurs as well as on the value of  $(G_{cc})_{\text{dS}}$ . The numerical simulation of Fig. 7.2 corresponds to  $G_{cc}(z=0) = 0.815G$ , with  $G_{bb}(z=0) = 1.095G$ .

In the right panel of Fig. 7.2, we plot the evolution of  $\delta_c$ ,  $\delta_b$ ,  $\delta_M$ , and  $\Phi$  for the same model parameters and background initial conditions as those used in the left. Here,  $\delta_M$  is the total density contrast defined by

$$\delta_M = \frac{\Omega_c}{\Omega_c + \Omega_b} \delta_c + \frac{\Omega_b}{\Omega_c + \Omega_b} \delta_b. \quad (7.178)$$

We numerically solve Eqs. (7.126) and (7.130) with Eqs. (7.127) and (7.131) derived under the quasi-static approximation for linear perturbations deep inside the sound horizon. We start to integrate the perturbation equations around the redshift  $z = 50$  by choosing the initial conditions  $\delta_c = \delta'_c = \delta_i$  and  $\delta_b = \delta'_b = \delta_i$ . The initial amplitude  $\delta_i$  is determined by reproducing today's observed matter density contrast  $\delta_M(z=0)$ , where we adopt the Planck2018 best-fit value  $\delta_M(z=0) = 0.811$  [1].

Since neither  $G_{cc}$  nor  $G_{bb}$  depends on the wavenumber  $k$ , the CDM and baryon perturbations exhibit scale-independent growth. In Fig. 7.2, we observe that the growth of  $\delta_c$  is suppressed relative to that of  $\delta_b$  for the redshift  $z \lesssim 1$ . This behavior is attributed to the gravitational interaction of CDM weaker than that of baryons. Since the CDM density is about five times as large as the baryon density, the total density contrast  $\delta_M$  is mostly affected

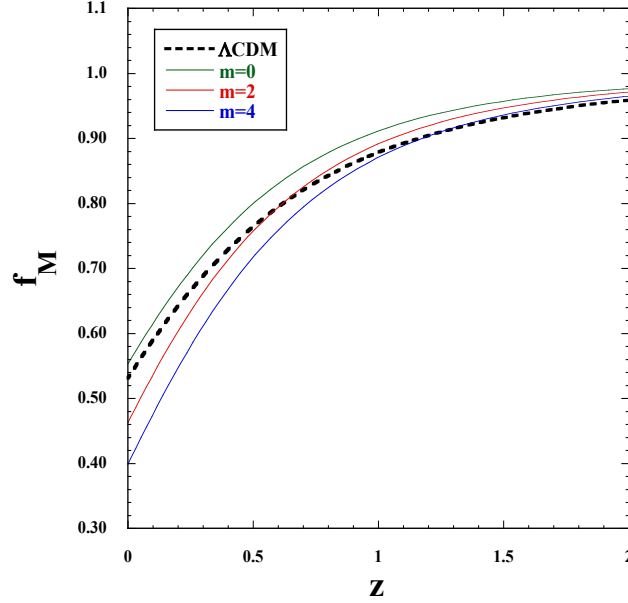


Figure 7.3: Evolution of  $f_M = \dot{\delta}_M / (H\delta_M)$  versus  $z$  for the same background initial conditions of density parameters as those used in Fig. 7.1. The model parameters are  $s = 1/5$ ,  $p_2 = 1$ , and  $r_\beta = 0.05$  with three different values of  $m$ . The dotted line corresponds to the evolution of  $f_M$  in the  $\Lambda$ CDM model.

by CDM perturbations and hence its growth is suppressed in comparison to the standard case with  $G_{cc} = G_{bb} = G$ . This should allow the possibility for alleviating the tension of  $\sigma_8$  between CDM and low-redshift measurements.

In our theory there is no anisotropic stress, so the gravitational potential  $\Psi$  and the weak lensing potential  $\psi_{\text{WL}} = (\Psi - \Phi)/2$  are equivalent to each other, i.e.,  $\Psi = \psi_{\text{WL}} = -\Phi$ . In some models like cubic-order uncoupled scalar Galileons where both  $G_{cc}$  and  $G_{bb}$  are larger than  $G$ ,  $|\psi_{\text{WL}}|$  grows even after the onset of cosmic acceleration [109, 110]. This typically induces a negative ISW-galaxy cross-correlation, which is disfavored observationally [213]. In our coupled GP theory,  $G_{cc}$  can be smaller than  $G$  at low redshifts, so it is possible to avoid the enhancement of  $|\psi_{\text{WL}}|$ . In the numerical simulation of Fig. 7.2, we observe that  $\Phi$  ( $= -\psi_{\text{WL}}$ ) decreases at low redshifts.

In Fig. 7.3, we show the evolution of the matter growth rate  $f_M = \dot{\delta}_M / (H\delta_M)$  for three different values of  $m$ , with the other model parameters and initial conditions same as those used in Fig. 7.2. When  $m = 0$ , we have  $q_c = 1$ ,  $\epsilon_c = 0$ , and  $c_S^2 = \hat{c}_S^2$  in Eqs. (7.126) and (7.127), so the equation of CDM density contrast reduces to the same form as that of baryons with the gravitational coupling  $G_{cc} = (1 + \alpha_B^2 / \hat{\nu}_S)G$ . Since  $G_{cc} = G_{bb} > G$  in this case, the growth rate  $f_M$  is larger than that in the  $\Lambda$ CDM model, see Fig. 7.3.

In contrast, for  $m\beta > 0$ , the CDM gravitational coupling  $G_{cc}$  can be smaller than  $G$  at low redshifts. In the numerical simulation of Fig. 7.3, the growth rate  $f_M$  for  $m = 2$  becomes smaller than that in the  $\Lambda$ CDM model at the redshift  $z < 0.62$ . For increasing  $m$ , the suppression of  $f_M$  tends to be more significant, see the case  $m = 4$  in Fig. 7.3. Thus, our coupled dark energy model with the momentum transfer offers a versatile possibility for realizing the weak cosmic growth rate.

## 7.5 Summary of Chapter 7

In this chapter, we considered the theory with the momentum transfer between CDM and vector dark energy. We derived the covariant equations of motion and obtained Eqs. (7.13) and (7.16). We also derived the background equations and the fluid continuity equations on flat FLRW space-time. When the dark energy is coupled to CDM with the momentum transfer alone, the fluid continuity equations do not have the interacting terms associated with the energy exchange. Moreover, we derived the conditions for ghosts and gradient instabilities for the cosmological perturbation, and we discussed the evolution of matter density perturbations under the quasi-static approximation. The effective gravitational coupling of CDM is quite different from that of baryons at late time, and the former can be smaller than the Newtonian gravitational constant  $G$ . Finally, we consider a concrete dark energy model given by the action Eq. (7.2) with Eq. (7.140). Since the  $Z$  dependence is the dark energy density parameter  $\Omega_{DE}$ , the dark energy equation of state given by Eq. (7.154) is the same form as Eq. (4.160) in the uncoupled case. We showed that there is the parameter space in which we realize a viable cosmology without ghosts or gradient instability. We also confirmed that, due to the existence of the momentum transfer, the linear growth rate of matter contrast around today could be smaller than that in  $\Lambda$ CDM. Then, our model has the possibility of reducing the  $\sigma_8$  tension in  $\Lambda$ CDM.

When our model is confronted with the observations of redshift-space distortions, however, we need to caution that the growth rates of  $\delta_c$  and  $\delta_b$  are different from each other. The analysis of how to constrain the model with the redshift-space distortion data is left for future work.

# Chapter 8

## Summary

In this thesis, we studied dark energy models based on vector-tensor theories in which a vector field is coupled to gravity. In such models, the late-time cosmic acceleration is driven by the vector field.

In Chap.2, we reviewed the standard cosmology and the observational evidence of dark energy. The equation of state  $w_{\text{DE}}$  is a key quantity to discuss the property of dark energy, and the condition for realizing the accelerating universe is given by  $w_{\text{DE}} < -1/3$ .

In Chap.3, we showed some dark energy models which are discussed in previous works. The  $\Lambda$ CDM based on a cosmological constant is a fiducial model in standard cosmology, but there are some problems such as cosmological constant problem,  $H_0$  tension, and  $\sigma_8$  tension. It means that the observational data might prefer alternative theoretical candidates for dark energy to the cosmological constant. As the general framework of scalar-tensor theories, we reviewed Horndeski theory which contains many dark energy models such as the quintessence, the Brans-Dicke theory, and Galileon.

In Chap.4, we introduce the generalized Proca theory which is one of the vector-tensor theories. We consider this theory on the FLRW background and derive the conditions for avoiding the ghost and Laplacian instabilities. Moreover, we show a concrete vector dark energy model, and the equation of state is always less than -1 without the theoretical instabilities.

In Chap.5, we placed observational constraints on a class of dark energy models in the framework of GP theories. The effect of intrinsic vector modes on the dimensionless gravitational couplings  $\mu$  and  $\Sigma$  arises through the quantity  $\lambda_V$  defined by Eq. (4.186), where  $q_V = 1$  for the model (4.140). This allows the possibility for realizing the values of  $\mu$  and  $\Sigma$  close to 1. Moreover, We provided a general formula for the ISW-galaxy cross-correlation spectrum  $C_l^{\text{IG}}$  for the scale-independent growth of linear perturbations. In Sec. 5.4, we performed the MCMC analysis for the dark energy model (4.140)

in cubic-order GP theories by using the ISW-galaxy cross-correlation data of the 2MASS and SDSS surveys combined with the CMB, BAO, SN Ia,  $H(z)$ , and RSD data. The evolution of the dark energy equation of state during the matter era is given by  $w_{\text{DE}} = -1 - s$ , where  $s$  is a positive constant. The parameter  $s$  is constrained to be  $s = 0.185^{+0.100}_{-0.089}$  at 95 % CL, so the model with  $s > 0$  is favored over the  $\Lambda$ CDM model ( $s = 0$ ). At the background level, this property is attributed to the fact that the presence of the additional parameter  $s$  to  $H_0$  and  $\Omega_{m0}$  can reduce the tensions of  $H_0$  between CMB and low-redshift measurements.

For the cosmic growth history, the model can be compatible with both the ISW-galaxy cross-correlation and RSD data thanks to the existence of intrinsic vector modes. From the MCMC simulation, we derived the  $2\sigma$  bound  $\lambda_V < 0.015$ . The likelihood analysis without the ISW-galaxy cross-correlation data placed the  $2\sigma$  constraint  $\lambda_V < 0.029$ . This means that inclusion of the ISW-galaxy data, in particular the SDSS data, provides the tighter constraint on  $\lambda_V$  compared to that obtained from the RSD data. The existence of intrinsic vector modes can make the model compatible with both the ISW-galaxy cross-correlation and RSD data by reducing  $\mu$  and  $\Sigma$  close to 1. As we see in Figs. 5.4 and 5.5, the evolution of  $w_{\text{DE}}$  in the best-fit case is clearly different from that in the  $\Lambda$ CDM model, while the evolution of perturbations is similar to each other. We would like to stress that not only the best-fit  $\chi^2$  but also the AIC and BIC in our model are smaller than those in the  $\Lambda$ CDM model.

In Chap.6, we studied the cosmology of GP theories in which a massive vector field  $A_\mu$  is coupled to CDM with the interacting action (6.3). We proposed a viable model of coupled vector dark energy given by the functions (6.78). For the power  $q = 2p_3$ , the coupling term in Eq. (6.79) grows in proportion to  $t^{1/2}$  in the radiation era and it reaches a constant value during the matter dominance. This interacting term starts to decrease after the onset of cosmic acceleration, which is followed by the approach to de Sitter solutions with  $\rho_c = 0$ . In other words, the effect of interactions between the vector field and CDM on cosmological observables mostly manifests itself from the onset of matter era to today. During the matter dominance, the dark energy equation of state  $w_{\text{DE}}$  is a constant smaller than  $-1$ , so the corresponding density parameter  $\Omega_{\text{DE}}$  grows in time. This property is different from the  $\varphi$ MDE of coupled scalar dark energy models in which  $\Omega_{\text{DE}}$  is a non-vanishing constant affected by the coupling  $\beta$ .

We found that the negative coupling  $Q$  leads to  $w_{\text{DE}}$  closer to  $-1$  relative to the uncoupled case. This is attributed to the fact that, for  $Q < 0$ , CDM decays to the vector field. The maximum value of  $w_{\text{DE}}$  reached during the matter era is determined by the CDM no-ghost condition (7.96). In this

case, the other stability conditions (6.74) and (6.77) of scalar perturbations are satisfied from the radiation era to the de Sitter attractor. For  $p_3 = 1, 2, 3$  the maximum values are given by  $w_{\text{DE}}^{(m)} = -1.52, -1.14, -1.07$ , respectively, which are larger than their corresponding values  $w_{\text{DE}} = -2, -1.33, -1.2$  for  $Q = 0$ . Thus, our coupled dark energy model alleviates the problem of observational incompatibility of uncoupled models with  $p_3 \leq 2$ .

In Chap.7, we studied the cosmology in coupled cubic-order GP theories given by the action (7.2) for the purpose of realizing the weak gravitational interaction on scales relevant to the growth of large-scale structures. The new interaction between the CDM four velocity  $u_c^\mu$  and the vector field  $A_\mu$ , which is weighed by the scalar product  $Z = -u_c^\mu A_\mu$ , exhibits very different properties in comparison to the standard coupled dark energy with the energy transfer. We proposed a concrete coupled dark energy model given by the functions (7.140). For the powers (7.143), the background cosmology satisfying the relation  $\phi^p H = \text{constant}$  ( $p > 0$ ) can be realized, with the new coupling constant  $\beta$  being absorbed into the definition of  $\Omega_{\text{DE}}$ . In other words, the interaction associated with the momentum transfer does not modify the cosmological background of uncoupled GP theories. We also showed that the ghosts are absent under the conditions (7.159) and (7.160). The scalar propagation speed squared in each cosmological epoch is given by Eqs. (7.164), (7.165), and (7.166), which are required to be all positive. The case shown in Fig. 7.1 is an example of the viable cosmology satisfying all the stability conditions. During the matter dominance, the CDM gravitational coupling  $G_{cc}$  is expanded in the form (7.170), which can be used to estimate the moment after which  $G_{cc}$  gets smaller than  $G$ . Provided that the condition (7.174) is satisfied, the transition to the regime  $G_{cc} < G$  occurs by today. On the future de Sitter attractor,  $G_{cc}$  is given by Eq. (7.176), which is always negative in the allowed parameter space constrained by the no-ghost and no-strong-coupling conditions ( $0 < p_2 \leq 1$ ). We showed that the weak gravitational interaction for CDM leads to the suppressed growth of total matter density contrast  $\delta_M$ , see Fig. 7.2. The lensing gravitational potential  $\psi_{\text{WL}} (= -\Phi)$  does not exhibit the enhancement at low redshifts, whose property should be consistent with the observations of ISW-galaxy cross-correlations. For increasing values of  $m$  and  $\beta$ , the growth rates of  $\delta_c$  and  $\delta_M$  tend to be smaller in comparison to the  $\Lambda$ CDM model, see Fig. 7.3.

We thus showed that the coupled GP theories with the momentum transfer offers a novel possibility for achieving the weak cosmic growth for CDM, in spite of the enhancement of baryon gravitational coupling. It will be of interest to investigate further whether the interacting model proposed in this paper reduces the observational tensions of  $\sigma_8$  and  $H_0$  present in the  $\Lambda$ CDM model.

# Bibliography

- [1] N. Aghanim *et al.* [Planck], Astron. Astrophys. **641**, A6 (2020) [arXiv:1807.06209 [astro-ph.CO]].
- [2] A. G. Riess *et al.* [Supernova Search Team], Astron. J. **116**, 1009 (1998) [astro-ph/9805201].
- [3] S. Perlmutter *et al.* [Supernova Cosmology Project Collaboration], Astrophys. J. **517**, 565 (1999) [astro-ph/9812133].
- [4] D. J. Eisenstein *et al.* [SDSS], Astrophys. J. **633**, 560-574 (2005) [arXiv:astro-ph/0501171 [astro-ph]].
- [5] G. B. Zhao, Y. Wang, A. Taruya, W. Zhang, H. Gil-Marín, A. de Mattia, A. J. Ross, A. Raichoor, C. Zhao and W. J. Percival, *et al.* [arXiv:2007.09011 [astro-ph.CO]].
- [6] S. Weinberg, Rev. Mod. Phys. **61**, 1-23 (1989).
- [7] J. Martin, Comptes Rendus Physique **13**, 566-665 (2012) doi:10.1016/j.crhy.2012.04.008 [arXiv:1205.3365 [astro-ph.CO]].
- [8] J. F. Koksma and T. Prokopec, [arXiv:1105.6296 [gr-qc]].
- [9] E. K. Akhmedov, [arXiv:hep-th/0204048 [hep-th]].
- [10] T. M. C. Abbott *et al.* [DES], Mon. Not. Roy. Astron. Soc. **480**, no.3, 3879-3888 (2018) [arXiv:1711.00403 [astro-ph.CO]].
- [11] L. Verde, T. Treu and A. G. Riess, Nature Astronomy, **3**, 891-895 (2019) [arXiv:1907.10625 [astro-ph.CO]].
- [12] H. Hildebrandt *et al.*, Mon. Not. Roy. Astron. Soc. **465**, 1454 (2017) [arXiv:1606.05338 [astro-ph.CO]].
- [13] T. M. C. Abbott *et al.* [DES], Phys. Rev. D **98**, no.4, 043526 (2018) doi:10.1103/PhysRevD.98.043526 [arXiv:1708.01530 [astro-ph.CO]].



- [14] Y. Fujii, Phys. Rev. D **26**, 2580 (1982).
- [15] L. H. Ford, Phys. Rev. D **35**, 2339 (1987).
- [16] B. Ratra and P. J. E. Peebles, Phys. Rev. D **37**, 3406 (1988).
- [17] C. Wetterich, Nucl. Phys. B **302**, 668 (1988) [arXiv:1711.03844 [hep-th]].
- [18] T. Chiba, N. Sugiyama and T. Nakamura, Mon. Not. Roy. Astron. Soc. **289**, L5 (1997) [astro-ph/9704199].
- [19] P. G. Ferreira and M. Joyce, Phys. Rev. Lett. **79**, 4740 (1997) [astro-ph/9707286].
- [20] R. R. Caldwell, R. Dave and P. J. Steinhardt, Phys. Rev. Lett. **80**, 1582 (1998) [astro-ph/9708069].
- [21] E. J. Copeland, A. R. Liddle and D. Wands, Phys. Rev. D **57**, 4686 (1998) [gr-qc/9711068].
- [22] P. G. Ferreira and M. Joyce, Phys. Rev. D **58**, 023503 (1998) [astro-ph/9711102].
- [23] C. Brans and R. H. Dicke, Phys. Rev. **124**, 925 (1961).
- [24] M. Ostrogradsky, Mem. Acad. St. Petersburg **6**, no.4, 385-517 (1850).
- [25] H. Motohashi and T. Suyama, Phys. Rev. D **91**, no.8, 085009 (2015) [arXiv:1411.3721 [physics.class-ph]].
- [26] G. W. Horndeski, Int. J. Theor. Phys. **10**, 363 (1974).
- [27] C. Deffayet, X. Gao, D. A. Steer and G. Zahariade, Phys. Rev. D **84**, 064039 (2011) [arXiv:1103.3260 [hep-th]].
- [28] T. Kobayashi, M. Yamaguchi and J. Yokoyama, Prog. Theor. Phys. **126**, 511 (2011) [arXiv:1105.5723 [hep-th]].
- [29] C. Deffayet, A. E. Gümrükçüoğlu, S. Mukohyama and Y. Wang, JHEP **04**, 082 (2014) doi:10.1007/JHEP04(2014)082 [arXiv:1312.6690 [hep-th]].
- [30] L. Heisenberg, JCAP **1405**, 015 (2014) [arXiv:1402.7026 [hep-th]].
- [31] A. A. Penzias and R. W. Wilson, Astrophys. J. **142**, 419-421 (1965).
- [32] G. F. Smoot *et al.* [COBE], Astrophys. J. Lett. **396**, L1-L5 (1992).

- [33] L. Amendola and S. Tsujikawa, “Dark Energy: Theory and Observations”, Cambridge Univ. Press (2010)
- [34] G. G. Fazio, R. Barkana, S. Tsujikawa and J. E. Kim, “The Encyclopedia of Cosmology: Volume 3: Dark Energy”, World Scientific (2018)
- [35] A. De Felice and S. Tsujikawa, Phys. Rev. Lett. **105**, 111301 (2010) [arXiv:1007.2700 [astro-ph.CO]].
- [36] A. De Felice and S. Tsujikawa, Phys. Rev. D **84**, 124029 (2011) [arXiv:1008.4236 [hep-th]].
- [37] S. Nesseris, A. De Felice and S. Tsujikawa, Phys. Rev. D **82**, 124054 (2010) [arXiv:1010.0407 [astro-ph.CO]].
- [38] S. Peirone, N. Frusciante, B. Hu, M. Raveri and A. Silvestri, Phys. Rev. D **97**, no.6, 063518 (2018) [arXiv:1711.04760 [astro-ph.CO]].
- [39] A. De Felice and S. Tsujikawa, JCAP **02**, 007 (2012) [arXiv:1110.3878 [gr-qc]].
- [40] A. De Felice and S. Tsujikawa, JCAP **03**, 025 (2012) [arXiv:1112.1774 [astro-ph.CO]].
- [41] N. Frusciante, S. Peirone, L. Atayde and A. De Felice, Phys. Rev. D **101**, no.6, 064001 (2020) [arXiv:1912.07586 [astro-ph.CO]].
- [42] A. G. Riess *et al.*, Astrophys. J. **826**, no. 1, 56 (2016) [arXiv:1604.01424 [astro-ph.CO]].
- [43] A. G. Riess *et al.*, Astrophys. J. **855**, 136 (2018).
- [44] A. De Felice, L. Heisenberg, R. Kase, S. Mukohyama, S. Tsujikawa and Y. I. Zhang, JCAP **1606**, 048 (2016) [arXiv:1603.05806 [gr-qc]].
- [45] A. De Felice, L. Heisenberg and S. Tsujikawa, Phys. Rev. D **95**, 123540 (2017) [arXiv:1703.09573 [astro-ph.CO]].
- [46] M. Hamuy, M. M. Phillips, R. A. Schommer, N. B. Suntzeff, J. Maza and R. Aviles, Astron. J. **112**, 2391 (1996) [arXiv:astro-ph/9609059 [astro-ph]].
- [47] N. Suzuki *et al.* [Supernova Cosmology Project Collaboration], Astrophys. J. **746**, 85 (2012) [arXiv:1105.3470 [astro-ph.CO]].

- [48] D. N. Spergel *et al.* [WMAP Collaboration], *Astrophys. J. Suppl.* **148**, 175 (2003) [astro-ph/0302209].
- [49] G. Hinshaw *et al.* [WMAP Collaboration], *Astrophys. J. Suppl.* **208**, 19 (2013) [arXiv:1212.5226 [astro-ph.CO]].
- [50] P. A. R. Ade *et al.* [Planck Collaboration], *Astron. Astrophys.* **571**, A16 (2014) [arXiv:1303.5076 [astro-ph.CO]].
- [51] P. A. R. Ade *et al.* [Planck Collaboration], *Astron. Astrophys.* **594**, A14 (2016) [arXiv:1502.01590 [astro-ph.CO]].
- [52] F. Beutler *et al.*, *Mon. Not. Roy. Astron. Soc.* **416**, 3017 (2011) [arXiv:1106.3366 [astro-ph.CO]].
- [53] A. J. Ross, L. Samushia, C. Howlett, W. J. Percival, A. Burden and M. Manera, *Mon. Not. Roy. Astron. Soc.* **449**, no. 1, 835 (2015) [arXiv:1409.3242 [astro-ph.CO]].
- [54] S. Alam *et al.* [BOSS Collaboration], *Mon. Not. Roy. Astron. Soc.* **470**, no. 3, 2617 (2017) [arXiv:1607.03155 [astro-ph.CO]].
- [55] L. Anderson *et al.* [BOSS Collaboration], *Mon. Not. Roy. Astron. Soc.* **441**, no. 1, 24 (2014) [arXiv:1312.4877 [astro-ph.CO]].
- [56] E. A. Kazin *et al.*, *Mon. Not. Roy. Astron. Soc.* **441**, no. 4, 3524 (2014) [arXiv:1401.0358 [astro-ph.CO]].
- [57] S. Weinberg, *Rev. Mod. Phys.* **61**, 1 (1989).
- [58] J. Martin, *Comptes Rendus Physique* **13**, 566 (2012) [arXiv:1205.3365 [astro-ph.CO]].
- [59] E. J. Copeland, M. Sami and S. Tsujikawa, *Int. J. Mod. Phys. D* **15**, 1753 (2006) [hep-th/0603057].
- [60] A. De Felice and S. Tsujikawa, *Living Rev. Rel.* **13**, 3 (2010) [arXiv:1002.4928 [gr-qc]].
- [61] T. Clifton, P. G. Ferreira, A. Padilla and C. Skordis, *Phys. Rept.* **513**, 1 (2012) [arXiv:1106.2476 [astro-ph.CO]].
- [62] A. Joyce, B. Jain, J. Khoury and M. Trodden, *Phys. Rept.* **568**, 1 (2015) [arXiv:1407.0059 [astro-ph.CO]].
- [63] L. Heisenberg, *Phys. Rept.* **796**, 1-113 (2019) [arXiv:1807.01725 [gr-qc]].

- [64] R. Kase and S. Tsujikawa, Int. J. Mod. Phys. D **28**, no.05, 1942005 (2019) [arXiv:1809.08735 [gr-qc]].
- [65] C. Armendariz-Picon, T. Damour and V. F. Mukhanov, Phys. Lett. B **458**, 209 (1999) [hep-th/9904075].
- [66] T. Chiba, T. Okabe and M. Yamaguchi, Phys. Rev. D **62**, 023511 (2000) [astro-ph/9912463].
- [67] C. Armendariz-Picon, V. F. Mukhanov and P. J. Steinhardt, Phys. Rev. Lett. **85**, 4438 (2000) [astro-ph/0004134].
- [68] C. Charmousis, E. J. Copeland, A. Padilla and P. M. Saffin, Phys. Rev. Lett. **108**, 051101 (2012) [arXiv:1106.2000 [hep-th]].
- [69] S. Tsujikawa, K. Uddin, S. Mizuno, R. Tavakol and J. Yokoyama, Phys. Rev. D **77**, 103009 (2008) [arXiv:0803.1106 [astro-ph]].
- [70] C. Umiltà, M. Ballardini, F. Finelli and D. Paoletti, JCAP **1508**, 017 (2015) [arXiv:1507.00718 [astro-ph.CO]].
- [71] M. Ballardini, F. Finelli, C. Umiltà and D. Paoletti, JCAP **1605**, no. 05, 067 (2016) [arXiv:1601.03387 [astro-ph.CO]].
- [72] W. Hu and I. Sawicki, Phys. Rev. D **76**, 064004 (2007) [arXiv:0705.1158 [astro-ph]].
- [73] A. A. Starobinsky, JETP Lett. **86**, 157 (2007) [arXiv:0706.2041 [astro-ph]].
- [74] S. A. Appleby and R. A. Battye, Phys. Lett. B **654**, 7 (2007) [arXiv:0705.3199 [astro-ph]].
- [75] S. Tsujikawa, Phys. Rev. D **77**, 023507 (2008) [arXiv:0709.1391 [astro-ph]].
- [76] C. Deffayet, O. Pujolas, I. Sawicki and A. Vikman, JCAP **1010**, 026 (2010) [arXiv:1008.0048 [hep-th]].
- [77] A. Nicolis, R. Rattazzi and E. Trincherini, Phys. Rev. D **79**, 064036 (2009) [arXiv:0811.2197 [hep-th]].
- [78] C. Deffayet, G. Esposito-Farese and A. Vikman, Phys. Rev. D **79**, 084003 (2009) [arXiv:0901.1314 [hep-th]].

- [79] A. De Felice, T. Kobayashi and S. Tsujikawa, Phys. Lett. B **706**, 123 (2011) [arXiv:1108.4242 [gr-qc]].
- [80] L. Amendola, M. Kunz, M. Motta, I. D. Saltas and I. Sawicki, Phys. Rev. D **87**, 023501 (2013) [arXiv:1210.0439 [astro-ph.CO]].
- [81] M. Raveri, B. Hu, N. Frusciante and A. Silvestri, Phys. Rev. D **90**, 043513 (2014) [arXiv:1405.1022 [astro-ph.CO]].
- [82] E. Bellini and I. Sawicki, JCAP **1407**, 050 (2014) [arXiv:1404.3713 [astro-ph.CO]].
- [83] M. Zumalacarregui, E. Bellini, I. Sawicki, J. Lesgourgues and P. G. Ferreira, JCAP **1708**, 019 (2017) [arXiv:1605.06102 [astro-ph.CO]].
- [84] G. Tasinato, JHEP **1404**, 067 (2014) [arXiv:1402.6450 [hep-th]].
- [85] G. Tasinato, Class. Quant. Grav. **31**, 225004 (2014) [arXiv:1404.4883 [hep-th]].
- [86] E. Allys, P. Peter and Y. Rodriguez, JCAP **1602**, 004 (2016) [arXiv:1511.03101 [hep-th]].
- [87] J. B. Jimenez and L. Heisenberg, Phys. Lett. B **757**, 405 (2016) [arXiv:1602.03410 [hep-th]].
- [88] E. Allys, J. P. Beltran Almeida, P. Peter and Y. Rodriguez, JCAP **1609**, 026 (2016) [arXiv:1605.08355 [hep-th]].
- [89] A. De Felice, L. Heisenberg, R. Kase, S. Mukohyama, S. Tsujikawa and Y. l. Zhang, Phys. Rev. D **94**, 044024 (2016) [arXiv:1605.05066 [gr-qc]].
- [90] A. De Felice, L. Heisenberg, R. Kase, S. Tsujikawa, Y. l. Zhang and G. B. Zhao, Phys. Rev. D **93**, 104016 (2016) [arXiv:1602.00371 [gr-qc]].
- [91] S. Nakamura, R. Kase and S. Tsujikawa, Phys. Rev. D **96**, 084005 (2017) [arXiv:1707.09194 [gr-qc]].
- [92] B. P. Abbott *et al.* [LIGO Scientific and Virgo Collaborations], Phys. Rev. Lett. **119**, 161101 (2017) [arXiv:1710.05832 [gr-qc]].
- [93] A. Goldstein *et al.*, Astrophys. J. **848**, no. 2, L14 (2017) doi:10.3847/2041-8213/aa8f41 [arXiv:1710.05446 [astro-ph.HE]].

- [94] B. P. Abbott *et al.* [LIGO Scientific and Virgo and Fermi-GBM and INTEGRAL Collaborations], *Astrophys. J.* **848**, no. 2, L13 (2017) [arXiv:1710.05834 [astro-ph.HE]].
- [95] T. Baker, E. Bellini, P. G. Ferreira, M. Lagos, J. Noller and I. Sawicki, *Phys. Rev. Lett.* **119**, 251301 (2017) [arXiv:1710.06394 [astro-ph.CO]].
- [96] P. Creminelli and F. Vernizzi, *Phys. Rev. Lett.* **119**, 251302 (2017) [arXiv:1710.05877 [astro-ph.CO]].
- [97] J. Sakstein and B. Jain, *Phys. Rev. Lett.* **119**, 251303 (2017) [arXiv:1710.05893 [astro-ph.CO]].
- [98] M. Crisostomi and K. Koyama, *Phys. Rev. D* **97**, 084004 (2018) [arXiv:1712.06556 [astro-ph.CO]].
- [99] R. Kase and S. Tsujikawa, *Phys. Rev. D* **97**, 103501 (2018) [arXiv:1802.02728 [gr-qc]].
- [100] J. M. Ezquiaga and M. Zumalacárregui, *Phys. Rev. Lett.* **119**, no. 25, 251304 (2017) [arXiv:1710.05901 [astro-ph.CO]].
- [101] L. Amendola, M. Kunz, I. D. Saltas and I. Sawicki, *Phys. Rev. Lett.* **120**, 131101 (2018) [arXiv:1711.04825 [astro-ph.CO]].
- [102] R. G. Crittenden and N. Turok, *Phys. Rev. Lett.* **76**, 575 (1996) [astro-ph/9510072].
- [103] N. Afshordi, Y. S. Loh and M. A. Strauss, *Phys. Rev. D* **69**, 083524 (2004) [astro-ph/0308260].
- [104] P. S. Corasaniti, T. Giannantonio and A. Melchiorri, *Phys. Rev. D* **71**, 123521 (2005) [astro-ph/0504115].
- [105] L. Pogosian, P. S. Corasaniti, C. Stephan-Otto, R. Crittenden and R. Nichol, *Phys. Rev. D* **72**, 103519 (2005) [astro-ph/0506396].
- [106] T. Giannantonio, R. Scrantonand, R. G. Crittenden, R. C. Nichol, S. P. Boughn, A. D. Myers and G. T. Richards, *Phys. Rev. D* **77**, 123520 (2008) [arXiv:0801.4380[astro-ph]].
- [107] T. Giannantonio, R. Crittenden, R. Nichol and A. J. Ross, *Mon. Not. Roy. Astron. Soc.* **426**, 2581 (2012) [arXiv:1209.2125 [astro-ph.CO]].

- [108] M. Ballardini, D. Paoletti, F. Finelli, L. Moscardini, B. Sartoris and L. Valenziano, *Mon. Not. Roy. Astron. Soc.* **482**, 2670 (2019) [arXiv:1712.02380 [astro-ph.CO]].
- [109] T. Kobayashi, H. Tashiro and D. Suzuki, *Phys. Rev. D* **81**, 063513 (2010) [arXiv:0912.4641 [astro-ph.CO]].
- [110] R. Kimura, T. Kobayashi and K. Yamamoto, *Phys. Rev. D* **85**, 123503 (2012) [arXiv:1110.3598 [astro-ph.CO]].
- [111] J. Renk, M. Zumalacarregui, F. Montanari and A. Barreira, *JCAP* **1710**, 020 (2017) [arXiv:1707.02263 [astro-ph.CO]].
- [112] B. F. Schutz and R. Sorkin, *Annals Phys.* **107**, 1 (1977).
- [113] J. M. Bardeen, *Phys. Rev. D* **22**, 1882 (1980).
- [114] L. Amendola, M. Kunz and D. Sapone, *JCAP* **0804**, 013 (2008) [arXiv:0704.2421 [astro-ph]].
- [115] Y. S. Song and K. Koyama, *JCAP* **0901**, 048 (2009) [arXiv:0802.3897 [astro-ph]].
- [116] S. Tsujikawa and T. Tatekawa, *Phys. Lett. B* **665**, 325 (2008) [arXiv:0804.4343 [astro-ph]].
- [117] G. B. Zhao, L. Pogosian, A. Silvestri and J. Zylberberg, *Phys. Rev. D* **79**, 083513 (2009) [arXiv:0809.3791 [astro-ph]].
- [118] R. Bean and M. Tangmatitham, *Phys. Rev. D* **81**, 083534 (2010) [arXiv:1002.4197 [astro-ph.CO]].
- [119] A. Silvestri, L. Pogosian and R. V. Buniy, *Phys. Rev. D* **87**, 104015 (2013) [arXiv:1302.1193 [astro-ph.CO]].
- [120] B. Boisseau, G. Esposito-Farese, D. Polarski and A. A. Starobinsky, *Phys. Rev. Lett.* **85**, 2236 (2000) [gr-qc/0001066].
- [121] N. Bolis, A. De Felice and S. Mukohyama, *Phys. Rev. D* **98**, 024010 (2018) [arXiv:1804.01790 [astro-ph.CO]].
- [122] D. J. Eisenstein and W. Hu, *Astrophys. J.* **496**, 605 (1998) [astro-ph/9709112].
- [123] D. J. Eisenstein and W. Hu, *Astrophys. J.* **511**, 5 (1997) [astro-ph/9710252].

- [124] L. M. Wang and P. J. Steinhardt, *Astrophys. J.* **508**, 483 (1998) [astro-ph/9804015].
- [125] S. Tsujikawa, R. Gannouji, B. Moraes and D. Polarski, *Phys. Rev. D* **80**, 084044 (2009) [arXiv:0908.2669 [astro-ph.CO]].
- [126] A. Pouri, S. Basilakos and M. Plionis, *JCAP* **1408**, 042 (2014) [arXiv:1402.0964 [astro-ph.CO]].
- [127] A. Rassat, K. Land, O. Lahav and F. B. Abdalla, *Mon. Not. Roy. Astron. Soc.* **377**, 1085 (2007) [astro-ph/0610911].
- [128] W. Hu and N. Sugiyama, *Astrophys. J.* **444**, 489 (1995) [astro-ph/9407093].
- [129] Y. Wang and M. Dai, *Phys. Rev. D* **94**, 083521 (2016) [arXiv:1509.02198 [astro-ph.CO]].
- [130] M. J. Hudson and S. J. Turnbull, *Astrophys. J. Let.* **751**, 30 (2012) [arXiv:1203.4814 [astro-ph.CO]].
- [131] F. Beutler *et al.*, *Mon. Not. Roy. Astron. Soc.* **423**, 3430 (2012) [arXiv:1204.4725 [astro-ph.CO]].
- [132] C. Howlett, A. Ross, L. Samushia, W. Percival and M. Manera, *Mon. Not. Roy. Astron. Soc.* **449**, 848 (2015) [arXiv:1409.3238 [astro-ph.CO]].
- [133] W. J. Percival *et al.* [2dFGRS Collaboration], *Mon. Not. Roy. Astron. Soc.* **353**, 1201 (2004) [astro-ph/0406513].
- [134] Y. S. Song and W. J. Percival, *JCAP* **0910**, 004 (2009) [arXiv:0807.0810 [astro-ph]].
- [135] C. Blake *et al.*, *Mon. Not. Roy. Astron. Soc.* **415**, 2876 (2011) [arXiv:1104.2948 [astro-ph.CO]].
- [136] J. Zheng, G. B. Zhao, J. Li, Y. Wang, C. H. Chuang, F. S. Kitaura and S. Rodriguez-Torres, *Mon. Not. Roy. Astron. Soc.* **484**, no.1, 442-450 (2019) [arXiv:1806.01920 [astro-ph.CO]].
- [137] S. de la Torre *et al.*, *Astron. Astrophys.* **557**, A54 (2013) [arXiv:1303.2622 [astro-ph.CO]].
- [138] T. Okumura *et al.*, *Publ. Astron. Soc. Jap.* **68**, 38 (2016) [arXiv:1511.08083 [astro-ph.CO]].



- [139] H. Akaike, IEEE Trans. Auto. Control, **19**, 716 (1974).
- [140] G. Schwarz, Annals of Statistics, **5**, 461 (1978)
- [141] G. Jungman, M. Kamionkowski and K. Griest, Phys. Rept. **267**, 195 (1996) [hep-ph/9506380].
- [142] G. Bertone, D. Hooper and J. Silk, Phys. Rept. **405**, 279 (2005) [hep-ph/0404175].
- [143] W. J. Percival *et al.* [2dFGRS Collaboration], Mon. Not. Roy. Astron. Soc. **353**, 1201 (2004) [astro-ph/0406513].
- [144] C. Blake *et al.*, Mon. Not. Roy. Astron. Soc. **415**, 2876 (2011) [arXiv:1104.2948 [astro-ph.CO]].
- [145] C. Wetterich, Astron. Astrophys. **301**, 321 (1995) [hep-th/9408025].
- [146] Y. Fujii and K. Maeda, “The scalar-tensor theory of gravitation,” Cambridge University Press (2003).
- [147] L. Amendola, Phys. Rev. D **62**, 043511 (2000) [astro-ph/9908023].
- [148] F. Piazza and S. Tsujikawa, JCAP **0407**, 004 (2004) [hep-th/0405054].
- [149] S. Tsujikawa and M. Sami, Phys. Lett. B **603**, 113 (2004) [hep-th/0409212].
- [150] B. Gumjudpai, T. Naskar, M. Sami and S. Tsujikawa, JCAP **0506**, 007 (2005) [hep-th/0502191].
- [151] A. R. Gomes and L. Amendola, JCAP **1403**, 041 (2014) [arXiv:1306.3593 [astro-ph.CO]].
- [152] A. R. Gomes and L. Amendola, JCAP **1602**, 035 (2016) [arXiv:1511.01004 [gr-qc]].
- [153] L. Amendola, D. Bettoni, G. Domenech and A. R. Gomes, JCAP **1806**, 029 (2018) [arXiv:1803.06368 [gr-qc]].
- [154] N. Frusciante, R. Kase, N. J. Nunes and S. Tsujikawa, Phys. Rev. D **98**, 123517 (2018) [arXiv:1810.07957 [gr-qc]].
- [155] N. Frusciante, R. Kase, K. Koyama, S. Tsujikawa and D. Vernieri, Phys. Lett. B **790**, 167 (2019) [arXiv:1812.05204 [gr-qc]].

- [156] L. Amendola, M. Quartin, S. Tsujikawa and I. Waga, Phys. Rev. D **74**, 023525 (2006) [astro-ph/0605488].
- [157] N. Dalal, K. Abazajian, E. E. Jenkins and A. V. Manohar, Phys. Rev. Lett. **87**, 141302 (2001) [astro-ph/0105317].
- [158] W. Zimdahl and D. Pavon, Phys. Lett. B **521**, 133 (2001) [astro-ph/0105479].
- [159] L. P. Chimento, A. S. Jakubi, D. Pavon and W. Zimdahl, Phys. Rev. D **67**, 083513 (2003) [astro-ph/0303145].
- [160] H. Wei and S. N. Zhang, Phys. Lett. B **644**, 7 (2007) [astro-ph/0609597].
- [161] L. Amendola, G. Camargo Campos and R. Rosenfeld, Phys. Rev. D **75**, 083506 (2007) [astro-ph/0610806].
- [162] Z. K. Guo, N. Ohta and S. Tsujikawa, Phys. Rev. D **76**, 023508 (2007) [astro-ph/0702015].
- [163] B. Wang, Y. g. Gong and E. Abdalla, Phys. Lett. B **624**, 141 (2005) [hep-th/0506069].
- [164] B. Wang, E. Abdalla, F. Atrio-Barandela and D. Pavon, Rept. Prog. Phys. **79**, no. 9, 096901 (2016) [arXiv:1603.08299 [astro-ph.CO]].
- [165] P. Fleury, J. P. B. Almeida, C. Pitrou and J. P. Uzan, JCAP **1411**, 043 (2014). [arXiv:1406.6254 [hep-th]].
- [166] M. Hull, K. Koyama and G. Tasinato, Phys. Rev. D **93**, 064012 (2016) [arXiv:1510.07029 [hep-th]].
- [167] E. Allys, P. Peter and Y. Rodriguez, JCAP **1602**, 004 (2016) [arXiv:1511.03101 [hep-th]].
- [168] J. B. Jimenez and L. Heisenberg, Phys. Lett. B **757**, 405 (2016) [arXiv:1602.03410 [hep-th]].
- [169] A. De Felice, L. Heisenberg, R. Kase, S. Mukohyama, S. Tsujikawa and Y. I. Zhang, Phys. Rev. D **94**, no. 4, 044024 (2016) [arXiv:1605.05066 [gr-qc]].
- [170] S. Nakamura, A. De Felice, R. Kase and S. Tsujikawa, Phys. Rev. D **99**, 063533 (2019) [arXiv:1811.07541 [astro-ph.CO]].

- [171] A. De Felice, J. M. Gerard and T. Suyama, Phys. Rev. D **81**, 063527 (2010) [arXiv:0908.3439 [gr-qc]].
- [172] L. Heisenberg, R. Kase and S. Tsujikawa, Phys. Rev. D **98**, 123504 (2018) [arXiv:1807.07202 [gr-qc]].
- [173] P. J. E. Peebles, Astrophys. J. **284**, 439 (1984).
- [174] P. J. E. Peebles, Astrophys. J. **263**, L1 (1982).
- [175] A. G. Riess, S. Casertano, W. Yuan, L. M. Macri and D. Scolnic, Astrophys. J. **876**, no. 1, 85 (2019) [arXiv:1903.07603 [astro-ph.CO]].
- [176] W. L. Freedman, B. F. Madore, D. Hatt, T. J. Hoyt, I. S. Jang, R. L. Beaton, C. R. Burns, M. G. Lee, A. J. Monson and J. R. Neeley, *et al.* doi:10.3847/1538-4357/ab2f73 [arXiv:1907.05922 [astro-ph.CO]].
- [177] K. C. Wong, S. H. Suyu, G. C. F. Chen, C. E. Rusu, M. Milon, D. Sluse, V. Bonvin, C. D. Fassnacht, S. Taubenberger and M. W. Auger, *et al.* Mon. Not. Roy. Astron. Soc. **498**, no.1, 1420-1439 (2020) [arXiv:1907.04869 [astro-ph.CO]].
- [178] M. J. Reid, D. W. Pesce and A. G. Riess, Astrophys. J. **886**, no. 2, L27 (2019) [arXiv:1908.05625 [astro-ph.GA]].
- [179] E. Macaulay, I. K. Wehus and H. K. Eriksen, Phys. Rev. Lett. **111**, 161301 (2013) [arXiv:1303.6583 [astro-ph.CO]].
- [180] S. Nesseris, G. Pantazis and L. Perivolaropoulos, Phys. Rev. D **96**, 023542 (2017) [arXiv:1703.10538 [astro-ph.CO]].
- [181] S. Joudaki *et al.*, Mon. Not. Roy. Astron. Soc. **474**, 4894 (2018) [arXiv:1707.06627 [astro-ph.CO]].
- [182] E. J. Copeland, M. Sami and S. Tsujikawa, Int. J. Mod. Phys. D **15**, 1753 (2006) [hep-th/0603057].
- [183] T. Chiba, A. De Felice and S. Tsujikawa, Phys. Rev. D **87**, 083505 (2013) [arXiv:1210.3859 [astro-ph.CO]].
- [184] S. Tsujikawa, Class. Quant. Grav. **30**, 214003 (2013) [arXiv:1304.1961 [gr-qc]].
- [185] W. Hu and I. Sawicki, Phys. Rev. D **76**, 064004 (2007) [arXiv:0705.1158 [astro-ph]].

- [186] S. Tsujikawa, K. Uddin, S. Mizuno, R. Tavakol and J. Yokoyama, Phys. Rev. D **77**, 103009 (2008) [arXiv:0803.1106 [astro-ph]].
- [187] A. Goldstein *et al.*, Astrophys. J. **848**, no. 2, L14 (2017) [arXiv:1710.05446 [astro-ph.HE]].
- [188] L. Lombriser and A. Taylor, JCAP **1603**, 031 (2016) [arXiv:1509.08458 [astro-ph.CO]].
- [189] L. Amendola, M. Kunz, I. D. Saltas and I. Sawicki, Phys. Rev. Lett. **120**, 131101 (2018) [arXiv:1711.04825 [astro-ph.CO]].
- [190] A. De Felice, C. Q. Geng, M. C. Pookkillath and L. Yin, JCAP **08**, 038 (2020) [arXiv:2002.06782 [astro-ph.CO]].
- [191] S. Nakamura, R. Kase and S. Tsujikawa, JCAP **1912**, 032 (2019) [arXiv:1907.12216 [gr-qc]].
- [192] L. G. Gomez and Y. Rodriguez, doi:10.1016/j.dark.2020.100759 [arXiv:2004.06466 [gr-qc]].
- [193] C. Wetterich, Astron. Astrophys. **301**, 321 (1995) [hep-th/9408025].
- [194] L. Amendola, Phys. Rev. D **62**, 043511 (2000) [astro-ph/9908023].
- [195] L. Amendola, Phys. Rev. D **69**, 103524 (2004) [astro-ph/0311175].
- [196] A. Pourtsidou, C. Skordis and E. J. Copeland, Phys. Rev. D **88**, 083505 (2013) [arXiv:1307.0458 [astro-ph.CO]].
- [197] C. G. Boehmer, N. Tamanini and M. Wright, Phys. Rev. D **91**, 123003 (2015) [arXiv:1502.04030 [gr-qc]].
- [198] C. Skordis, A. Pourtsidou and E. J. Copeland, Phys. Rev. D **91**, 083537 (2015) [arXiv:1502.07297 [astro-ph.CO]].
- [199] J. Dutta, W. Khyllep and N. Tamanini, Phys. Rev. D **95**, 023515 (2017) [arXiv:1701.00744 [gr-qc]].
- [200] T. S. Koivisto, E. N. Saridakis and N. Tamanini, JCAP **1509**, 047 (2015) [arXiv:1505.07556 [astro-ph.CO]].
- [201] A. Pourtsidou and T. Tram, Phys. Rev. D **94**, 043518 (2016) [arXiv:1604.04222 [astro-ph.CO]].

- [202] R. Kase and S. Tsujikawa, Phys. Rev. D **101**, 063511 (2020) [arXiv:1910.02699 [gr-qc]].
- [203] R. Kase and S. Tsujikawa, Phys. Lett. B **804**, 135400 (2020) [arXiv:1911.02179 [gr-qc]].
- [204] F. N. Chamings, A. Avgoustidis, E. J. Copeland, A. M. Green and A. Pourtsidou, Phys. Rev. D **101**, no.4, 043531 (2020) [arXiv:1912.09858 [astro-ph.CO]].
- [205] L. Amendola and S. Tsujikawa, JCAP **06**, 020 (2020) [arXiv:2003.02686 [gr-qc]].
- [206] A. De Felice, L. Heisenberg, R. Kase, S. Tsujikawa, Y. Zhang and G. Zhao, Phys. Rev. D **93**, 104016 (2016) [arXiv:1602.00371 [gr-qc]].
- [207] M. C. Pookkillath, A. De Felice and S. Mukohyama, Universe **6**, no.1, 6 (2019).
- [208] J. D. Brown, Class. Quant. Grav. **10**, 1579 (1993) [gr-qc/9304026].
- [209] A. De Felice, J. M. Gerard and T. Suyama, Phys. Rev. D **81**, 063527 (2010) [arXiv:0908.3439 [gr-qc]].
- [210] B. Boisseau, G. Esposito-Farese, D. Polarski and A. A. Starobinsky, Phys. Rev. Lett. **85**, 2236 (2000) [gr-qc/0001066].
- [211] S. Tsujikawa, Phys. Rev. D **76**, 023514 (2007) [arXiv:0705.1032 [astro-ph]].
- [212] A. De Felice, T. Kobayashi and S. Tsujikawa, Phys. Lett. B **706**, 123 (2011) [arXiv:1108.4242 [gr-qc]].
- [213] J. Renk, M. Zumalacarregui, F. Montanari and A. Barreira, JCAP **1710**, 020 (2017) [arXiv:1707.02263 [astro-ph.CO]].
- [214] J. B. Durrive, J. Ooba, K. Ichiki and N. Sugiyama, Phys. Rev. D **97**, no.4, 043503 (2018) [arXiv:1801.09446 [astro-ph.CO]].